Characterisation of pH and Glucose Sensors for use in Cell Culture

by

Suket Singhal

January 2009

A thesis submitted for
the degree of Doctor of Philosophy of Imperial College

Institute of Biomedical Engineering
Imperial College of Science, Technology and Medicine

To Amma & my family

I declare that the work in this thesis is my own.
Suket Singhal

Acknowledgements

I would like to thank my supervisor Prof. A.E.G. Cass for all the help and encouragement that he has accorded me during the completion of this work. His supervision has allowed me to grow in a lot of respects. His method of allowing exploration of science has given me a deep appreciation of scientific principles and the ability to understand technology easily.

This project would not have been possible without the collaboration and help of Sakis Mantalaris and Maya Lim from Chemical Engineering, who were responsible the culture of stem cells. Also, Manos Drakakis and Dr. Alex Yue, who supplied the electronic and data acquisition equipment. Most importantly I would like to thank Dr. Anna Radomska for all her expertise in the preparation of the sensors and for being one of the most astounding sounding boards of ideas and potential stumbling blocks. The work of the team was essential in the completion of the project and it is a model of collaborative working. NIr Grossman was responsible for the culture of HL-N! cells and the work done with him provided invaluable insight.

There are numerous people to thank in the Institute of Biomedical Engineering & Department of Biomedical Engineering for all their inspiration and numerous ideas; along with all the numerous ideas and plans that were formed during a few beers and food. There are far too may to name individually and i am sure that I will leave out a number of people as well.

Finally and by no means the least, I would like to thank my family who provided me with lots of support and encouragement throughout. They might have thought that I was crazy to begin with, but they let me try and find out myself!

Abstract

The long term monitoring of cell cultures, to study their dynamic nature is important, although devices capable of doing this aren't available. Primiarily the reason for this is the bio-compatability of the devices and this refers to both the devices' compatibility with the culture as well as its compatibility with the device.

Glucose sensors fabricated in electropolymerised poly(phenol) were used for the study. The reproducibility of these devices was checked to assess their viability for large scale deployment. It was found that the intra–batch variation was within the norms of experimental error, although the inter–batch variation was significant. This is a feature that is inherent to hand made devices and some methods to mitigate this are discussed.

The surface characterisation of the sensors showed that the polymer and enzyme sit mutually exclusive to each other on the surface. Using cyclic voltammetry, with ferrocyanide as the probe molecule, it was confirmed that the diffusion profile to the surface of the sensor was semi-infinite planar and that the electrochemistry was quasi-reversible. Infra–red and Raman spectroscopy and scanning electrochemical microscopy were used as well to study the films' morphology.

The sensors were not toxic to 3T3 cell cultures, as the yield and cell viability were consistent with those of the control cultures. It was also seen that the initial degradation of the sensors' response was not entirely due to the loss in enzyme activity. Non-polarised sensors showed a decrease in sensitivity to glucose and a threshold concentration ca. 3 mM below which they showed no response to glucose, when they were removed from the culture. These effects were not seen before the sensors were placed in the culture and in protein free media, they were partially reversed over time.

The effect of surface treatment on gold electrodes is also studied to assess whether the sensitivity to pH can be improved. Acid etching and gold nanoparticle deposition are the surface treatments used.

Contents

1 Introduction **21**

1.1 Aims and Objectives 21

1.2 Theory 21

1.2.1 Electrochemical Theory 22

1.2.2 Electrochemical Techniques 26

1.2.3 Enzyme Theory 37

1.2.4 Biosensor Theory 38

1.3 Literature Review 43

1.3.1 Iridium oxide devices 43

1.3.2 Electrochemical Enzyme Sensors 47

1.3.3 Osmium containing polymers 57

1.3.4 Scanning Electrochemical Microscopy 64

1.3.5 *In-vitro* monitoring of cell cultures 68

1.4 Summary 73

2 Materials and methods **87**

2.1 Introduction 87

2.2 Materials 88

2.3 Details of equipment used 88

2.3.1 Electrochemical instrumentation 88

2.4 Details of the electrochemical cells used 89
2.4.1 Counter electrode 90
2.4.2 Working electrodes 91
2.5 Iridium oxide pH electrodes 95
2.5.1 Precipitation solution 96
2.5.2 Galvanostatic deposition 96
2.5.3 Surface treatment before galvanostatic deposition 97
2.5.4 pH calibration 98
2.6 Redox mediated enzyme sensors 99
2.6.1 Synthesis of the metallopolymer 100
2.6.2 Surface immobilisation 102
2.7 Enzyme films encapsulated in poly(phenol) 106
2.8 Testing the sensitivity of the devices for glucose 108
2.9 Study of the film morphology 108
2.9.1 Optical studies 109
2.9.2 Electrochemical studies 109
2.10 Off-line media analysis 111
2.11 Sensor performance *In-Vitro* 112
2.11.1 Toxicity tests 112
2.11.2 Life time of sensors *in-vitro* 112
2.12 Summary 113

3 Iridium oxide pH sensors 116

3.1 Introduction 116
3.2 Optimisation of film production 116
3.3 Surface treatment to improve iridium oxide film characteristics 120
3.3.1 Surface Modification 121
3.3.2 Sensor performance 127

3.4 Summary and Conclusions 132

4 Glucose sensors mediated by an osmium complex metallopolymer 135

4.1 Introduction 135

4.2 Covalent attachment. 136

4.3 Encapsulation in electro-deposition paint 143

4.4 Summary and Conclusions 149

5 Glucose sensors fabricated from electropolymerised poly(phenol) films 153

5.1 Introduction 153

5.2 Glucose oxidase procured from Biozyme 153

5.3 Optimisation using the new enzyme 155

5.3.1 Phenol concentration 155

5.3.2 pH optimisation 159

5.4 The importance of pre-adsorption 163

5.5 Control studies 166

5.6 Intra–batch variability 170

5.7 Life–time analysis of the sensors 171

5.8 Summary 175

6 Surface characterisation of glucose sensors 178

6.1 Introduction 178

6.2 Optical analysis 178

6.2.1 FT–IR spectroscopy 179

6.2.2 Raman spectroscopy 181

6.3 Cyclic Voltammetry 186

6.3.1 Validation 186

6.3.2 Study of the film's diffusion profile and e^- transfer 195

6.4 Scanning Electrochemical Microscopy 212

6.5 Summary 224

7 Sensors and Cell Cultures. 228

7.1 Introduction 228

7.2 Off - line analysis of Cardiomyocyte cultures 228

7.2.1 Primary test for validation 228

7.2.2 Interference from norepinephrine. 232

7.2.3 Long term monitoring of cardiomyocytes 235

7.3 *In-vitro* chracterisation and use. 240

7.3.1 Toxicity tests 240

7.3.2 *In-vitro* life time analysis of the enzyme sensors 240

7.3.3 The use of H_2O_2 to assess the degradation of the performance of the sensors. 253

7.4 Summary 256

8 Conclusion and recommendations for future work 259

8.1 Conclusions 259

8.2 Recommendations for future work 263

List of Figures

1.1 Schematic showing the features of the double layer. 25

1.2 Schematic showing the difference in time taken to sweep between the same switching potentials (E_λ) at different scan rates ($\dot{v}$). 27

1.3 A cyclic voltammogram of 10mM $Ru[NH_3]_6^{2+}$ in 100mM KCl at a 200 μm platinum disc electrode at a scan rate of 100 mVs^{-1}. The labels indicate the important features of the scan. 28

1.4 CVs of 100mM $Ru[NH_3]_6^{2+}$ in 100mM KCl at a gold disc electrode. The scan rates for each CV are shown in the legend. 30

1.5 Schematic of a 2–step chronoamperogram 33

1.6 Schematic showing the modes of SECM 36

1.7 Schematic showing the structure of the glucose oxidase active centre. [8] . . 38

1.8 Schematic showing the operating principle of a biosensor 39

1.9 Schematic showing the e^- transfer path for a glucose sensor. The sensor is made using glucose oxidase on a platinum electrode with the mediator in solution. 42

1.10 Rate of acidification of 3T3 cells as shown by Ges et. al. [34]. 46

1.11 Mechanism of the polymerisation of phenol 53

1.12 Schematic of CNT 'ensemles' from Lin et. al. [55]. 56

1.13 CV of (Os-bpy$_2$)Cl showing surface bound characteristics as shown by Forster et. al. [66]. 58

1.14 Michaelis-Menten and Lineweaver-Burke plots for glucose sensors made by Gregg and Heller [70]. 60

1.15 Schematic representation of the device patented by Heller [74]. 61

1.16 Entrapment of Os complex in poly(phenol), CVs as shown by Pravda et. al. [81]. 63

1.17 Line scan over a glucose oxidase substrate, using an enzyme modified tip, with a synthetic redox mediator to complete the redox cycle. The drop in current indicates that the tip has move off the H_2O_2 producing area, shown by Horrocks et. al. [87]. 66

1.18 SECM images of a platinum substrate electrolysing water, using a carbon fibre tip modified with IrOx to sense pH, shown by Wipf et. al. [88]. The side bars indicate the pH range recorded at the tip and A to E are experiments performed in unbuffered solution whereas F to J are performed in phosphate buffer. The substrate potentials are -0.2V (A, F); -0.4 (B. G); -0.6 V (C, H); -1.0 V (D, I) and -1.2 V (E, J). 67

1.19 Surface scan of a lactate oxidase modified surface with HMF as a mediator, as shown by Parra et. al. [92]. 69

1.20 Cell culture parameters of yeast cultures as measured and presented by Vojinovic et. al. [96]. 72

2.1 A schematic of the working electrodes housed in a glass capillary body. . . . 92

2.2 Schematic illustrating the method used to form an SU8 layer on the platinum wire. 93

2.3 Schematic comparing an ideal SU8 film with the inconsistencies of the films that could easily be produced. 94

2.4 Schematic showing the construction of the working electrode. 95

2.5 Reaction scheme showing the polymerisation of vinylimidazole. 100
2.6 Scheme for the synthesis of Os(dmo-bpy)chloride. 101
2.7 The reaction scheme for the precipitation of the osmium complex, in the presence of sodium dithionite [4]. 102
2.8 Reaction scheme showing the synthesis of Os(dmo-bpy)Cl–PVI from its two independent constituents. 103
2.9 Small volume cell used to precipitate resydrol on glassy carbon electrode. . 105
2.10 Potential pulse profile used to precipitate Resydrol. 106

3.1 Trace showing the open circuit potential of four sensors with iridium oxide deposited using a current density of 0.1 mA cm^{-2}, during a pH titration. . 117
3.2 Calibration curves for iridium oxide deposited at 0.1 mA cm^{-2}. 117
3.3 Calibration curves for iridium oxide films deposited galvanostatically at 0.6 mA cm^{-2}. 119
3.4 Variations in sensor performance with the optimised protocol. 120
3.5 Calibration variations with the new protocol, using a current density of 10 A m^{-2} for galvanostatic deposition of iridium oxide on gold substrates. . . . 120
3.6 CVs of 5 mM ruthenium hexaamine(III) in 100 mM KCl at a scan rate of 100 mV s^{-1} that show the comparison between the surfaces of the gold disc electrodes before and after etching with aqua regia. 122
3.7 CVs of 5 mM ruthenium hexaamine(III) in 100 mM KCl at a scan rate of 100 mV s^{-1} that show the comparison between the surfaces of the gold disc electrodes before and after the physisorption of gold nano-particles. 123
3.8 CVs of 5 mM ruthenium hexaamine(III) in 100 mM KCl at a scan rate of 100 mV s^{-1} that show the comparison between the surfaces of the gold disc electrodes before and after etching with nitric acid. 123

3.9 CVs of 5 mM ruthenium hexaamine(III) in 100 mM KCl at a scan rate of 100 mV s^{-1} that show the comparison between the surfaces of the gold disc electrodes before and after etching with nitric acid. The surface of this electrode indicates that the acid etching increased its surface area. 124
3.10 Peak currents for each of the surface modifications. 125
3.11 Comparison of the C_d of the gold electrodes before and after each surface treatment. 126
3.12 pH calibration curves for iridium oxide electrodes, prepared on 200μm gold disc electrodes etched with aqua regia. 127
3.13 pH calibration curves for iridium oxide electrodes, prepared on 200μm gold disc electrodes etched with nitric acid. 128
3.14 pH calibration curves for iridium oxide electrodes, prepared on 200μm gold disc electrodes with gold nanoparticles physisorbed on their surfaces. 128
3.15 pH calibration curves for iridium oxide electrodes, prepared on 200μm polished gold disc electrodes. 129
3.16 pH calibration curves for iridium oxide electrodes, prepared on 200μm polished gold disc electrodes with a 1% nafion film deposited as a protective layer. 129
3.17 Variations in the sensitivity to pH for each type of electrode preparation technique. 130

4.1 Scheme showing the formation of the epoxide bonds between (a) the amine group in the enzyme and the functional end of the PEG, (b) the free nitrogen on the vinylimidazole pendant and the functional group of the PEG. [5] . . 136
4.2 CVs of osmium complex attached covalently to the electrode surface. 137
4.3 Loss in osmium content of film while in PBS. 138
4.4 Glucose titration using a covalently attached osmium complex film. 140
4.5 No sensor response from a glucose titration. 141

4.6 Current trace recorded during a glucose titration using a covalently attached PVI and glucose oxidase film. The labelled arrows show the change in glucose concentration in mM during the course of the titration. 142
4.7 Calibration curve for the glucose oxidase and PVI film. 142
4.8 Currents recorded during the electro-deposition of resydrol. 145
4.9 CVs of the osmium complex containing films, encapsulated using resydrol in PBS. $\dot{v} = 50\text{mV s}^{-1}$. 145
4.10 CVs of osmium complex encapsulated in resydrol, showing minimal loss of the complex from the surface. $\dot{v} = 100\text{mV s}^{-1}$. 146
4.11 CVs at different scan rates of the osmium complex encapsulated in resydrol. 147
4.12 The CV at 1 mV s^{-1}, from Figure 4.11. 147
4.13 CV of osmium complex cured with resydrol in the curing mixture, on the surface of a glassy carbon electrode. Scan rate = 1 mV s^{-1}. 148
4.14 Glucose titration trace using film cured with resydrol in the curing mix. The labelled arrows show the change in glucose concentration in mM during the course of the titration. 149

5.1 Calibration curves of devices using glucose oxidase from Biozyme Labs. . . 154
5.2 1^{st} scan of phenol at the shown bulk concentrations, on a 200μm platinum disc electrode with glucose oxidase preadsorbed on the platinum surface. The bulk electrolyte is 100mM PBS and the scan rate is 100mV s^{-1}. 156
5.3 2^{nd} scan of phenol at the shown bulk concentrations, on a 200μm platinum disc electrode with glucose oxidase preadsorbed on the platinum surface. The bulk electrolyte is 100mM PBS and the scan rate is 100mV s^{-1}. 157
5.4 3^{rd} scan of phenol at the shown bulk concentrations, on a 200μm platinum disc electrode with glucose oxidase preadsorbed on the platinum surface. The bulk electrolyte is 100mM PBS and the scan rate is 100mV s^{-1}. 157

5.5 Current recorded for a glucose titration on a 200μm platinum electrode with glucose oxidase entrapped in a poly(phenol) film made using 5 mM phenol. The arrows indicate the concentration of glucose in mM during the course of the titration. 158

5.6 Current recorded for a glucose titration on a 200μm platinum electrode with glucose oxidase entrapped in a poly(phenol) film made using 15 mM phenol. The concentration of glucose in mM is shown using the labelled arrows. . . 158

5.7 Glucose calibration curves for a single batch of devices made using 25mM phenol in the polymerisation cell. These calibration curves demonstrate the intra–batch variability inherent with the process. 159

5.8 Current recorded during a glucose titration for two sensors polymerised in a supporting electrolyte with pH = 4.56. The labelled arrows show the concentration of glucose during the titration. 161

5.9 Current recorded during a glucose titration for two sensors polymerised in a supporting electrolyte with pH = 4.66. The concentration of glucose in the bulk solution is shown by the labelled arrows within the figure. 161

5.10 Currents recorded during a glucose titration for two sensors that were polymerised in a supporting electrolyte consisting of only 100mM PBS. (pH $\simeq$ 7.2) The arrows indicate the glucose concentration during the titration; in mM. 162

5.11 Currents recorded using sensors made with PBS as the supporting electrolyte and an acetate 'spike' during electropolymerisation. The labelled arrows show the concentration of glucose, in mM, during the sequential aliquot addition. 163

5.12 CV of 50 mM phenol an a platinum disc electrode that has not been allowed to stand in glucose oxidase solution. Therefore there has been no pre-adsorption of enzyme on the platinum surface. 164

5.13 Currents recorded during the glucose calibration of three sensors prepared without the pre-adsorption step. The arrows show the glucose concentration, in mM during the titration. 165
5.14 Calibration curves obtained from the titration of glucose; for three sensors prepared, as described without any pre-adsorption. The CV in Figure 5.13 corresponds to the trace shown here for sensor 1 165
5.15 Currents recorded on a functional glucose sensor during a standard glucose titration (experiment) and the titration of 100mM PBS (negative control). The concentration of glucose in the cell was increased step wise, this is indicated by the labelled arrows in the figure. 167
5.16 CVs for a the oxidation of 50mM phenol on a 1 mm bare platinum disc without any glucose oxidase in the cell and the same electrode with pre-adsorbed glucose oxidase and present in the polymerisation cell. 168
5.17 Currents recorded during a glucose titration on two 1 mm diameter platinum electrodes. One of the electrodes is a functional glucose sensor and the other is a poly(phenol) film electro-oxidised on the platinum surface. The arrows show the bulk glucose concentration in the cell during the titration. 169
5.18 Variations in the calibrated responses to glucose on days 1, 4, 5 and 6, for sensor 'A'. 171
5.19 Glucose calibration curves, for sensor 'B' on days 1,2 and 3. 172
5.20 Glucose calibration for sensor 'B' on days 4, 5 and 6. 172
5.21 Glucose calibration curves for sensor 'C', from days 1 to 3. 173
5.22 Glucose calibration curves for sensor 'C' from days 4 to 7. 173
5.23 Daily variations in the calibration slopes for 7 days. 174

6.1 IR absorbance spectra for glucose oxidase, obtained using ATR from pressed powder. 180
6.2 IR spectra from the sensor's surface. 180

6.3 A second IR spectra from the glucose sensor's surface. 181
6.4 Raman spectra for crystals of phenol placed on a glass slide. 182
6.5 Raman spectra for glucose oxidase dried from solution on a reflective substrate. 183
6.6 Raman scattering for poly(phenol) polymerised on a polished platinum substrate. Two different laser powers were used to assess whether the signal from the thin film could be improved. 183
6.7 Raman scattering for a glucose sensor at different laser power settings. . . . 184
6.8 Raman spectra from the surface of a glucose sensor showing weak bands. . 185
6.9 Raman scattering from the surface, at points of little or no signal. 185
6.10 Ferrocyanide CV for a bare 1 mm platinum disc electrode. 187
6.11 Ferrocyanide CVs for a poly(phenol) coated and an enzyme platinum disc electrode. 188
6.12 Types of diffusion layers. 189
6.13 The structure of a quasi–linear diffusion profile, adapted from [6]. 190
6.14 Daily glucose calibration curves for the glucose sensors used in this experiment. The sensor is made on a 1 mm platinum disc with pre-adsorbed glucose oxidase encapsulated in a poly(phenol) film. 193
6.15 CVs of 10mM ferrocyanide in 100mM KCl from the functional glucose sensor on days 1 and 2. 194
6.16 CVs of 10mM ferrocyanide in 100mM KCl from the functional glucose sensor on days 3 to 5. 195
6.17 Initial calibration curves for '1' and '2' before CV trials. 196
6.18 CV of 50mM ferrocyanide in 100mM KCl on three 1mm bare platinum disc electrodes, $\dot{v} = 100$ mV s^{-1}. 197
6.19 Daily CVs of 50 mM ferrocyanide in 100mM KCl for electrode '3' at a $\dot{v}$ of 50 mV s^{-1}. 198

6.20 Differences in the polymerisation CVs for a poly(phenol) film. Both CVs are for 50mM phenol in 100mM PBS on bare 1mm platinum disc electrodes. Both electrodes have been prepared by abrasive polishing with alumina. . . 199
6.21 Daily CVs of 50mM ferrocyanide at electrode '1', $\dot{v} = 10$ mV s^{-1}. 200
6.22 Daily CVs of 50mM ferrocyanide at electrode '2', $\dot{v} = 10$ mV s^{-1}. 200
6.23 Scan rate dependence of 50mM ferrocyanide electrochemistry at electrode '1' on day 1. 202
6.24 Scan rate dependence of 50mM ferrocyanide electrochemistry at electrode '2' on day 1. 202
6.25 Scan rate dependence of 50mM ferrocyanide electrochemistry at electrode '2' on day 4. 203
6.26 Scan rate dependence of I_p for electrodes '1' and '2' on day 1. 203
6.27 I_p vs. $\sqrt{\dot{v}}$ for electrode '1'. 204
6.28 I_p vs. $\sqrt{\dot{v}}$ for electrode '2'. 204
6.29 Daily variations in C_d for each of the three electrodes. 206
6.30 Approach curve on the epoxy surround of the substrate. a 100μm tip was used and the bulk electrolyte was 10mM ferrocyanide in 100mM KCl. The tip moved from the its original position in 10μm steps. 213
6.31 Line scans on the bare platinum substrate. The probe distance was set using the approach curve and the bulk electrolyte was 10mM ferrocyanide in 100mM KCl. Each step of the probe was 50μm with a collection time of 2s. 214
6.32 Area scan of a bare platinum disc in GC mode with 10mM ferrocyanide in 100mM KCl. This is a 1000 $\times$ 500μm scan, 50μm steps are used in both the x and y directions. a) shows the profile of the reduction current and b) shows the plan view mapped substrate. 215

6.33 Preliminary area scan of a glucose sensors' surface in GC mode with 10mM ferrocyanide in 100mM KCl. The 600 × 300μm area is scanned using 50μm steps along both the axes. The profile of the probe current is shown in (a) whereas (b) shows the plan view of the map. 216

6.34 Surface scan of a functional glucose sensor as the substrate using a 5 μm probe in GC mode.The bulk electrolyte is 50mM ferrocyanide in 100mM KCl. The area was mapped using 10μm steps in both the x and y directions. 217

6.35 Comparison of calibration curves pre and post drying. 218

6.36 Preliminary area scan of the surface of a dried sensor using GC mode with 50mM ferrocyanide in 100mM KCl. A 100μm probe was used and the steps in both directions were 50μm. 219

6.37 Preliminary area scan of the surface of a dried sensor using GC mode; collecting enzymatically generated H_2O_2 at the tip. A 100μm tip was used for this scan and 50μm steps were used to traverse the substrate in both directions.220

6.38 A negative control surface scan, with only PBS in the cell. 220

6.39 Area scan of a functional glucose sensor with only 100mM PBS as the electrolyte. The profile of the probe current is shown in (a) and this is shown as a plan view in (b). The tip was used was 100μm in diameter and 50μm steps were used to travel across the designated area of the substrate. 222

6.40 Area scans of the same region of the substrate performed consecutively. In (a) the electrolyte is 50mM ferrocyanide in 100mM KCl and in (b) this is changed to glucose in 100mM PBS. All other experimental conditions are the same 223

7.1 Measuring the concentration of glucose in a media aliquot. The raw trace is as taken from the culture (V_{tot}=50 μl) and the dilute trace is the same sample that has been diluted using 100 mM PBS by a factor of 4 (V_{tot}=200 μl). 229

7.2 Change in glucose concentration not accounting for the norepinephrine, for both trials 'A' and 'B'. 231
7.3 Change in glucose concentration when the norepinephrine has been accounted for, for both trials 'A' and 'B'. 231
7.4 Cyclic voltammogram of 100 μM norepinephrine, prepared in 100 mM PBS as per manufacturers specifications. The electrode used is a functional glucose sensor made using glucose oxidase in a poly(phenol) film. $\dot{v} = 100mVs^{-1}$. 233
7.5 Chronoamperometery for a 100 μM titration of norepinephrine in a cell with 100 mM PBS. The electrodes used were functional glucose sensors made using glucose oxidase and poly(phenol). 234
7.6 Differences in the calibration curve and background current in fresh media. 234
7.7 Change in the concentration of glucose in Claycomb media during the culture of cardiomyocyte cells, without the removal of the background current. . . . 236
7.8 Change in the concentration of glucose in Claycomb media during the culture of cardiomyocyte cells, once the estimated background current, has been mathematically removed. 236
7.9 Cell growth over 7 days of the second off-line test 239
7.10 Initial calibration curve for sensors before operating *in-vitro*. 242
7.11 Calibration curves for sensors 1 and 2 after one day *in-vitro*. 242
7.12 Calibration curves for sensors 3 and 4 after 2 days in *in-vitro*. 243
7.13 Calibration curve for sensor 5 and 6 after 3 days in the 3T3 culture vessel. . 243
7.14 Linear section of calibration curves for sensors 1 and 2 on day 1. 244
7.15 Linear section of calibration curves for sensors 3 and 4 on day 2. 245
7.16 Schematic showing the flux of glucose at the enzyme film. 247
7.17 Calibration curve for sensors 1 and 2 on day 2. 248
7.18 Calibration trace for sensor 1 as repeated on day 2. 249
7.19 Calibration trace for sensor 2 as repeated on day 2. 249

7.20 Calibration trace for sensor 3 as repeated on day 2. 250
7.21 Calibration trace for sensor 4 as repeated on day 2. 250
7.22 The transient nature of the responses of sensors 1 and 2 before they were placed in the culture and during their daily calibrations once they had been removed from the culture after 24 hours. 251
7.23 The sensitivity of sensors 3 and 4 before being placed in culture compared to their responses on removal from the media. 251
7.24 A comparison of the calibration curves for sensor 1 and 2 on day 3 compared to the same devices before they were placed in the culture. 252
7.25 A comparative of the calibration curves for sensor 3 and 4 on day 3 and before they were placed in the culture 252
7.26 Comparative response to H_2O_2 for sensors 1, 2 and 3 before and after being placed *in-vitro*. 254
7.27 Comparative response to H_2O_2 for sensors 4, 5 and 6 before and after being placed *in-vitro*. 255
7.28 Comparative response to H_2O_2 for sensors 7, 8 and 9 before and after being placed *in-vitro*. 255

List of Tables

1.1 Details of poly(phenol) and glucose oxidase film thickness on HOPG as reported by Arrigan and Bartlett [52]. 54

2.1 Composition of buffer. 88
2.2 Sample, set points for pH calibration of iridium oxide electrodes, as obtained from a glass electrode. 99
2.3 Volumetric ratios and concentrations of the components of the curing mixture. 104
2.4 Protocol to make enzyme buffer 107
2.5 Preparation of the pre adsorption and polymerisation solutions. 107
2.6 Conditions used for cyclic voltammetry to polymerise phenol. 108
2.7 Composition of Claycomb Media. (As per the manufacturers' specifications) 111

3.1 Operating characteristic of the iridium oxide deposition. 118
3.2 Operating characteristics of pH sensors 130

5.1 Characteristics of sensors made using glucose oxidase from Biozyme Labs. . 154
5.2 Oxidation peak characteristics for the electro–polymerisation of phenol at the shown bulk concentrations of phenol (C_b). 156
5.3 Operating slope of a single batch of glucose sensors. 170

5.4 Analysis of inter-batch variance of the operating characteristics of glucose sensors. Obtained by performing and ANOVA on the batches and comparing the homogeneity of variance using Levene's test. 175

6.1 Vibrational bands of functional groups expected to be found in the glucose sensors. 179
6.2 Nomenclature of electrodes used for ferrocyanide CV tests. 196
6.3 Initial operating characteristics of '1' and '2'. 197
6.4 Slopes of fits from I_p vs. $\dot{v}^{1/2}$ analysis. 205
6.5 Capacitance of disc electrodes. 206
6.6 Daily ΔE_p for '1'. 208
6.7 Daily ΔE_p for '2'. 208
6.8 Daily kinetic parameters for '1'. 209
6.9 Daily kinetic parameters for '2'. 210
6.10 Daily $E_{1/2}$ values for '1'. 210
6.11 Daily changes in $E_{1/4} - E_{3/4}$ for '1'. 211
6.12 Armstrong's tests for '2'. 211

7.1 Calibration curve data 229
7.2 Calibration curve data, for the sensors used during the long term monitoring of the media. The sample numbers indicate the calibrations performed before that particular sample was tested. 235
7.3 pH of samples diluted with 100mM PBS after being removed from media during the long term monitoring of cardiomyocyte cultures. 238
7.4 Results of the toxicity tests 241
7.5 Sensor nomenclature for *in-vitro* test. 241
7.6 Change in linear sensitivity when the sensors are withdrawn from the culture. 246
7.7 Activity of H_2O_2 verified using a $KMnO_4$ titration. 253

List of abbreviations

AFM	Atomic force microscopy
APTES	Aminopropyl triethoxy siloxane
C_b, C_{bulk}	Bulk concentration
C_d	Double layer capacitance
C_o, C_r	Concentration of the oxidised and reduced species, respectively
CMOS	Complimentary metal oxide semiconductor
CNT	Carbon nanotube
CTC	Cyano-ditolyltetrazolium chloride
CTF	Fluorescent red formazan
CV	Cyclic voltammetry
d	Distance between two plates of a capacitor
D_{eff}	Effective diffusion coefficient
ϵ, ϵ_0	Dielectric constants
E^0	Standard electrochemical potential
ECM	Extra cellular matrix
EDP	Electrodeposition paint
EQCM	Electrochemical quartz crystal micro balance
F	Faraday constant
FAD	Flavine Adenine Dinucleotide
FIA	Flow injection Analysis
FT–IR	Fourier transform infrared spectroscopy
GC	Generation collection
HMF	Hydroxymethylferrocene
HOMO	Highest unoccupied molecular orbital
HOPG	Highly ordered pyrolytic graphite
HPLC	High pressure liquid chromatography
HUMO	Highest unoccupied molecular orbital

I_p	Peak current
i_{ss}	Steady state current
i_T	Tip current
IHP	Inner Helmholtz plane
ISFET	Ion selective field effect transistor
$J_{glucose}$	Flux of glucose
K_m	Michaelis-Menten constant
MMO	Metal metal oxide
MWCNT	Multi-walled carbon nanotube
n	Number of electrons
NHE	Normal hydrogen electrode
OHP	Outer Helmholtz plane
PBS	Phosphate buffered saline
PEG	poly(ethylene glycol)
ploy(DAB)	poly(diamino benzene)
PVI	poly(vinylimidazole)
QCM	Quartz crystal microbalance
R	Ideal gas constant
R/G	Ratio of electrode radius and glass surround radius in SECM tip
RDE	Rotating disc electrode
S/N	Signal to noise ratio
SAM	Self assembled monolayer
SCE	Saturated calomel electrode
SECM	Scanning electrochemical microscope
SEM	Scanning electron microscopy
σ	Charge stored in the double layer
T	Temperature
UME	Ultra microelectrode
V	Potential / Voltage
$\dot{v}$	Scan rate

Chapter 1

Introduction

1.1 Aims and Objectives

The aim of this collaborative project was to devise an end to end platform that would allow the on-line monitoring of stem cell cultures in biological real time. Three independent aspects were used to make the system; the cell culture vessels, the electronics that would control the sensors as well as log the data and the sensors themselves. In this work glucose and pH sensors are studied with this end use in mind. Previously available and published technology is used to make the sensors and their surfaces are characterised to gain a greater insight into their optimum performance under cell culture conditions.

1.2 Theory

The theoretical aspects of the techniques and concepts discussed in this thesis are described in this section. This includes the theory of electrochemistry, enzymes and chemical and biosensors.

1.2.1 Electrochemical Theory

Electrochemistry is the study of the reactions of chemical species at electrified interfaces. The reactions can involve the transfer of electrons and/or ions across the interfacial region. In particular this work will concentrate on the redox activities of chemical species, across two different phases, usually these are the solid phase (electrode) and the liquid phase (electrolyte). It will be shown later that most of these reactions occur in the inter-facial region of these two phases. If we consider a single chemical species that undergoes redox chemistry as shown in equation 1.1; where the forward reaction is oxidation.

$$A - e^- \rightleftharpoons A^+ \tag{1.1}$$

The oxidation of species A takes place when an e^- leaves its Highest Occupied Molecular Orbital (HOMO) and during the reduction process an electron is gained by species A in its Highest Unoccupied Molecular Orbital (HUMO), correspondingly the electron transfer process takes place to and from the Fermi levels of the electrodes. The standard electrode potentials (E^0) for this couple can be estimated from these [1].

All electrochemical redox reactions can be written as a series of half reactions and then the formal potential of these reactions can be calculated using the Nernst Equation. Let us consider one such reaction between zinc and copper in solution.

$$\begin{aligned} Zn_{(s)} &\longrightarrow Zn^{2+}_{(aq)} + 2e^- \qquad (E^0 = -0.76V) \\ Cu^{2+}_{(aq)} + 2e^- &\longrightarrow Cu_{(s)} \qquad (E^0 = 0.34V) \\ Zn_{(s)} + Cu^{2+}_{(aq)} &\longrightarrow Zn^{2+}_{(aq)} + Cu_{(s)} \qquad (E^0_{cell} = 1.10V) \end{aligned} \tag{1.2}$$

The two half reactions and the combined chemical reaction are shown in equations 1.2, all potentials are given with respect to a NHE from Bard and Faulkner [1]. The electrochemical potential of the cell is calculated using Hess's Law. The actual potential of the cell can be calculated from here using the Nernst Equation, equation 1.3 [1]. Where R is the ideal gas

constant, T is the temperature, n is the number of electrons, F is the Faraday constant and C_o and C_r are the concentrations of the oxidised and reduced species in solution.

$$E^{0\prime} = E^0 + \frac{RT}{nF} ln \frac{C_o}{C_r} \tag{1.3}$$

Mass Transport in Electrochemistry

In an electrochemical system there are three main modes of mass transport that can take place:

- Diffusion
- Migration
- Forced Convection

The mass transfer to the electrode is defined by the Nernst – Planck equation, which for 1-D mass transfer is given by equation 1.4 [1].

$$J_i(x) = -D_i \frac{\partial C_i(x)}{\partial x} - \frac{z_i F}{RT} D_i C_i \frac{\partial \phi(x)}{\partial x} + C_i v(x) \tag{1.4}$$

Where D is the diffusion coefficient for each regime, C_i is the bulk concentration, z is the ionic charge, ϕ is the potential and v is the velocity with which an element of solution moves past the surface. In eqaution 1.4 the first term is the diffusion term, from Fick's second law, the second term is the migration term used for the migration of ions and the third term describes convection.

In order to maximise the utility and reliability of electrochemical measurements the concentration of the supporting electrolyte is always maintained at a level that the potential gradient is minimal and therefore migration is assumed to be negligible. Secondly most experiments are performed without any convection, this means that diffusion is the sole mode of mass transport. This makes systems reproducible and mass transport easy to model.

The electrical double layer

The electrical double layer is a structure that occurs at the interface of the solution and the surface of the electrode and displays capacitive behaviour. The double layer is best described as a capacitor that is formed with only a single plate, or as an electrolytic capacitor.

Electrodes being metal can not store excess charge at any point apart from the edges, or surfaces. Therefore when an electrode is poised at a constant potential or swept from one potential to another there is charge stored on its surface. This excess charge needs to be balanced in the interfacial region between the electrode and bulk solution. As all supporting electrolytes contain by definition ions, it is these ions that perform the task of balancing the charge. The double layer is schematically represented in Figure 1.1.

Various models have been proposed for the formation of the double layer with each model describing the structure of the layer in increasing detail. The simplest of these models was proposed by Helmholtz and is known as the Helmholtz double layer theory. Being the first to think about interfacial charges he proposed a two layer model, as shown in Figure 1.1. In the model he proposed that there are two layers of charge known as the Inner Helmholtz Plane (IHP) and the Outer Helmholtz Plane (OHP).

The IHP is a compact layer with greater charge storing capacity and is made up of the ions that complement the surface charge which the electrode carries. The ions in this plane tend not to be solvated, so they experience no shielding effects and are able to approach at the closest point. In well made supporting electrolytes this layer tends to be a few $\mathring{A}$ in thickness [1].

The OHP is a more diffuse layer and it consists of primarily solvated ions that gradually equilibrate the charge between the IHP and the bulk solution. In total the thickness of both the IHP and OHP tends to be of the order of a few nanometres [1].

The capacitance of a two plate capacitor is given in equation 1.5, where σ is the stored charge density, ϵ and ϵ_0 are the dielectric constants of the medium and the vacuum respectively and V the voltage drop [1]. This implies that the the double layer capacitance C_d is

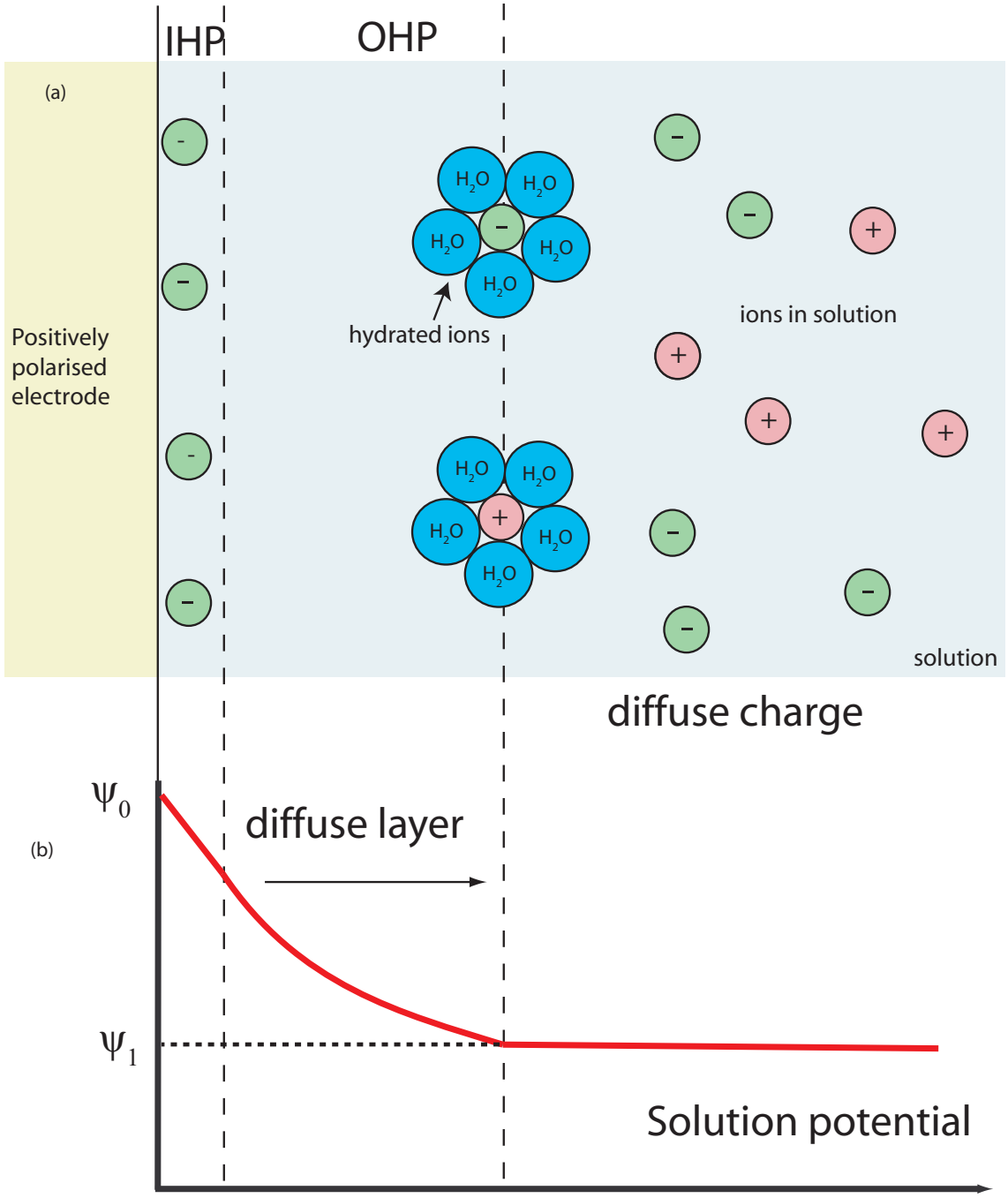


Figure 1.1: Schematic showing the features of an electrochemical double layer (a) is a representation of the ionic distribution within the cell itself and (b) is the profile of the potential from the applied potential at the electrode to the potential of the bulk solution. Adapted from [1]

constant, again shown in equation 1.6. This is a weakness in the model as practically this is not strictly true.

$$\sigma = \frac{\varepsilon\varepsilon_0}{d} v \tag{1.5}$$

$$\frac{\delta\sigma}{\delta V} = C_d = \frac{\varepsilon\varepsilon_0}{d} \tag{1.6}$$

Subsequently to overcome these weaknesses in the Helmholtz model Gouy–Chapman proposed a more refined one to which Stern made some further modifications [1]. Both these new models relied on a similar physical model as that proposed by Helmholtz; but using a different set of assumptions and they were able to predict with greater accuracy the potential profiles across both these layers. Gouy-Chapman viewed the solution near the surface of the electrode as finite elemental laminae whose thickness decreased as the distance from the electrode increased. This approach involves a physical assumption that modelled the decreasing electrostatic charge across the increased distance. Stern's modification added the size of the molecule and its hydration shell to the model to describe the plane of closest approach for the ions. Both these modifications showed that the charge storage was, not constant across the double layer, to confirm practical observations [1].

For the purpose of this work it is adequate to make the Helmholtz approximation for analysis and therefore the other two models were not used and are not described in any more detail.

1.2.2 Electrochemical Techniques

Electrochemistry is the study of the redox chemistry of chemical species and the potentials and currents associated with them. Electrochemical techniques are powerful analytical tools that can be used to study mass and electron transport, chemical reactions along with the structure and morphologies of surface modified electrodes. There are numerous techniques that can be utilised to study the above phenomenon; for the purpose of this chapter we shall

concentrate on the techniques listed below, because the other techniques are very diverse and fall outside the remit of this work.

- Cyclic voltammetry (CV)
- Chronoamperometry at a constant potential
- Scanning electrochemical microsscopy (SECM)

Cyclic Voltammetry

CV is one of the more powerful and widely used techniques in electrochemistry; it involves the study of the currents associated with redox reactions; when the potential is swept in a linear ramp, in both the forward and reverse directions, between two switching potentials (E_λ). Typically E_λ are chosen such that the redox potentials are in the middle, the importance of this is discussed later. This linear sweep of the voltage at different scan rates ($\dot{v}$) is schematically represented in Figure 1.2, where the slope of each line is the $\dot{v}$; this plays a significant role in the relationships that will be described later.

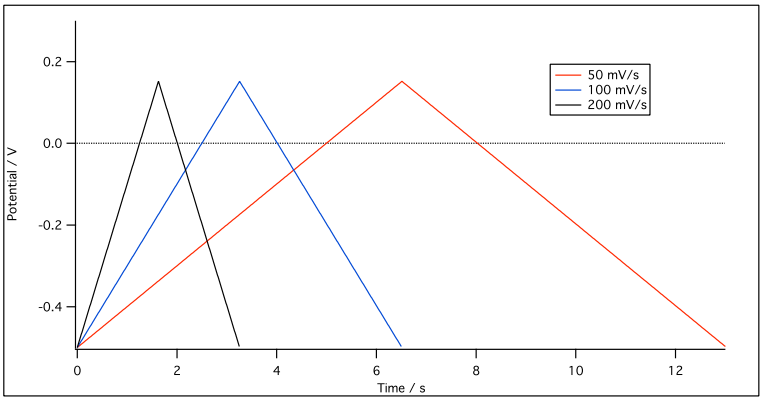


Figure 1.2: Schematic showing the difference in time taken to sweep between the same switching potentials (E_λ) at different scan rates ($\dot{v}$).

The currents recorded at a disc electrode, under the conditions of a linear sweep, produce a current–potential trace, shown in Figure 1.3. This is a very typical trace for a single step, single electron transfer reaction. In this case, the initial concentration of the reduced species

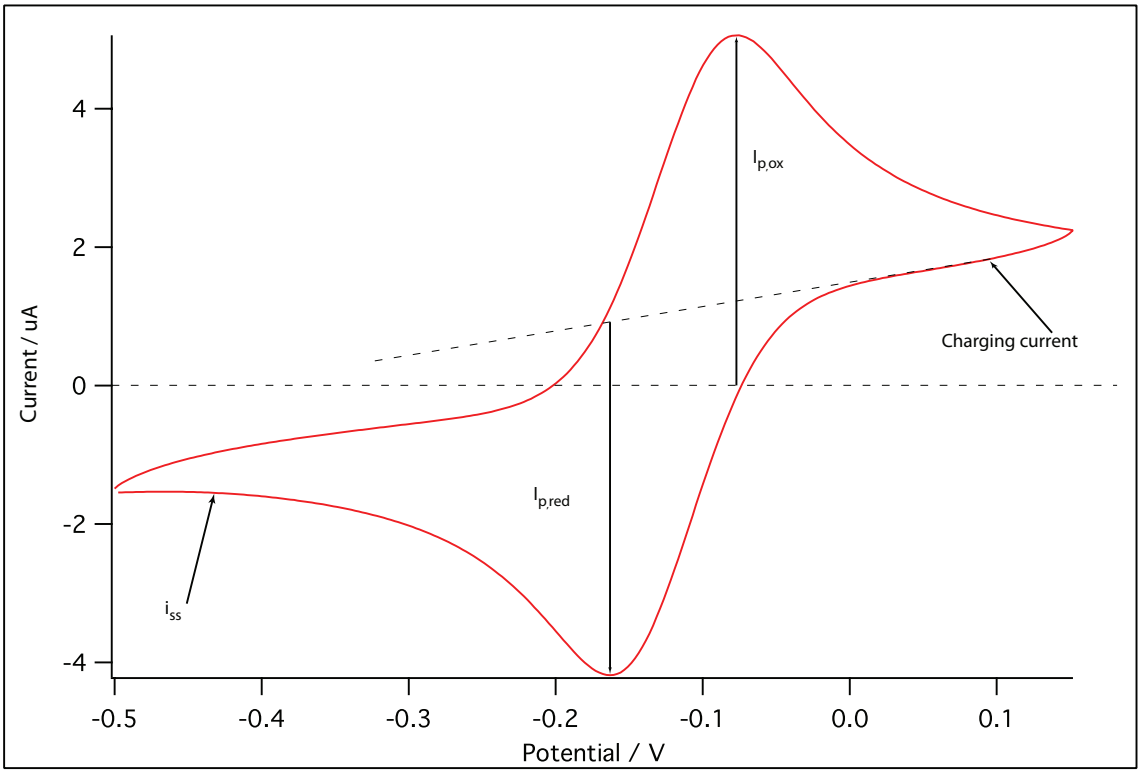


Figure 1.3: A cyclic voltammogram of 10mM $Ru[NH_3]_6^{2+}$ in 100mM KCl at a 200 μm platinum disc electrode at a scan rate of 100 mVs^{-1}. The labels indicate the important features of the scan.

in the electrolyte was assumed, to be zero; therefore the voltage was first changed in the positive direction. At potentials more negative than the oxidation potential no reaction takes place. As the potential approaches the oxidation potential there is an increase in the recorded current, until the peak current I_p, the potential at this point is known as the peak potential $E_{p,ox}$. During the production of the oxidised species the concentration of the reduced species decreases in the diffusion layer, therefore the current also decreases at potentials more positive than E_p, until a steady state value is reached, at which point the currents are diffusion limited. This steady state current is shown during the reverse scan, i_{ss}.

At the second E_λ the linear sweep of the voltage is reversed and this results in the reversal of the initial charging current, at potentials more positive than $E_{p,red}$. It is at this point that the E_λ becomes significant, as the estimation of $I_{p,red}$ is dependant on it. In both portions of the linear sweep, the charging current is roughly constant and is super imposed on the Faradaic processes, this has to be removed to obtain accurate estimations of the peak currents. The fact that the charging currents can not be considered to be exactly reversed at the second E_λ increases the errors of estimation [1]. In the case of the CV in Figure 1.3, the base line for the estimation of $I_{p,red}$ is shown as a linear baseline of the charging current observed before the E approaches $E_{p,red}$. This bas line changes depending on the value of $E_\lambda - E_{p.ox}$ [1]. The peak to peak separation (ΔE_p) is also a function of E_λ and is shown by Bard and Faulkner [1].

The scan rate of the CV also, plays an important role in its characteristics; a succession of CVs at different scan rates are shown in Figure 1.4. From the figure there are two main features that are affected by altering the scan rate; I_p and the charging current. The charging current increases along with the scan rates, this can be seen by studying the i_{ss} of the reverse scans from Figure 1.4. The charging current is constant during each scan and it can be estimated from the i_{ss} using equation 1.7; therefore we know that the charging

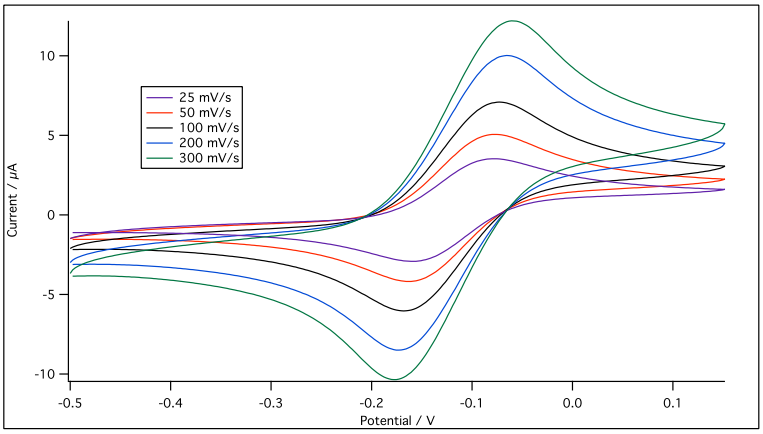


Figure 1.4: CVs of 100mM $Ru[NH_3]_6^{2+}$ in 100mM KCl at a gold disc electrode. The scan rates for each CV are shown in the legend.

current is a function of the $\dot{v}$ [1].

$$i_{ss} \simeq \dot{v} C_d \tag{1.7}$$

The peak current I_p also increases with the increasing scan rate, again clearly visible in Figure 1.4. The relationship between I_p and $\dot{v}$ for a reversible system at a disc electrode is given in equation 1.8; where D is the diffusion coefficient, A is the area of the electrode, C_r is the concentration of the reduced species in the bulk, n is the number of electrons involved in the redox reaction, and F is the Faraday constant. This equation is derived from Ficks' Second Law, with system specific boundary conditions and can be found in detail in Bard and Faulkner [1].

$$i_p = (2.69 \times 10^5) n^{3/2} A D^{1/2} C_r \dot{v}^{1/2} \tag{1.8}$$

The peak separation for a reversible system is supposed to be independent of $\dot{v}$, but in practice ΔE_p can increase from the Nernstian value of $59/n$ mV at higher scan rates. At these higher scan rates the electron transfer kinetics can not keep up with the changing potential and therefore ΔE_p seems to increase. This is to say that no matter how fast the rate of e^- transfer, at high enough scan rates the CVs will always show quasi-reversible character. The life time of a chemical reaction with a rate constant k can be defined as

$t' = 1/k$ for a first order reaction. The time window or characteristic time for CV is defined as $\tau = RT/F\dot{v}$, based on the instrumentation and other experimental parameters. If $\tau >> t'$ then the electron transfer kinetics will lag behind the actual potential applied [1].

The previous discussions have all centred on systems that are known as Nernstian or reversible; these are systems that exhibit fast electron transfer kinetics. There are however other electrochemical systems where this is not the case. For these systems, that show intermediate rates of electron transfer, the shapes of the CVs and the other peak parameters are characteristic. Nicholson proposed a method to measure these intermediate reaction kinetics and it is now known as the *Method of Nicholson*. He defined a kinetic parameter ψ which can be used to calculate the effective rate constant k [2].

$$\psi = \frac{k}{\sqrt{\pi a D}} \tag{1.9}$$

$$a = \frac{nF\dot{v}}{RT}$$

He proposed that most systems operate in the region of $0.3 < \alpha < 0.7$ and that ψ is generally indpendent of α within these limits. Using the table presented by him it is possible to estimate ψ for the system from the ΔE_p and therefore calculate the rate constant and then ascertain the electron transfer kinetics [2]. The ranges proposed by Matsuda and Ayabe to classify electron transfer kinetics are shown below [1]. The significance and definition of these parameters are discussed in chapter 6.

$$\text{Reversible } \Lambda \geq 15;\ k_0 \geq 0.3\dot{v}^{1/2} \text{ cm/s}$$

$$\text{Quasi-reversible } 15 \geq \Lambda \geq 10^{-2(1+\alpha)};\ 0.3\dot{v}^{1/2} \geq k_0 \geq 2 \times 10^{-5}$$

$$\text{Irreversible } \Lambda \leq 10^{-2(1+\alpha)};\ k_0 \leq 2 \times 10^{-5}$$

The ability to draw information about the mass and electron transport properties, chemical reactions and information about the surfaces of the electrodes are the reasons that CV

is such a powerful analytical tool and why it is so widely used. This techniques does have a few limitations and some other special cases, these special cases are not relevant for the work described in this thesis, so have not been discussed. The main limitation of this techniques arises from the fact that the constant charging current from the C_d is continuously super imposed on the Faradaic processes. This means that it is not easy to differentiate between the two types of processes, when the C_{bulk} is less that 10^{-6} M. At higher scan rates this hindrance is exacerbated because the charging current increases as a function of $\dot{v}$, whereas I_p increases as a function of $\dot{v}^{1/2}$.

Electrodes that have a diameter small enough to change the diffusion profile to their surface are known as micro-electrodes. There is no consensus on the electrode diameter that constitutes a micro-electrode; but their diffusion profile is known to be semi-hemispherical as opposed to semi-infinite planar. This feature increases the flux at the surface of the electrode and also creates a steady state concentration gradient. It is this steady state concentration profile that gives CVs using micro-electrodes the characteristic shape of sampled voltammograms [1].

Both the above cases define the transport and electrical processes that occur when the species is in solution and freely diffusing. If the species is bound to the surface, then the operating parameters are different. Close contact with the electrode's surface means that bulk mass transport does not occur, as a result the electrochemistry takes place at the standard potentials and surface bound CVs are symmetric about the peaks [1].

Chronoamperometry

Chronoamperometry is the study of electrochemical reactions under conditions of a constant applied potential. In these experiments a potential step is applied at the electrode, usually this potential is chosen such that the current is mass transport limited; that is the potential is chosen in the plateau region of a sampled or steady state voltammogram. More positive oxidation potentials are necessary to study the reactions during chronoamperometry as

the uncertainty of e^- transfer kinetics can be removed. The currents recorded during a chronoamperometry experiment are represented in Figure 1.5.

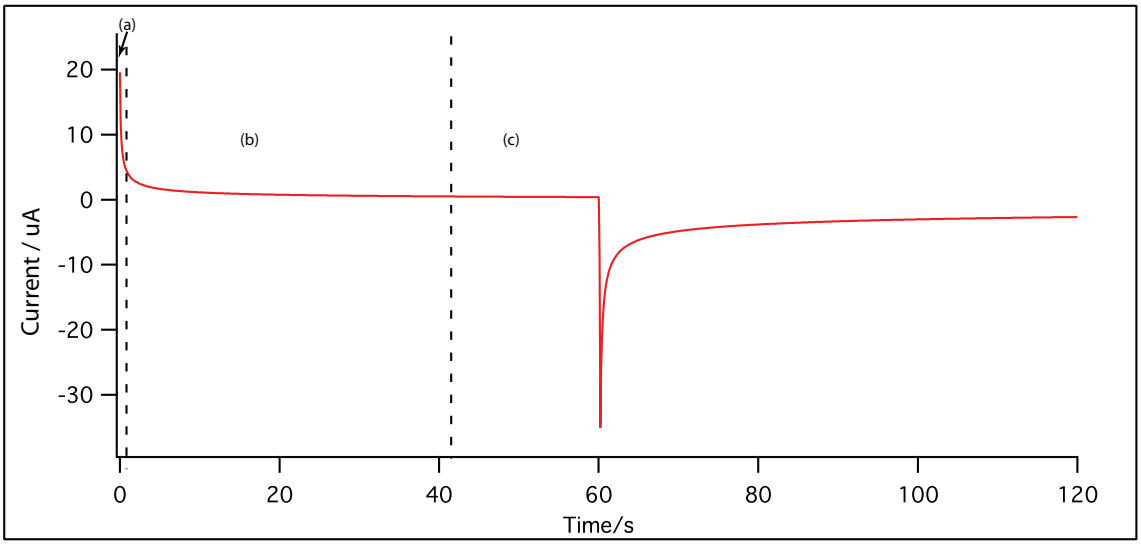


Figure 1.5: Schematic of a two–step chronoamperrogram; (a) is the charging current region, (b) is the Cottrell region and (c) is the region that shows i_{ss}.

This chronoamperogram shows a two potential step process, where the oxidation reaction is studied first and then at $t = 60$ s, the potential is reversed to reduce the species. The charging current can be seen for duration of time that it takes to reorganise the double layer. It is usually a higher current than the other phenomenon and a short time to dissipate; of the order of a few 100 μs. The next part of the amperrogram shows the Cottrell current which takes longer to dissipate; in most systems this has dissipated after a few seconds. The Cottrell current is dependant on time and is transient because it shows the development of the concentration profile, of the species to the surface of the electrode, the Cottrell relationship is shown in equation 1.10.

$$i(t) = \frac{nFAD^{1/2}C_r}{\pi^{1/2}t^{1/2}} \tag{1.10}$$

When the flux of the electroactive species has reached steady state to and from the surface of the electrode, the current achieves steady state and its response becomes independent of

time. To study the extents of chemical reactions, for example during a titration of H_2O_2 it is imperative to wait for the onset of i_{ss} so as to obtain correct and reproducible results. The areas under both the oxidation and reduction steps, in Figure 1.5, should be the same within experimental error and in the absence of any complicating chemical reactions.

Scanning Electrochemical Microscopy

It has been shown to be possible to use scanning probe techniques to study the redox behaviour of surfaces [3]. Scanning probe microscopy experiments are set up to measure differences in the redox behaviour of species and using this data information about the substrate can be inferred. This means that for SECM it is necessary to have an indication of the substrate being scanned, so that it is possible to set up the experiment with appropriate probe molecules.

The set up for this technique involves the use of a substrate and a probe as part of a single electrochemical cell, along with the requisite reference and counter electrodes. Both the substrate and the probe are controlled independently using a two channel potentiostat. The probe is attached to a piezo–resistive stage, which makes it possible to scan the surface of the substrate in the x–y direction (at constant z) or the diffusion layer of the substrate by varying the z [3].

The physical property that SECM relies on is the diffusion profile of an ultra micro electrode. The diffusion profile of the tip, has to be completely encased within the insulator that protects it; this hinders lateral diffusion from the bulk. This determines the R/G ratio of the tip; the R/G is the ratio of the tip diameter and the outer diameter of the insulator, as represented in Figure 1.6 (a). To meet the condition of the diffusion profile, there is a minimum R/G which is dependant on the electrode size; also the larger the R/G of the tip the bigger the collection area, therefore decreased spatial resolution [4]. The tip current in the bulk electrolyte is characteristic of a UME and is shown in equation 1.11, where a is

the radius of the electrode [5].

$$i_{T,\infty} = 4nFCDa \tag{1.11}$$

There are two main modes of operating a SECM; these are dictated by the condition of the substrate during the experiment.

- Feedback Mode
- Generation – Collection mode

In feedback mode the tip current (i_T) is monitored, as at fixed z, i_T is characteristic depending on whether the tip is passing over the insulating or conducting parts of the substrate. Changes in i_T occur due to different Faradaic processes that take place on the tips surface. The distance between the tip and the substrate is d and radius of the tip is a; as $d/a \rightarrow 0$ the i_T current is affected by the surface under it. As $d/a \rightarrow 0$ the diffusion of the redox species to the surface of the tip becomes hindered, therefore as it traverses an insulating substrate the $i_T \rightarrow 0$ as well [6]. When the same scan is made across a conducting substrate the redox species is regenerated at the conductor and the i_T increases as a result of an increased Faradaic response; these processes are both shown schematically in Figure 1.6 (b) and (c).

In generation collection mode the substrate is scanned by the tip, with a similar set up, except that in this case the Faradaic response of i_T, is a result of species generated at the substrate, this is schematically shown in Figure 1.6 (d). In most cases the substrate is held at a constant potential E_s and this accounts for the generation of redox species, that are picked up by the probe; although it is also possible to generate a redox species with the substrate at open circuit. In this case, a chemical reaction takes place at the surface which produces redox species through a chemical reaction [5].

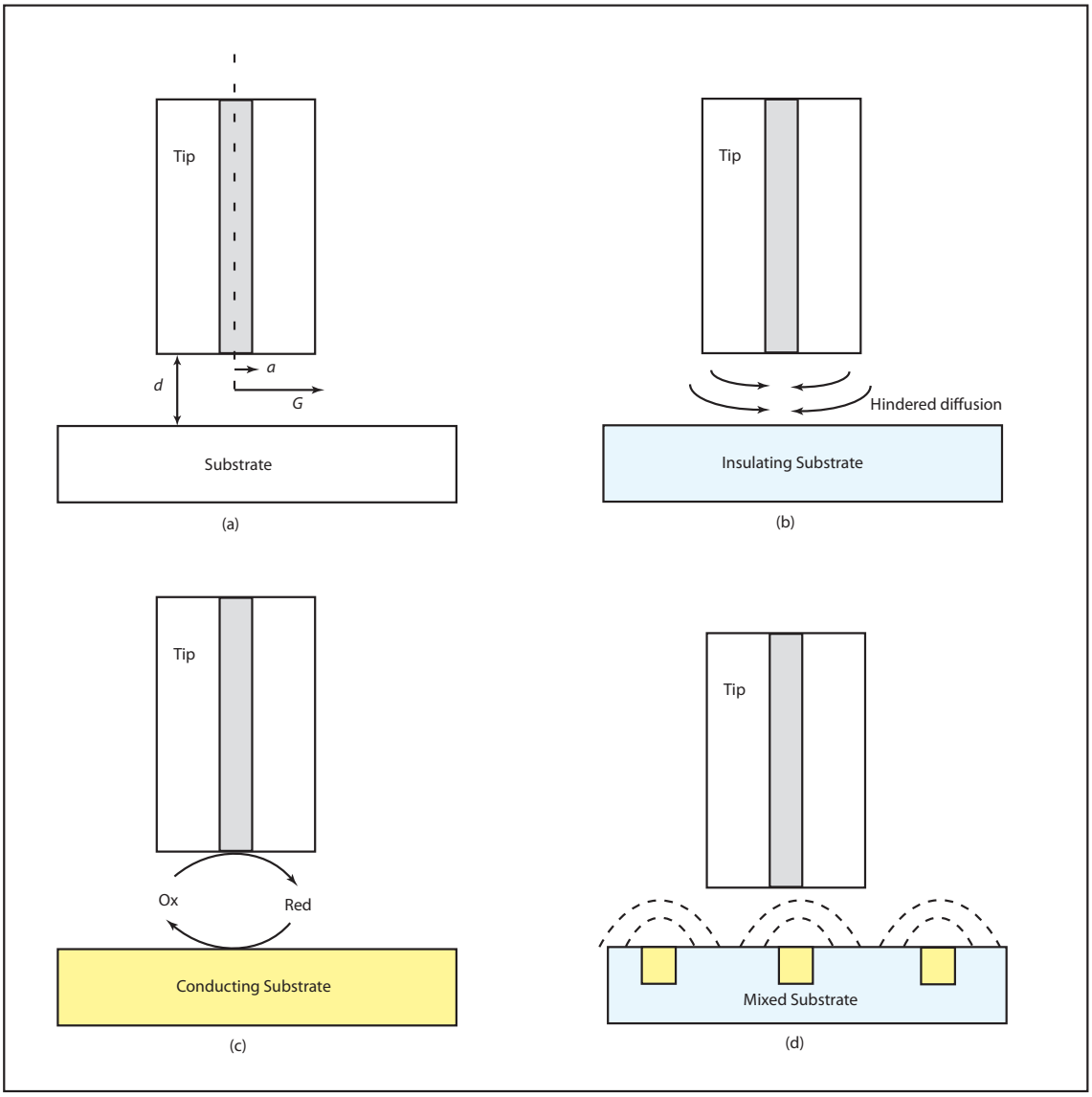


Figure 1.6: Schematic showing the features and modes of SECM, (a) The tip and substrate orientation and the important dimensions associated with these, (b) Feedback mode on an insulated substrate with hindered diffusion, (c) Feedback mode on a conductor with the regeneration of the oxidised species at the substrate, (d) Scanning in generation – collection mode on a substrate generating at the conductors.

1.2.3 Enzyme Theory

Enzymes are proteins with active centres that catalyse reactions for specific molecules. As these are naturally occurring molecules the operating conditions under which they provide maximum catalytic effects fall within a very narrow band. Enzymes operate most efficiently at certain temperatures and pH; mathematically there is a single maximum efficiency point for both operating temperature and pH. On either side of this value the efficiency of the enzyme decreases.

Another key feature of enzymes is that they act on very specific molecules. In general the active centres of enzymes are only able to act on molecules with the correct structure and orientation, there are some exceptions to this rule. This is one of the biggest advantages of using enzymes to facilitate catalysis for analytical purposes. The noise and disturbances that are part of the metrics logged tend to be inherent to the transducer chosen. Although, it is possible to mitigate some of the noise introduced by the transducer.

Enzymes are classified based on the recommendations of the nomenclature committees of the ICBMB and IUPAC method of classification. The nomenclature follows a 4 level hierarchy with the first category defining the types of reactions catalysed; e.g. oxidoreductases, transferases, hydrolases. The second tier classification defines the functional groups whose reaction the enzyme catalyses. The final two numbers narrow the enzyme down to the molecule it acts on and/or the source of the enzyme [7]. The classification number for glucose oxidase from *Asper. Niger* is E.C.1.1.3.4; this is because it belongs to the oxidoreductase class of enzymes, it acts on the CH–OH group and it uses O_2 as the electron acceptor (co-factor).

Each of the dimers of glucose oxidase has one active centre within and the active centre is FAD. The structure of the active centre is represented in Figure 1.7. The active structure consists of three parts, riboflavin (vitamin B2), adenine and the phosphodiester linking them [8].

The FAD active centre in glucose oxidase is very specific to and oxidises β D-glucose

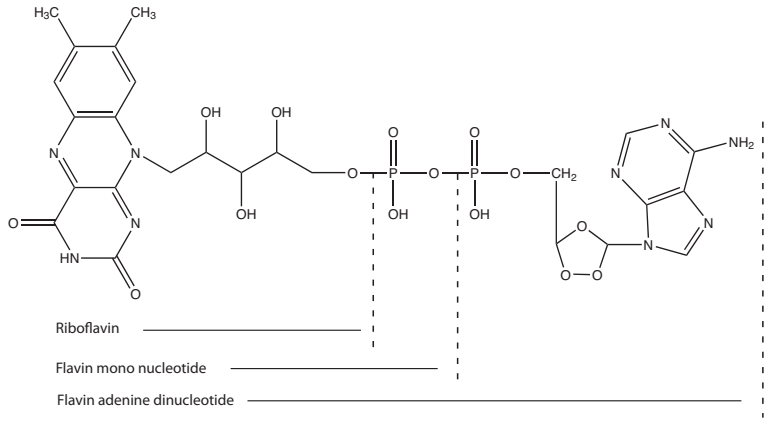


Figure 1.7: Schematic showing the structure of the glucose oxidase active centre. [8]

according to the scheme in equation 1.12. In fact because glucose oxidase only recognises the β anomer of D–glucose, this means that all standard glucose solutions have to be allowed to mutarotate for 24 hours prior to use. When the solution has been left to mutarotate for 24 hours it can be assumed that the two anomers are in equilibrium. During this reaction the glucose oxidase, itself, gets reduced and the reduction is reversed with the use of molecular O_2 as the final electron acceptor. The temperature dependence of the activity of glucose oxidase is described by Gibson et. al. and the pH dependence of the same mechanism is described by Weibel and Bright [9, 10].

$$\begin{aligned} D-glucose + FAD &\xrightarrow{GOx} D-gluconolactone + FADH_2 \\ FADH_2 + O_2 &\longrightarrow FAD + H_2O_2 \end{aligned} \tag{1.12}$$

1.2.4 Biosensor Theory

Devices that use a biological molecule as the analyte recognition element are termed biosensors. The analyte specific film undergoes a chemical and/or biological change, which is then picked up by a compatible transducer and recorded as a signal, this path is schematically represented in Figure 1.8.

In Figure 1.8 there are 2 different analytes, only one of these is specific to the recognition

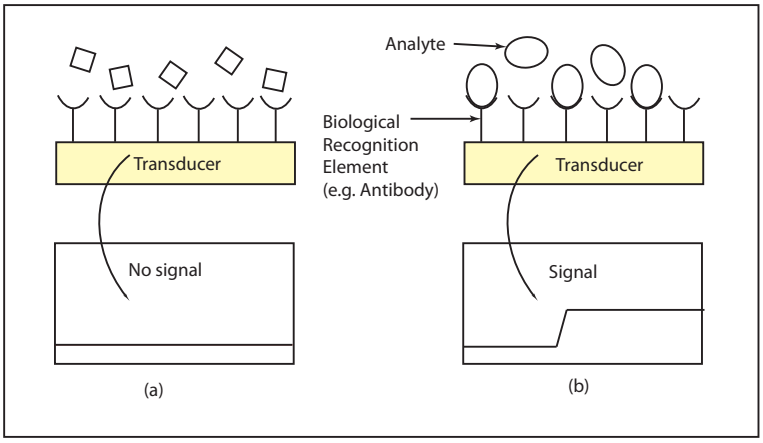


Figure 1.8: Schematic showing the principle of operation for a biosensor: (a) the analyte in solution is not specific, therfore no signal is produced; (b) the analyte in solution is specific to the recognition element, so a signal is produced and recorded.

element of the film; it is only this analyte, (b), that produces a signal which is recorded by the data acquisition module. Different types of biological molecules can be incorporated into biosensors; the use of enzymes, DNA, aptamers and antibodies has been reported [11, 12]. The choice of recognition element is dependant on the analyte. That is, there has to be a known and established interaction between the two, and more importantly the recognition element has to show a high specificity to the analyte, otherwise a non specific signal will always be super imposed onto the true signal.

Once the recognition element has been identified a suitable transducer has to be chosen as well; the role of the transducer is the conversion of the biological or chemical signal, produced by the presence or removal of the analyte, to a physical property that can be measured. The choice of transducer is dictated by the recognition element being used; families of biological molecules can be used with certain kinds of transducers. Thermal, optical, mechanical, acoustic and electrochemical transduction methods are widely reported in literature as part of biosensing devices [13, 14, 15, 16, 11]. One important point of note here, is that although in most cases only some methods of signal transduction are compatible with families of analyte specific biological molecules it is always possible to

engineer biological molecules to make them compatible with other transducers. If native molecules are available, their use is preferred, because it is more beneficial to change the type of transducer, as opposed to re-engineer a biological molecule. In some cases this is not possible, therefore there are a number of reports in literature that describe the use of engineered molecules [12, 17, 18, 19].

The next stage in the development of a biosensor is the attachment of the biological molecule to the surface of, or in contact with the transducer. This is a critical stage of the development process, because the dynamic range of the sensor is directly linked to the effectiveness of the surface loading, but mass transport of the analyte should not be hindered as this limitss the flux of the analyte at the film's surface. There are three main categories of surface attachment:

- Entrapment behind a membrane: in this case the recognition element is kept in contact with the surface of the transducer behind a perm-selective membrane that does not allow the molecule to cross, because of size and/or charge exclusion. One such example is glucose oxidase entrapped behind a cellulose acetate membrane [20].

- Encapsulation within a polymer: here the recognition element is held in place within a matrix, consisting of itself and the polymer. This is a versatile technique and is widely used because of its ease of fabrication; although charge and steric hindrances are possible problems that can lead to poor reproducibility of these sensors. The electropolymerisation of poly(DAB) in the presence of glucose oxidase, as described by Malitesta et. al. is an example of this method of surface immobilisation [21].

- Covalent attachment to the surface: chemical bonds are used to hold the molecules in place on the surface of the transducer. This mode of surface immobilisation requires more attention as often the chemistry by which this attachment is made can be complicated; although sensors produced using these techniques give maximum reproducibility in the sensors' responses. Also, the distribution on the surface is the

most reliable in this case. There are two popular methods of covalent attachment, firstly alkane thiols are used to form self assembled monolayers (SAM) on gold surfaces and then appropriate chemical treatments are performed for the immobilisation procedure. One such example is reported by Steel et. al. where they have quantified the amount of DNA immobilised on gold substrates [22]. The second popular method is the use of silanisation to prepare the substrate and then attach the molecules in a manner similar to that for SAM. Suri and Mishra report using silanisation to activate piezoelectric crystal surfaces to attach proteins to make an immunosensor [15].

The choice of analyte dictates the development of a biosensor, as there are numerous combinations of transducers and surface immobilisation that can be used to design suitable devices. During the process of development there are two important operating characteristics, that have to be maximised:

1. Sensitivity: this is the measured change in signal that is achieved when there is a unit change in the analyte concentration of the sample.

2. Linear range: the concentration of analyte that the device can measure before any further increase in its concentration does not result in a similar change in the signal.

Enzyme Sensors

Biosensors are widely reported in the literature and it is possible to use an array of biological moieties coupled with the correct transducers to design sensors that serve the required purposes.

In particular enzyme sensors that incorporate an oxidoreductase in the analyte specific layer, it is the transfer of e^- that is studied. This transfer of electrons is conducted by the use of a co-factor and it is at this stage where the transducer measures the e^- transfer activity. It is not easy to monitor the primary e^- transfer step because of the inability to get to the active centre through the glycoprotein shell, although there have been reports of

the direct electrochemistry of glucose oxidase [23].

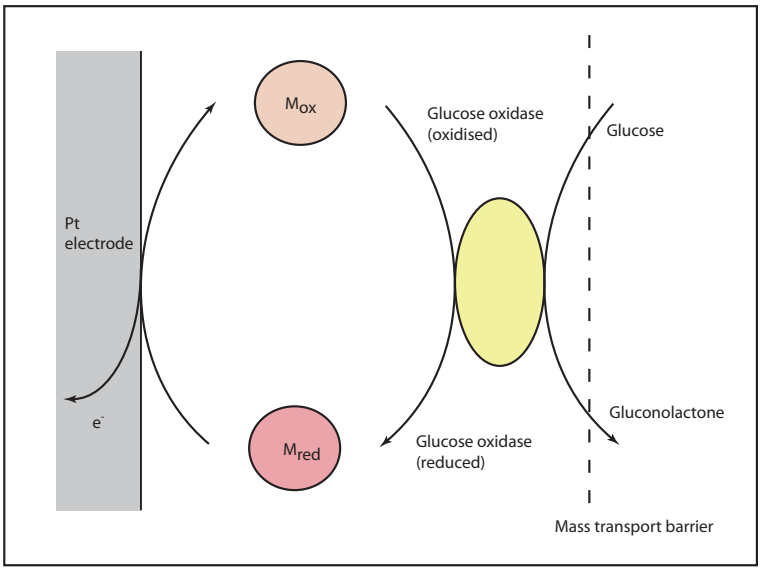


Figure 1.9: Schematic showing the e^- transfer path for a glucose sensor. The sensor is made using glucose oxidase on a platinum electrode with the mediator in solution.

In the case of unmediated glucose sensors the FAD active centre is re-oxidised with molecular O_2 available in solution, the product of this oxidation step is H_2O_2, which is then oxidised at the electrode's surface, as shown in equation 1.12. Using unmediated sensors is advantageous because there is no need to incorporate any other reagent or chemical in the preparation of the sensor, which makes them easier to manufacture although their linear range will be limited by the availability of the co-substrate required. The biggest disadvantage with using unmediated devices is the need to operate at more positive potentials; this increase in operating potential increases the risk of electrochemical interference, from the oxidation of other electro-active species in solution.

Cass et. al. first reported the use of a ferrocene mediated glucose sensor, where this was the oxidant for the regeneration of the enzyme and therefore the device was measuring glucose content by studying the oxidation current of ferrocene [24]. Such devices are known as mediated sensors and recent advances and trends in this field are discussed in more detail in section 1.3.2.

1.3 Literature Review

1.3.1 Iridium oxide devices

The use of metal–metal oxide (MMO) electrodes to sense pH has been widely reported; the primary metal used for this purpose was and to some extent still is antimony (Sb). The earliest found reference for the use of Sb–SbO_3 films as pH sensitive devices is by Roberts and Wheeler [25]. Although the first report of iridium oxide as pH sensitive films was not till 1942, by Perley et. al. [26]. In their patent application they report the formation of the iridium films by electroplating, evaporation and sputtering. Their methods of manufacture were restricted by the technologies that were available to them. The iridium oxide films were sensitive for the entire range of pH and gave and open circuit potential of +700 mV at pH 0 and -100 mV at pH 14; this implies a Nernstian range if a linear response is assumed [26].

Theory of pH sensing using iridium oxide films

There are different modes of sensing pH in a solution. The most widely used and commercially available technique is the use of glass electrodes with an integrated reference electrode. The internal solution of the electrode is at a fixed pH and the changes in the proton concentration of the bulk are recorded as changes in the open circuit potential of the glass electrode, according to the Nernst equation, equation 1.3. These devices are reliable but, their biggest disadvantage is the amount of sample that is required to make measurements.

The use of metal–metal oxide layers is one way to miniaturise pH sensors. As metal–metal oxide sensors do not require the use of a liquid junction they are smaller in size and modern external reference electrodes are also sufficiently small to use in small volume analysis. Metal–metal oxide sensors are also used in the open circuit potential mode of operation. Changes in the bulk pH are monitored by studying the changing potential due to chemical changes in the metal oxide film. The development and overview of metal metal

oxide electrodes is given in section 1.3.1.

Amorphous iridium(IV) oxide gets reduced to iridium(II) and iridium(III) oxide in the presence of H^+ ions, as shown in equation 1.13 [27]. This chemical reaction will result in a Nernstian response from the sensors of 59 mV decade^{-1}.

$$\begin{aligned} IrO_2 + H^+ + e^- &\rightleftharpoons IrO \cdot OH \\ 2IrO_2 + 2H^+ + 2e^- &\rightleftharpoons Ir_2O_3 + 2H_2O \end{aligned} \tag{1.13}$$

The use of hydrated iridium oxide alters the pathway by which the Iridium(IV) oxide is reduced to Iridium(II) oxide, in the presence of protons,as shown in equation 1.14 [27]. This shows us that the stoichiometric ratio of the uptake of protons and e^- is 1.5; it is this ratio that results in the super–Nernstian response of the sensors.

$$2[IrO_2(OH)_2 \cdot 2H_2O]^{2-} + 3H^+ + 2e^- \rightleftharpoons [Ir_2O_3(OH)_3 \cdot 3H_2O]^{3-} + 3H_2O \tag{1.14}$$

The hydrated film can thus theoretically provide a response that can be 1.5 times of a Nernstian response. This is rarely the case because of the actual composition of the deposited film. Even with this practical limitation hydrated iridium oxide films do produce a super–Nernstian response and this increased sensitivity along with the smaller form of the sensor makes these devices beneficial. For the case of iridium oxide electrodes the Nernst equation in terms of pH is shown in equation 1.15 [28].

$$E = E^0 - 2.303\frac{RT}{F}pH \tag{1.15}$$

During the synthesis of the precipitation solution, iridium chloride is converted to a complex of iridium oxalate, in a basic solution. This synthesis is performed because both iridium chloride and iridium oxide are sparingly soluble in aqueous solutions and at higher pH these tend to precipitate. Whereas iridium oxalate has been reported to be more stable in solution [29]. The presence of H_2O_2 in the solution is probably to increase the stability

of the solution, similar to a finding reported by Kruszyna et. al. [30]. They report that the use of excessive Ce(IV) in the solution increased the stability of the iridium oxalate and the presence of H_2O_2 in Yamanaka's protocol would provide a similar stability.

In the recent past the use of iridium oxide sensors to monitor the pH of samples has been widely reported; on a variety of substrates and using each of the techniques described by Perley et. al. (with some modifications) [26]. O'Hare et. al. and Hitchman and Ramanathan report the formation of iridium oxide films on iridium substrates using anodic and thermal deposition [28, 31]. Yamanka reported the formation of iridium oxide films using galvanoststic deposition, for their electrochromic properties [29]. Marzouk reported the use of iridium oxide films on Ti substrates using the protocol reported by Yamanaka; the use of Ti decreased the cost of the sensors [32].

The noble metals have found the most wide spread use as substrates for the deposition of iridium oxide films probably due to their ease of use and the ability to prepare them in various shapes, forms and as part of other devices. Galvanostatic deposition on platinum substrates has been reported by Marzouk et. al. and Ges et. al. as parts of microfluidic based devices, wires and planar substrates [33, 27, 34]. Ges et. al. have deposited iridium oxide films on substrates smaller than 500 μm^2; these are reported to display super-nernstian behaviour and excellent long term stability. The measurement volume required for these cells is 25 nL [32]. The ability to do small volume measurements is the biggest advantage of iridium oxide devices, over conventional glass electrodes, although some small sample glass probes are now commercially available.

Due to the many advantages of glass probes and the stability of iridium oxide pH sensors, their use has been reported widely and for numerous applications. Smiechowski and Lvovich have reported the use of iridium oxide films to monitor the pH in non-aqueous media [35]. These devices exhibit a slightly worse correlation in diesel, than for aqueous media, but this is to be expected, due to weaker dissociation in organic liquids. Physiological applications of iridium oxide have been popular as well, although O'Hare et. al. report that the presence

of physiological concentrations of albumin causes irreversible deterioration of the films, as the protein promotes the corrosion of the film [28]. A widely used method for the protection of iridium oxide films in physiological media is to coat them using nafion [28, 32, 27]. As reported by O'Hare et. al. the cyclic voltammograms of iridium oxide films thus protected and then dipped in physiological albumin showed no differences to fresh sensors, whereas unprotected devices showed no characteristic features at potentials more positive than 800 mV.

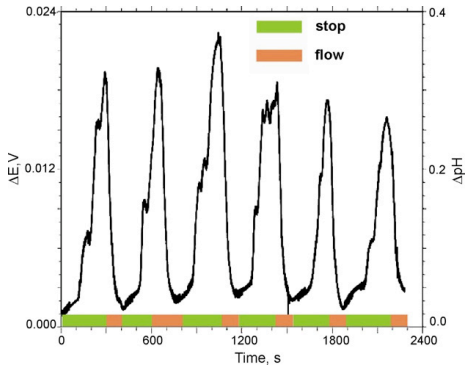


Figure 1.10: Rate of acidification of 3T3 cells as shown by Ges et. al. [34].

It is also possible to make devices that are matched so well to each other, that they can be employed in differential sensing mode, as reported by Ges et. al. [34]. Using a stop flow configuration in a perfused culture vessel of nI cells, they were able to accurately measure the acidification rate of the cells, their results are shown in Figure 1.10. The reported acidification rate of the cells is 0.19 pH min^{-1} [34]. The ability to use differential sensing between fresh media and extra-cellular culture media on the same device adds extra power to the use of iridium oxide electrodes. As their applications can extend to large scale *in-vitro* monitoring, monitoring the onset of hypoxia in tissue and other anaerobic growth conditions that result in biological levels of pH variation.

1.3.2 Electrochemical Enzyme Sensors

In the past enzyme sensors have seen progress in research and development and also commercial success. This has been led primarily by the need for blood glucose monitoring devices, so as to allow better glycemic control for patients suffering from *diabetes*.

Leland C Clark is widely considered as the 'father of biosensors' having developed an electrode that was able to sense the concentration of dissolved oxygen, using a polarised platinum plate, now known as the Clark type electrode. The electrode was made by dipping a Pt electrode and a AgCl wire in to a KCl solution, protected from the bulk electrolyte using a permselective Teflon membrane. When the platinum electrode was polarised at -600 mV molecular oxygen was reduced as shown by the schemes in equations 1.16. The e^- balance was achieved at the anode, where the silver was oxidised to AgCl, equation 1.17.

$$\begin{aligned} O_2 + 2H^+ + 2e^- &\longrightarrow H_2O_2 \\ O_2 + 4H^+ + 4e^- &\longrightarrow 2H_2O \end{aligned} \tag{1.16}$$

$$Ag + Cl^- \longrightarrow AgCl + e^- \tag{1.17}$$

In 1962, Clark and Lyons proposed a development of this architecture and coined the term enzyme electrode. Replacing the Teflon membrane for a sandwich dialysis membrane with glucose oxidase in between, they were able to sense glucose concentrations by reversing the potential to +600 mV [20]. It is reported that the system was later developed and the first fully functional sensor is attributed to Hicks and Updike [8].

From here on the development of biosensors is considered to have progressed through three generations.

- First generation sensors relied on the principles of the Clark electrode and development concentrated on the ability to increase the enzyme loading and thus improve performance. Yellow Spring Labs released the first commercial glucose analyser, which was a bench top instrument, relying on the same principles [36]. This is still consid-

ered to be the most accurate method to analyse the concentration of glucose in off–line sample analysis.

- Second generation sensors replaced molecular O_2 as the electron acceptor for the enzyme. The use of synthetic molecules allowed the e^- transfer between the enzyme and the electrode to take place at lower oxidising potentials. This was advantageous, as electrochemical interference decreased along with more negative oxidation potentials. These redox mediators were freely diffusing in solution.

- The third generation of biosensors again employed synthetic redox mediators, but these were surface bound. This mode of operation improved the e^- transfer ability of the system and improved integration and performance. These types of sensors are not discussed in any more detail here, but will be dealt with separately in section 1.3.3.

- All the latest research in the field of biosensors consists of some or all of the previous principles using the properties of new materials that have become available with the advent of time. In this section I will primarily deal with these types of sensors.

First generation sensors tend to be the easiest to develop, with the key parameter being the extent of the enzyme loading that can be achieved. This and the availability of molecular oxygen in solution play a key role in the final operating characteristics of these devices. In the recent past devices using this architecture are fabricated either by:

1. Attaching functional groups to the surface of the electrode and then attaching groups that are complimentary to the enzyme at the other end; that is through the use of carbodiimide chemistry to make covalent bonds. One such example is reported by Masson et. al. where they have used alkane thiol chemistry to create a SAM on gold microelectrodes and then attached glucose oxidase to the SAM [37].

2. The encapsulation of the enzyme within polymer matrices. This has seen a lot of interest, as the ability to electrochemically encapsulate the enzyme allows the freedom

for miniaturisation. Both conducting and non conducting polymers can be used for the purpose of enzyme encapsulation and both their uses have been reported [38, 39, 40].

Conducting polymers gain this trait due to an overlap in their molecular orbitals and half filled shells that allow the free movement of electrons. Examples of conducting polymers are poly(pyrrole) poly(aniline), poly(acetylene) and poly(thionine).

Conducting polymers should improve the devices performance, especially when used in conjunction with oxidoreductases where the transfer of electrons is important, as this will improve the e^- transfer process through the film however conducting polymers suffer from the lack of reproducibility during the fabrication of the film. The only exception to this case is the formation of the film using chronocoulometery. In all other case the thickness and structure of the film will vary, as there are no mechanisms to control them.

Due to their physical properties films of non-conducting polymers are self limiting in nature; when fabricated electrochemically. The initiation of the polymerisation is reliant on the activation energy supplied by the electrode, but once the film has reached a certain thickness, this is no longer available to the monomers in bulk solution.

A well studied insulating polymer is poly(1,2-diaminobenzene) or poly(DAB); Sasso et. al. reported the use of this polymer to make a glucose sensor coupled with flow injection analysis (FIA) [40]. Platinised vitreous carbon electrodes were used as the substrate onto which the enzyme was covalently bound with glutaraldehyde. Then poly(DAB) was polymerised on the surface, primarily to act as a perm-selective barrier [40]. This structure of the film meant that the poly(DAB) was not encapsulating the enzyme, but merely acting as a substrate for the immobilisation. Their results strongly indicate that poly(DAB) serves its purpose as a perm-selctive barrier to common electro-active interference and the apparent Michaelis-Menten characteristics of the devices were promising as well.

The first report of an enzyme electrode made, solely, using poly(DAB) is by Malitesta et. al. They do not use any pre-adsorption during the fabrication of the films, but films made using a constant potential and CV showed consistent performances. The K'_m and

i_{max} are 14.2 mM and 12.8 μA, respectively [21]. This was already an improvement on the architecture proposed by Sasso et. al. [40]. Again the films show excellent selectivity to glucose, as the electrochemistry of ascorbic acid was significantly suppressed by the poly(DAB) film [21].

More recently Reyes and co-workers have combined the advantages of platinum black deposition to those of poly(DAB) as a perm-selective film. With current densities of $192 \pm 48\mu$A cm^{-2}mM^{-1} and a linear range up to 25 mM, this architecture holds some promise [41]. It is very difficult to reproduce large numbers of platinised films and it seems that the reproducibility of the sensors in this report, suffers as a result; but the better operating characteristics outweigh these manufacturing inconsistencies, in such a research context. One interesting point the authors make is the relationship between surface roughness and the polymerisation charge, it was noticed that both charge and surface roughness increased, until a certain point when the charges levelled off [41]. The authors suggest that the cause for this is because an increased roughness means that the monomer diffusion through the platinum deposits is slower, that is a smaller D_{eff} to the active centres for polymerisation [41]. It is possible that this change could seen because of a change in the diffusion profile; increasing the surfaces roughness beyond a certain point would mean that the diffusion profile will tend to semi-infinite planar. This change will decrease the flux of the monomer at the electrode surface.

Yang et al. have reported a lactate sensor using the poly(DAB) architecture, by adding a second semi-permeable membrane, the life of this device was increased to 7 day continuous operation and it showed a linear range of at least 15 mM [42]. An enzyme containing poly(DAB) film has been further characterised by Chung et. al. using an EQCM. Their analysis suggests that in this architecture the majority of the enzyme sits on the outside of the membrane [43]. This would agree with the model proposed first by Sasso et. al. [40].

Another novel method of electrodeposition is described by Kurzawa et. al., using an aqueous colloid of a mixture of polymers, sold under the commercial name Resydrol [44].

The colloid is sensitive to pH and is stable in the near neutral region. It is this property that they have exploited to perform electrodeposition. Using a pulse technique, the pH at the surface of the electrode is decreased by electrolysis for a short period and then it is allowed to re-equilibriate with the bulk [44]. This configuration shows a linear range up to and a current density of 14.59 mA cm^{-2} M^{-1}. Also, they have reported excellent stability over 5000 samples in a flow injection system and the ability to deposit these films on different electrode configurations [44].

Also, of a great deal of interest is the structure of this polymer film; as the colloid is a mixture of the copolymers of acrylates and because of the method of deposition [45]. In their paper the authors show a CV of an as deposited and a thermally cured film in $Ru(NH_3)_6^{3+}$ and the thermally cured film shows a damped I_p. The peak current for the as deposited film is ca. 6 nA and than for the cured film is ca. 3 nA [44]. In my opinion a peak current ca. 3 nA at a 1 mm electrode in a 5 mM solution is very small compared to a bare electrode; but they claim good permeability; but the real point to note is the shape of both the CVs, neither of which displays steady state character. What these CVs show is that the film is labile and permeable and dehydrolysing it does not significantly change its character, which are good characteristics for enzyme biosensors.

Bartlett et. al. reported the use of phenol and its derivatives as other insulating polymers that can be used to fabricate enzyme films [46]. The monomers that they used were phenol, pyrogallol, 3-nitrophenol, 4-hydroxybenzenesulfonic acid and bromophenol blue. Of these they found the poly(phenol) films to give the most sensitive devices [46]. This was probably because these formed the most insulating films and thus had maximum coverage.

The chemical mechanism for the electrochemical polymerisation of phenol was shown by Gatrell and Kirk [47]. In Figure 1.11 we can see that it is a free radical reaction that is initiated by the electrochemical formation of the phenoxy radical. It was proposed, by the authors, that at low concentrations of phenol the oxidation proceeds along the path of the formation of soluble products such as, the quinones. They also proposed that just prior to

the formation of a passivating film there was a critical mass that built up just in front of the electrode's surface. There after further polymerisation took place via electron tunnelling, until the tunelling distance is too great, at this point the film is fully passivated [47]. A further study of this reaction mechanism has been conducted by Arslan et. al. and they suggested that the polymerisation of phenol exhibited a pH and temperature dependence [48].

A further investigation of these films by Bartlett and Caruana was conducted, on this occasion they deposited the films on microelectrodes [49]. The reproducibility of the devices was good and they showed excellent permselectivity to uric acid. The exclusion of ascorbic acid and acetoamidophenol was not as distinct, but the responses were still some what suppressed. They have also incorporated amino acid oxidase in the film and it responded to changes in the concentration of D-alanine [49].

Another phenol derivative that has been reported is amino-phenol; although there is no improvement in the operating characeristics as reported by Eddy et. al. [50]. Nakabayashi et. al. used the selective permeability properties of poly(phenol) to make a ferrocene mediated carbon paste electrode [51].

In their original report, Bartlett and co workers had used the charge under the oxidation peak to estimate the thickness of the poly(phenol) and glucose oxidase film to be about 38 nm [46]. This was roughly four times that suggested by Mallitesta et. al. for poly(DAB); but it was only an estimate. Arrigan and Bartlett, then used scanning force microscopy to study the surface of the enzyme films in more detail, using a highly ordered pyroltic graphite (HOPG) substrate, so as to minimise any surface topologies [52].Their scans of the substrate with a poly(phenol) film showed no surface features with surface roughness of 1.0 nm. The surface roughness of the film that incorporated the enzyme was calculated as 1.9 nm; the film thickness as reported by Arrigan and Bartlett are shown in Table 1.1. The film thickness were calculated by nanodozing them; that is by applying force from the scanning tip and scratching off a portion of the film.

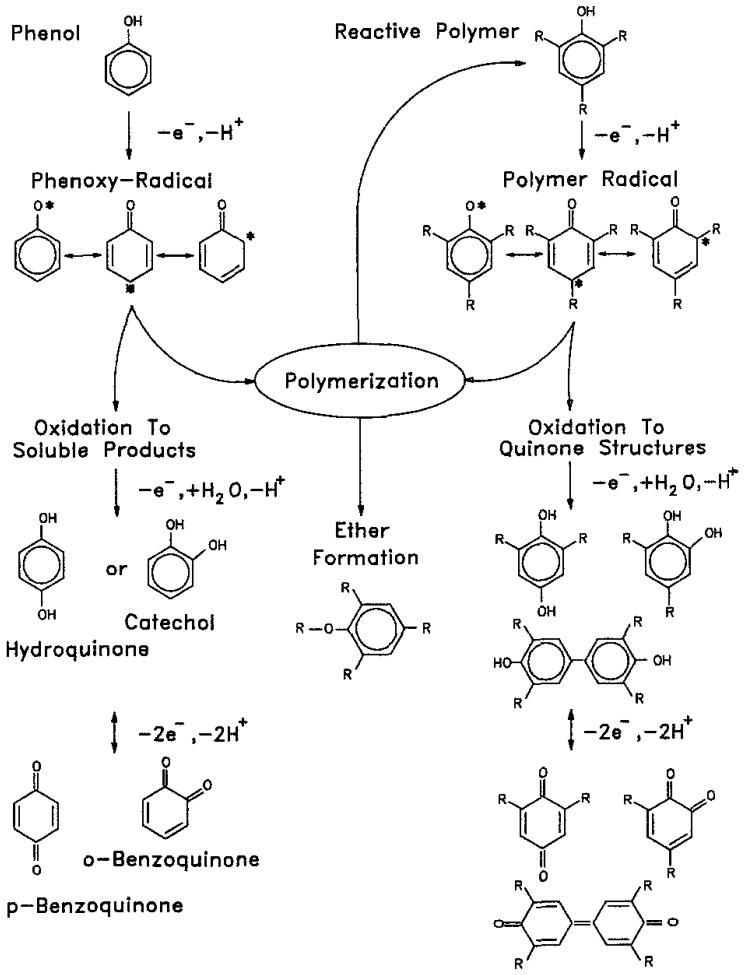


Figure 1.11: Mechanism of the polymerisation of phenol; R represents either a hydrogen atom or a monomer, as reported by Gattrell and Kirk [47].

Film details		Measurement / nm
poly(phenol) only	mean thickness	3.0 ± 1.2
poly(phenol) + GOx	mean thickness	7.4 ± 0.8
	maximum thickness	9.7 ± 1.7
	minimum thickness	6.4 ± 0.9

Table 1.1: Details of poly(phenol) and glucose oxidase film thickness on HOPG as reported by Arrigan and Bartlett [52].

To conclude the authors suggested that the structure of the film was continuous and free of any pinholes [52]. This is contradictory to what was reported by Wang et. al. in 1994 [17]. The paper by Wang et. al. described the interaction that proteins have with different surfaces. One of the examples they used was glucose oxidase in a poly(phenol) film. Optical microscopy, both reflective and fluorescent were the tools used by the authors. The film was constructed in a similar manner to Arrigan and Bartlett; but the proteins were fluorescently labelled. In addition to this the fluorescence of the cyano-ditolyltetrazolium chloride (CTC) and fluorescent red formazan (CTF) showed the porosity of the film. What the author's imaging results showed was that the enzyme tended to agglomerate on the surface in 'clumps' and the phenol polymerised around these clumps. Because of this there were regions of the surface that showed porosity to large synthetic molecules like (CTC) [17].

Both these reports of the structure of the enzyme and polymer film are interesting, as they show very different characteristics. With these two reports it would seem that the enzyme interacts differently to a platinum surface and a carbon surface. Neither of the two sets of authors report any pre-treatment of the surfaces, so no inferences can be made about them. Also, there was no electrochemical data from Wang et. al. that can be used to compare the enzymatic activity of the two films; which might have indicated the nature of the two different interactions.

A couple of recent reviews written by Wang and Merkoci et. al. describe the use

of carbon nano tubes (CNT) as parts of analytical devices [53, 54]. The reviews contain many recent reports of enzyme sensors, amongst others, being made using CNTs. The use of the direct electrochemistry of glucose oxidase is reported, along with a host of other architectures [53]. Merkoci et. al. are more descriptive in their review and elucidate the use of CNTs as pastes and composites and as parts of modified electrodes [54]. From these reviews and the number of recent publications it is very evident that the use of new materials such as CNT accord advantageous characteristics to enzyme electrodes. What follows is a brief summary of the types of architecture that incorporate CNTs and the properties of such devices. This is by no means an exhaustive review, as the number of papers is extremely large, but an attempt has been made to cover as many different aspects of these novel sensors as possible.

Lin et. al. describe the fabrication of CNT 'ensembles' onto which they attach glucose oxidase, using carbodiimide chemistry. The ensembles themselves are made by setting CNTs in a passivating epoxy, with a small portion of exposed CNT on the surface and a schematic from their paper is shown in Figure 1.12. These electrodes show a characteristic steady state CV, for ferrocyanide, when no enzyme had been attached. Then using the reduction of H_2O_2, they were able to sense changes in the glucose concentration at -200 mV with a linear range of 20 mM [55].

Wang and Musameh incorporated CNTs and enzyme in a poly(pyrrole) film. This sensor showed a linear range up to 50 mM glucose and a sensitivity of 2.33 nA/mM [56]. These sensors were still operated at +900 mV, so it was unlikely that the CNTs added any catalytic properties for the oxidation of H_2O_2 and it is more likely that the increased surface area and the affinity between the enzyme and CNTs improved the performance of the device, by incorporating more enzyme and increasing the area available for peroxide oxidation. Another report for a similar structure was presented by Shirsat and co-workers; the substrate they used was platinised polyvinylidene fluoride, with a layer-by-layer structure of poly(pyrrole), CNT and enzyme [57]. Again the operating potential for these devices was +700 mV, so

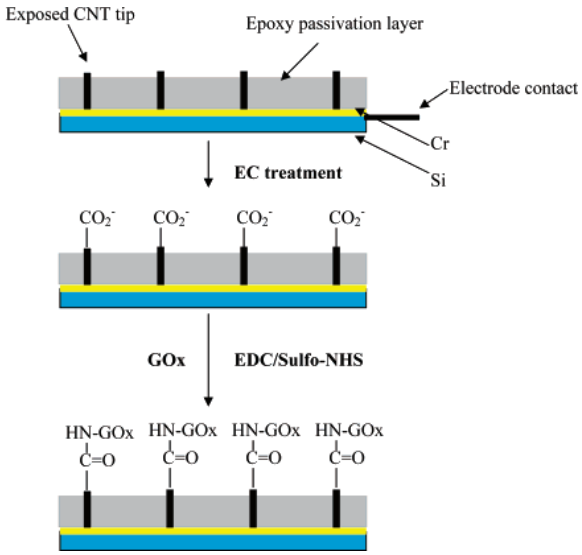


Figure 1.12: Schematic of CNT 'ensemles' from Lin et. al. [55].

the CNT are most likely not catalysing the oxidation of H_2O_2. This architecture can even be used to sense the reduction of H_2O_2, as reported by Zhu et. al. and Wang and Musameh [58, 59].

Another reported method that benefits from the affinity between glucose oxidase and CNTs is their incorporation in plasma polymerised films. Muguruma et. al. report that the plasma treatment increased the performance of the sensors 4-16 fold as compared to either just the CNTs or plasma treatment [60]. Again as the sensors were polarised at a high oxidising potential, the plasma treatment of the CNTs must increase their affinity, by altering the surface charge, with the enzyme, which resulted in the improved performance.

The use of MWCNTs coated with a cationic polymer, poly(diallylmethylammonium chloride), is reported to catalyse the oxidation of H_2O_2, in fact the authors report that oxidation currents for peroxide are measured at +100 mV (vs. Ag|AgCl) [61]. The apparent Michaelis-Menten constants for this device are K_M =10.12 mM and I_{max} =32,25 μA, with a reproducibility of 5% and a stability of ca. 15 days, when stored at 4 °C [61]. The authors claim that the CNTs are catalytically active for H_2O_2 because of increased electrostatic

interactions between them and the enzyme, although they present no evidence for this supposition.

Reports from Joshi et. al. and Antiochia and Gorton combine the properties of CNTs and osmium redox polymers [62, 63]. Joshi et. al. cast the polymer and enzyme solution on a glassy carbon electrode that had a CNT film dried on its surface. They also incubated the CNTs in the casting solution and then cured the mixture in one step [62]. The performance of the latter preparation was better and so were the CVs of the complex film, both of which are indicative of better e^- transport mechanisms. The CNTs can facilitate better kinetics, because of their size and structure and also because of their own electron distribution. The devices made by Joshi et. al. were linear till ca. 20 mM and current gave densities >1 mA cm^{-2} [62].

The reported use of platinum nano-particles in enzyme films also tends to rely on the increased surface area of the electrode and greater number of active sites that become available, especially in the case of H_2O_2 sensing. Although no catalytic advantage is drawn from the use of these novel materials, they are still useful in fabricating electrochemical sensors, as they are able increase the surface area of the electrode by orders of magnitude, without there being an increase in its physical size. Also with structures as described by Lin et. al. it is possible to increase the flux to the enzyme sites, because the diffusion profile changes to semi-hemispherical [55]. All of these are important gains in the developments of analytical devices that may be useful although the use of these new materials has to be assessed in biological applications.

1.3.3 Osmium containing polymers

Osmium and ruthenium complexes with bidentate ligands have been reported as early as the 1960's [64]. The earliest report of these complexes being combined with polymer chains is by Forster and Vos [65]. They have described the synthesis protocol for poly(vinylpyridine) and poly(vinylimidazole) with both Os and Ru containing active centres. The complex of

interest to this treatise is Osmium bipyridine chloride [(Os-bpy)Cl]. These polymer films were cured on the surface of carbon electrodes and then analysed with CV, by Forster and Vos [65]. Reports in the literature showed that the complexes exhibit surface bound characteristics at $\dot{v} < 20$ mV/s, as seen in figure 1.13 and at higher scan rate they begin to exhibit diffusive characteristics [65]. Also the redox potentials of the osmium active centres was less positive than that for the ruthenium centres. The authors also used UV-vis and emission spectroscopy to study the metallopolymers [65]. The redox potentials and the ability of these polymers to form redox active films led to a rapid increase in their reported use.

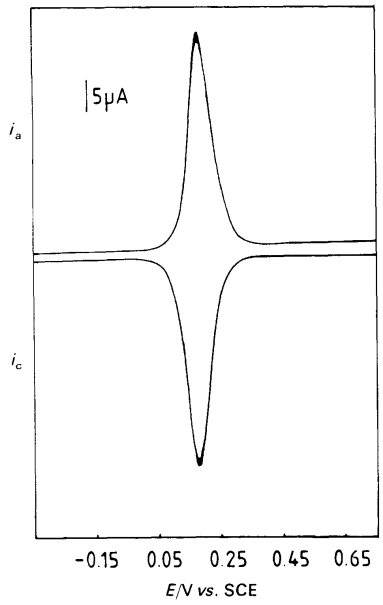


Figure 1.13: CV of (Os-bpy$_2$)Cl showing surface bound characteristics as shown by Forster et. al. [66].

In two papers published in 1991 Forster and Vos in conjunction with Lyons then went on to study the charge transport character of these films. They showed that increasing the number of active sites on the surface increased, the Faradaic processes; this was achieved by decreasing the number of monomers in the polymer backbone [66]. This is not an enirely surprising result, but it confirms that it is the bidentate ligands that give the osmium

active centres their properties. The authors proposed that the rate limiting step was the self exchange of e^- between the active centres, or electron hopping [66]. These observations are supported by the results of the second paper, that indicated increased k^0 values when the counter ion concentration was higher and the film was not compact [67]. Increasing the active centre loading to its maximum did not allow the film to be as labile, which hindered the charge transfer through the film to the surface of the electrode. Therefore the authors suggested that although redox activity was linked to the number of active sites, most favourable e^- transfer kinetics are observed at higher electrolyte concentrations when the osmium loading was below maximum [67]. Forster and Vos go on to confirm the self exchange of electrons in these polymer films [68].

While Forster and Vos had reported the electrochemical properties of the metallopolymer, Gregg and Heller reported the formation of the same films using a functional PEG to form epoxide bonds; this is the earliest report of its kind [69]. They too found that the films showed surface bound characters during CV, at low scan rates up to 5 mV s^{-1}. This transition point was at a lower scan rate than that reported by Forster and Vos, but as a result of using a long chain PEG the lability of the film could have increased. The authors also showed that the films were permeable to organic molecules, using hydroquinone as the model. The authors found that increasing the level of cross-linking did not affect the transfer kinetics of their system, this was contrary to the popular belief of the e^- transfer kinetics. They claim that this was probably a result of using a long chain binder, which might be the case; but at the point of publication they were not privy to the results of Forster et. al. that showed electron hopping as the e^- transfer pathway [69, 66, 67]. (Forster and Vos published their results toward the end of the same year.)

In conjunction with their study of the epoxide bonded films, Gregg and Heller published a second paper incorporating glucose oxidase in to the redox film [70]. This too is the first report of its kind in the literature. Using a rotating disk electrode (RDE) they were able to calibrate the response of glucose at +400 mV vs. SCE, the plots of which are shown

in Figure 1.14. They reported that the kinetics of the electrode were not restricted by the mass transport of glucose to the surface of the film, implying that e^- transfer kinetics played a significant role [70]. Their enzyme electrodes exhibited an excellent linear range and sensitivity to glucose. Following on from the work of Forster and Vos and Gregg and Heller there have been a number of reports of enzyme sensors made using these molecules.

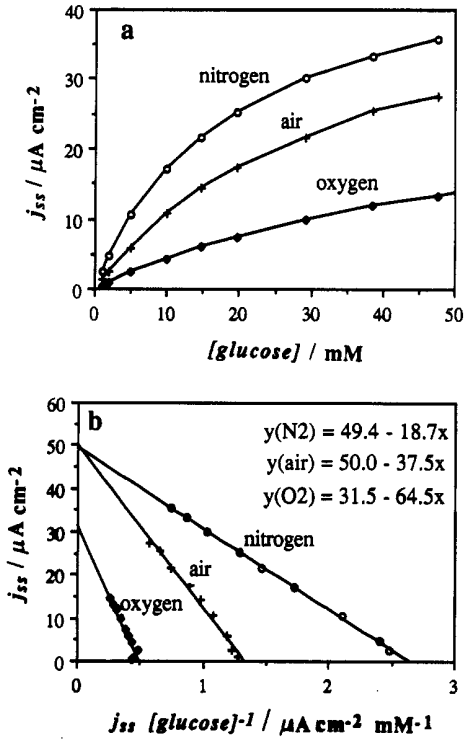


Figure 1.14: Michaelis-Menten and Lineweaver-Burke plots for glucose sensors made by Gregg and Heller [70].

Heller reported the fabrication of these films on a 7 μm carbon fibre that exhibited sensitivities for glucose as high as 1 A cm^{-2} M^{-1}, with only a 2% loss in signal per day when stored at 25 °C [71]. Ohara et. al. use poly(vinylimidazole) as the backbone for the metallopolymer and report similar results for glucose sensors, although their current densities are slightly lower in comparison to those reported by Heller [72, 71]. This suppression could be as a result of the use of a 3 mm electrode, as opposed to the use of a micro electrode.

This would in turn imply that sensitivity of the sensors was not dependant on the enzyme loading, due to rapid turnover.

Using a slightly different bidentate ligand on the osmium centre, Ohara et. al. have shown that the redox potentials for the electrodes are more negative than before. The new ligand was (4,4'-dimethylbpy)$_2$Cl and the new potential at which the electrooxidation current could be sensed was +200 mV [73]. In addition to this the authors showed that the same sensor design can be used to sense lactate by replacing the enzyme to lactate oxidase. The operating features of these films were similar to the other reports. Glucose sensors of this style were fabricated by Csoregi et. al. and subcutaneously implanted in a rat and glucose levels monitored. The modification that they made prior to implanting the sensor was the addition of a mass transport film, using poly(ester sulphonic acid) and a copolymer of polyaziridine and poly(vinyl pyridine). In order to make it biocompatible the outer most layer was made from tetraacrylated poly(ethylene oxide) [74]. This same configuration was filed as a patent by Heller, a schematic of this device is shown in Figure 1.15 [75].

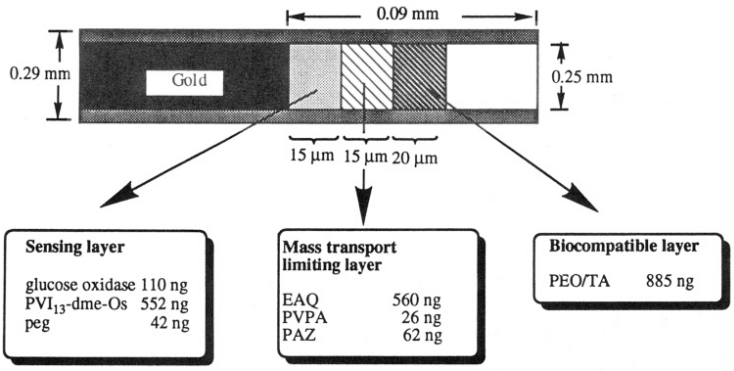


Figure 1.15: Schematic representation of the device patented by Heller [74].

A small change in the oxidation potential was reported with the use of 4,4'-dimethoxy-bpy to make the osmium complex; the new potential for this configuration was reported to be +50 mV vs. SCE by Taylor et. al. [76]. These incremental changes demostrate development, but it is not believed that there are any significant advantages in this slightly

more negative operating potential, as there were limited electroactive interference at the previously reported potentials of +200 mV vs. SCE. Vijaykumar and co workers developed this concept further by incorporating alcohol oxidase in to the film and making it sensitive to alcohol with a working potential of -50 mV vs. Ag|AgCl [77]. By incorporating soybean peroxidase in to the recognition layer Kenausis et. al. coupled the enzymatic redox of H_2O_2 with the metallopolymer and report a stable output over 12 and 8 day continuous operation for glucose and lactate sensors, respectively [78]. Heller and his co workers have also reported the use of these sensors in deoxygenated calf serum and when implanted in the jugular veins of rats [79, 80].

Although there have been a number of reports that elucidate the properties of these metallopolymers when they are covalently bound to the surface of electrodes, there have also been a few reported developments using other methods of surface immobilisation. The co-immobilisation of glucose oxidase, osmium complex and poly(phenol) is reported by Pravda et. al. [81]. They report that the best performing devices were obtained when a 1 μl aliquot of 1% osmium polymer was allowed to dry on the surface, thereafter glucose oxidase and poly(phenol) were deposited on the surface concomitantly. The devices exhibit linear responses to glucose up to 7 mM and current densities of ca. 1 μA cm^{-2} [81]. The linear range shown by their sensor is relatively low and implies that the amount of enzyme loaded on the surface was not adequate. The polymerisation CVs as reported by the authors can be seen in, Figure 1.16. when polymerising phenol on the surface of the bare platinum, the I_{ox} is $\simeq 22\mu$A, but in the presence of the osmium complex in solution this is decreased to $1/3^{rd}$ of this value at $\simeq 8\mu$A and the I_{ox} when the osmium complex has been cured on the surface is $\simeq 14\mu$A [81]. This would mean that the area available for the oxidation of phenol was minimised by the complex in solution, presumably because of the mechanics of the process of entrapment. This would suggest that this method should produce sensors that perform better, but the titration data indicated quite the opposite. This might be because the heterogeneity in the distribution of the metallopolymer and enzyme inhibits

efficient e^- transfer.

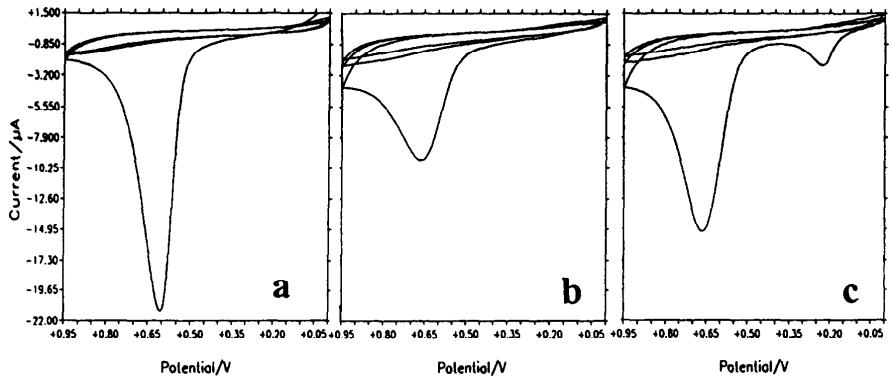


Figure 1.16: Entrapment of Os complex in poly(phenol), CVs as shown by Pravda et. al. [81].

Further to the work of Kurzawa et. al. described in section 1.3.2 Vilkanauskyte et. al. have described the encapsulation of the osmium complex in a similar manner, using alcohol dehydrogenase. The authors show an improved performances in comparison to devices made excluding the osmium complex [45].

In addition to all of the above architectures there have even been reports of chemically modifying pyrrole with the osmium metallopolymer and then electrodepositing this new compound on to the surfaces of electrodes [82, 83, 84]. This technique has the added advantage of only allowing for the deposition of the sensing layer on areas that are electrically connected. That is, it will be possible to fabricate different kinds of sensing layers on an electrode array without affecting the performance of each electrode.

There is a litany of literature that describes the use of osmium metallopolymers as mediators for enzyme sensors. Each report develops the concept a little further and shows greater promise. As described in section 1.3.2 with the advent of new materials this method seems to have seen a slight decline in interest. Many of the sensors described are not suited to manufacturing on a large scale.

1.3.4 Scanning Electrochemical Microscopy

The use of SECM as an analytical tool has become popular in the recent past. In the past Bard and co-workers catalogued most of the theory that defines this type of scanning probe analysis; they defined the Faradaic and non-Faradaic processes that take place at the UME tip, which is used as the scanning probe [3, 4, 6, 5]. These have been discussed in section 1.2.2.

There are many advantages that make this technique particularly suitable for biological applications, these have also been described by Roberts et. al. in a recent review [85]. Firstly it is relatively easy to develop experimental procedures; the only factor to think about in detail is the use of a suitable redox couple, as a number of biological samples produce electroactive species naturally. Sample preparation tends to be relatively easy, as there is no need to make it optically compatible, as needed for fluorescence spectroscopy, or to slice it up accurately as required for atomic force microscopy. One of the greatest advantages of this form of analysis is the ability to study biological samples using conditions that are as closely aligned to *in-vivo* as possible; the only difference is the presence of a redox mediator.

The principle of hindered diffusion at the surface of the tip that underpins the operation of this technique also provides it with its Achilles' heel. It is possible to use very small tips to probe the surface, but the R/G of these probes must be > 5, this means that the collection area increases by a factor of 5 as well. The i_T is proportional to the area of the tip therefore, making the tip smaller decreases the signal which makes the S/N ratio worse. To a certain degree this can be mitigated by increasing the concentration of the electroactive species in solution, but it still might be difficult to separate the background currents from the signal; this could also lead to losing some of the signal by mistakenly treating it as noise.

Albeit with a few disadvantages this is a very powerful analytical technique and there have been wide spread reports of its use in numerous applications. Roberts et. al. in their review of the application of SECM for biochemical systems report diverse uses from

the characterisation of DNA modified substrates, to a litany of work performed on enzyme imaging and kinetic studies and the imaging of single cells and tissue [85]. This technique does have numerous non-biological applications as well, as it can be used to characterise different components of micro-fabricated devices, such as ion selective field effect transistors, as long as the devices can be submerged in elecrtolytic solutions.

Ciobanu et. al. report the use of enzyme modified SECM tips to study the glucose uptake and lactate production of single fibroblasts and cancer cells [86]. The tips are prepared using glucose and lactate oxidase for the two tests, respectively. These tips are then rastered across the sample and measurements recorded. The shapes and sizes of the cell images are comparable to the expected values; although the signals that they are being able to pick up are of the order of 10 pA [86]. This is to be expected because the enzyme loading on a platinum UME with a 7 μm diameter is going to be low and hence the signal produced weak. Also they operate in the H_2O_2 mode of sensing, which could poison such a small electrode during the experiment.

This particular problem has been mitigated to a certain extent by Horrocks et. al., by using a redox mediator that 'wires' the enzyme and enhances e^- transport [87]. In feedback mode, they noticed an increase in the tip current as the tip approached the substrate (glassy carbon with immobilised glucose oxidase) until the tip was close enough to block the diffusion of glucose and oxygen, removing the production of H_2O_2 under the collection area. A line scan in GC mode also shows a clear transition from an area with enzyme to one without [87]. The main advantage of their tip modification is the ability to see changes in current of the order of a 100 pA, which improves the S/N ratio.

Another example of a modified tip being utilised in SECM is by Wipf et. al., who have deposited iridium oxide on an 8 μm carbon fibre and have used it to study the pH profiles of substrates [88]. Studying the local changes in pH due to the electrochemical reduction of H_2O they have reported some very discrete images that also show that at more anodic potentials the localised changes are higher due to increased electrolysis. Their study

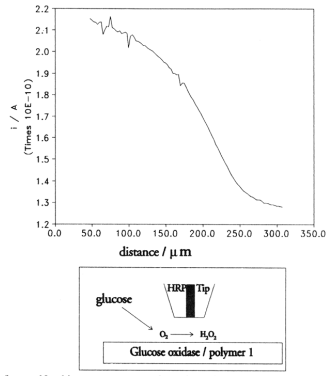


Figure 1.17: Line scan over a glucose oxidase substrate, using an enzyme modified tip, with a synthetic redox mediator to complete the redox cycle. The drop in current indicates that the tip has move off the H_2O_2 producing area, shown by Horrocks et. al. [87].

of immobilised glucose oxidase with a ferrocinium mediator showed less promising results. The generation of H^+ ions by the enzyme was observed, probably due to bulk diffusion that is difficult to differentiate from the background [88]. Using the potentiometric mode of sensing for pH, there are fewer restrictions on the size of tip that can be used as the signal is not reliant on tip's surface area, although mechanical considerations do limit the size as well. Secondly there are not too many bioanalytical applications that can be engineered to allow the study of ions, apart from those related to ion discharge and uptake, but for those scanning ion conductance microscopy is better suited.

There have been numerous reports of the use of SECM to scan surfaces that have enzymes immobilised on them. A preliminary report by Bard et. al. described the feedback characteristics of a nylon film loaded with glucose oxidase [5]. The actual feedback currents showed a correlation for those predicted by theory and therefore this technique might be used for further characterisation of surfaces and reaction kinetics.

Oliviera and Heinze use glucose oxidase and horse radish peroxidase to characterise anodically and chemically grown titanium dioxide surfaces [89]. The enzymes were attached using a SAM made from aminopropyltriethoxysilane (APTES) and carbodiimide chemistry. The quality of the SAMs made on chemically prepared TiO_2 seemed to be better as they

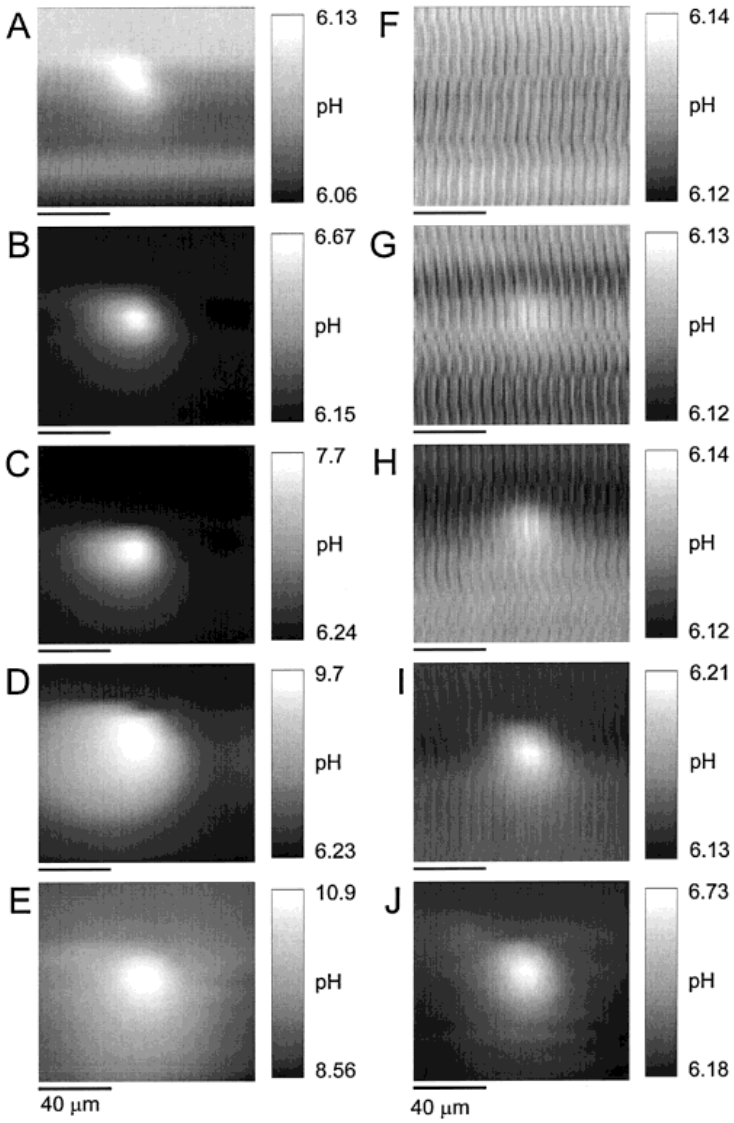


Figure 1.18: SECM images of a platinum substrate electrolysing water, using a carbon fibre tip modified with IrOx to sense pH, shown by Wipf et. al. [88]. The side bars indicate the pH range recorded at the tip and A to E are experiments performed in unbuffered solution whereas F to J are performed in phosphate buffer. The substrate potentials are -0.2V (A, F); -0.4 (B. G); -0.6 V (C, H); -1.0 V (D, I) and -1.2 V (E, J).

show increased enzymatic activity at the UME [89]. This also showed that the enzyme immobilisation on a SAM gave excellent uniformity in coverage, even though it was not always possible to ascertain the smaller features using SECM.

Another study of the enzymatic activity of glucose oxidase has been reported by Deng et. al. [90]. Using a layer-by-layer configuration they showed that when the substrate was polarised to oxidise the enzymatically generated H_2O_2 the feedback current was only 10% of that seen at open circuit [90]. This showed that the collection efficiency of hydrogen peroxide with their lbl structure is conducive to better signals for glucose analysis.

Surfaces with lactate oxidase and cholesterol oxidase have also been imaged using this technique [91, 92]. For the case of cholesterol oxidase the enzymatic by-product H_2O_2 was detected at the tip and the surface scans show a difference in i_T of ca. 600 pA between no cholesterol and cholesterol in the electrochemical cell, although no surface features can be observed due to lateral diffusion [91]. Using hydroxymethylferrocene (HMF) in the case of lactate oxidase imaging showed discrete enzyme distribution on the glassy carbon substrate, a picture of this can be seen in Figure 1.19. This distribution is supported by some high contrast images provided in the same study [92].

A brief review of the literature available for SECM studies on enzymatic systems shows that there is great promise and it is relatively easy to design experiments to study these systems. The majority of the work seen was not able to distinguish surface features, because the enzyme distribution in most cases was not discrete enough for the limited spatial resolution that this technique accords. Also lateral diffusion of species away from the surface affects the ability to distinguish small variations in film structure.

1.3.5 *In-vitro* monitoring of cell cultures

The monitoring of the extra-cellular matrix (ECM) during cell culture is very important as it makes available information about the transient characteristics of the ECM which, in turn can allow informed optimisation of culture protocols and save time. For example,

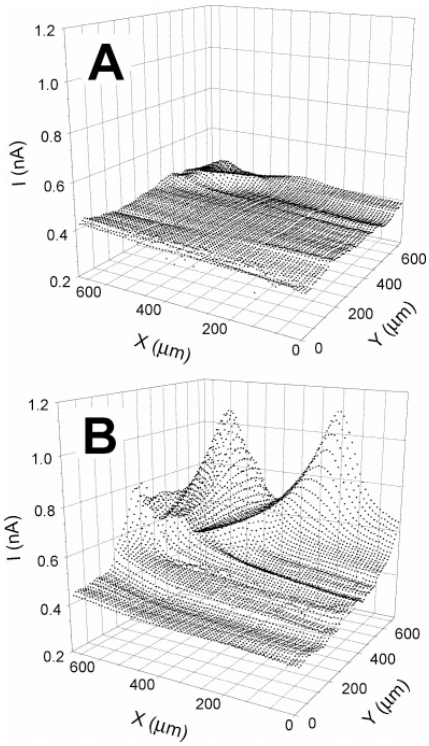


Figure 1.19: Surface scan of a lactate oxidase modified surface with HMF as a mediator, as shown by Parra et. al. [92].

indications of apoptosis from the culture prior to its onset, would allow preventitive action to be taken. At present there are three possible methods that can be used to monitor culture parameters.

- Off-line analysis: here regular samples are withdrawn from the culture, usually from the waste media and these samples are analysed by commercially available bench-top instruments. The advantage of this method is that the data produced can be reliable, because of the ability to use equipment that can be calibrated prior to each sample being tested, or practically in a regular and scheduled fashion. It is also possible to test a number of different parameters from a single sample. There are numerous disadvantages to this mode of operation as well, primarily the fact that removing a few aliquots during a culture does not necessarily portray the transient characteristics

accurately. Also some commercial equipment requires extensive sample pre-treatment before the sample can be analysed and this makes the process laborious and time consuming.

- On-line analysis using flow injection: the sensors are set up ourtside the main culture vessel and regular small volume samples are withdrawn from the culture automatically. In some case these samples are returned to the culture vessel, but mostly they are treated as waste material. In this scenario elaborate perfusion mechanisms have to be set up to ensure that both ends of the delivery system do not break the sterility barrier and that the sample delivery is uninhibited for the duration of the culture. This is usually achieved through the use of HPLC hardware, due to its reliability and standardised fittings. This system is beneficial to the user in terms of the sensor reliability; it is easier to build in redundancy in to the system which allows for the regular calibration of the devices which can also be replaced if required, allowing for more accurate data collection. Although this setup can only be employed if the culture is going to be operated in perfused mode, otherwise the media will get depleted at a rate that harms the growth of the cells.

- *In-vitro* monitoring: when the sensing devices are placed directly in to the culture vessel, the data acquisition rate can be decided on by the user as there are no restrictions in breaking the sterility barrier or depletion of media. This mode of operation accords the maximum flexibility in terms of operating the culture as per the needs of the culture and not the monitoring logistics. There are two very important problems associated with this mode; firstly it is imperative that the devices themselves or any part thereof do not prove toxic to the cells being grown. Secondly, cell culture media are heterogeneous environments with various components. These components have been known to affect the surfaces of sensors, in a process known as bio–fouling.

On-line non invasive methods of sensing are most widely reported in the literature; although often this mode of sensing requires sample delivery systems or other equipment to interrogate the media, Some of these reports are described below.

Rhiel and co workers reported the monitoring of glucose and lactate in a rotating wall perfused reactor, using near infra-red spectroscopy [93]. Their measurements have shown an excellent inverse correlation between cell density and glucose and vice versa for lactate. These trends were reversed after a period of 70 hours when the cells begin to die [93]. The standard error of prediction they have reported is within acceptable norms as well. Ozturk et. al. performed similar tests using a commercially available analyser for concentrations of glucose and lactate; their responses and relationships with cell growth for the duration of the culture are exceptional as well [94].

Xu and co-workers devised a glucose control system in a perfused rotating wall bioreactor to monitor and control the media for 55 days, with only three two point calibrations in the interim [95]. Using a H_2O_2 sensing electrode, even in FIA mode this is a challenging feat. There is a small deviation in their measurements from the standard analysis used by them, but they claim adequate control for this time period; although they provide no cell data to support it [95]. Multiple analyte sensing using fluidised bed enzyme reactors, for a yeast culture, have been reported by Vojinovic et. al. They have monitored glucose, lactate, ethanol, galactose and l-amino acids using oxidoreductases with FIA. In yeast culture the authors were able to show the inverse correlation between concentrations of galactose and ethanol; their results can be seen in Figure 1.20 [96].

There are a few reports of placing sensors *in-vitro* to monitor culture parameters. One such report is by Ceriotti et. al. using 3T3 fibroblast cultures. Their sensing mechanism was made of a miniaturised Clark type electrodes and ISFETs to sense O_2 and pH respectively [97]. Seeding an increasing number of cells they were able to show that the trend for O_2 consumption and that the pH of the media decreased, over a 24 hour period. In a separate experiment run for a 24 hour period, they showed that the introduction of toxic effects such

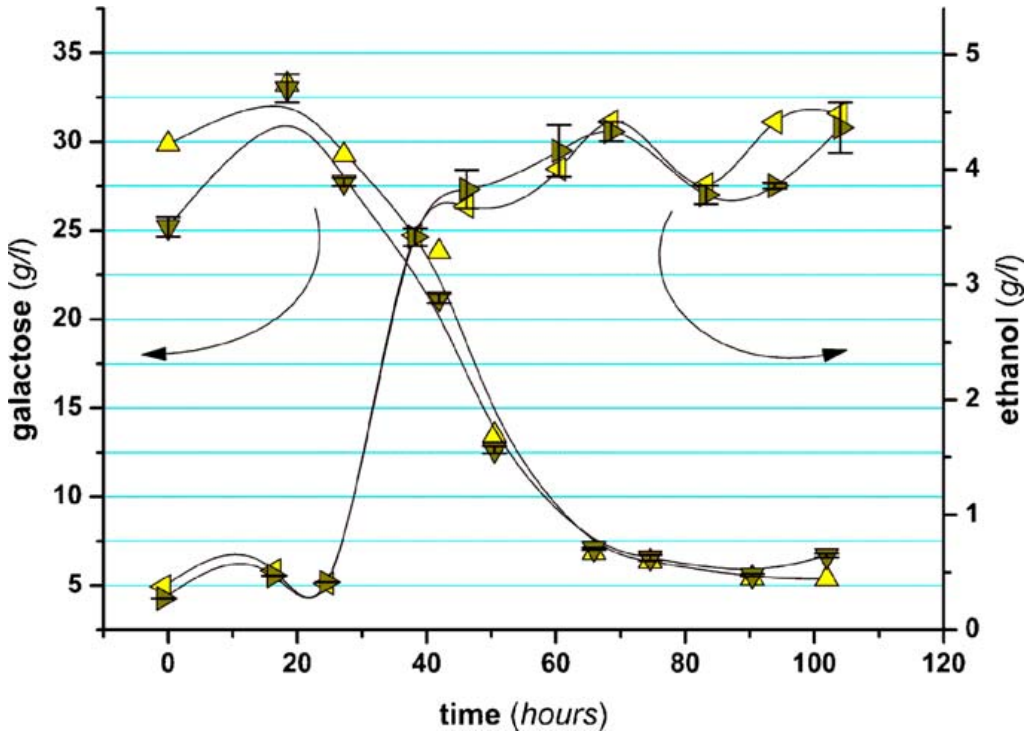


Figure 1.20: Cell culture parameters of yeast cultures as measured and presented by Vojinovic et. al. [96].

as sodium arsenite, cadmium chloride and *cis*-platinum decreased the O_2 consumption and the pH did not change to the same extent; these results are to be expected [97]. These are an excellent set of experiments, but the short time span might suggest that the sensors were prone to fouling and could not deliver useful data for longer periods.

With the aid of a modified ISFET Lehmann et. al. have presented reports of monitoring the pH and respiration in cell culture. The link between these two is as expected and holds promise [98]. The use of a pH sensor for 124 days *in-vitro* was shown by Jeevarajan and co-workers. Using the optical properties of the phenol red present in the media, they were able to accurately monitor the pH for this period [99]. This technique has the advantage of interrogating the media and not requiring an analyte recognition element. Phenol red is a well known pH indicator and because the culture media never approaches its pK_a while

the culture is healthy it has an excellent sensitivity.

A search for the work published in this field did not produce many results, as a consequence of all the issues elucidated before. Most of the progress in monitoring cell cultures has been reported, using non invasive sensing, probably as it is possible to build in redundancy to the system and also because the difficulty in setting up the equipment is not as great as developing sensors that can be placed in to the culture directly.

The lack of progress for *in-vitro* sensors is probably due to the fact that the life spans of the sensors are small, although improvements have been reported in the sensor's life time by modifying their surface; the sensors themselves proved toxic to the cells in question [100]. Also the repeated reports of sensors made using CMOS technology might indicate that miniaturisation will play an important role in cell culture monitoring. With the advent of more cost effective methods of producing devices, the number of these reports should see an increase. In the course of this work, no reports were found that mechanistically explain the degradation of sensors when placed in cell cultures.

1.4 Summary

This chapter described in detail the principles of electrochemistry and biosensors. These principles will be built upon in the subsequent chapters to understand the results derived and the conclusions drawn from the presented work. Along with a review of the theoretical concepts of the work, a brief review of the published literature is also presented. This review sets the frame work that describes the work that has already been performed in this field and subsequently published. This is by no means an exhaustive literature review, because the published literature in the field of biosensors, and in particular glucose sensors, is very vast; but this review presents a flavour of all the work reported historically and also the direction that future research might take.

References

[1] A. J. Bard and L. R. Faulkner, *Electrochemical Methods: Fundamentals and Applications 2nd ed.* J. Wiley, 2001.

[2] R. S. Nicholson, "Theory and application of cyclic voltammetry for measurement of electrode reaction kinetics," *Analytical Chemistry*, vol. 37, no. 11, pp. 1351–1355, 1965.

[3] A. J. Bard, F. F. Fu-Ren, J. Kwak, and O. Lev, "Scanning electrochemical microscopy. introduction and principles," *Anal. Chem.*, vol. 61, no. 2, pp. 132–138, 1989.

[4] J. Kwak and A. J. Bard, "Scanning electrochemical microscopy. theory of the feedback mode," *Anal. Chem.*, vol. 61, no. 11, pp. 1221–1227, 1989.

[5] A. J. Bard, F. F. Fu-Ren, D. T. Pierce, P. R. Unwin, D. O. Wipf, and F. Zhou, "Chemical imaging of surfaces with the scanning electrochemical microscope," *Science*, vol. 254, no. 2, pp. 68–74, 1991.

[6] J. Kwak and A. Bard, "Scanning electrochemical microscopy. apparatus and two-dimesional scans of conductive and insulating substrates," *Anal. Chem.*, vol. 61, no. 17, pp. 1794–1799, 1989.

[7] NC-ICBMB and E. C. Webb, *Enzyme Nomenclature 1992.* Academic Press, 1992.

[8] D. O'Hare, *The development of electrochemical sensors for the study of intervertebral disc nutrition.* PhD thesis, Imperial College, London, 1991.

[9] Q. T. Gibson, B. E. P. Swooda, and V. Massey, "Kinetics and mechanism of action of glucose oxidase," *The Journal of Biological Chemistry*, vol. 239, no. 11, pp. 3927–3934, 1964.

[10] M. K. Weibel and H. J. Bright, "The glucose oxidase mechanism: Interpretation of the ph dependence," *The Journal of Biological Chemistry*, vol. 246, no. 9, pp. 2734–2744, 1971.

[11] B. J. Privett, J. H. Shin, and M. H. Schoenfisch, "Electrochemical sensors," *Anal. Chem.*, vol. DOI: 10.1021/ac8007219, 2008.

[12] B. Leca-Bouvier and L. J. Blum, "Biosensors for protein detection: A review," *Analytical Letters*, vol. 38, no. 10, pp. 1491–1517, 2005.

[13] K. Ramanathan and B. Danielsson, "Principles and applications of thermal biosensors," *Biosensors & Bioelectronics*, vol. 16, no. 6, pp. 417–423, 2001.

[14] J. Homola, S. S. Yee, and G. Gauglitz, "Surface plasmon resonance sensors: review," *Sensors and Actuators B-Chemical*, vol. 54, no. 1-2, pp. 3–15, 1999.

[15] C. R. Suri and G. C. Mishra, "Activating piezoelectric crystal surface by silanization for microgravimetric immunobiosensor application," *Biosensors & Bioelectronics*, vol. 11, no. 12, pp. 1199–1205, 1996.

[16] B. F. Serra, A. Tzoris, and E. A. H. Hall, "Manometric transduction in enzyme biosensors," *Biosensors & Bioelectronics*, vol. 22, no. 1, pp. 94–101, 2006.

[17] J. H. Wang, L. W. Ruddock, and A. E. G. Cass, "Microscopic investigations of the interaction of proteins with surfaces," *Biosensors & Bioelectronics*, vol. 9, no. 9-10, pp. 647–655, 1994.

[18] A. Wada, M. Mie, M. Aizawa, P. Lahoud, A. E. G. Cass, and E. Kobatake, "Design and construction of glutamine binding proteins with a self-adhering capability to

unmodified hydrophobic surfaces as reagentless fluorescence sensing devices," *Journal of the American Chemical Society*, vol. 125, no. 52, pp. 16228–16234, 2003.

[19] X. Chen, N. Matsumoto, Y. Hu, and G. Wilson, "Electrochemically mediated electrodeposition/electropolymerization to yield a glucose microbiosensor with improved characteristics," *Analytical Chemistry*, vol. 74, no. 2, pp. 368–372, 2002.

[20] L. Clark, "Electrode systems for continuous monitoring in cardiovascular surgery," *Annals of the New York Academy of Science*, vol. 102, pp. 29–45, 1962.

[21] C. Malitesta, F. Palmisano, L. Torsi, and P. G. Zambonin, "Glucose fast-response amperometric sensor based on glucose-oxidase immobilized in an electropolymerized poly(ortho-phenylenediamine) film," *Analytical Chemistry*, vol. 62, no. 24, pp. 2735–2740, 1990.

[22] A. B. Steel, T. M. Herne, and M. J. Tarlov, "Electrochemical quantitaion of dna immobilised on gold," *Analytical Chemistry*, vol. 70, no. 22, pp. 4670–4677, 1998.

[23] A. Chaubey and B. D. Malhotra, "Mediated biosensors," *Biosensors & Bioelectronics*, vol. 17, no. 6-7, pp. 441–456, 2002.

[24] A. E. G. Cass, G. Davis, G. D. Francis, H. A. O. Hill, W. J. Aston, I. J. Higgins, E. V. Plotkin, L. D. L. Scott, and A. P. F. Turner, "Ferrocene-mediated enzyme electrode for amperometric determination of glucose," *Analytical Chemistry*, vol. 56, no. 4, pp. 667–671, 1984.

[25] E. J. Roberts and F. F, "The antimony-antimony trioxide electrode and its use as a measure of acidity," *Journal of the American Chemical Society*, vol. 50, pp. 2125–2142, 1928.

[26] G. A. Perley, P. Wyncote, J. Godshalk, and M. Bowie, "Cells for pH measurement," tech. rep., United States Patent Office, 1947.

[27] I. A. Ges, B. L. Ivanov, D. K. Schaffer, E. A. Lima, A. A. Werdich, and F. J. Baudenbacher, "Thin-film IrOx pH microelectrode for microfluidic-based microsystems," *Biosensors and Bioelectronics*, vol. 21, no. 2, pp. 248–256, 2005.

[28] D. O'hare, K. H. Parker, and C. P. Winlove, "Metal-metal oxide pH sensors for physiological application," *Medical Engineering & Physics*, vol. 28, no. 10, pp. 982–988, 2006.

[29] K. Yamanaka, "Anodically electrodeposited iridium oxide-films (aeirof) from alkaline-solutions for electrochromic display devices," *Japanese Journal of Applied Physics Part 1-Regular Papers Short Notes & Review Papers*, vol. 28, no. 4, pp. 632–637, 1989.

[30] H. G. Kruszyna, I. Bodek, L. K. Libby, and R. M. Milburn, "Preparation and reactivity of tris(oxalato)iridate(iv) ion in aqueous acidic solution," *Inorganic Chemistry*, vol. 13, no. 2, pp. 434–438, 1974.

[31] M. L. Hitchman and S. Ramanathan, "Evaluation of iridium oxide electrodes formed by potential cycling as pH probes," *Analyst*, vol. 113, no. 1, pp. 35–39, 1988.

[32] S. A. M. Marzouk, "Improved electrodeposited iridium oxide pH sensor fabricated on etched titanium substrates," *Analytical Chemistry*, vol. 75, no. 6, pp. 1258–1266, 2003.

[33] S. A. M. Marzouk, S. Ufer, R. P. Buck, T. A. Johnson, L. A. Dunlap, and W. E. Cascio, "Electrodeposited iridium oxide pH electrode for measurement of extracellular myocardial acidosis during acute ischemia," *Analytical Chemistry*, vol. 70, no. 23, pp. 5054–5061, 1998.

[34] I. A. Ges, B. L. Ivanov, A. A. Werdich, and F. J. Baudenbacher, "Differential pH measurements of metabolic cellular activity in nl culture volumes using microfabricated

iridium oxide electrodes," *Biosensors and Bioelectronics*, vol. 22, no. 7, pp. 1303–1310, 2007.

[35] M. F. Smiechowski and V. F. Lvovich, "Iridium oxide sensors for acidity and basicity detection in industrial lubricants," *Sensors and Actuators B: Chemical*, vol. 96, no. 1-2, pp. 261–267, 2003.

[36] B. D. Malhotra and A. Chaubey, "Biosensors for clinical diagnostics industry," *Sensors and Actuators B-Chemical*, vol. 91, no. 1-3, pp. 117–127, 2003.

[37] J.-F. Masson, C. Kranz, K. S. Booksh, and B. Mizalkoff, "Improved sensitivity and stability of amperometric enzyme microelectrodes by covalent attachment to gold electrodes," *Biosensors & Bioelectronics*, vol. 23, no. 3, pp. 355–361, 2008.

[38] S. Cosnier, "Affinity biosensors based on electropolymerized films," *Electroanalysis*, vol. 17, no. 19, pp. 1701–1715, 2005.

[39] D. Olea, O. Viratelle, and C. Faure, "Polypyrrole-glucose oxidase biosensor - effect of enzyme encapsulation in multilamellar vesicles on analytical properties," *Biosensors & Bioelectronics*, vol. 23, no. 6, pp. 788–794, 2008.

[40] S. V. Sasso, R. J. Pierce, R. Walla, and A. M. Yacynych, "Electropolymerized 1,2-diaminobenzene as a means to prevent interferences and fouling and to stabilize immobilized enzyme in electrochemical biosensors," *Analytical Chemistry*, vol. 62, no. 11, pp. 1111–1117, 1990.

[41] J. I. Reyes De Corcuera, R. P. Cavalieri, and J. R. Powers, "Improved platinization conditions produce a 60-fold increase in sensitivity of amperometric biosensors using glucose oxidase immobilized in poly-o-phenylenediamine," *Journal of Electroanalytical Chemistry*, vol. 575, no. 2, pp. 229–241, 2005.

[42] Q. Yang, P. Atanasov, and E. Wilkins, "Needle-type lactate biosensor," *Biosensors and Bioelectronics*, vol. 14, no. 2, pp. 203–210, 1999.

[43] T. D. Chung, R. A. Jeong, S. K. Kang, and H. C. Kim, "Reproducible fabrication of miniaturized glucose sensors: preparation of sensing membranes for continuous monitoring," *Biosensors & Bioelectronics*, vol. 16, no. 9-12, pp. 1079–1087, 2001.

[44] C. Kurzawa, A. Hengstenberg, and W. Schuhmann, "Immobilization method for the preparation of biosensors based on ph shift-induced deposition of biomolecule-containing polymer films," *Analytical Chemistry*, vol. 74, no. 2, pp. 355–361, 2002.

[45] A. Vilkanauskyte, T. Erichsen, L. Marcinkeviciene, V. Laurinavicius, and W. Schuhmann, "Reagentless biosensors based on co-entrapment of a soluble redox polymer and an enzyme within an electrochemically deposited polymer film," *Biosensors & Bioelectronics*, vol. 17, no. 11-12, pp. 1025–1031, 2002.

[46] P. N. Bartlett, P. Tebbutt, and C. H. Tyrrell, "Electrochemical immobilization of enzymes .3. immobilization of glucose-oxidase in thin-films of electrochemically polymerized phenols," *Analytical Chemistry*, vol. 64, no. 2, pp. 138–142, 1992.

[47] M. Gattrell and D. W. Kirk, "A study of electrode passivation during aqueous phenol electrolysis," *Journal of the Electrochemical Society*, vol. 140, no. 4, pp. 903–911, 1993.

[48] G. Arslan, B. Yazici, and M. Erbil, "The effect of ph, temperature and concentration on electrooxidation of phenol," *Journal of Hazardous Materials*, vol. 124, no. 1-3, pp. 37–43, 2005.

[49] P. N. Bartlett and D. J. Caruana, "Electrochemical immobilization of enzymes .5. microelectrodes for the detection of glucose based on glucose-oxidase immobilized in a poly(phenol) film," *Analyst*, vol. 117, no. 8, pp. 1287–1292, 1992.

[50] S. Eddy, K. Warriner, I. Christie, D. Ashworth, C. Purkiss, and P. Vadgama, "The modification of enzyme electrode properties with nonconducting electropolymerized films," *Biosensors & Bioelectronics*, vol. 10, no. 9-10, pp. 831–839, 1995.

[51] Y. Nakabayashi, M. Wakuda, and H. Imai, "Amperometric glucose sensors fabricated by electrochemical polymerization of phenols on carbon paste electrodes containing ferrocene as an electron transfer mediator," *Analytical Sciences*, vol. 14, no. 6, pp. 1069–1076, 1998.

[52] D. W. M. Arrigan and P. N. Bartlett, "A scanning force microscopy study of poly(phenol) films containing immobilized glucose oxidase," *Biosensors & Bioelectronics*, vol. 13, no. 3-4, pp. 293–304, 1998.

[53] J. Wang, "Carbon-nanotube based electrochemical biosensors: A review," *Electroanalysis*, vol. 17, no. 1, pp. 7–14, 2005.

[54] A. Merkoci, M. Pumera, X. Llopis, B. Perez, M. del Valle, and S. Alegret, "New materials for electrochemical sensing vi: Carbon nanotubes," *Trac-Trends in Analytical Chemistry*, vol. 24, no. 9, pp. 826–838, 2005.

[55] Y. H. Lin, F. Lu, Y. Tu, and Z. F. Ren, "Glucose biosensors based on carbon nanotube nanoelectrode ensembles," *Nano Letters*, vol. 4, no. 2, pp. 191–195, 2004.

[56] J. Wang and M. Musameh, "Carbon-nanotubes doped polypyrrole glucose biosensor," *Analytica Chimica Acta*, vol. 539, no. 1-2, pp. 209–213, 2005.

[57] M. D. Shirsat, C. O. Too, and G. G. Wallace, "Amperometric glucose biosensor on layer by layer assembled carbon nanotube and polypyrrole multilayer film," *Electroanalysis*, vol. 20, no. 2, pp. 150–156, 2008.

[58] L. D. Zhu, R. L. Yang, J. G. Zhai, and C. Y. Tian, "Bienzymatic glucose biosensor based on co-immobilization of peroxidase and glucose oxidase on a carbon nanotubes electrode," *Biosensors & Bioelectronics*, vol. 23, no. 4, pp. 528–535, 2007.

[59] J. Wang and M. Musameh, "Enzyme-dispersed carbon-nanotube electrodes: a needle microsensor for monitoring glucose," *Analyst*, vol. 128, no. 11, pp. 1382–1385, 2003.

[60] H. Muguruma, Y. Shibayama, and Y. Matsui, "An amperometric biosensor based on a composite of single-walled carbon nanotubes, plasma-polymerized thin film, and an enzyme," *Biosensors and Bioelectronics*, vol. 23, no. 6, pp. 827–832, 2008.

[61] K. M. Manesh, H. T. Kim, P. Santhosh, A. I. Gopalan, and K. P. Lee, "A novel glucose biosensor based on immobilization of glucose oxidase into multiwall carbon nanotubes-polyelectrolyte-loaded electrospun nanofibrous membrane," *Biosensors & Bioelectronics*, vol. 23, no. 6, pp. 771–779, 2008.

[62] P. P. Joshi, S. A. Merchant, Y. D. Wang, and D. W. Schmidtke, "Amperometric biosensors based on redox polymer-carbon nanotube-enzyme composites," *Analytical Chemistry*, vol. 77, no. 10, pp. 3183–3188, 2005.

[63] R. Antiochia and L. Gorton, "Development of a carbon nanotube paste electrode osmium polymer-mediated biosensor for determination of glucose in alcoholic beverages," *Biosensors & Bioelectronics*, vol. 22, no. 11, pp. 2611–2617, 2007.

[64] D. A. Buckingham, F. P. Dwyer, and H. A. Goodwin, "Mono- and bis-(2.2'-bipyridine) and (1,10-phenanthroline) chelates of ruthenium and osmium," *Australian Journal of Chemistry*, vol. 17, pp. 325–336, 1964.

[65] R. J. Forster and J. G. Vos, "Synthesis, characterization, and properties of a series of osmium-containing and ruthenium-containing metallopolymers," *Macromolecules*, vol. 23, no. 20, pp. 4372–4377, 1990.

[66] R. J. Forster, J. G. Vos, and M. E. G. Lyons, "Controlling processes in the rate of charge transport through [os(bipy)$_2$(pvp)$_n$cl]cl redox polymer-modified electrodes," *Journal of the Chemical Society-Faraday Transactions*, vol. 87, no. 23, pp. 3761–3767, 1991.

[67] R. J. Forster, J. G. Vos, and M. E. G. Lyons, "Thermodynamics and kinetics of heterogeneous electron-transfer at glassy-carbon osmium-containing metallopolymer

interfaces," *Journal of the Chemical Society-Faraday Transactions*, vol. 87, no. 23, pp. 3769–3774, 1991.

[68] R. J. Forster and J. G. Vos, "Ionic interactions and charge-transport properties of metallopolymer films on electrodes," *Langmuir*, vol. 10, no. 11, pp. 4330–4338, 1994.

[69] B. A. Gregg and A. Heller, "Redox polymer-films containing enzymes .1. a redox-conducting epoxy cement - synthesis, characterization, and electrocatalytic oxidation of hydroquinone," *Journal of Physical Chemistry*, vol. 95, no. 15, pp. 5970–5975, 1991.

[70] B. A. Gregg and A. Heller, "Redox polymer-films containing enzymes .2. glucose-oxidase containing enzyme electrodes," *Journal of Physical Chemistry*, vol. 95, no. 15, pp. 5976–5980, 1991.

[71] A. Heller, "Electrical connection of enzyme redox centers to electrodes," *Journal of Physical Chemistry*, vol. 96, no. 9, pp. 3579–3587, 1992.

[72] T. J. Ohara, R. Rajagopalan, and A. Heller, "Glucose electrodes based on cross-linked $[os(bpy)(2)]^{(+/2+)}$ complexed poly(l-vinylimidazole) films," *Analytical Chemistry*, vol. 65, no. 23, pp. 3512–3517, 1993.

[73] T. J. Ohara, R. Rajagopalan, and A. Heller, "Wired enzyme electrodes for amperometric determination of glucose or lactate in the presence of interfering substances," *Analytical Chemistry*, vol. 66, no. 15, pp. 2451–2457, 1994.

[74] E. Csoregi, D. W. Schmidtke, and A. Heller, "Design and optimization of a selective subcutaneously implantable glucose electrode based on wired glucose-oxidase," *Analytical Chemistry*, vol. 67, no. 7, pp. 1240–1244, 1995.

[75] A. Heller, "Subcutaneous glucose electrode," tech. rep., United States Patent Office, 1997.

[76] C. Taylor, G. Kenausis, I. Katakis, and A. Heller, "Wiring of glucose-oxidase within a hydrogel made with polyvinyl imidazole complexed with [(os-4,4'-dimethoxy-2,2'-bipyridine)cl]$^{(+/2+)}$," *Journal of Electroanalytical Chemistry*, vol. 396, no. 1-2, pp. 511–515, 1995.

[77] A. R. Vijayakumar, E. Csregi, A. Heller, and L. Gorton, "Alcohol biosensors based on coupled oxidase-peroxidase systems," *Analytica Chimica Acta*, vol. 327, no. 3, pp. 223–234, 1996.

[78] G. Kenausis, Q. Chen, and A. Heller, "Electrochemical glucose and lactate sensors based on "wired" thermostable soybean peroxidase operating continuously and stably at 37c," *Analytical Chemistry*, vol. 69, no. 6, pp. 1054–1060, 1997.

[79] D. Schmidtke and A. Heller, "Accuracy of the one-point in vivo calibration of "wired" glucose oxidase electrodes implanted in jugular veins of rats in periods of rapid rise and decline of the glucose concentration," *Analytical Chemistry*, vol. 70, no. 10, pp. 2149–2155, 1998.

[80] N. Gajovic, G. Binyamin, A. Warsinke, F. Scheller, and A. Heller, "Operation of a miniature redox hydrogel-based pyruvate sensor in undiluted deoxygenated calf serum," *Analytical Chemistry*, vol. 72, no. 13, pp. 2963–2968, 2000.

[81] M. Pravda, C. M. Jungar, E. I. Iwuoha, M. R. Smyth, K. Vytras, and A. Ivaska, "Evaluation of amperometric glucose biosensors based on coimmobilization of glucose-oxidase with an osmium redox polymer in electrochemically generated polyphenol films," *Analytica Chimica Acta*, vol. 304, no. 2, pp. 127–138, 1995.

[82] S. Gaspar, K. Habermller, E. Csregi, and W. Schuhmann, "Hydrogen peroxide sensitive biosensor based on plant peroxidases entrapped in os-modified polypyrrole films," *Sensors and Actuators B: Chemical*, vol. 72, no. 1, pp. 63–68, 2001.

[83] K. Habermuller, A. Ramanavicius, V. Laurinavicius, and W. Schuhmann, "An oxygen-insensitive reagentless glucose biosensor based on osmium-complex modified polypyrrole," *Electroanalysis*, vol. 12, no. 17, pp. 1383–1389, 2000.

[84] W. Schuhmann, C. Kranz, H. Wohlschlager, and J. Strohmeier, "Pulse technique for the electrochemical deposition of polymer films on electrode surfaces," *Biosensors and Bioelectronics*, vol. 12, no. 12, pp. 1157–1167, 1997.

[85] W. S. Roberts, D. J. Lonsdale, J. Griffiths, and S. P. J. Higson, "Advances in the application of scanning electrochemical microscopy to bioanalytical systems," *Biosensors and Bioelectronics*, vol. 23, no. 3, pp. 301–318, 2007.

[86] M. Ciobanu, D. Taylor, J. Wilburn, and D. Cliffel, "Glucose and lactate biosensors for scanning electrochemical microscopy imaging of single live cells," *Analytical Chemistry*, vol. 80, no. 8, pp. 2717–2727, 2008.

[87] B. R. Horrocks, D. Schmidtke, A. Heller, and A. J. Bard, "Scanning electrochemical microscopy. 24. enzyme ultramicroelectrodes for the measurement of hydrogen peroxide at surfaces," *Anal. Chem.*, vol. 65, no. 24, pp. 3605–3614, 1993.

[88] D. O. Wipf, F. Y. Ge, T. W. Spaine, and J. E. Bauer, "Microscopic measurement of pH with iridium oxide microelectrodes," *Analytical Chemistry*, vol. 72, no. 20, pp. 4921–4927, 2000.

[89] E. M. Oliveira, S. Beyer, and J. Heinze, "Secm characterization of immobilised enzymes by self-assembled monolayers on titanium dioxide surfaces," *Bioelectrochemistry*, vol. 71, no. 2, pp. 186–191, 2007.

[90] C. Deng, M. Li, Q. Xie, M. Liu, Q. Yang, C. Xiang, and S. Yao, "Construction as well as eqcm and secm characterizations of a novel nafion/glucose oxidase-glutaraldehyde/poly(thionine)/au enzyme electrode for glucose sensing," *Sensors and Actuators B: Chemical*, vol. 122, no. 1, pp. 148–157, 2007.

[91] A. Parra, E. Casero, F. Pariente, L. Vzquez, and E. Lorenzo, "Bioanalytical device based on cholesterol oxidase-bonded sam-modified electrodes," *Analytical & Bioanalytical Chemistry*, vol. 388, no. 5, pp. 1059–1067, 2007.

[92] A. Parra, E. Casero, L. Vazquez, J. Jin, F. Pariente, and E. Lorenzo, "Microscopic and voltammetric characterization of bioanalytical platforms based on lactate oxidase," *Langmuir*, vol. 22, no. 12, pp. 5443–5450, 2006.

[93] M. H. Rhiel, M. B. Cohen, M. A. Arnold, and D. W. Murhammer, "On-line monitoring of human prostate cancer cells in a perfusion rotating wall vessel by near-infrared spectroscopy," *Biotechnology and Bioengineering*, vol. 86, no. 7, pp. 852–861, 2004.

[94] S. S. Ozturk, J. C. Thrift, J. D. Blackie, and D. Naveh, "Real-time monitoring and control of glucose and lactate concentrations in a mammalian cell perfusion reactor," *Biotechnology and Bioengineering*, vol. 53, no. 4, pp. 372–378, 1997.

[95] Y. Xu, J. Sun, G. Mathew, A. S. Jeevarajan, and M. M. Anderson, "Continuous glucose monitoring and control in a rotating wall perfused bioreactor," *Biotechnology and Bioengineering*, vol. 87, no. 4, pp. 473–477, 2004.

[96] V. Vojinovic, F. M. F. Esteves, J. M. S. Cabral, and L. P. Fonseca, "Bienzymatic analytical microreactors for glucose, lactate, ethanol, galactose and l-amino acid monitoring in cell culture media," *Analytica Chimica Acta*, vol. 565, no. 2, pp. 240–249, 2006.

[97] L. Ceriotti, A. Kob, S. Drechsler, J. Ponti, E. Thedinga, P. Colpo, R. Ehret, and F. Rossi, "Online monitoring of balb/3t3 metabolism and adhesion with multiparametric chip-based system," *Analytical Biochemistry*, vol. 371, no. 1, pp. 92–104, 2007.

[98] M. Lehmann, W. Baumann, M. Brischwein, H.-J. Gahle, I. Freund, R. Ehret, S. Drechsler, H. Palzer, M. Kleintges, U. Sieben, and B. Wolf, "Simultaneous measurement of

cellular respiration and acidification with a single cmos isfet," *Biosensors and Bioelectronics*, vol. 16, no. 3, pp. 195–203, 2001.

[99] A. S. Jeevarajan, S. Vani, T. D. Taylor, and M. M. Anderson, "Continuous ph monitoring in a perfused bioreactor system using an optical ph sensor," *Biotechnology and Bioengineering*, vol. 78, no. 4, pp. 467–472, 2002.

[100] A. Radomska, S. Singhal, H. Ye, M. Lim, A. Mantalaris, X. Yue, E. Drakakis, C. Toumazou, and A. Cass, "Biocompatible ion selective electrode for monitoring activity during the growth and cultivation of human cells," *Biosensors & Bioelectronics*, vol. DOI: 10.1016/j.bios.2008.04.026, 2008.

Chapter 2

Materials and methods

2.1 Introduction

The aim of this chapter is to describe the various experimental techniques that were used in the fabrication and characterisation of the electrochemical sensors referred to in chapter 1. It is a detailed overview of the chemical and practical aspects that were imperative when making and testing both the metal–metal oxide (MMO), chemical sensors and the enzyme, biosensors.

Firstly, all the instrumentation and materials used during the course of the work, are detailed. Thereafter the construction of the electrodes and various forms of packaging are discussed. The formation of the analyte specific layers for each of the two different types of sensors are also discussed, along with the chemical basis and necessity of each of the procedures. Methods and techniques used for the characterisation of these surfaces are described. Lastly, the work carried out to monitor cell cultures, both on and off line is elaborated.

2.2 Materials

All the reagents used were AnalaR grade or better. Reagents were used as received, where this was not the case, the preparation steps taken are described in detail. All experiments were performed using 18.2 MΩ water from a Millipore system.

Glucose oxidase [E.C. 1.1.3.4] was obtained from two different sources; each of these was a different formulation:

1. A lypophilised powder from Sigma Aldrich; whose activity was ca. 200 U mg^{-1} of powder. Stock solutions as described in section 2.5 using the specific activity of each individual batch.

2. The enzyme obtained from Biozyme Labs U.K. was in solution and its activity was ca. 8000 U/ml. The enzyme was dissolved in an acetate and phosphate buffer as per the manufacturers specifications shown in Table 2.1.

Reagent	Final concentration
Acetate	100 mM
Phosphate	50 mM
Thiomersal	0.004% w/v
Potassium chloride	250 mM

Table 2.1: Composition of buffer.

2.3 Details of equipment used

2.3.1 Electrochemical instrumentation

All electrochemical measurements and film fabrications were performed on one of the two instruments listed below:

1. μAutolab III from Eco Chemie was used with their proprietary software; General Purpose Electrochemical Software.

2. CHI 1000A from CH Instruments along with their supplied software. This is an 8 channel potentiostat that can be used to monitor and control up to 8 independent channels. All the work here was done in a single electrochemical cell using one counter and reference electrode with multiple working electrodes.

Where necessary the use of a particular instrument has been referred to in the text, although the choice of instrument was based on convenience and ease of use.

The model M370 system, from UniScan Instruments was used for all the SECM analyses. This system consists of a bi-potentiostat that works in combination with a piezo-resistive x-y-z stage.

2.4 Details of the electrochemical cells used

Most of the electrochemical measurements were performed in a three electrode cell; made up of a Ag|AgCl reference electrode, a platinum mesh counter electrode and a working electrode.

The Ag|AgCl reference electrodes were obtained from CH Instruments and used as received.

For quality control purposes the reference electrodes were tested on a regular basis. The test was performed to ensure that the quality of the AgCl film had not deteriorated and that the potentials being supplied in the cell were accurate. A small beaker with 3 M KCl was used as the electrolyte, along with a Saturated Calomel Electrode (SCE), to supply the reference potential. Both the test electrode and the SCE were dipped in the electrolyte and the potential across the two terminals was measured, using a pH meter. The expected potential for this measurement is 24mV and a measured potential within $\pm$10mV of this value was considered acceptable.

If the Ag|AgCl electrode failed the above test, it was regenerated as follows:

1. The AgCl wire was removed from the body of the electrode along with the filling solution.
2. 1M HCl was filled into the body of the electrode using a syringe and the body was immersed in a beaker of 1M HCl for a couple of hours.
3. The HCl was removed and the body was rinsed thoroughly with water.
4. 3 M KCl solution was filled inside the body of the electrode to $\frac{2}{3}^{rd}$ of its height, as per the manufacturers instructions.
5. The AgCl film was abraded from the electrode wire along with any oxidised silver, using a sand paper and then the wire was rinsed using dI water.
6. The clean wire was dipped for a few seconds in a $FeCl_3$ solution to form a new layer of AgCl on its surface.
7. The wire was rinsed and inserted back in to the body of the electrode as soon as possible.
8. The electrode was left to stand over night in 3 M KCl storage solution.

2.4.1 Counter electrode

The counter electrode was made in the lab from of a piece platinum mesh, obtained from Advent Research Materials. The mesh was connected to a piece of copper contact wire, using a small length of 200μm platinum wire as the connector. A platinum wire was used so as to ensure that there was no contamination from other electroactive ions in the electrochemical cell.

2.4.2 Working electrodes

The surfaces of the working electrodes were treated in one of the two ways listed below; this was done to ensure that the quality of the surface could be ascertained and that the measurements were reproducible.

1. Polishing using an aqueous slurry of alumina

    - The surfaces were polished on a nylon pad, sequentially with 1μm, 0.3μm and 0.05μm alumina. In between each stage of polishing the electrodes were placed in an ultrasonic bath for 10 minutes. This method of preparation resulted in a smooth, mirror polished surface.

2. Electrochemical cleaning in 0.5M H_2SO_4

    - The working electrode was repeatedly cycled between +1100 mV and −240 mV for 120 complete cycles.($\dot{v}$ = 50 mV s^{-1})

The glassy carbon electrodes were discs with a 1 mm diameter and were obtained from CH Instruments. The platinum and gold working electrodes were made in the lab, as discussed below.

Fabrication of working electrodes

The large number of sensors that were required in the bio-reactor for on-line measurements meant that the use of commercially fabricated electrodes was not viable. The diameter of the platinum disc electrodes was 250μm and that of the gold disc electrodes was 200μm.

A disc was chosen, because it has a simple geometry and the mass transfer properties for this particular shape are well documented. Therefore it would be possible to use conventional means for the purposes of analyses.

Two key features that had to be controlled during the manufacturing process were:

1. The mechanical robustness of the device.

2. The level of electrical insulation provided along the length of the electrode and the permeability of the film used.

The first sensors were fabricated using a glass capillary as the body of the electrode. The capillary was pulled to a fine tip with a pipette puller and the metal was threaded through its fine end. Once this had been performed a small amount of silver loaded conducting epoxy was placed on the end of a contact wire, typically either copper or silver, which was passed through the capillary until it made contact with the electrode metal. The epoxy was then cured at a high temperature for half an hour. A digital multi-meter was used to test the quality of the electrical connection. To ensure that the glass tip was perfectly sealed a small amount of Super Glue was placed on it. The structure of the electrode was now ready and its schematic is shown in Figure 2.1.

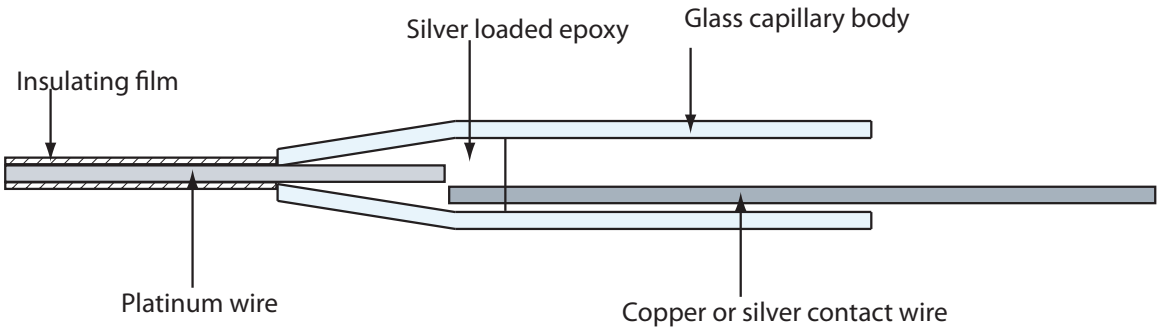


Figure 2.1: A schematic of the working electrodes housed in a glass capillary body.

The insulating film along the length of the electrode, proved to be a little more challenging. The initial plan was to package the electrode in as thin a sheath as possible, while still matching the necessary performance criteria. In order to obtain this, the first insulator that we tried was SU8. This is a negative photoresist, with excellent electrical insulation which is readily available and the curing process takes place under UV light. We thought that one of its biggest advantages was its viscosity, as this would have allowed control of the film thickness. The process used to form the film is described below:

- Fresh piranha solution was prepared, in a fume hood. (This is a 3:1 mixture of

concentrate H_2SO_4 and 30% w/v H_2O_2) WARNING: EXTREMELY CORROSIVE

- The platinum wire was dipped into the piranha solution to remove all traces of organic material. This too was done in a fume hood.
- SU8 was dispensed into a pipette tip using a syringe and needle. The fine end of the pipette tip had a dimater slightly larger than 250 μm.
- The electrode was introduced in to the tip through the fine end and left there for a few seconds.
- It was then withdrawn from the tip along its longitudinal axis. This was done carefully and slowly to avoid damaging the film.
- Finally the electrode was cured under a UV lamp for one minute. The exposure time was critical, as overexposure made the SU8 brittle and prone to cracking.

Cutting the distal tip of the electrode yielded a disc shaped electrode. A schematic of the film formation process can be seen in Figure 2.2.

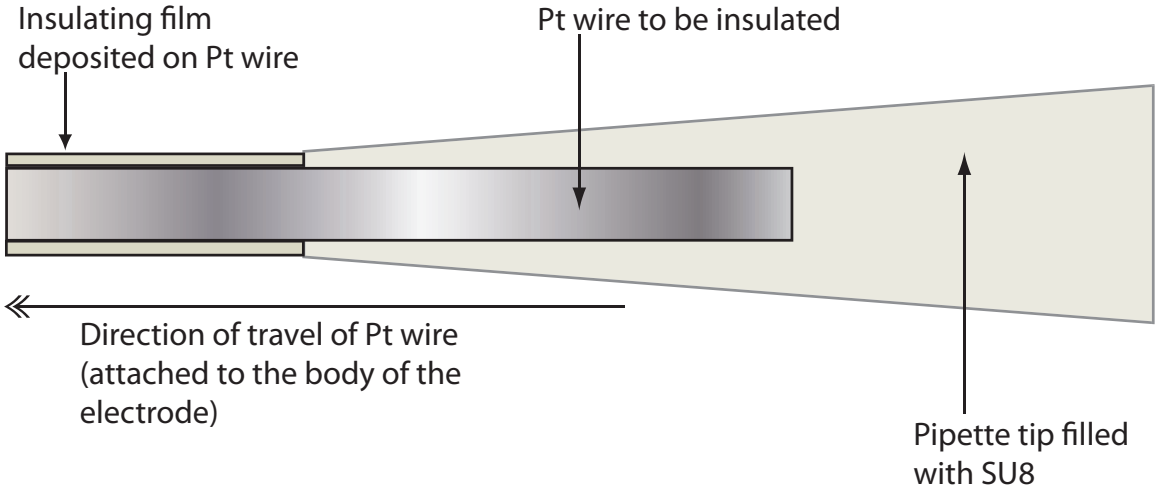


Figure 2.2: Schematic illustrating the method used to form an SU8 layer on the platinum wire.

This method of fabrication was unsuitable because of a number of problems. Primarily, it

was found that the thickness of the film that could be produced with ease, did not provide the necessary electrical insulation. Also, while curing it seemed that the SU8 tended to collect in small 'baubles', probably as a result of its surface tension. As a consequence of the 'baubles' there were lengths of the electrode, where there was little or no insulation. This process lacked consistency and hence could not be used. Figure 2.3 shows the quality of an ideal film and also the films that could actually be produced in this manner.

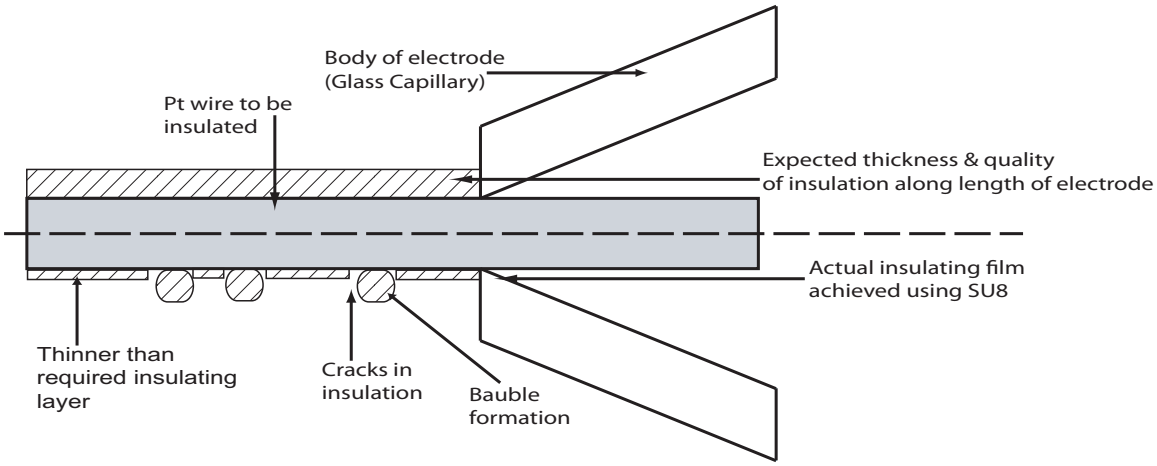


Figure 2.3: Schematic comparing an ideal SU8 film with the inconsistencies of the films that could easily be produced.

In order to achieve both the mechanical robustness and electrical insulation, it was necessary to use a material that closely emulated the insulating and mechanical properties of glass. Glass itself was not a viable option as it is difficult and dangerous to work with. A second epoxy resin which could provide the desired electrical insulation and also gave the electrodes mechanical strength was found. Resin Araldite MY750 and Aradur hardener were procured from Robnor Resins (U.K.) and used as received. The curing mixture was made using two parts resin and one part hardener.

Noble metal wires were wound around a copper contact wire and a small amount of solder was used to hold them in place. This connection was checked before the electrodes were packaged using a digital multi-meter. A sealed 200 μL pipette tip was used as the mould. A syringe was used to fill the pipette tip with the curing mixture. The electrode

and contact wires were inserted into the mould and cured at 100 °C for 90 minutes. Once the electrodes had cooled to room temperature their distal end were cut using a rotating diamond saw; so as to cause minimal damage to the electrodes' surface. Once the electrode was removed from the mould it was polished using alumina, as described earlier, to produce a mirror polished surface.

This was a longer and more involved fabrication but, the quality of the insulation was reproducible and the electrodes mechanically robust. Also, the ability to repeatedly polish the surfaces meant that the electrodes could be reused. A schematic of the construction can be seen in Figure 2.4 and this was the style of construction used for both the gold and platinum electrodes.

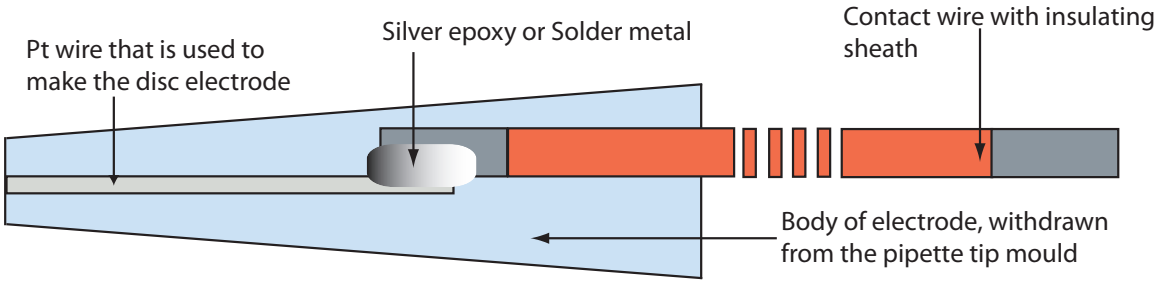


Figure 2.4: Schematic showing the construction of the working electrode.

2.5 Iridium oxide pH electrodes

This section describes in detail, the steps used to form the MMO layer to make pH sensitive devices. Firstly, the synthesis of the iridium oxalate solution and then the method used to generate the iridium oxide layer on the substrates are described. Finally, the surface modifications of the gold substrates are described.

2.5.1 Precipitation solution

The synthesis of iridium oxalate is shown in equation 2.1. The protocol used for this was the same as that described by Yamanaka [1].

$$IrCl_4 \cdot 2H_2O + (COOH)_2 \cdot 2H_2O \longrightarrow [Ir(C_2O_4)_3]^{3-} \tag{2.1}$$

- 150 mg of iridium chloride hydrate was dissolve thoroughly in 100 ml of water by stirring for thirty minutes .
- 1 ml of hydrogen peroxide (30% w/v) was added to this and the solution stirred for another 10 minutes.
- 500 mg of oxalic acid was added and stirred for a further 10 minutes.
- Anhydrous potassium carbonate was added to the mixture, slowly, till the pH of the solution was 10.5.
- Lastly, this solution was left to stand in a dark bottle for 48 hours to stabilise.

2.5.2 Galvanostatic deposition

The gold substrates were prepared by abrasive polishing, providing mirror polished surfaces on which the iridium oxide films were formed.

The precipitation of iridium oxide from iridium oxalate was performed using anodic electrochemical deposition [2]; the reaction is shown in equation 2.2.

$$[Ir(COO)_2(OH)_4]^{2-} \longrightarrow IrO_2 + 2CO_2 + 2H_2O + 2e^- \tag{2.2}$$

A two electrode cell was used, consisting of a 250μm gold disc electrode and a Ag|AgCl reference electrode; in this instance the counter electrode was shorted to the reference. The lack of space in a small volume cell necessitated the use of a two electrode system. The cell

was well stirred, magnetically, to allow the formation of an uniform layer, as reported by Yamanaka [2].

The reported current density during the galvanostatic deposition process is 1.6A m^{-2} [1]. The area of our disc electrodes was calculated as 4.9×10^{-4} cm^2, implying that the currents to be used were of the order of 10^{-8}A. Deposition with this current density resulted in inconsistent devices. To improve the reproducibility currents of the order of 10^{-7}A were used. The relative benefits of each deposition current are discussed later. The films were deposited at room temperature in an air conditioned lab over a period of 600 s.

2.5.3 Surface treatment before galvanostatic deposition

The gold surfaces were prepared to a smooth mirror polish using alumina. It was found that even at the higher current densities there were some inconsistencies in the sensitivities of the electrodes produced. These deviations warranted a closer look at the surface of the substrates to ascertain, whether they could be eliminated. It was thought that the reason for these deviations was a result of variations in the number of nucleation sites that were present on the gold substrates prior to deposition as discussed in more detail in section 3.3.

To increase and control the number of nucleation sites available prior to deposition it was decided to acid etch the polished surfaces. HNO_3 and aqua regia were chosen as the two etching agents; aqua regia would dissolve the gold substrate indiscriminately whereas concentrated HNO_3 would result in a more controlled etch.

Prior to the surface modifications cyclic voltammetry was performed on each of the electrodes. A 5 mM ruthenium hexaamine solution was prepared in 100 mM KCl and degassed with N_2 for 45 minutes. Cyclic voltammetry was performed from -500 mV to $+100$ mV at a scan rate of 100 mV s^{-1}, under a N_2 blanket.

Once the electrodes had been tested, they were placed in a sonic bath with water for a few minutes. Then the surface modifications were carried out as described below.

- Aqua regia etching was carried out by placing the electrodes in 20 ml of aqua regia

for 1 minute. These were then rinsed and sonicated in water for a couple of minutes.

- The electrodes were etched in 10 ml of concentrate nitric acid for 5 minutes. Immediately after the etching they too were rinsed and sonicated in water.

- The electrodes were dipped in a solution containing gold nanoparticles (obtained from Chris Johnson, a colleague in the lab) and then allowed to dry at room temperature for 30 minutes; to deposit a thin film of gold nano-particles on their surface.

Cyclic voltammetry was repeated as before in 5mM ruthenium hexaamine. Thereafter the iridium oxide layer was deposited as described in section 2.5.2.

2.5.4 pH calibration

The open circuit potentials were measured against a SCE. Two different techniques were used to vary the pH and quantify the electrode's responses.

1. A three point calibration using standard pH solutions

    - Three, commercially available, standard solutions of pH: 4.01, 7.00 and 9.21 were used. The devices were dipped into each of the standards respectively. Once a steady state potential had been recorded, they were withdrawn and rinsed with water. Thereafter they were inserted in the next pH standard.

    - This method had various disadvantages

        – A three point calibration curve is not a rigourous calibration. Although, the buffers chosen straddle the region of interest and the response of the sensors was linear, it would be better practice to calibrate the devices using more than three points.

        – This mode of calibration did not tell us much about the transient responses of the electrodes; as the electrodes were removed from one solution and re-inserted into another one.

2. A multiple point pH calibration was used to overcome these weaknesses.

    - 10 mM phosphate buffer was used as the bulk electrolyte.
    - 100 mM HCl and NaOH were titrated into the buffer to obtain a multiple point calibration plot.
    - Prior to testing the iridium oxide electrodes, a freshly calibrated glass pH probe and meter were used to record the pH values after the addition of each aliquot of acid or alkali. As an example, the volumes of each of the aliquots and the resulting pH values, as obtained from the glass electrode are shown in Table 2.2. Iridium oxide electrodes were subjected to identical titrations and the data used to make the required calibration curves.

Reagent	Volume added / (μl)	pH
	0	7.19
100 mM HCl	450	6.88
	1000	6.17
	1000	3.19
100 mM NaOH	500	4.51
	1000	6.57
	1000	7.10
	1000	7.87
	500	9.39

Initial volume of 10mM Phosphate buffer = 50 ml.

Table 2.2: Sample, set points for pH calibration of iridium oxide electrodes, as obtained from a glass electrode.

2.6 Redox mediated enzyme sensors

The redox mediators used were based on the osmium containing polymers described by Forster and Vos [3]. The synthesis of these polymers and their incorporation into enzyme sensors is discussed here.

2.6.1 Synthesis of the metallopolymer

The metallopolymer chosen as a redox mediator in this work was poly(vinylimidazole) (PVI) complexed with [osmium–(4,4'- dimethoxy-2,2'-bipyridine)Cl] (Os–dmo-bpy). A three step synthesis was used.

1. The synthesis and purification of the poly(vinylimidazole) (PVI) backbone.
2. Synthesis and purification of the osmium complex. Synthesised by modifying a chloro osmium salt with the required organic ligands.
3. Attaching the osmium complex to the polymer backbone and collecting the product.

Synthesis and purification of PVI

The synthesis of PVI is an addition reaction, where the carbon–carbon double bond from the vinyl group forms the new covalent bonds between individual monomer units, as shown in Figure 2.5. The polymerisation is aided by the use of an initiator, which was 1,1'–azobis(cyclohexanecarbonitrile). 6 ml of vinylimidazole was added to 500 mg of the initiator in a round bottom flask. The polymerisation reaction was carried in an inert atmosphere and a well stirred vessel, at 70 °C for 2 hours [3].

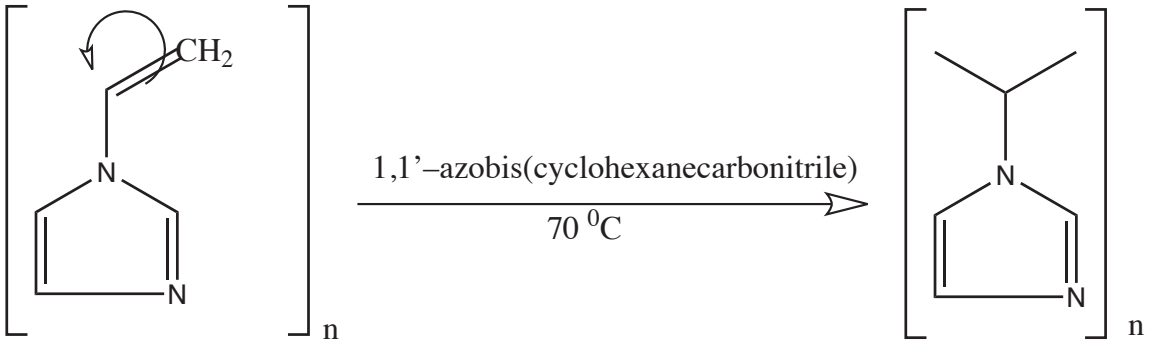


Figure 2.5: Reaction scheme showing the polymerisation of vinylimidazole.

On removal from the water bath and once the flask had cooled to room temperature, 10 ml of methanol was added to the reaction vessel and stirred rapidly for 15 to 20 minutes,

or until the dark yellow precipitate had dissolved completely. The resulting solution was added, drop-wise, to 200 ml of vigourously stirred acetone. This was then filtered under vacuum using a 0.45 μm filter paper on top of a glass frit. The purification process was repeated twice.

After the final purification, the polymer obtained was weighed and made into a 100 mg ml^{-1} stock solution in ethanol.

Synthesis of the osmium complex

This synthesis is a substitution reaction, where the ammonium and chloro groups from ammonium hexachloro-osmate are replaced by the dimethoxy-bipyridine (dmo-bpy) ligands. The reaction scheme can be seen in Figure 2.6.

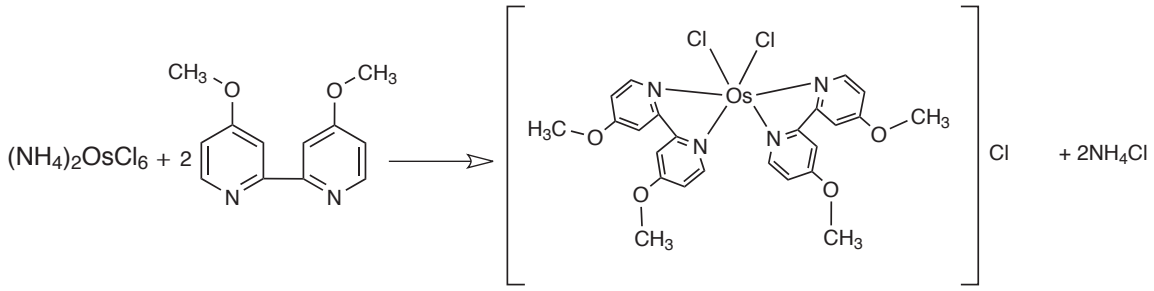


Figure 2.6: Scheme for the synthesis of Dichlorobis(bipyridine)osmium(III)chloride. Modified from [4]

The reaction was carried out, as reported by Taylor et. al.[5], in ethylene glycol. Stoichiometric amounts of dmo-bpy and $(NH_4)_2OsCl_6$ were added with a marginal excess of the former. The solution was degassed with argon for 45 minutes and the reaction carried out at 200 °C for 1 hour. When the vessel had cooled to room temperature 10 ml of 1M sodium dithionite solution was added. This reduced the complex as shown by the reaction scheme in Figure 2.7, allowing it to precipitate [4]. The reaction mixture is stirred for 3 minutes in an ice bath and then filtered under vacuum. Post filtration the residue was collected and allowed to dry overnight at room temperature.

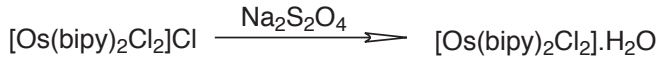


Figure 2.7: The reaction scheme for the precipitation of the osmium complex, in the presence of sodium dithionite [4].

Attaching the osmium complex to PVI

The coupling of the osmium complex and the polymer backbone is also a substitution reaction, as shown by the reaction scheme in Figure 2.8. The synthesis was carried out as reported by Forster and Vos. [3]. 104 mg of PVI and 57 mg of Os–(dmo-bpy) were added to 100 ml of absolute ethanol and degassed with N_2. This mixture was then refluxed in a 70 °C water bath for 72 hours, after which it was allowed to cool to room temperature. Thereafter it was filtered through a 0.45 μm filter paper under vacuum. The filtrate was then added drop-wise into a large volume of, vigourously stirred, diethyl ether, allowing the product to precipitate. Decanting the supernatant left the purified compound.

Finally, the precipitate was dissolved in a small volume of ethanol and decanted into a vessel of known weight. The ethanol was then extracted to ascertain the weight of Os–(dmo-bpy)-Cl synthesised. This was then made in to a stock solution with a known concentration and stored at 4 °C.

2.6.2 Surface immobilisation

There are a number of methods that have been reported to immobilise similar osmium complex metallopolymers and glucose oxidase on the electrodes' surfaces to form analyte specific films. This work concentrates on the use of two of these methods:

1. A covalently bonded film using a functionalised PEG. The PEG forms epoxide bonds between the osmium complex, itself and glucose oxidase.

2. Concurrent entrapment in an electrodeposition paint that is precipitated on the electrode surface by decreasing the local pH.

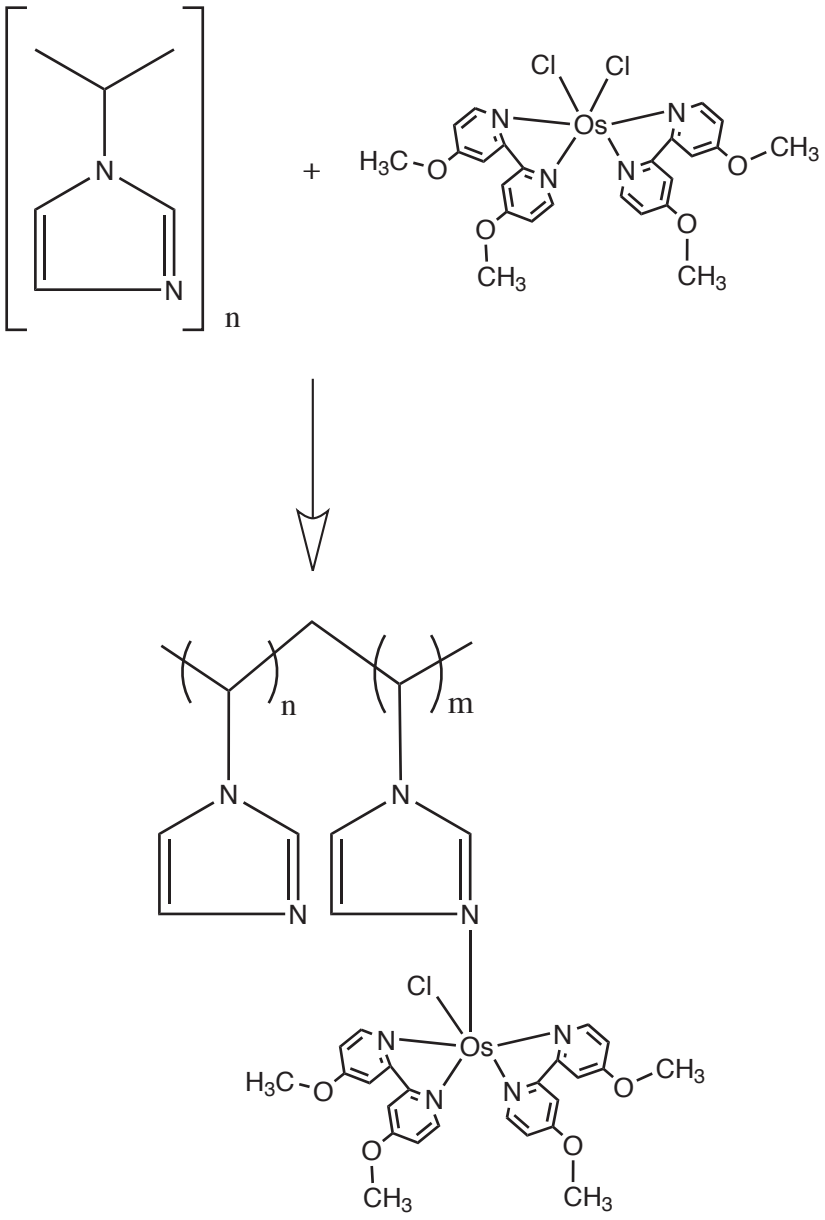


Figure 2.8: Reaction scheme showing the synthesis of Os(dmo-bpy)Cl–PVI from its two independent constituents. Modified from [6].

Reagent	Volume/(μl)	Concentration/(mg ml^{-1})
Osmium complex	2	20
PEGDGE	1	5.6
Glucose Oxidase	1	16
Total	4	

Table 2.3: Volumetric ratios and concentrations of the components of the curing mixture.

Covalent immobilisation

A functionalised poly(ethylene glycol) (PEG) was used to form epoxide bonds between the amides of the enzyme and imidazole ring of the polymer backbone, as shown in the reaction scheme in Figure 4.1. Table 2.3 shows the ratios and concentrations that made up the 4μl aliquot, that was dispensed on to the surface of the glassy carbon electrode. The film, once deposited, was allowed to cure at room temperature for up to 36 hours.

Encapsulation in an electrodeposition paint

The encapsulation of the redox mediator and enzyme was performed using an electrodeposition paint (EDP) that precipitated out of an aqueous solution when the pH of the solution was lowered. The EDP is a colloid of alkyds and acrylates that destabilise at low pH [7].

In readiness for the encapsulation the electrodes were prepared by polishing with alumina. Thereafter the procedure described below was used to load the enzyme and redox mediator:

- A 10 mg ml^{-1} solution of the Osmium complex was prepared in water and 10 μl of this was deposited on the electrode surface and allowed to dry at room temperature.
- In the mean time a 75 μl_{stock} ml^{-1}_{water} Resydrol solution with 120 U ml^{-1} glucose oxidase was prepared.
- The pH of this solution was adjusted to 7.10 using 100 mM HCl.

- The solution was then allowed to incubate at 4 °C for 30 minutes.

A small volume cell was fashioned for the glassy carbon electrode, with the dried osmium complex film. The electrode sat in the cell face up and the cell was fashioned using a 1.5 ml Eppendorf tube. The conical end of the Eppendorf tube was cut so that the electrode would be a snug fit. Then the electrode was carefully inserted in to this end and held in place vertically with a clamp. The two electrode cell was completed by dispensing 100 μl of the resydrol and enzyme solution on the working electrode and using a Ag|AgCl wire as the quasi–reference electrode; the cell arrangement can be seen in Figure 2.9

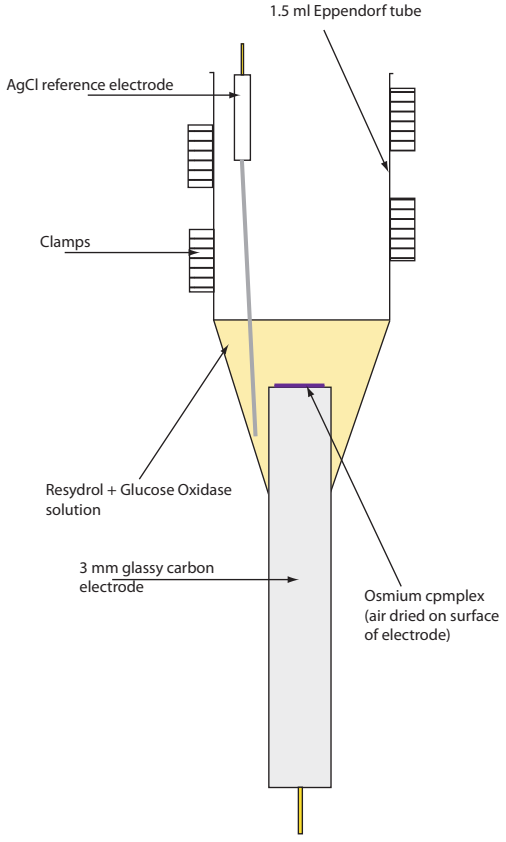


Figure 2.9: Small volume cell used to precipitate resydrol on glassy carbon electrode; not to scale.

To perform the deposition, an electrochemical pulse technique was employed to decrease the pH in the vicinity of the electrode surface [7]. The potentials were pulsed for 20 cycles,

with a profile as shown in Figure 2.10:

1. +2200 mV for 0.2 s
2. +800 mV for 1 s
3. 0 mV for 5 s

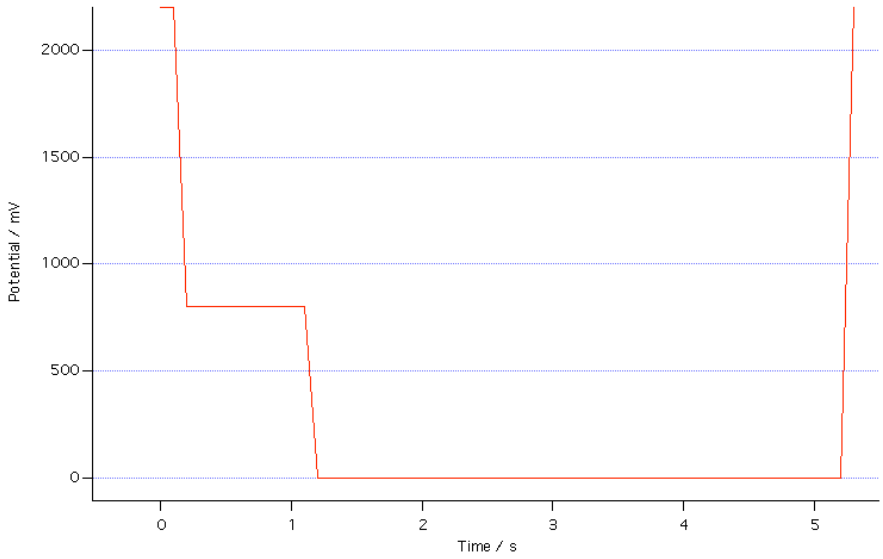


Figure 2.10: Potential pulse profile used to precipitate Resydrol.

2.7 Enzyme films encapsulated in poly(phenol)

Enzyme electrodes were made by encapsulating glucose oxidase in a poly(phenol) layer deposited electrochemically, using cyclic voltammetry. Enzyme from both the sources, mentioned earlier, were used for these sensors and the formulation obtained from Biozyme was used as received. The powder from Sigma–Aldrich was solubilised in an acetate buffer, the particulars of which are shown in Table 2.4.

In both cases, the protocol was similar and involved two steps. Firstly, the enzyme was allowed to preadsorb on the electrode surface after which poly(phenol) was formed on

Reagant	Concentration	Vol. added
Sodium phosphate dibasic	500 mM	5 mL
Thiomersal	2%	100 μL
Sodium acetate (pH=3.9)	500 mM	As required to adjust the pH to 4.5
Sodium acetate (pH=4.5)	500 mM	As required to make up acetate conc.
KCl	3 M	4.17 mL
dI	–	To make up to 50 mL

Table 2.4: Protocol to make enzyme buffer

Enzyme Source	Reagent	Stock concentrations	Pre–adsorption solution	Polymerisation solution
Sigma	Glucose oxidase	10,000 U ml^{-1}	667 U ml^{-1}	667 U ml^{-1}
	Phenol	50 mM	0 mM	25 mM
	PBS	100 mM	100 mM	100 mM
Biozyme	Glucose oxidase	7,500 U ml^{-1}	500 U ml^{-1}	500 U ml^{-1}
	Phenol	50 mM	0 mM	25 mM
	PBS	100 mM	100 mM	100 mM

Table 2.5: Preparation of the pre adsorption and polymerisation solutions.

it. The stock and final concentrations of each of the reagents that constituted the pre–adsorption and polymerisation solutions are shown in Table 2.5.

The electrodes were prepared by abrasive polishing. Once ready, they were placed in a beaker containing the pre–adsorption solution. The sensors were left to incubate in the solution for up to 2 hours. The phenol solution was always freshly prepared, but it was allowed to incubate with the enzyme, at room temperature, for up to an hour before use.

Phenol was polymerised on the electrode surface using cyclic voltammetry in a three electrode cell, using the μAutolab III. The conditions used for the cyclic voltammetry are shown in Table 2.6. Once prepared the electrodes were rinsed and placed in 100 mM PBS, over night, to allow any loosely bound enzyme to wash away from their surfaces; after this they were ready to be tested.

Particular	Condition
Initial Potential	+200 mV
Time held at initial potential	10 s
1^{st} switching potential	+200 mV
2^{nd} switching potential	+1000 mV
Polarity of 1^{st} scan	Positive
Scan rate	10 mV/s
No. of scans	3

Table 2.6: Conditions used for cyclic voltammetry to polymerise phenol.

2.8 Testing the sensitivity of the devices for glucose

The response of all the devices to glucose was tested using chronoamperometry. The potential used depended on the configuration of the sensor and the electrochemical species that was being sensed. In each case, the chosen potential sat in the plateau region of the current, so as to ensure that the response of the sensor was purely limited by mass transfer. This meant using an oxidation potential at least 150 mV more positive than the peak potential. Before any measurements were taken the electrodes were left in a polarised state for 180 seconds. This was to ensure that the charging and Cottrell currents had dissipated.

As with the MMO, pH sensors, a multi point calibration was conducted, by titrating a 1 M glucose solution in to the cell. All measurements were carried out in a cell that was mildly stirred with a magnetic stirrer. The initial volume of the cells was either 10 ml or 50 ml of 100mM PBS.

2.9 Study of the film morphology

The structure and the morphology of the poly(phenol) encapsulated glucose sensors was studied using optical and electrochemical techniques.

2.9.1 Optical studies

FT-IR and Raman spectroscopy were used to interrogate the electrode surface to analyse the composition of the film. In both cases the substrate was a home made platinum disc electrode with a diameter of 1 mm. A bigger electrode was chosen here, so that a larger area would be available to map. As both instruments had conventional optical stages, a simple modification was made to hold the cylindrical electrode in place and perpendicular to the optical beam.

A 10 mm thick, sheet of poly(methyl-methacrylate) was cut to the same shape and size of conventional glass slides. After removing the backing paper two of these were dipped in to a beaker containing chloroform. After a short while, both pieces were removed from the beaker and held together tightly, by hand. Once the chloroform had evaporated, both pieces were joint together and we had a slide with a thickness of ca. 20 mm. This slide was held in place on the stage of a pillar drill and a hole the exact size of the electrode body drilled into it. The thickness of the slide and the use of a pillar drill ensured that the electrode was stable on the optical stages and also perpendicular to the beam.

Platinum electrodes with just a layer of poly(phenol) and with an enzyme encapsulated layer were mapped using both these techniques.

2.9.2 Electrochemical studies

The electrochemical behaviour of the enzyme sensors was studied using transition metal complexes as probes.

Cyclic voltammetry

A 10 mM solution of potassium ferrocyanide was used to study the morphology of the film. In the first instance poly(phenol) was polymerised on the surface of a 1 mm platinum disc electrode and this electrode was cycled in the above solutionn between -150 mV and $+400$ mV at a scan rate of 100 mV s^{-1}.

Thereafter, a poly(phenol) film which incorporated the enzyme was studied using the same method, for seven days.

Scanning electrochemical microscopy

The SECM probes used were 100 μm and 5 μm diameter platinum discs (RG $\simeq$ 15). The probes were prepared for use by electrochemical cleaning in H_2SO_4. Prior to area scans being conducted, the procedure used to position the stage was:

1. Cyclic voltammetry of hexacyanoferrate(II) with 100 mM KCl as the supporting electrolyte. This was the redox couple used for the succeeding two steps as well.
2. Negative feedback approach curves, on the insulator, to set the initial height of the probe.
3. Line scans in the x and y directions, to determine the starting co-ordinates of the map.

SECM area scans were conducted on three different substrate configurations, as shown in the list below:

1. Bare platinum disc electrode with a 1 mm diameter.
2. Platinum disc electrode with a poly(phenol) film
3. Platinum disc electrode with glucose oxidase encapsulated in a poly(phenol) film

In order to study the morphology of the film, the machine was operated in substrate generation and probe collection mode. Two redox couples were used for these maps, as described below:

1. Hexacyanoferrate(II)
    - The substrate was used to electrochemically generate the oxidised form of the species and the probe current interrogated the reduction current

2. Glucose

   - Glucose solution was used as the bulk electrolyte and the probe was used to oxidise the H_2O_2 produced by the enzymatic reaction on the substrate.

2.10 Off-line media analysis

HL-Cardiomyocyte cells were cultured in T-25 flasks in a temperature and CO_2 controlled environment. All the tests described were performed once the cells had become confluent and were split. Cells were cultured in Claycomb Media; this is a proprietary media obtained from JRH Biosciences. Only a few details are known about the concentration of the media and these are shown in Table 2.7.

Reagent	Final concentration
Claycomb Media	n/a
Fetal Bovine Serum	10%
Penicillin : Streptomycin	100 Uml : 100 μg ml^{-1}
Norepinephrine	0.1 mM
L-Glutamine	2 mM
Glucose	22.55 mM

Table 2.7: Composition of Claycomb Media. (As per the manufacturers' specifications)

Two different tests were carried out for the off-line analysis. The first test was a preliminary experiment to ascertain the viability of off-line analysis. Here a 500 μl aliquot was withdrawn from the T-flask on a daily basis and its glucose concentration was tested. Amperometric measurements using non-mediated sensors were conducted on the raw media, these were repeated once the raw media had been diluted with 100 mM PBS. The measurements were performed for 200 s at +700 mV after the Cottrell current had been allowed to dissipate for 180 s.

Once the plausibility of the off-line analysis had been confirmed, a second test was

conducted on the same cell line, using two different cultures grown concurrently. One culture was used as the control and it was grown under normal conditions with its media being changed daily. The second culture vessel was set up as normal, but the media in this vessel was not changed or replenished during the course of the experiment.

Samples for the measurements were acquired on a daily basis from both cultures. The waste media from the control culture was used and the sample form the second culture was a small aliquot withdrawn from it. In both cases the glucose concentration was measured using the raw sample and dilutions. The dilutions were made using a per sample judgement.

2.11 Sensor performance *In-Vitro*

The following steps were carried out, sequentially, *in-vitro*:

1. Toxicity tests of the sensors

2. Life time analysis of the sensors in the culture

2.11.1 Toxicity tests

Four culture vessels were set up for a 7 day culture of fibroblasts, cell type 3T3. The cultures were carried out in Dulbecco's Modified Eagle's Media at 37 °C. Two of the vessels were kept as controls and no sensors were placed in them. Four sensors were placed in each of the other two culture vessels. All four vessels were seeded with 20,000 cells and the yield and viability were assessed at the end of the culture.

2.11.2 Life time of sensors *in-vitro*

Eight sensors were fabricated using glucose oxidase and poly(phenol) as described earlier and these were subjected to the same calibration process. As above four cultures were set up, this time each of the 4 vessels had 2 sensors placed in them. After the start of the culture period the sensors were withdrawn from each vessel on days 1, 2, 3 and 7.

Once the sensors had been removed from the culture they were calibrated using the same procedure as in section 2.8. In addition to this each pair of sensors was also tested as follows, in the interim they were stored in 100 mM PBS:

1. Sensors 1 and 2 on days 2, 3 and 7. They were also tested twice on day 2
2. Sensors 3 and 4 on days 3 and 7. These too were tested twice on day 2.
3. Sensors 5 and 6 on day 7.

In order to assess the effects of fouling a similar analysis was performed using a smaller probe. Changes in the sensitivity of the sensors to H_2O_2 was tested, once they had spent time *in-vitro*. Each of the sensors was calibrated for its response to H_2O_2 before being placed *in-vitro* and their responses were tested once they were removed from the culture on days 1, 2 and 3.

The specific concentration of H_2O_2 used, was calculated prior to each titration using $KMnO_4$. The H_2O_2 was diluted 10 times in dI and 2 ml of 4M H_2SO_4 was added to it. Then 20 mM $KMNO_4$ was titrated into the solution. This was repeated three times. These steps are described in more detail along with the calculations in chapter 7.

2.12 Summary

This chapter described the equipment and the experimental techniques that were employed during the course of this work. For the electrochemical experiments, experiment specific conditions are mentioned at the relevant places in the succeeding chapters. The optimisation process that allowed us to arrive at the conditions in this chapter are also described in more detail where applicable.

References

[1] K. Yamanaka, "The electrochemical-behavior of anodically electrodeposited iridium oxide-films and the reliability of transmittance variable cells," *Japanese Journal of Applied Physics Part 1-Regular Papers Short Notes & Review Papers*, vol. 30, no. 6, pp. 1285–1289, 1991.

[2] K. Yamanaka, "Anodically electrodeposited iridium oxide-films (aeirof) from alkaline-solutions for electrochromic display devices," *Japanese Journal of Applied Physics Part 1-Regular Papers Short Notes & Review Papers*, vol. 28, no. 4, pp. 632–637, 1989.

[3] R. J. Forster and J. G. Vos, "Synthesis, characterization, and properties of a series of osmium-containing and ruthenium-containing metallopolymers," *Macromolecules*, vol. 23, no. 20, pp. 4372–4377, 1990.

[4] D. A. Buckingham, F. P. Dwyer, and H. A. Goodwin, "Mono- and bis-(2.2'-bipyridine) and (1,10-phenanthroline) chelates of ruthenium and osmium," *Australian Journal of Chemistry*, vol. 17, pp. 325–336, 1964.

[5] C. Taylor, G. Kenausis, I. Katakis, and A. Heller, "Wiring of glucose-oxidase within a hydrogel made with polyvinyl imidazole complexed with [(os-4,4'-dimethoxy-2,2'-bipyridine)cl]$^{(+/2+)}$," *Journal of Electroanalytical Chemistry*, vol. 396, no. 1-2, pp. 511–515, 1995.

[6] T. J. Ohara, R. Rajagopalan, and A. Heller, "Glucose electrodes based on cross-linked [os(bpy)(2)]$^{(+/2+)}$ complexed poly(l-vinylimidazole) films," *Analytical Chemistry*, vol. 65, no. 23, pp. 3512–3517, 1993.

[7] C. Kurzawa, A. Hengstenberg, and W. Schuhmann, "Immobilization method for the preparation of biosensors based on ph shift-induced deposition of biomolecule-containing polymer films," *Analytical Chemistry*, vol. 74, no. 2, pp. 355–361, 2002.

Chapter 3

Iridium oxide pH sensors

3.1 Introduction

In this chapter I will discuss the steps taken to optimise the fabrication of iridium oxide sensors for pH measurement. The formation of a reproducible iridium oxide layer on gold substrates and a possible method of improving the performance is discussed. An attempt at increasing the number of nucleation sites on the gold surface is studied; this should aid the precipitation of iridium oxide from the iridium oxalate in solution.

3.2 Optimisation of film production

All iridium oxide electrodes were made on 250 μm diameter discs, giving each electrode a surface area of 4.19×10^{-4} cm^2. The reported current density for galvanostatic deposition is 0.1 mA cm^{-2} [1]. This value was used to calculate the current for deposition, which is 4.19×10^{-8} A, as described in section 2.5.2. Figure 3.1 shows the performance of the iridium oxide film prepared using the reported current density. Of the four sensors that were deposited under these conditions, two showed no responses to changes in pH [sensors 3 and 4]. The other two exhibited reproducible changes, although when their calibration curve is analysed the responses are seen to be sub-Nernstian, Figure 3.2. As a comparison, a super-Nernstian

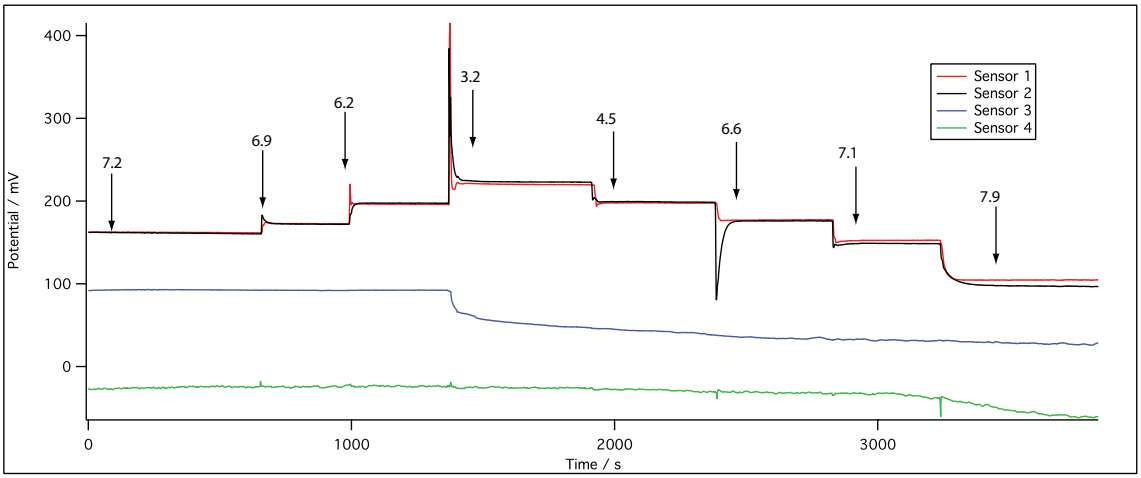


Figure 3.1: Trace showing the open circuit potential of four sensors with iridium oxide deposited using a current density of 0.1 mA cm^{-2}, during a pH titration. The inset labels show the pH of the bulk electrolyte as measured by a glass electrode after the addition of each aliquot of acid or base.

sensor has been shown in the same figure and the responses to pH from this current density are perceptibly different. The slopes of sensors 1 and 2 are -20.5 mV $decade^{-1}$ and -18.8 mV $decade^{-1}$, respectively. The responses of these sensors indicated that the precipitation

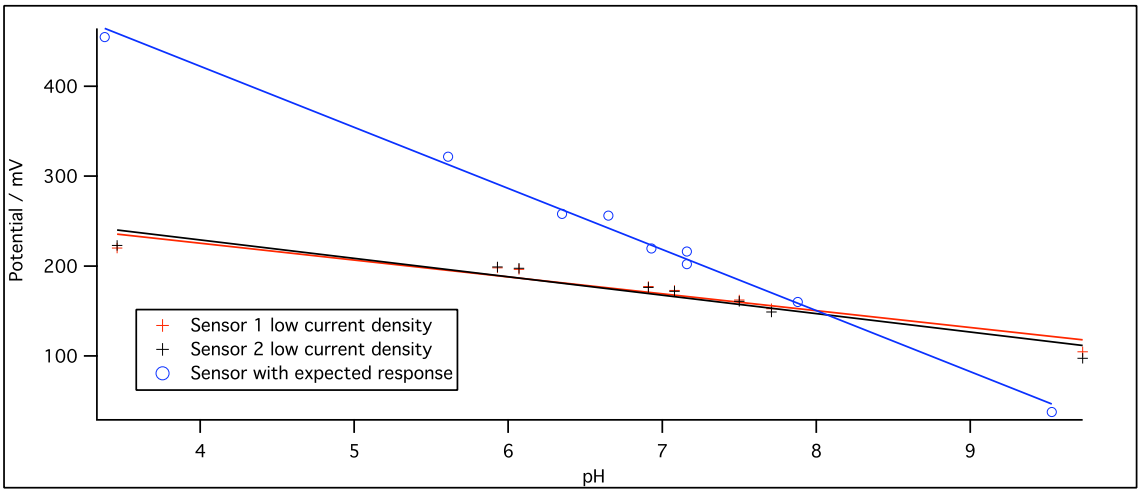


Figure 3.2: Calibration curves for iridium oxide deposited at 0.1 mA cm^{-2}. The potentials were read from the potential–time trace after the addition of each aliquot once steady state had been reached. The sensor with the expected Super-Nernstian response was prepared under optimal conditions and show that the responses of sensors 1 and 2 are weak.

of iridium oxide did not yield films that were capable of showing super-Nernstian responses, probably as a result of their crystal structure. It has been reported that the current density required for iridium oxide precipitation on platinum is higher than that needed for gold, which is in the region of 0.5 - 1 mA cm^{-2} [2]. Therefore in order to try and rectify the weaker responses of sensors 1 and 2, a higher current density was used.

The same report also indicates that the surface structure is an important feature in determining the efficiency of the precipitation of iridium oxide. The films prepared by Yamanaka [1], were on an inidium-tin oxide substrate, so it was thought that a higher current density might be required for our films. Therefore, deposition at a current of 3.14 $\times 10^{-7}$ A was attempted; this equates to a current density of 0.6 mA cm^{-2}.

The calibration curves for devices made using galvanostatic deposition at 3.14 $\times 10^{-7}$ A can be seen in Figure 3.3 and the operating characteristics are shown in Table 3.1. Sensors 3 and 5 show an excellent super-Nernstian response to changes in pH. The three other sensors do not exhibit such a high response to pH, although they are well matched to each other.

It was found that this new set of conditions resulted in too much intra-batch variability, so a current density exactly one order of magnitude higher than reported by Yamanaka [3] was tried. The operating characteristics of these devices can be seen in Table 3.1. Figure 3.4 shows data from sensors 1 and 3, which were made by galvanostatic deposition at 4.19 $\times$ 10^{-7} A (10 A m^{-2}). The responses of sensor 3 are smaller than those for sensor 1. In fact the response from sensor 3 is very sub-Nernstian and this feature can be seen repeated in the calibration curves of Figure 3.5. Sensors 1 and 4 show a well matched and super-Nernstian response.

Protocol	Mean slope \ mV pH^{-1}	Mean intercept
0.6 mA cm^{-2}	-63 $\pm$ 13.3	579.2 $\pm$ 103.7
1 mA cm^{-2}	-49 $\pm$ 14.7	431.5 $\pm$ 193.4

Table 3.1: Operating characteristic of the iridium oxide deposition. ($n = 6$)

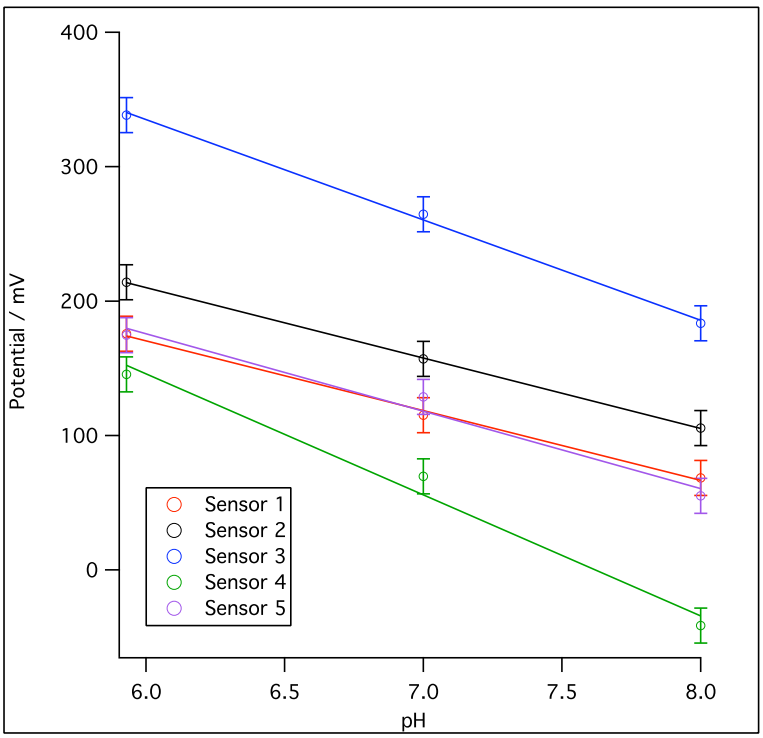


Figure 3.3: Three point pH calibration curves for five different iridium oxide sensors. The iridium oxide films were deposited galvanostatically with a current density of 0.6 mA cm^{-2} on 200μm gold disc electrodes.

The increased current density does impart some operating benefits to the electrodes, made at a deposition current density of 10 A m^{-2}, although the data in Table 3.1 shows them to be less reproducible than those made at 0.6 mA cm^{-2}. The number of failed sensors made at this higher deposition current was greater than with those deposited at 1 mA cm^{-2}. The variation in the intercept of Figure 3.1 is described toward the end of this chapter.

Altering the deposition current had made it possible to produce iridium oxide films with improved operating characteristics. However the spread in their responses was still appreciable and it was thought prudent to try improve the precision of the sensors. Hitchman and Ramanathan have reported that thicker iridium oxide films give better responses to changes in pH and more reproducible behaviour [4], so surface modification of the substrates prior to deposition may help in achieving this.

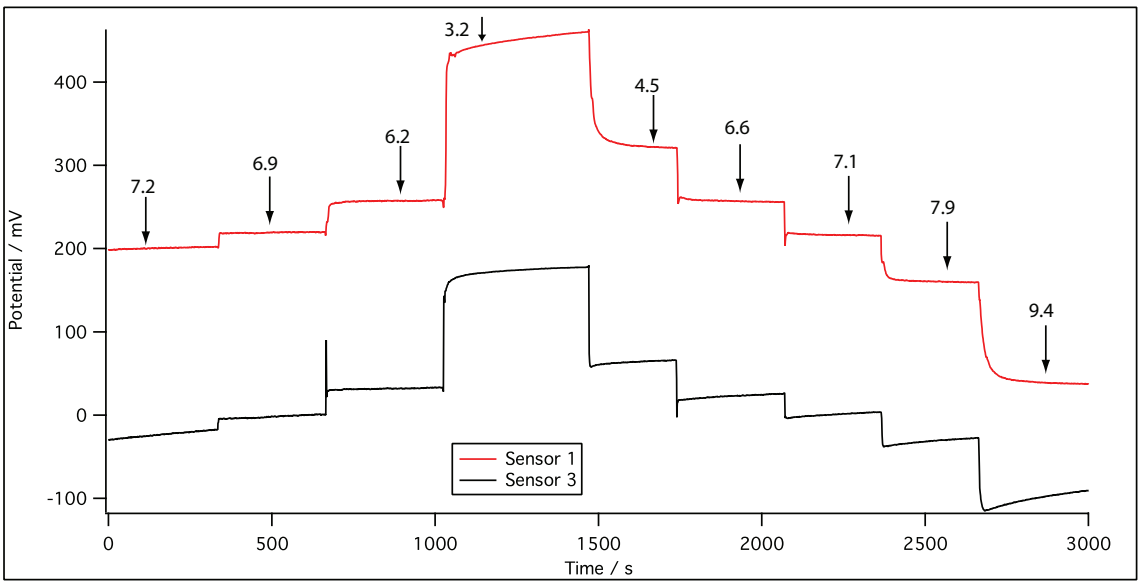


Figure 3.4: Trace showing the open circuit potential of iridium oxide sensors deposited at a current density of 10 A m^{-2}. The inset labels indicate the pH of the cell after the addition of each aliquot of acid or base.

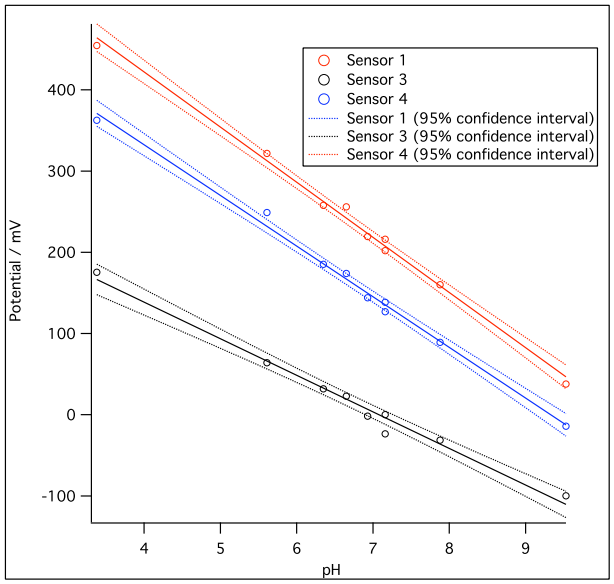


Figure 3.5: Calibration variations with the new protocol, using a current density of 10 A m^{-2} for galvanostatic deposition of iridium oxide on gold substrates.

3.3 Surface treatment to improve iridium oxide film characteristics

The optimised protocol developed in section 3.2 resulted in iridium oxide sensors with a super-Nerstian response, but there was still some inter and intra batch variation in their

responses. It was thought that this may be due to a non uniform number of nucleation sites being available to initiate the precipitation reaction, shown in equation 3.1. Firstly, I shall discuss the steps taken to alter the gold surface of the electrode and then I will discuss the quality of the sensors that were formed as a result.

$$[Ir(COO)_2(OH)_4]^{2-} \longrightarrow IrO_2 + 2CO_2 + 2H_2O + 2e^- \tag{3.1}$$

3.3.1 Surface Modification

An attempt was made to increase and control the number of nucleation sites that were available on the gold surface for use in the precipitation reaction. Three different methods were tried to achieve this:

- Acid etching using concentrated nitric acid
- Acid etching using aqua regia
- Physisorbing gold nanoparticles on the surface

The mechanism for the dissolution of gold in aqueous media has been discussed by Marsden and House [5]. The overall dissolution of gold relies on the formation of complex ions with suitable complimentary groups such as cyanides, chlorides and other halides [6]. The overall mechanism as reported by Geoffroy and Cardarelli is shown in equation 3.2 [6].

$$Au^0 + 4HCl + HNO_3 \rightarrow HAuCl_4 + NO + 2H_2O \tag{3.2}$$

The step wise mechanism proposed by Marsden and House states that probably both the Au(I) and Au(III) chloride complexes are formed in solution, as shown in equation 3.3 [5]. In the first step a Au(I) chloride ion is formed at the surface of the gold, which is then oxidised stage wise to the Au(III) ion [5]. The authors propose that the role of nitric acid

in aqua regia is to act as a strong oxidising agent to facilitate the formation of Au(I) ions.

$$\begin{aligned} 2Au + 2Cl^- &\rightleftharpoons 2AuCl + 2e^- \\ AuCl_2^- + 2Cl^- &\rightleftharpoons AuCl_4^- + 2e^- \end{aligned} \tag{3.3}$$

Cyclic voltammetry of ruthenium hexaamine(III) was used to study the gold surfaces, both before and after each surface treatement. The conditions for cyclic voltammetry have been described in section 2.5.3. In most cases the cyclic voltammograms (CVs) did not show any significant differences before and after treatments; figures 3.6, 3.7, 3.8 and 3.9 show CVs for each of the three treatments. Acid etching with nitric acid showed some surfaces were unaffected, figure 3.8 but in another instance the redox currents were shown to increase, figure 3.9.

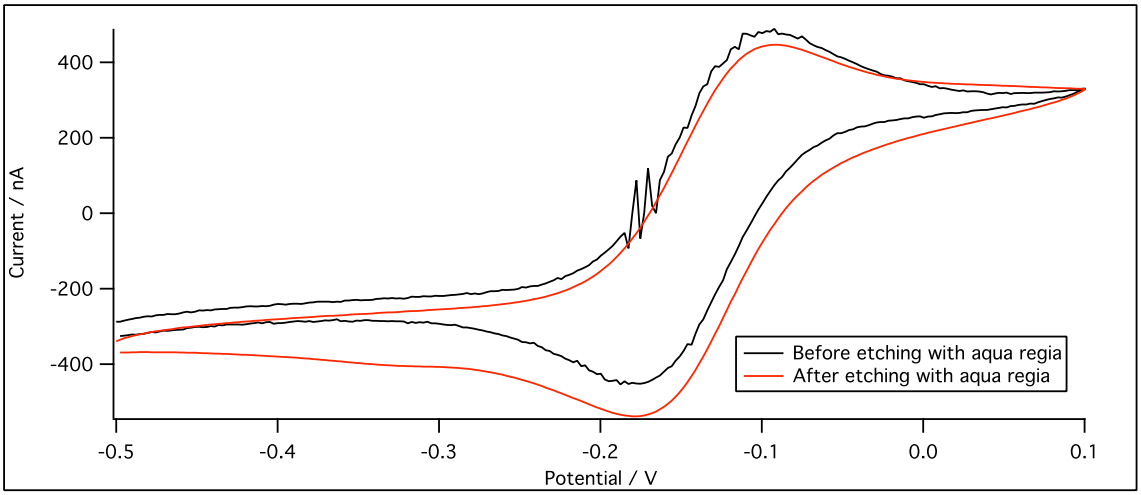


Figure 3.6: CVs of 5 mM ruthenium hexaamine(III) in 100 mM KCl at a scan rate of 100 mV s^{-1} that show the comparison between the surfaces of the gold disc electrodes before and after etching with aqua regia.

Increased peak currents for both the reduction and oxidation scans shows that acid etching has had an effect on the polished gold surface, although a single instance may not be significant. Later it will be shown what effect, if any, this particular surface had on the performance of the iridium oxide layer. A comparison of the peak currents for each

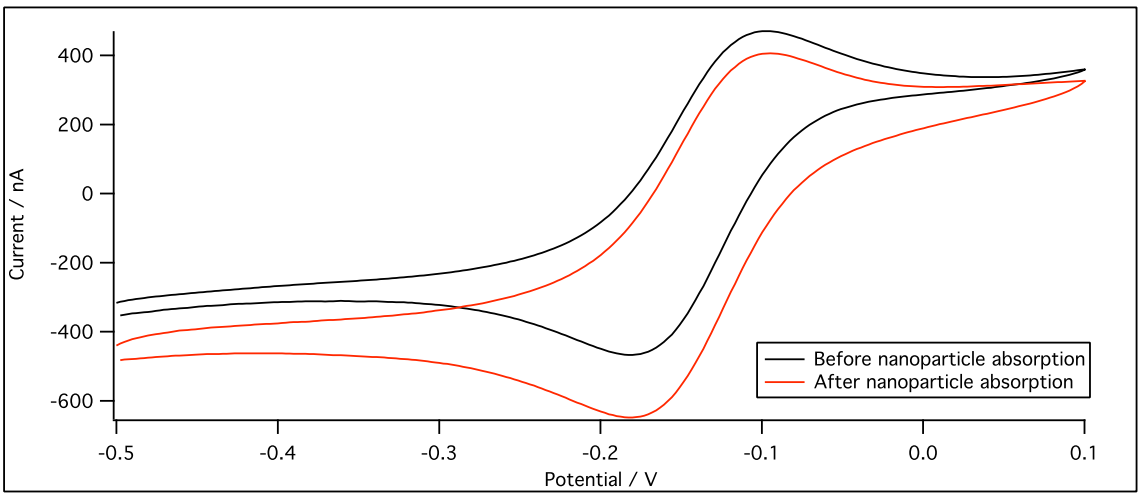


Figure 3.7: CVs of 5 mM ruthenium hexaamine(III) in 100 mM KCl at a scan rate of 100 mV s^{-1} that show the comparison between the surfaces of the gold disc electrodes before and after the physisorption of gold nano-particles.

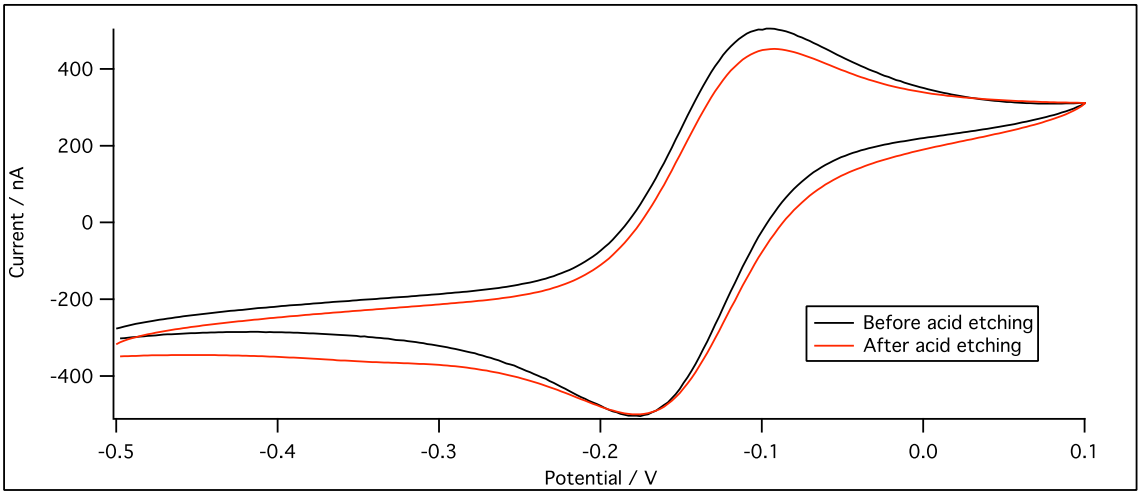


Figure 3.8: CVs of 5 mM ruthenium hexaamine(III) in 100 mM KCl at a scan rate of 100 mV s^{-1} that show the comparison between the surfaces of the gold disc electrodes before and after etching with nitric acid.

of the surface treatments can be seen in figure 3.10. This clearly indicates that each of the three treatments did not alter the surface characteristics or area in a manner that can be picked up, purely, with the aid of cyclic voltammetry. The surfaces have changed in a manner that does not affect the diffusion profile of the electrode, nor does it affect the sites

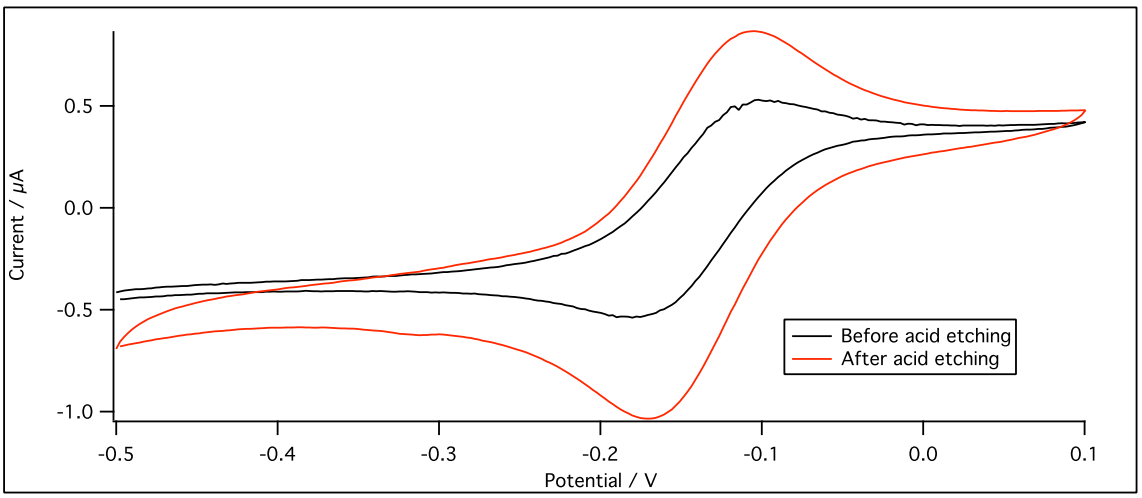


Figure 3.9: CVs of 5 mM ruthenium hexaamine(III) in 100 mM KCl at a scan rate of 100 mV s^{-1} that show the comparison between the surfaces of the gold disc electrodes before and after etching with nitric acid. The surface of this electrode indicates that the acid etching increased its surface area.

that are available for electron transfer to ruthenium. One of the primary reasons for using ruthenium hexaamine as the probe redox couple was that it is not affected by the oxide content on the electrodes surface. Its electrochemical behaviour is less affected by surfaces of heterogeneous termination, than some of the other redox couples that might be used.

One piece of information that might indicate changes in the surface of the electrode is the double layer capacitance (C_d). As cyclic voltammetry is a transient potential process, the steady state current from a CV can be used to estimate C_d, as shown in equation 3.4 [7].

$$i_{ss} = v.C_d \tag{3.4}$$

The C_d of the electrode is much more sensitive to changes on its surface, than the apparent peak currents. The data clearly shows that each of the treatments carried out on the gold surfaces resulted in an increase in their double layer capacitance, Figure 3.11. Both the nanoparticle treatment and etching with nitric acid resulted in a comparable increase in the electrodes' capacitive behaviour. This change was less on the surfaces etched with aqua

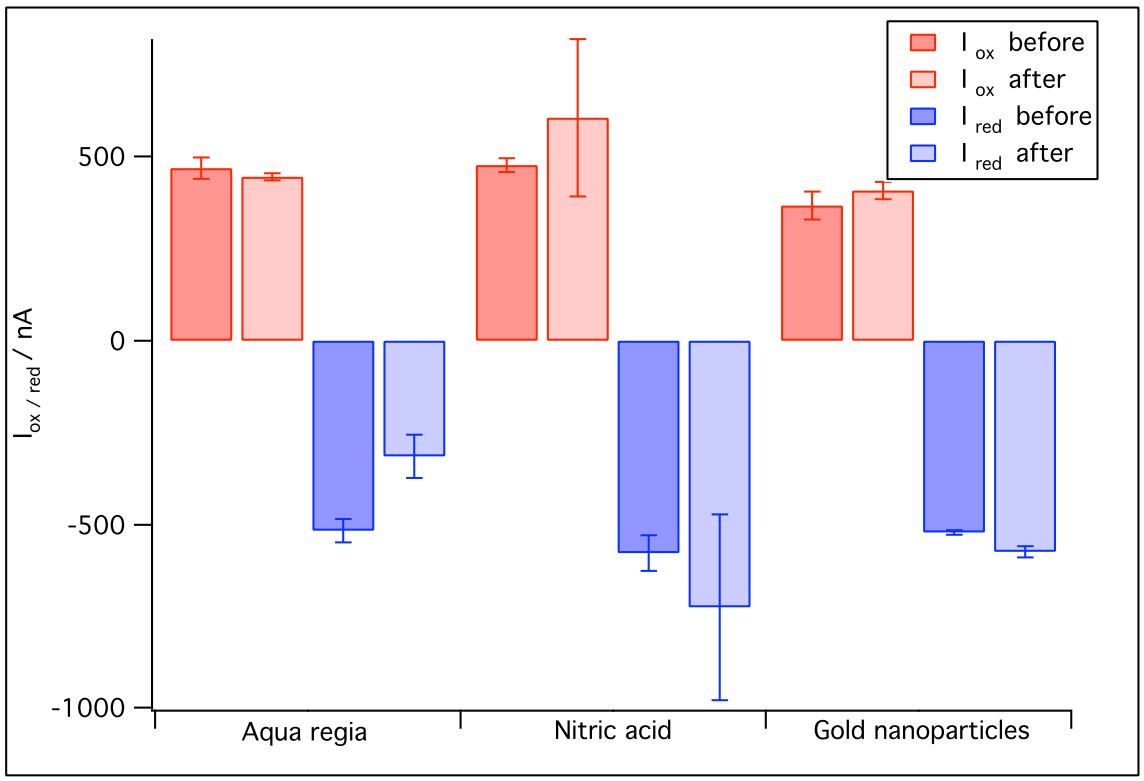


Figure 3.10: Changes to the peak oxidation and reduction currents as seen from 5mM ruthenium hexaamine(III) CVs before and after each of the surface treatments used.

regia. This may be because etching with aqua regia occurs indiscriminately and possibly the length of time used to etch the surface resulted in the formation of a well. In contrast, the controlled etch using nitric acid would have resulted in a large number of very small etched sites, thereby resulting in a larger increase in capacitance. Similarly the physisorption of gold nanoparticles alters the structure of the surface, resulting in an increased C_d.

The change in capacitance results from a change in the surface area of the electrode, the charge storage capacity and the dielectric constant, equation 3.5. The estimation we have used does not allow us to separate the reason for this increase in capacitance, into its individual parts; but each of these terms is dependant on each other. A thorough study of the surface, using techniques such as SEM, impedance spectroscopy and chronoamperometry, would be the only method to accurately assess the surface area of the gold surface. The

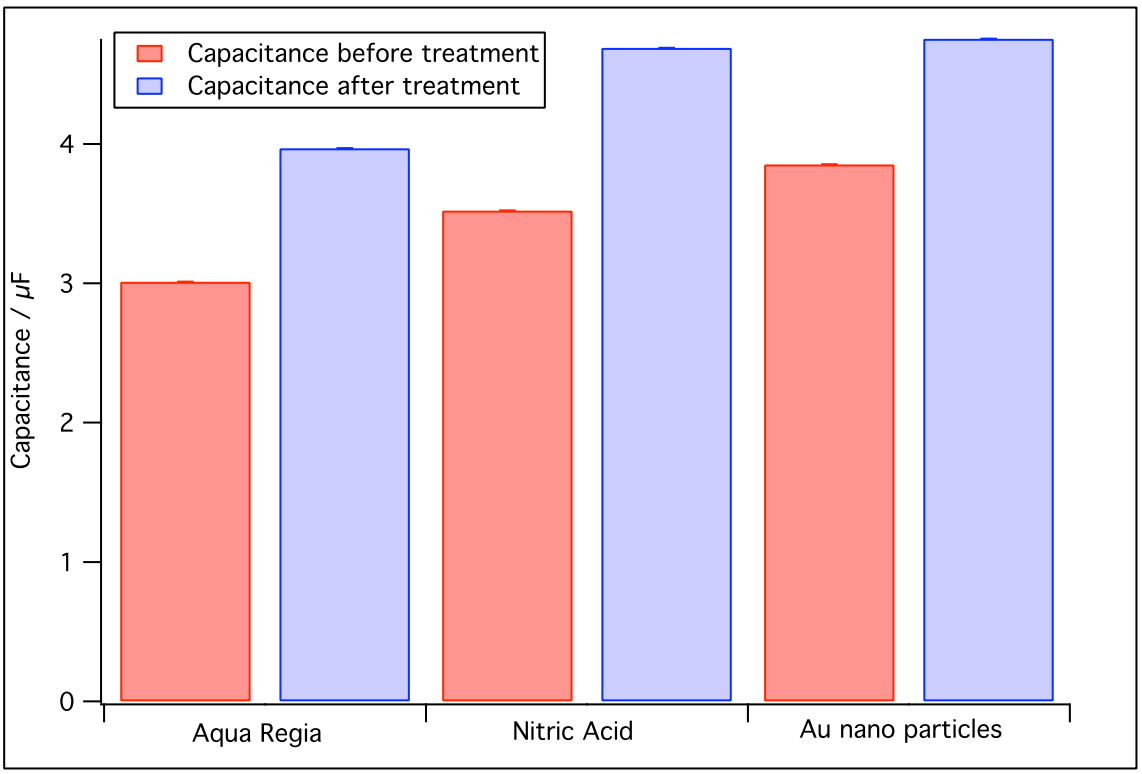


Figure 3.11: Comparison of the C_d of the gold electrodes before and after each surface treatment.

use of a.c. voltammetry too, will allow the separation of the Faradaic and non-Faradaic components of the current.

$$C_d = \frac{\epsilon_o.\epsilon_r.A}{d} \tag{3.5}$$

The increases in capacitance are not easily seen in the peak currents, I_p, of cyclic voltammograms as they are not due to an increase in area alone. The 30% increase is caused by a change in $\epsilon_r.A$, therefore the change in surface area can not be quantified with any greater accuracy, than shown above.

Using the capacitance it is possible to be certain of a change in the surfaces of the treated gold electrodes. Therefore, it is still to be seen whether these new nucleation sites will improve the precipitation and formation of iridium oxide, allowing for the production of sensors with smaller deviations in operating characteristics.

3.3.2 Sensor performance

As mentioned previously each of the sensors produced were subject to calibration and their performances were then analysed. The surface treatment may have introduced new nucleation sites on the gold, but do these new sites affect the quality of the iridium oxide film that is formed? The deposition procedure for the films was the one that had been optimised for the untreated gold surfaces. The two important parameters to judge the effectiveness of adding a process to the production would be the sensitivity of each electrode and their accuracy.

For each of the production methods, figures 3.12, 3.13, 3.14, 3.15 and 3.16 are sample calibration curves. These are a fair representation of the electrodes that were tested. Figure 3.16 show calibration curves for the same untreated sensors as used in figure 3.15, but with 1% nafion deposited on them as a protective layer. The sensor characteristics are shown

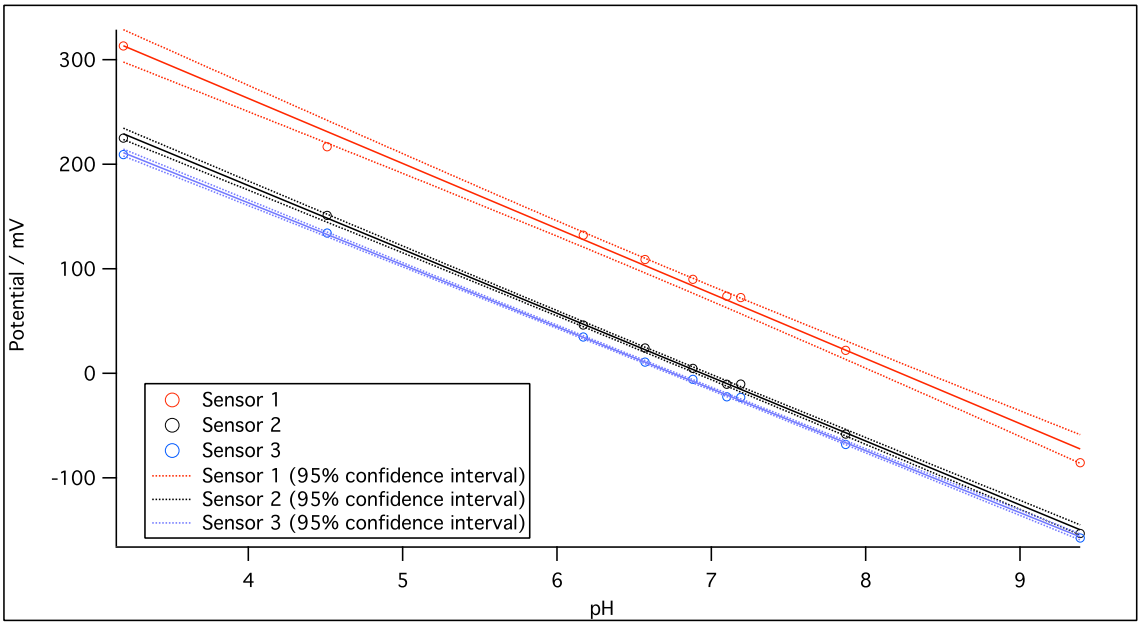


Figure 3.12: pH calibration curves for iridium oxide electrodes, prepared on 200μm gold disc electrodes etched with aqua regia.

in Table 3.2; where it can be seen that each of the four electrode types showed super-Nernstian responses, although there were still some intra-batch variabilities. The variation

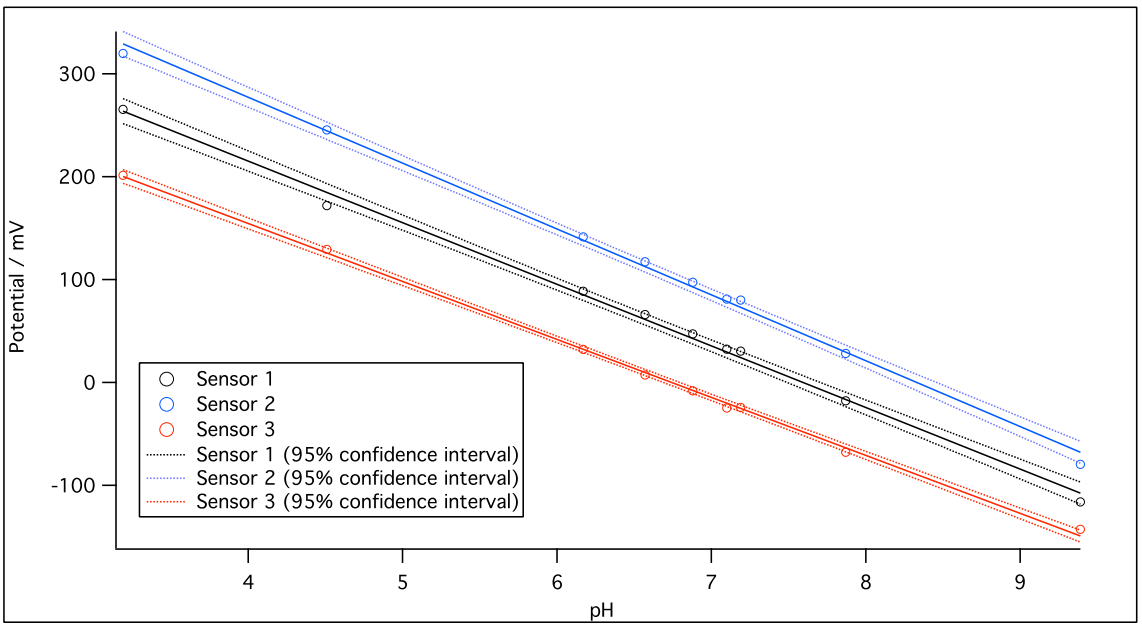


Figure 3.13: pH calibration curves for iridium oxide electrodes, prepared on 200μm gold disc electrodes etched with nitric acid.

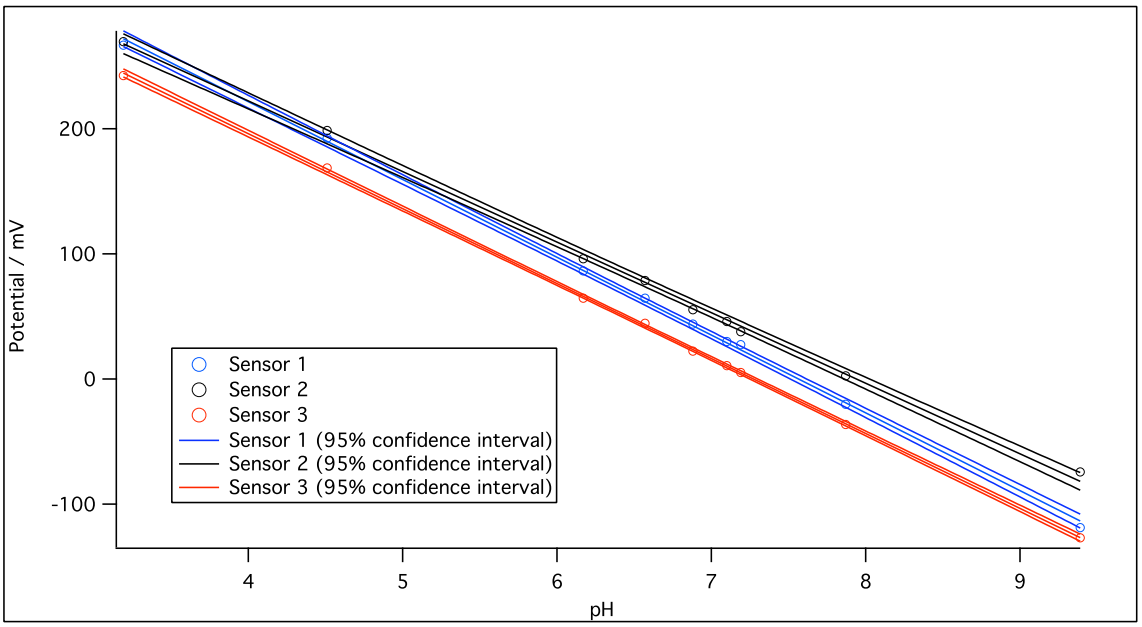


Figure 3.14: pH calibration curves for iridium oxide electrodes, prepared on 200μm gold disc electrodes with gold nanoparticles physisorbed on their surfaces.

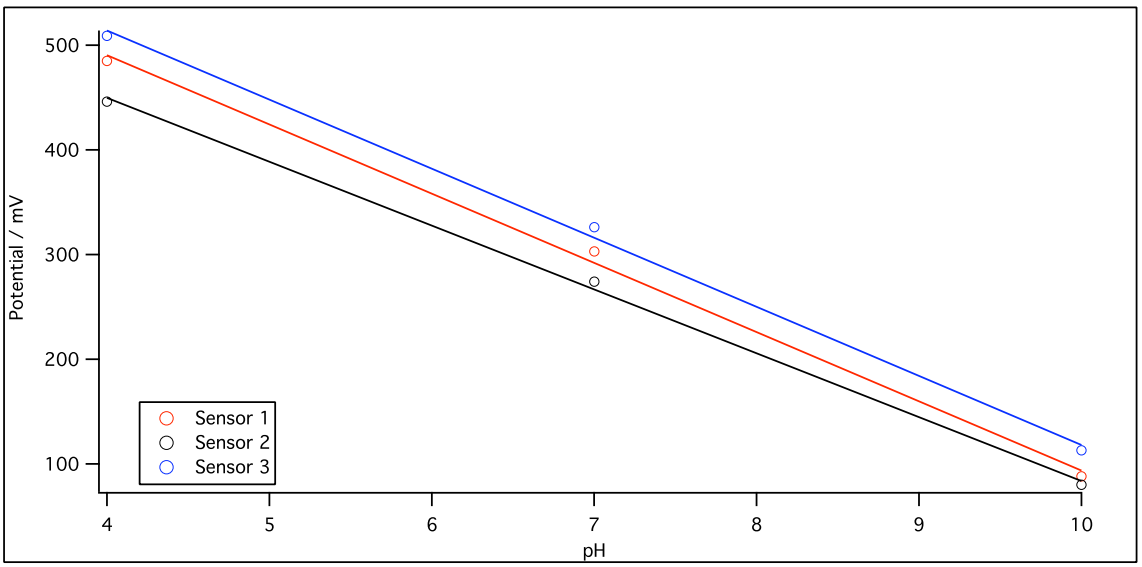


Figure 3.15: pH calibration curves for iridium oxide electrodes, prepared on 200μm polished gold disc electrodes.

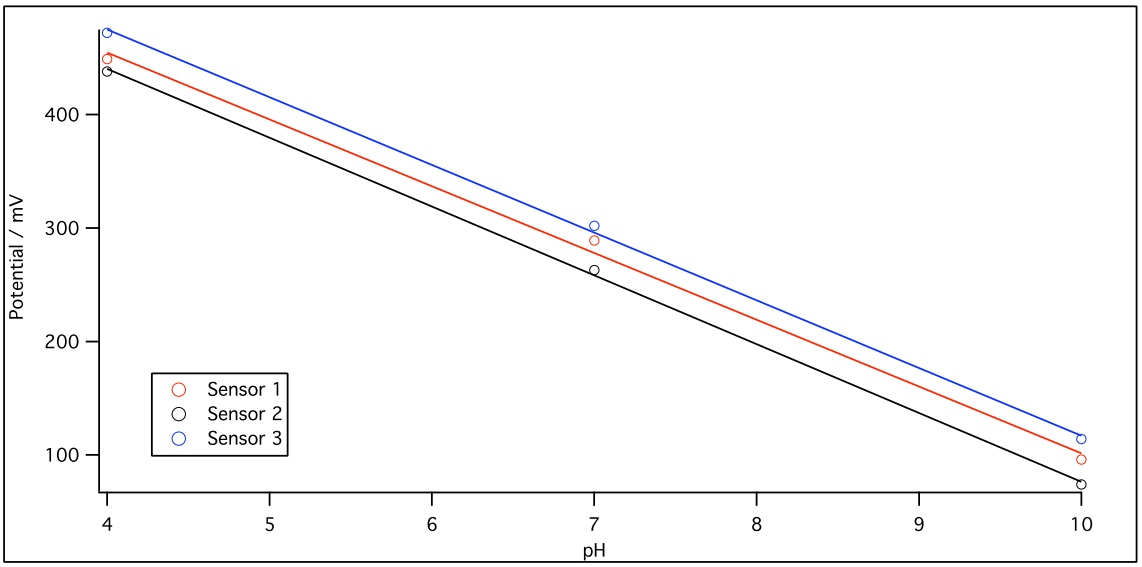


Figure 3.16: pH calibration curves for iridium oxide electrodes, prepared on 200μm polished gold disc electrodes with a 1% nafion film deposited as a protective layer.

in slope is represented in figure 3.17, here it can be seen that the mean response from all electrodes types is super-Nernstian. The effect of each surface treatment was analysed using at least four different devices, all made in the same batch. We know that nitric

Surface treatment	Mean slope / mV pH^{-1}	Mean intercept / mV
Aqua regia	-62.29 ± 2.53	502.69 ± 100.49
Nitric acid	-57.69 ± 5.72	433.25 ± 77.4
Gold nanoparticles	-60.68 ± 5.19	495.11 ± 109.24
No treatment	-66.35 ± 2.1	748.09 ± 26.86
No treatment + nafion	-60.63 ± 2.69	690.04 ± 26.15

Table 3.2: Operating characteristics of pH sensors

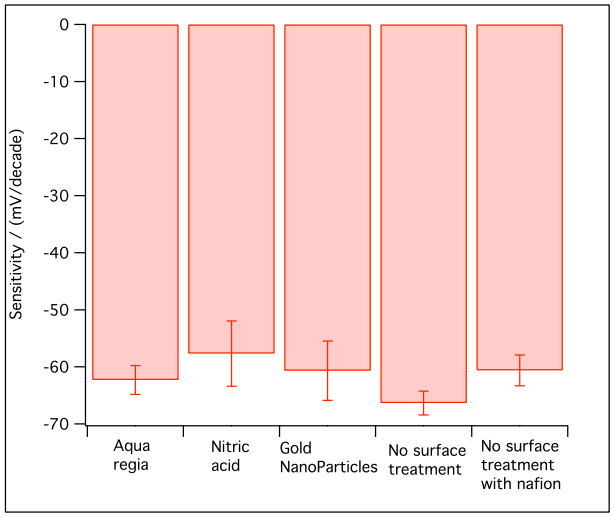


Figure 3.17: Variations in the sensitivity to pH for each type of electrode preparation technique.

acid treatment produces the least sensitive devices and that the other two treatments yield better responses. There is still some variation in the devices that have been treated with gold nanoparticles. When treated surfaces are compared to untreated surfaces that have been very carefully prepared, their responses were found to be similar. When compared to the sensors described earlier (operating characteristics defined in table 3.1), these untreated surfaces show increased and more precise responses. A more important point to note is the very small standard deviation for the untreated surfaces. These two points in tandem indicate that careful preparation of the gold surfaces will yield devices that exhibit super-

Nernstian responses and these responses will be more reproducible.

The presence of chloride (Cl^-) ions in the solution causes the iridium oxide to become soluble iridium chloride [8]. This is harmful for the sensors as it decreases their sensitivity, due to the deterioration in the iridium oxide film structure. Marzouk et. al. have reported the use of a nafion film on the iridium oxide sensor that minimises the degradation. They achieved this by dip coating the sensors in a 5% solution of nafion and then curing the film [2]. We formed a similar film of nafion by dip-coating the electrodes in a 1% solution of nafion. Moussy and Harrison have reported that the use of nafion films inhibits the degradation of Ag|AgCl electrodes when implanted in tissue, they mention that Cl^- exclusion is a result of a mass transport barrier and charge exclusion [9]. O'Hare et. al. refute this and report that even the use of nafion did not exclude Cl^- from the surface of the iridium oxide , although the presence of the layer resulted in no significant changes in the sensitivities of the electrode when in chloride containing media [8]. This would mean that Cl^- ions can enter the iridium oxide layer and form soluble iridium chloride, but due to size exclusion, the iridium chloride does not cross the nafion barrier. As a result, the crystal structure of the iridium oxide film can not degrade indefinitely. We too noticed that the presence of nafion did not result in the degradation of the performance of the iridium oxide films.

Finally it is worth considering the y-intercept for each of the calibration curves. Each of the electrodes that were made after surface modifications show vastly different intercepts, as seen in table 3.2. There are two possible reasons for this discrepancy between devices. Firstly the Debye length which, is a potential off-set that exists at the metal–solution interface, or possible differences at the substrate–iridium oxide interface. The Debye length is represented by equation 3.6 and the parameters affecting it are ionic strength (I), dielectric constant (ϵ_0) and permittivity of free space (ϵ_r).

$$\kappa^{-1} = \sqrt{\frac{\epsilon_0 \epsilon_r kT}{2N_A e^2 I}} \tag{3.6}$$

As each of the sensors from each batch were calibrated together none of these parameters

will result in these intra-batch variations, this means that the off-sets probably arise due to changes in potential at the gold–iridium oxide interface. O'Hare et. al. also speculate about the effect that the supporting substrate has in establishing the open circuit potential, although they to do not propose any reasons for this [8]. This observation is supported by the fact that the untreated electrodes, both before and after treatment with nafion, exhibit very small vertical off-sets combined with similar slopes.

The surface treatment of the gold substrate does yield super-Nernstian pH sensors and they tend to give reproducible data, but the same can also be true for untreated gold surfaces. If due care and attention is taken when preparing exacting surfaces then there is no need to add an extra step during the production of these iridium oxide electrodes. Also the surface treatment tends to introduce changes to the substrate that exhibit themselves during the calibration process and these are undesirable when large numbers of sensors are to be used.

3.4 Summary and Conclusions

Iridium oxide sensors show an excellent super-Nernstian response to changes in pH and are viable for use *in-vitro*. If the surfaces of the substrate are prepared with due care, then the performance of the entire batch is found to be super-Nerstian and the sensors sensitivities are very well matched to each other.

Each of the three treatments used on the gold surfaces showed some changes to their surface characteristics. Cyclic voltammetry on its own is not sensitive enough to be able to pick up these small surface variations. To achieve a better understanding of these treatments and the effect that they have on the gold surfaces, these surfaces need to be studied in more detail. The addition and control of nucleation sites does affect the precipitation of iridium oxide, but the addition of another process in the fabrication procedure is not warranted if substrates of equivalent quality can be readily prepared.

References

[1] K. Yamanaka, "Anodically electrodeposited iridium oxide-films (aeirof) from alkaline-solutions for electrochromic display devices," *Japanese Journal of Applied Physics Part 1-Regular Papers Short Notes & Review Papers*, vol. 28, no. 4, pp. 632–637, 1989.

[2] S. A. M. Marzouk, S. Ufer, R. P. Buck, T. A. Johnson, L. A. Dunlap, and W. E. Cascio, "Electrodeposited iridium oxide pH electrode for measurement of extracellular myocardial acidosis during acute ischemia," *Analytical Chemistry*, vol. 70, no. 23, pp. 5054–5061, 1998.

[3] K. Yamanaka, "The electrochemical-behavior of anodically electrodeposited iridium oxide-films and the reliability of transmittance variable cells," *Japanese Journal of Applied Physics Part 1-Regular Papers Short Notes & Review Papers*, vol. 30, no. 6, pp. 1285–1289, 1991.

[4] M. L. Hitchman and S. Ramanathan, "Evaluation of iridium oxide electrodes formed by potential cycling as pH probes," *Analyst*, vol. 113, no. 1, pp. 35–39, 1988.

[5] J. O. Marsden and I. House, *The Chemistry of Gold Extraction*. SME, 2006.

[6] N. Geoffroy and F. Cardarelli, "A method for leaching or dissolving gold from ores or precious metal scrap," *Journal of the Minerals, Metals & Materials Society*, vol. 57, no. 8, pp. 47–50, 2005.

[7] A. J. Bard and L. R. Faulkner, *Electrochemical Methods: Fundamentals and Applications 2nd ed.* J. Wiley, 2001.

[8] D. O'hare, K. H. Parker, and C. P. Winlove, "Metal-metal oxide pH sensors for physiological application," *Medical Engineering & Physics*, vol. 28, no. 10, pp. 982–988, 2006.

[9] F. Moussy and D. J. Harrison, "Prevention of the rapid degradation of subcutaneously implanted Ag|AgCl reference electrodes using polymer-coatings," *Analytical Chemistry*, vol. 66, no. 5, pp. 674–679, 1994.

Chapter 4

Glucose sensors mediated by an osmium complex metallopolymer

4.1 Introduction

The use of transition metal complexes as mediators for enzyme sensors lowers the operating potential of the sensors and improves their linear range. Due to these two advantages it was decided to employ the 'wiring' of the enzyme to an osmium complex metallopolymer. The first reports of the synthesis of these molecules was by Forster and Vos in 1990 [1]. Since then the use of these molecules has been widely reported in the literature [2, 3, 4].

In this chapter the combination of these polymers and glucose oxidase is discussed along with the structure of the films and the operating characteristics of the devices. Two different methods of film fabrication are discussed along with the problems encountered when employing each method.

4.2 Covalent attachment.

The primary mode of 'wiring' glucose oxidase and the transition metal complex is by the formation of epoxide bonds between the amine group of the enzyme and the polymer backbone, as represented in Figure 4.1 [3]. The films were prepared by curing a mixture of the enzyme, polymer and functionalised cross linker on the surface of 3 mm glassy carbon disc electrodes, as described in Table 2.3.

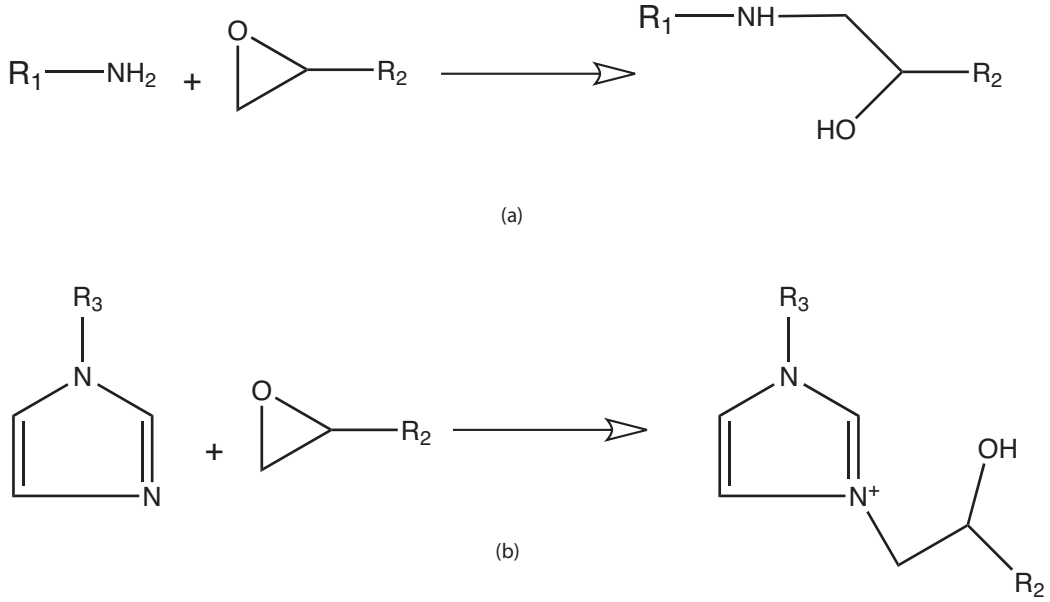


Figure 4.1: Scheme showing the formation of the epoxide bonds between (a) the amine group in the enzyme and the functional end of the PEG, (b) the free nitrogen on the vinylimidazole pendant and the functional group of the PEG. [5]. Where: R_1 represents the remainder of the enzyme, R_2 represents the remainder of the PEG chain and R_3 is the rest of the polymer backbone and the osmium complex, both of which make up one metallopolymer molecule

Once the electrodes had been prepared their electrochemical properties were tested using cyclic voltammetry. This method can be used to study the morphology of the film and the electrochemistry of the osmium complex. The response of each electrode to changes in glucose concentrations was then tested.

Batches of the polymer were synthesised and a number of electrodes were tested to study

the electrochemistry of the osmium complex. In most cases the films formed were not stable enough to remain absorbed and in electrical contact with the carbon surface of the elctrode once they had been dipped into the the bulk electrolyte, PBS. Figures 4.2 and 4.3 show two electrodes used to produce cyclic voltammograms.

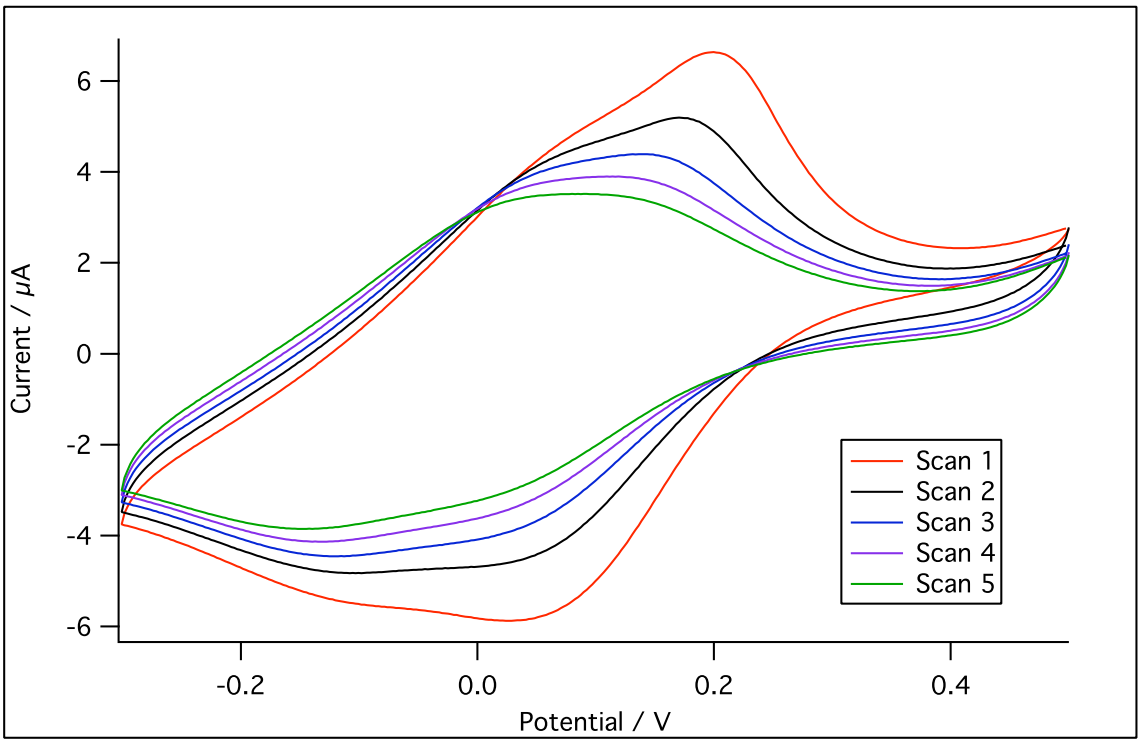


Figure 4.2: Successive CVs of osmium complex attached covalently to form a film on the surface of the electrode. Each scan was performed under the same set of conditions ($\dot{v}$ = 100 mV s^{-1}) and without removal from the bulk electrolyte. Potentials vs. Ag|AgCl.

In Figure 4.2 the oxidation peak of the first scan is small but generally well defined, although the shape of the reduction peak is broader, than that of the oxidation peak. The size of the redox peaks for consecutive scans becomes smaller, indicating that the osmium complex became detached from the surface. By the 4^{th} scan the electrochemical behaviour of the complex was greatly decreased and the peak potentials were in the expected region, as reported for these complexes by Taylor et. al [6]. The diameter of the electrodes was 3 mm, yet the density of the loaded osmium complex on their surfaces is not as high as expected

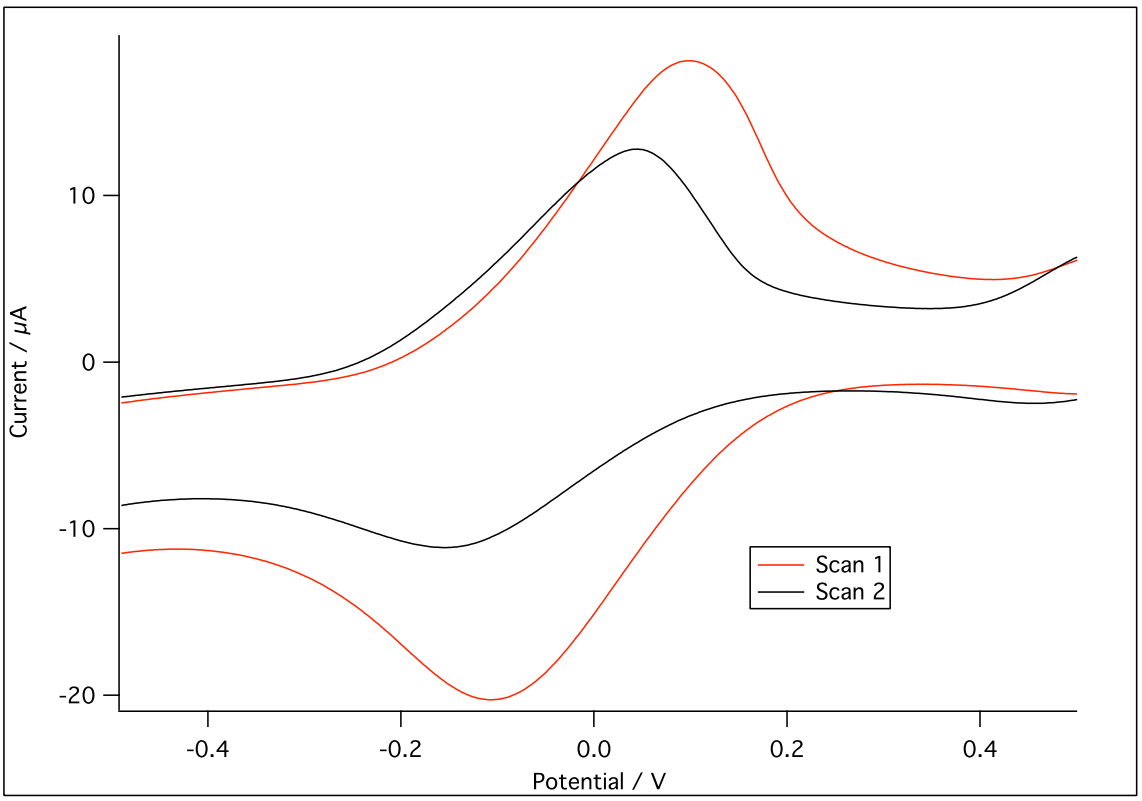


Figure 4.3: Successive CVs of an osmium complex, formed using covalent attachment to a functionalised PEG, film on a glassy carbon electrode performed at $\dot{v} = 100$ mV s^{-1}. The successive scans show that the film degrades once it has been placed in PBS.

[6]. More importantly, the structure of the film is very different to that reported by Gregg and Heller [3]. These authors first reported the use of these organic metallopolymers as enzyme sensors and the CVs obtained by them show surface bound characteristics at low to medium scan rates, with some separation at the higher scan rates [3].

Further trials yielded some improvements in the morphology of the film, showing more classically diffusive voltammograms, shown in Figure 4.3. Even when some improvements were seen in the electrochemistry of the complex, the mechanical stability of the film was still poor, and the second consecutive scan indicated that the film was becoming detached from the surface of the electrode. The reduction and oxidation peaks of the 1^{st} scans are comparable, $I_{p,ox} \simeq 1.81 \times 10^{-5}$ A and $I_{p,red} \simeq 1.89 \times 10^{-5}$ A. This means that $I_{p,ox}/I_{p,red} \simeq$

1, within the error of estimating the peak currents. During the second scan $I_{p,ox}$ has decreased by approximately 30% to 1.28×10^{-5} A and the ratio of the peak currents is much smaller than 1. It also seems that the electron transfer kinetics for this set of measurements is slow. The ΔE_p for the first and second scans are 205 and 195 mV, respectively. Ohara et. al. have reported that the peak to peak separation for all ranges of cross linking studied is $\simeq$ 100 mV [5]. The values obtained in these experiments are well in excess of the reported separation, which is indicative of slower electron transfer kinetics. This strongly indicates that the structural properties of the film are not the same as those reported in the literature [1, 3]. Figure 4.3, did show an improved CV, although only one electrode out of four showed this response, even though all 4 electrodes were made in the same manner at the same time. This high failure rate was not acceptable and so it was necessary to improve on this.

The responses of the films to changes in glucose concentration were analysed using chronoamperometery at a constant potential of +450 mV; these data can be seen in Figures 4.4 and 4.5. The titration in Figure 4.4 shows that the first addition of glucose, to a concentration of 10 mM in the cell, produced a significant response at the elctrode. However, the current then slowly decayed toward the background level. Further additions of glucose did not cause any perturbations to this decay, although there is a slight shoulder, at ca.400s caused by one addition of glucose. This implies that the film decaying and therefore showed no response to further changes in glucose concentration. These results were in stark contrast to the values reported in the literature. For example, Heller reported a saturation current density of approximately 900 $\mu A cm^{-2}$ at a concentration of approximately 40 mM glucose [7]. Currents of this order are also reported by Csoregi et.al. for monitoring the glucose concentration subcutaneously [8]. The authors report a linear range of $\simeq$20 mM and a corresponding oxidation current of 40 nA [8]. The substrate of the sensor has an area of 5×10^{-4} cm^2 which implies similar current densities to those reported by Heller.

Figure 4.5 is more representative of the responses that were obtained from most of the sensors. The method of titration was the same as described before, with the one exception

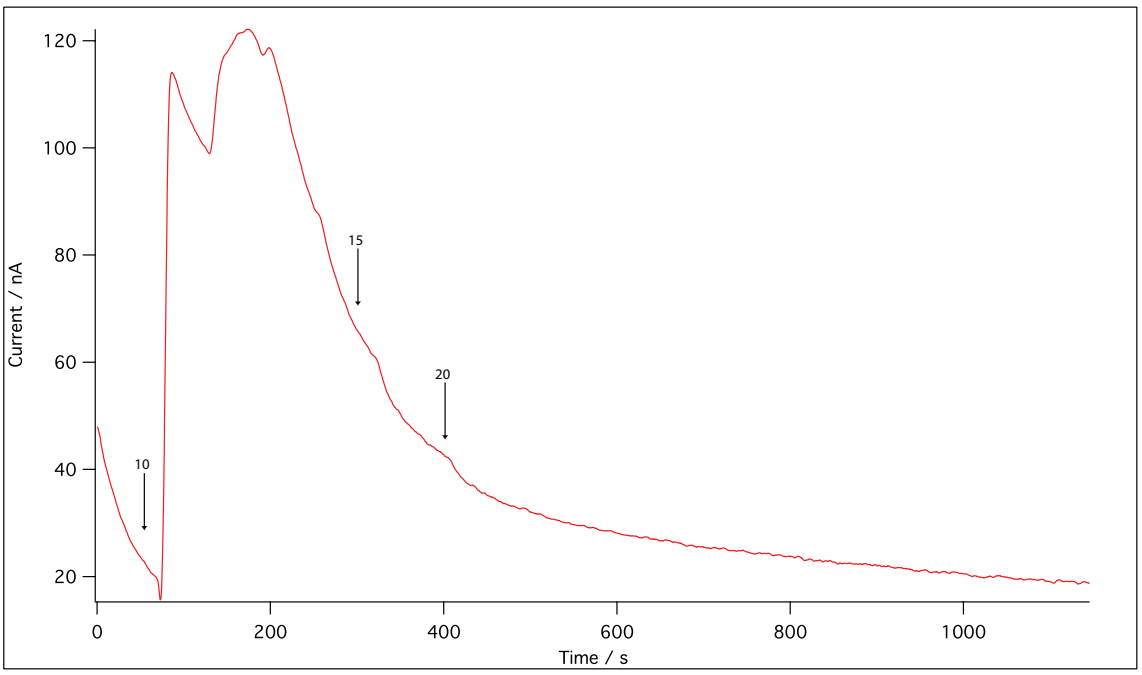


Figure 4.4: Glucose titration using a covalently attached osmium complex film with glucose oxidase. The spike at cf.100s occurs when the glucose concentration in the cell is 10 mM. The current decays toward the background and no further additions of glucose alter the signal. The labelled arrows show the glucose concentration, in mM, during the titration.

being the decay of the Cottrell current. In this case, the decay of the Cottrell current was recorded and therefore the titration of glucose was begun after 200 s. (Figure 4.5 only shows the data recorded from this point onwards.) Here there was no response to any addition of glucose. During the titration of glucose, the cell was stirred to ensure a rapid and uniform mixing of each aliquot: the shear caused by this at the film – solution interface might have resulted in rapid loss of film.

From the synthesis of the polymer to the curing of the film there were several parameters that could have caused problems with the mechanical stability of the film. One final test was carried out in an attempt to pin point the problem in their manufacture, so that this could be rectified.

The mechanical properties of the film were tested in the absence of osmium complex; the polymer backbone of vinylimidazole was used to form the film along with glucose oxidase.

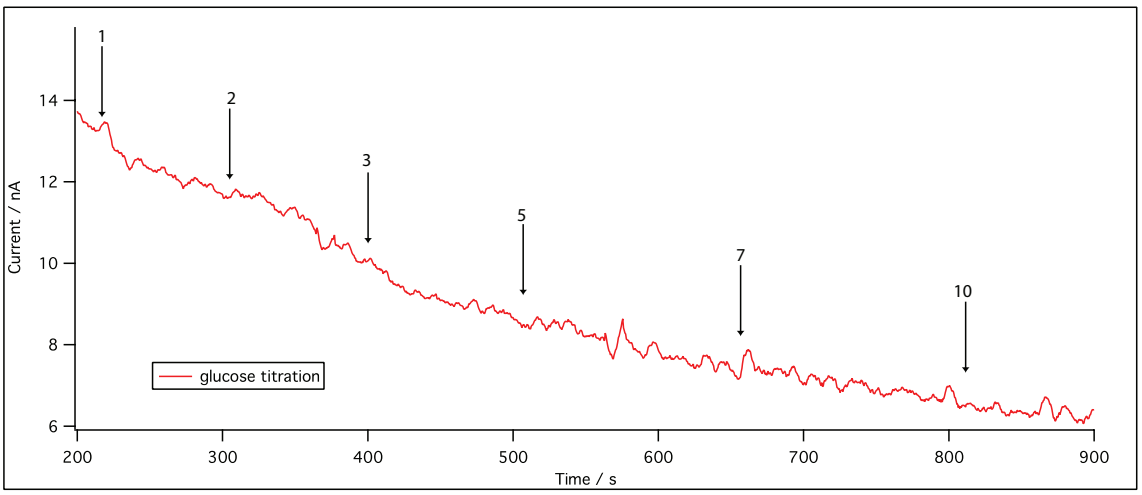


Figure 4.5: No sensor response from a glucose titration. The electrode was held at the oxidation potential and sequential titration of a standard glucose solution was performed; and there was no change in the currents recorded. The labels show the addition of the glucose aliquots and the resulting concentrations in the cell.

Then the H_2O_2 mode of sensing was used to see if the film remained attached to the carbon surface. The resultant current trace and calibration curve are shown in Figures 4.6 and 4.7. The current recorded showed quick and well defined changes on the addition of each glucose aliquot, until the enzyme was saturated at a glucose concentration of 1.2mM in the cell. The responses from the trial indicated that even though the S/N ratio was acceptable, the linear range of the sensor was limited by the enzyme loading of the film or the concentration of dissolved oxygen in the bulk electrolyte.

Formation of a structurally sound film of the polymer and enzyme meant that the epoxide bonding of each of the two types of molecules to each other was adequate This indicated that the composition of the curing mixture was correct and that the time given for curing was adequate. More importantly it showed that the quality of the carbon surface was high enough for the covalent attachment of the glucose sensitive film. Polishing the surface left it hydrophilic and this in turn meant that the curing mixture sat exclusively on the surface of the carbon: this was the same preparation technique as reported by Gregg and Heller [3]. This ruled out possibilities of error during synthesis other than the coupling of

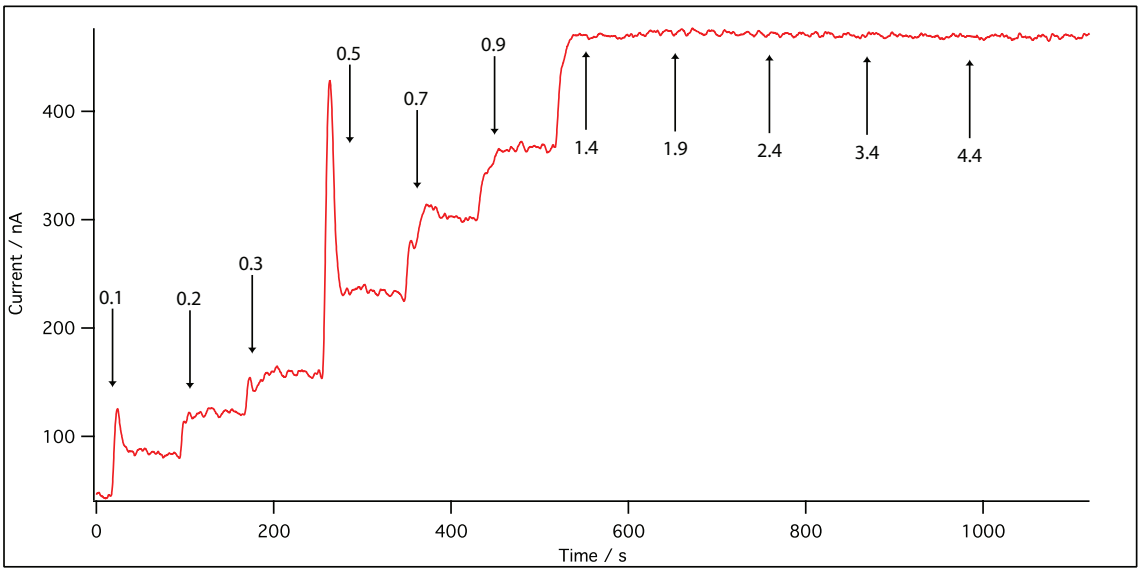


Figure 4.6: Current trace recorded during a glucose titration using a covalently attached PVI and glucose oxidase film. The labelled arrows show the change in glucose concentration in mM during the course of the titration.

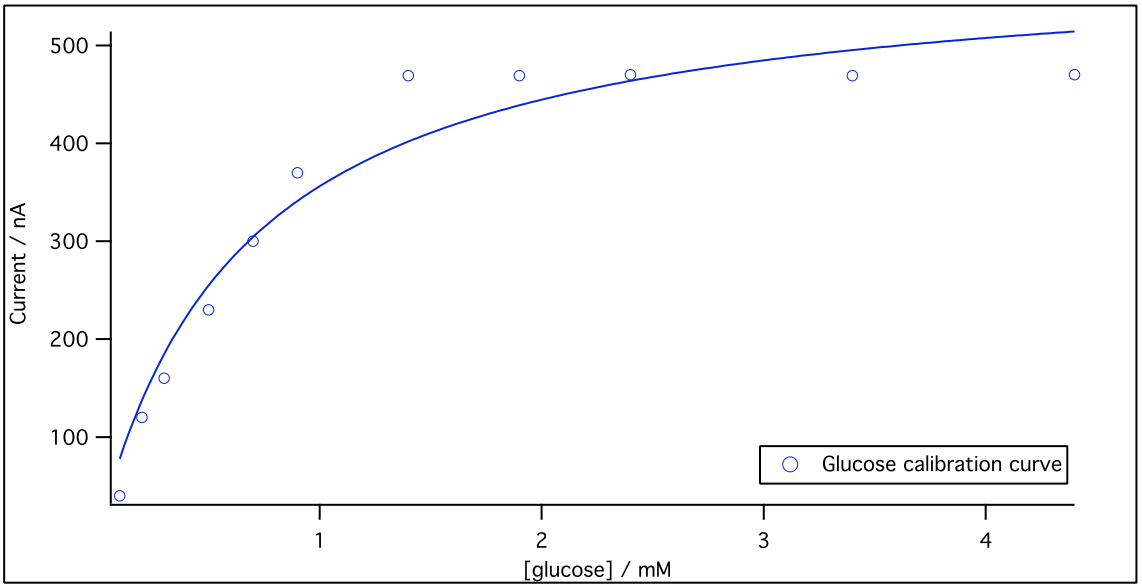


Figure 4.7: Calibration curve for the glucose oxidase and PVI film.

the osmium complex and the polymer backbone as the weak films, showed that the osmium complex synthesised was acceptable. Further attempts were made to improve on this, but to no avail.

All of the evidence indicated that an inadequate film quality contributed to a very high electrode failure rate. Therefore, other methods of encapsulating the enzyme and osmium complex were tried, including those that did not rely on the coupling of the osmium complex and vinylimidazole backbone.

4.3 Encapsulation in electro-deposition paint

The use of an electro-deposition paint would mean that the coupling of the osmium complex and polymer backbone would not affect the mechanical strength of the film. This method would therefore be more forgiving to variations during the synthesis. Resydrol was chosen as the paint; this is an aqueous suspension of copolymer of acrylates and acrylate esters [9]. The stability of this colloid is sensitive to pH and it is this property that allowed its use in electro-deposition.

The typical currents recorded during each multiple pulse cycle are represented in Figure 4.8. Each set of points represents the currents at each potential. For a single cycle twenty such cycles were performed for the deposition. This is the optimum number of cycles as reported by Kurzawa et.al.[10]. The short pulse of 2.2 V for 0.2 s decreases the local pH at the surface of the electrode, which destabilises the colloid. The pH is then allowed to equilibrate for the remainder of the cycle.

Cyclic voltammetry of these films was performed to ascertain the quality of the osmium complex loading. The CV for the first electrode made using this method can be seen in Figure 4.9, this was performed at $\dot{v} = 50\text{mV s}^{-1}$. The data showed that the initial loading of osmium complex on to the electrode's surface was lower than that seen using covalent attachment, Figure 4.3, although the films were stronger. The loss of electrochemical activity during successive scans is less in this instance. The loss in the oxidation peak current

between the 1^{st} and the 2^{nd} scans is 7.9×10^{-7} A and between the 2^{nd} and the 3^{rd} scans is 2.8×10^{-7} A, which is less than a 25% loss in activity.

Figure 4.10 shows films produced for a different batch in the same manner, but here the loading of osmium is lower than before and the loss during successive scans is negligible. The data from this particular electrode, was not as expected since these CVs were performed at a scan rate of 100 mV s^{-1}, rather than at 50 mV s^{-1}. If the structure and content of the film were the same as the electrode in Figure 4.9 then doubling the scan rate should have doubled the charging currents and increased the peak current as well. This was clearly not the case, so there was still substantial variability in the production of the enzyme and complex films.

The use of resydrol and the new method of encapsulation had improved the mechanical stability of the films, but not the osmium loading of the electrodes and the sensors still showed no responses to changes in the concentration of glucose.

Another example showing improved film stability from single electrode tests at different scan rates; the resultant CVs are shown in Figures 4.11 and 4.12. This robustness had never been seen prior to the use of this encapsulation technique. It is more important to note that the amount of complex attached in this film was less than that seen with the few covalently formed films that showed any electrochemical behaviour.

For each technique used to prepare the films, the concentrations of the complex and enzyme cured on the surface was equal. This showed that covalent attachment retained a large proportion of the material loaded on its surface, although it was not attached to the carbon with any degree of strength. The opposite was true when the electro–deposition paint was used.

To incorporate the advantages of both of these techniques, resydrol was added to the curing mixture, so the osmium complex, enzyme and colloid were all cured on the carbon surface together. The resultant cyclic voltammogram can be seen in Figure 4.13. This figure clearly demonstrates that the osmium loading in this instance was good and that the film

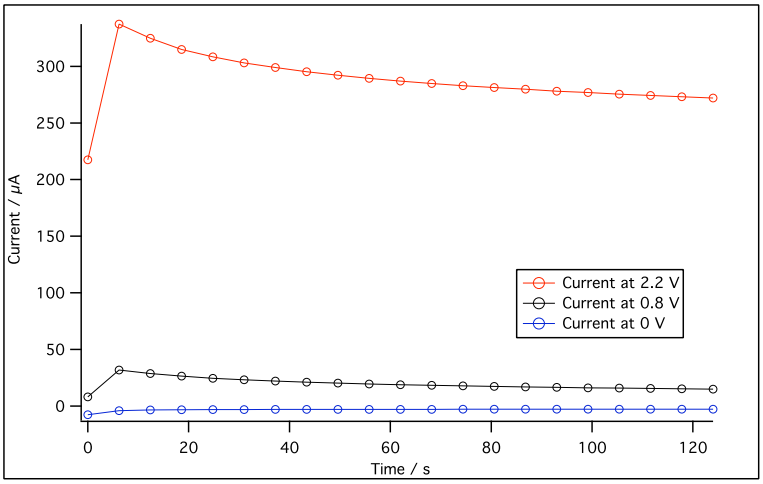


Figure 4.8: The current recorded during the pulsed electro-deposition of resydrol on a glassy carbon electrode which, had an osmium film dried on its surface. Each set of points at the three different potentials represents one complete deposition cycle. Twenty such cycles were used for a single deposition.

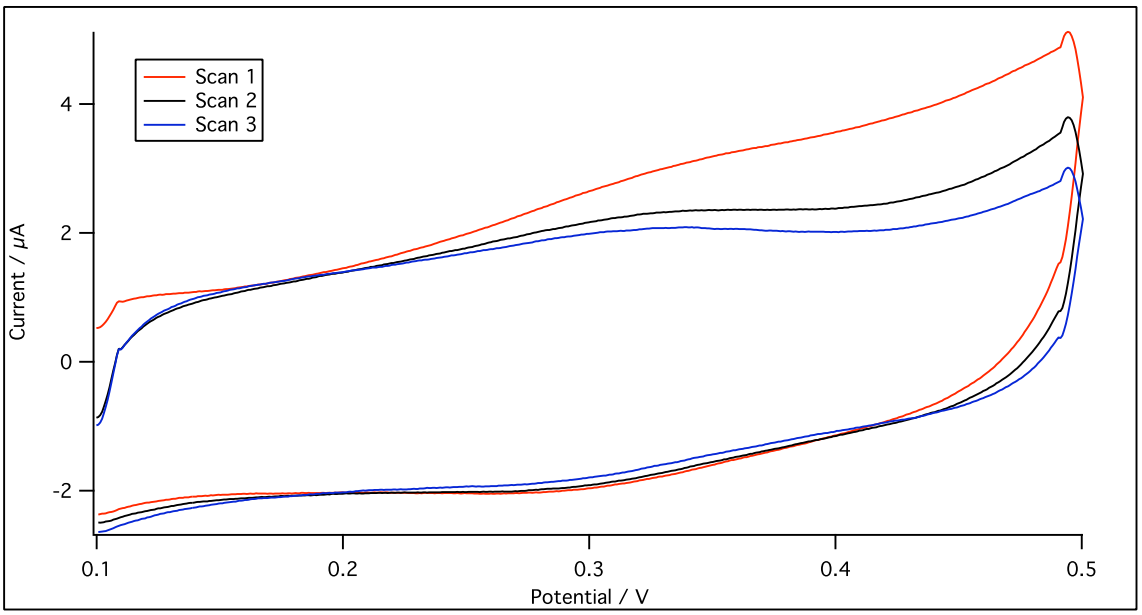


Figure 4.9: CVs of the osmium complex containing films, encapsulated using resydrol in PBS. $\dot{v} = 50\text{mV s}^{-1}$.

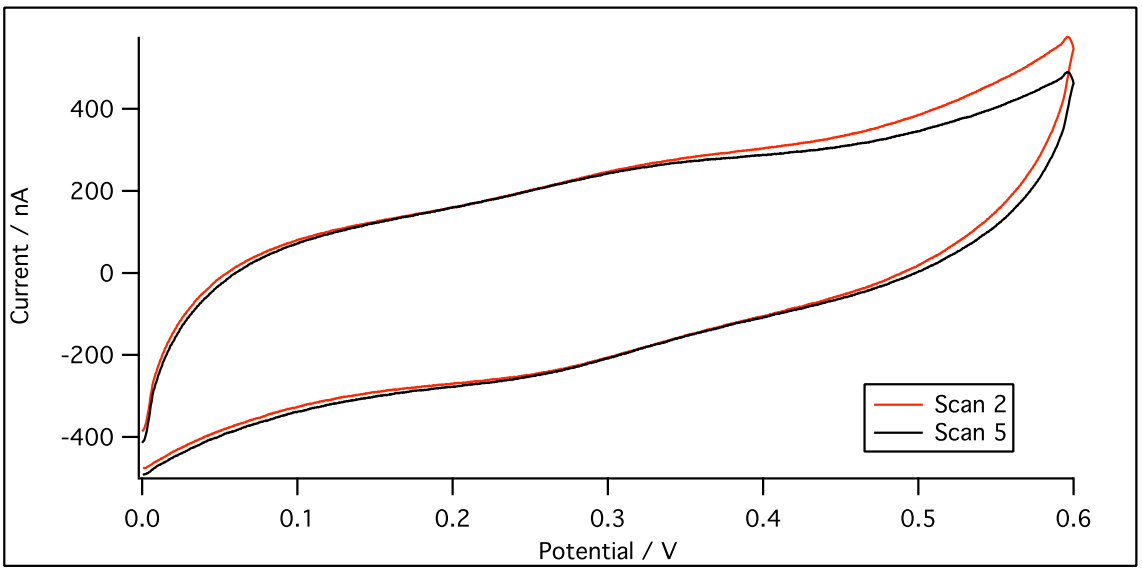


Figure 4.10: CVs of osmium complex encapsulated in resydrol, showing minimal loss of the complex from the surface. $\dot{v} = 100\text{mV s}^{-1}$.

was robust enough not to deteriorate when it was hydrated. The scan was performed at 1 mV s^{-1}, which means that the film was robust enough to show a reproducible reduction after approximately 30 minutes in buffer. Therefore, this method of fabrication showed some promise as a useful method.

The voltammogram in Figure 4.13 did not show any surface bound characteristics, which indicated that the film was flexible and that mass transport through the film should not be hindered. Analysing the results further it became evident that the peak to peak separation was 65 mV. This is outside the range that indicates a Nernstian response, especially considering that $\dot{v}$ was as low as 1 mV s^{-1}. The electron transfer kinetics for the osmium complex were not expected to display quasi-reversible behaviour, as reported by others [10]. This implies that the encapsulation in resydrol might have had an effect on the kinetics. This could prove to be a problem with this method of encapsulation as the use of the osmium complex as a mediator is reliant on efficient electron transfer between the enzyme and itself.

The same electrode, from Figure 4.13, was studied to find its response to a glucose titration; the resultant current trace is shown in Figure 4.14. The titration was performed

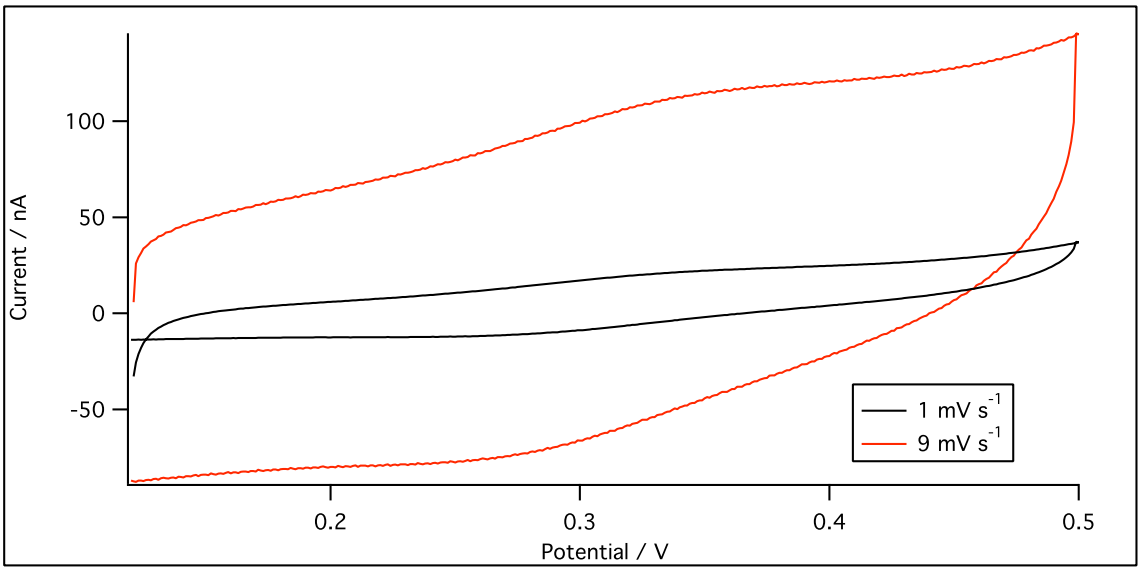


Figure 4.11: CVs of the osmium complex, encapsulated in resydrol, performed in 100 mM PBS at the scan rates shown in the legend.

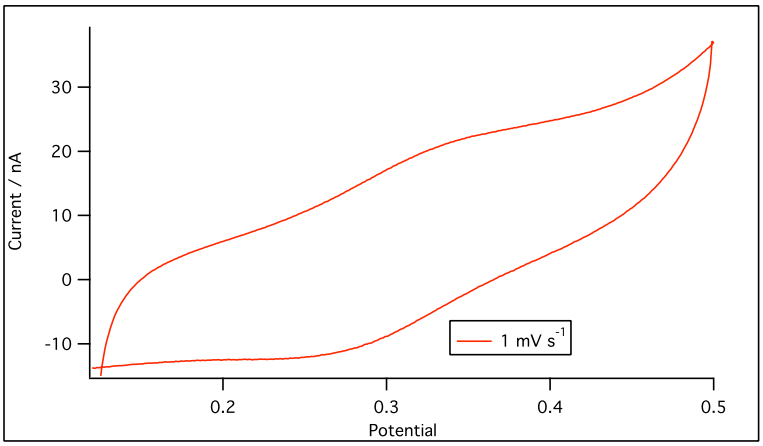


Figure 4.12: The CV at 1 mV s^{-1}, from Figure 4.11.

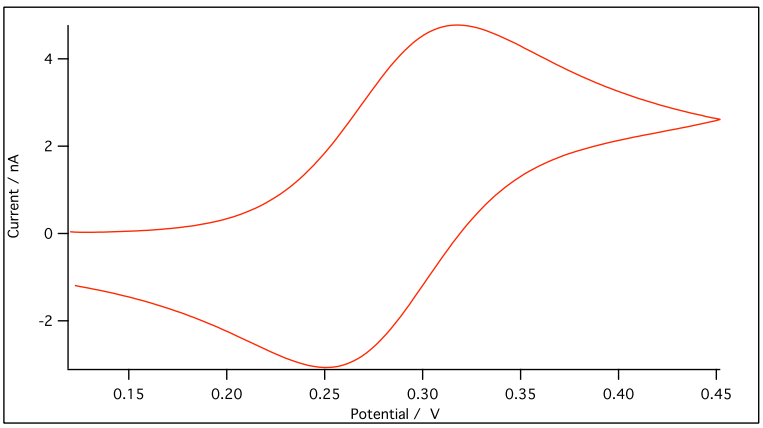


Figure 4.13: CV of osmium complex cured with resydrol in the curing mixture, on the surface of a glassy carbon electrode. Scan rate = 1 mV s^{-1}.

to study the oxidation of the osmium complex. In this case the Cottrell current was again recorded so it has been omitted from the trace shown in Figure 4.14. There was no response from the sensor on addition of glucose until about 750 s, where there was a small increase in the current. However, this increase was not much more than the noise of the amperogram and by this time the concentration of glucose in the cell was 15 mM, which is a high concentration for the first response from a glucose sensor.

Their are two possibilities that can be ascribed to this symptom, firstly if the permeability of the cured film was low then it would not possible to see small changes in the concentration of glucose in the cell. The electrode can provide a signal at high concentrations that might indicate a mass transfer hindrance as opposed to the electron transfer between the complex and the enzyme not being efficient. Covalently bonded films and encapsulated films formed by potential pulsing have been shown to be permeable to many different molecules that are similar in size to glucose [5, 3, 4, 10, 9], therefore, it might be possible that this is not the reason.

The second reason might be that the e^- transfer kinetics between the osmium centre and the FAD centre of the enzyme are slow. Increasing the concentration of glucose in the cell will mean that there is a higher turnover of the enzyme; in turn this increased turnover

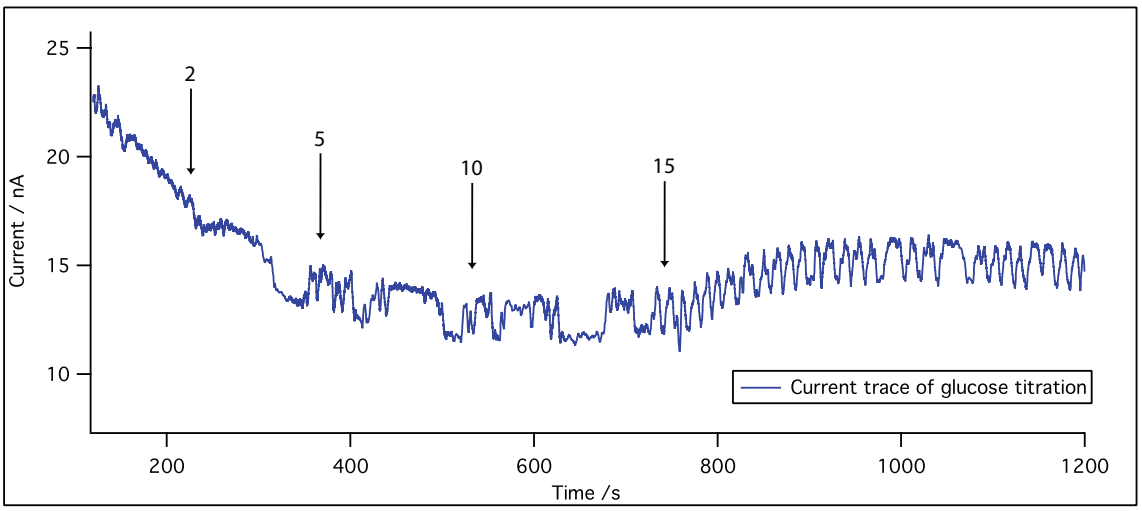


Figure 4.14: Glucose titration trace using film cured with resydrol in the curing mix. The labelled arrows show the change in glucose concentration in mM during the course of the titration.

increases the probability of e^- transfer between the two active centres. There was also anecdotal evidence that suggested that the age of the polymer complex was key to the 'wiring' of the enzyme, no specifics were available for this. As this particular enzyme containing film was formed using Resydrol in the curing mixture, its structure and morphology would have been different from those reported and it might have been this difference that created the symptom of sensing only high concentrations of glucose.

Encapsulation also showed some promise as a method of producing glucose sensors, but both the synthesis of the osmium metallopolymer and the fabrication of the film gave very low yields per batch.

4.4 Summary and Conclusions

It was not possible to use films made using the covalent attachment of the osmium complex and enzyme on the glassy carbon surface due to mechanical frailties of the film. The failure rate of the films was so high that it was not possible to reproduce the promising results in order to improve the process.

In order to understand the bonding process and remove a number of unknowns from the film making process, the enzyme was covalently bound to a poly(vinylimidazole) backbone. This yielded a stronger film and it was possible to sense changes in the glucose concentration, with a small linear range up to 1.2 mM. Using this information, attempts were made to optimise the coupling of the osmium complex and polymer backbone during synthesis, but no further improvements could be made.

To mitigate the frailties in the synthesis of the metallopolymer, an encapsulation technique was used to make the films more robust. It was found that the strength of the films in this case was slightly improved although the loading of the transition metal complex was lower. These sensors showed no responses to glucose in the cell as a result of the enzyme and complex not being 'wired'; that is the structure of the film did not provide the required e^- transfer kinetics.

Although this mode of operation has been widely reported with enzyme sensors, we were unable to reproduce the films. As a result of this lack of reproducibility it was decided not to pursue these sensors any further and the use of non–mediated sensors was chosen.

References

[1] R. J. Forster and J. G. Vos, "Synthesis, characterization, and properties of a series of osmium-containing and ruthenium-containing metallopolymers," *Macromolecules*, vol. 23, no. 20, pp. 4372–4377, 1990.

[2] T. J. Ohara, R. Rajagopalan, and A. Heller, "Wired enzyme electrodes for amperometric determination of glucose or lactate in the presence of interfering substances," *Analytical Chemistry*, vol. 66, no. 15, pp. 2451–2457, 1994.

[3] B. A. Gregg and A. Heller, "Redox polymer-films containing enzymes .1. a redox-conducting epoxy cement - synthesis, characterization, and electrocatalytic oxidation of hydroquinone," *Journal of Physical Chemistry*, vol. 95, no. 15, pp. 5970–5975, 1991.

[4] B. A. Gregg and A. Heller, "Redox polymer-films containing enzymes .2. glucose-oxidase containing enzyme electrodes," *Journal of Physical Chemistry*, vol. 95, no. 15, pp. 5976–5980, 1991.

[5] T. J. Ohara, R. Rajagopalan, and A. Heller, "Glucose electrodes based on cross-linked [os(bpy)(2)]$^{(+/2+)}$ complexed poly(l-vinylimidazole) films," *Analytical Chemistry*, vol. 65, no. 23, pp. 3512–3517, 1993.

[6] C. Taylor, G. Kenausis, I. Katakis, and A. Heller, "Wiring of glucose-oxidase within a hydrogel made with polyvinyl imidazole complexed with [(os-4,4'-dimethoxy-2,2'-

bipyridine)cl]$^{(+/2+)}$," *Journal of Electroanalytical Chemistry*, vol. 396, no. 1-2, pp. 511–515, 1995.

[7] A. Heller, "Electrical connection of enzyme redox centers to electrodes," *Journal of Physical Chemistry*, vol. 96, no. 9, pp. 3579–3587, 1992.

[8] E. Csoregi, D. W. Schmidtke, and A. Heller, "Design and optimization of a selective subcutaneously implantable glucose electrode based on wired glucose-oxidase," *Analytical Chemistry*, vol. 67, no. 7, pp. 1240–1244, 1995.

[9] A. Vilkanauskyte, T. Erichsen, L. Marcinkeviciene, V. Laurinavicius, and W. Schuhmann, "Reagentless biosensors based on co-entrapment of a soluble redox polymer and an enzyme within an electrochemically deposited polymer film," *Biosensors & Bioelectronics*, vol. 17, no. 11-12, pp. 1025–1031, 2002.

[10] C. Kurzawa, A. Hengstenberg, and W. Schuhmann, "Immobilization method for the preparation of biosensors based on ph shift-induced deposition of biomolecule-containing polymer films," *Analytical Chemistry*, vol. 74, no. 2, pp. 355–361, 2002.

Chapter 5

Glucose sensors fabricated from electropolymerised poly(phenol) films

5.1 Introduction

Glucose sensors using glucose oxidase film on platinum surfaces entrapped in an electropolymerised poly(phenol) film were made after studying various factors involved in the fabrication procedure. In this chapter the effect of monomer concentration in the cell and the pH and acetate composition of the enzyme stock are reviewed. The optimised protocol provided reproducible devices whose characteristics are shown along with their *in-vitro* life time.

5.2 Glucose oxidase procured from Biozyme

In section 2.7 the use of a liquid formulation of glucose oxidase, procured from Biozyme Labs, is described. This enzyme stock was used as received and glucose sensitive films

were made, as stated in section 2.7. This was based on the work reported by Bartlett and Caruana [1]. These devices provided suitable operating characteristics as glucose sensors, as shown in Table 5.1. The data from a single batch of 5 sensors is shown in, Figure 5.1 and shows that the devices exhibit a linear range up to 17 mM. One of these sensors was only 40% as sensitive as the others, but this was considered acceptable as this level of variation could be improved upon.

Sensor	Slope / (nA mM^{-1})	Intercept / nA
1	1.25	1.57
2	1.04	1.62
3	0.97	1.44
4	0.52	1.15
5	0.91	1.53

Mean slope = 0.94 ± 0.02 nA mM^{-1}

Table 5.1: Characteristics of sensors made using glucose oxidase from Biozyme Labs.

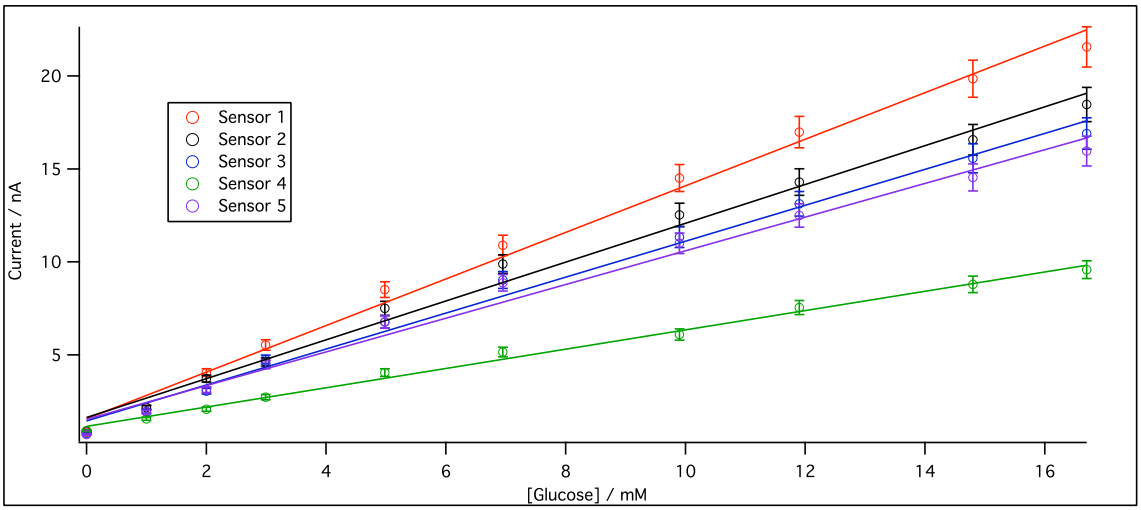


Figure 5.1: Calibration curves of devices using glucose oxidase from Biozyme Labs.

When using the enzyme formulation, the sensors showed linearity of response up to 16mM glucose and their intra–batch variability was 2.1%, including sensor 4, which had a

sensitivity of 520 pA mM^{-1}. Due to supply problems with the manufacturer, long term use of this enzyme formulation was not possible. As a result, a new source was used for the enzyme.

5.3 Optimisation using the new enzyme

Glucose oxidase in the form of a lypophilised powder was obtained from Sigma-Aldrich. It was dissolved in a stock buffer that was optimised, to yield the best sensor performance. The factors that proved important in the production of good sensors were the pH and acetate concentration of the enzyme buffer; along with the concentration of phenol in the electrolytic cell. The sensor optimisation procedure was based on the glucose oxidase formulation provided by Biozyme Labs.

5.3.1 Phenol concentration

Bartlett et.al. have reported the use of 25 mM phenol in the electrolytic cell. They used this to form a poly(phenol) layer that they estimated to be 38 nm thick, based on the area of the electrode and the charge passed during oxidation [2]. Arslan et.al. however, reported the use of a concentration of 12.5 mM phenol to form poly(phenol) films on platinum surfaces [3]. It was also reported by Gattrell and Kirk that when using a concentration lower than 12 mM, the oxidation products of phenol do not form a polymer [4]. Therefore, it was necessary to study the minimum phenol requirement in the cell during polymerisation.

The performance of the sensors was investigated using phenol concentrations of 5, 15 and 25 mM phenol during electro-polymerisation. The polymerisation voltammograms for each of the three concentrations are shown in Figures 5.2 to 5.4. The first scans, in figure 5.2 show that there are marked differences in the I_p for each of the phenol concentrations. It was expected that the peak currents would increase as a function of the bulk phenol concentration, but clearly that was not the case. The areas under the oxidation peaks do not follow this trend either. The data for both these parameters is in Table 5.2.

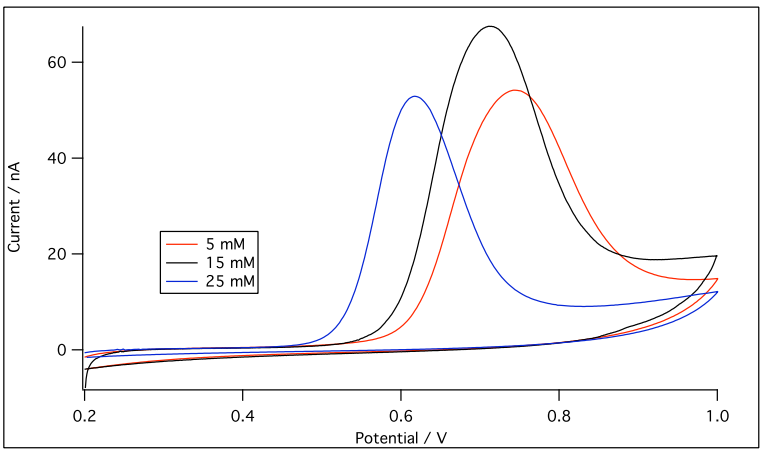


Figure 5.2: 1^{st} scan of phenol at the shown bulk concentrations, on a 200μm platinum disc electrode with glucose oxidase preadsorbed on the platinum surface. The bulk electrolyte is 100mM PBS and the scan rate is 100mV s^{-1}.

[phenol] / mM	I_p / nA	Area / $\times 10^{-6} C$
5	66	6.7
15	67	12.7
25	53	3.3

Table 5.2: Oxidation peak characteristics for the electro–polymerisation of phenol at the shown bulk concentrations of phenol (C_b).

The peak current and area under the peak do not show a linear relationship with the concentration of phenol because the available active areas of each of these electrodes is not the same. The pre-adsorption of glucose oxidase decreases the active area and this change is not necessarily consistent for each electrode. The peak currents for each of the three cases above are suppressed by about 40% when compared to bare electrodes of the same diameter without any adsorbed enzyme. This indicates that the enzyme on the platinum surface partially blocks the active area. Therefore, the parameter used to compare these electrodes is the background current at +1000 mV, which indicates the level of insulation provided by the polymer and enzyme. For each of the three scans, the background current decreased as the concentration of phenol in the cell was increased. This showed that at high

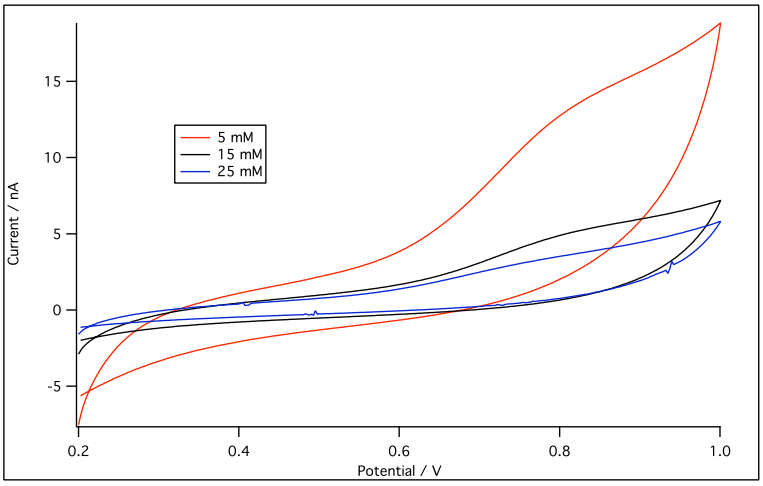


Figure 5.3: 2^{nd} scan of phenol at the shown bulk concentrations, on a 200μm platinum disc electrode with glucose oxidase preadsorbed on the platinum surface. The bulk electrolyte is 100mM PBS and the scan rate is 100mV s^{-1}.

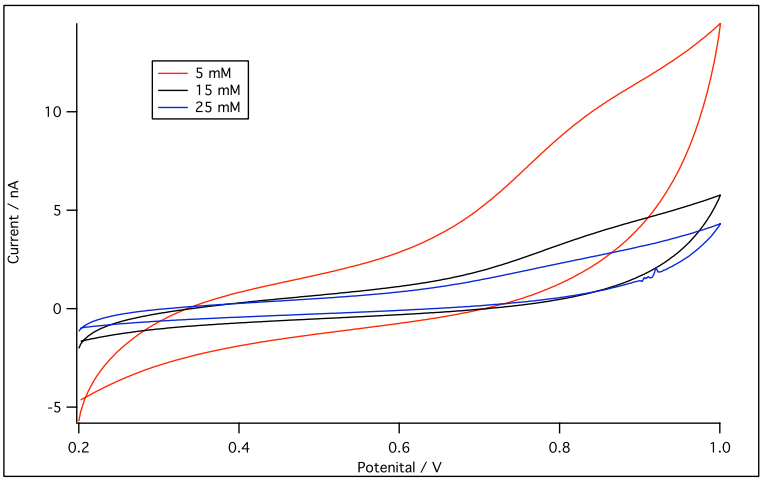


Figure 5.4: 3^{rd} scan of phenol at the shown bulk concentrations, on a 200μm platinum disc electrode with glucose oxidase preadsorbed on the platinum surface. The bulk electrolyte is 100mM PBS and the scan rate is 100mV s^{-1}.

phenol concentrations the polymerisation pathway and therefore electrode passivation was predominant, which is the same observation as reported by Gattrell and Kirk [4].

To see what effect the different C_b of phenol had on the performance of the sensors, their responses to a glucose titration were assessed. Prior to the titration the sensors were left in PBS for 18 hours to allow any weakly adsorbed enzyme to wash away.

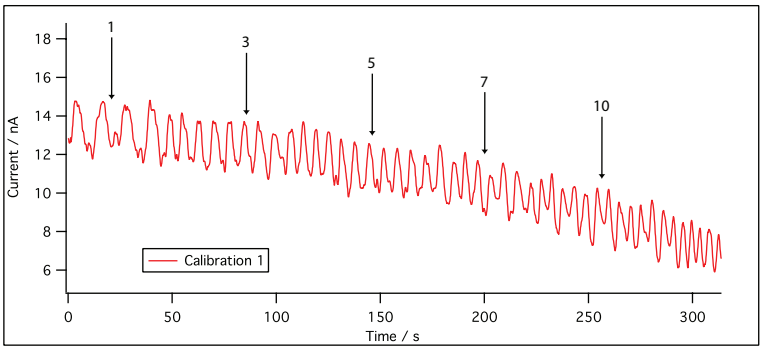


Figure 5.5: Current recorded for a glucose titration on a 200μm platinum electrode with glucose oxidase entrapped in a poly(phenol) film made using 5 mM phenol. The arrows indicate the concentration of glucose in mM during the course of the titration.

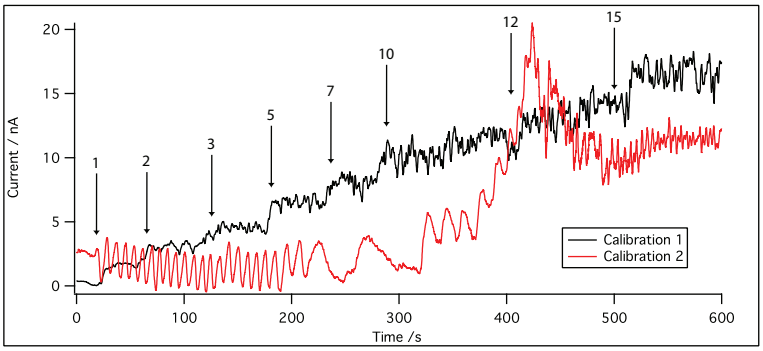


Figure 5.6: Current recorded for a glucose titration on a 200μm platinum electrode with glucose oxidase entrapped in a poly(phenol) film made using 15 mM phenol. The concentration of glucose in mM is shown using the labelled arrows.

There was no response from the device made using 5 mM phenol, Figure 5.5, indicating that the weakly adsorbed enzyme had washed away from the surface during the wash out period. The background current was also elevated compared to higher phenol concentrations. This suggested that less insulation was present, resulting form the loss in enzyme and

lower poly(phenol) coverage. This confirmed that the oxidation of phenol at low concentrations did not proceed down the path of polymerisation as reported by Gattrell and Kirk [4]. The first calibration from the second device made at 15mM phenol showed more promise, but a repeat titration showed that even in this case the enzyme had become detached. The data showed that the consistencies of these devices was poor. Therefore, it was decided to carry out the polymerisation in a cell that contained 25 mM phenol, the titration curves for which can be seen in Figure 5.7.

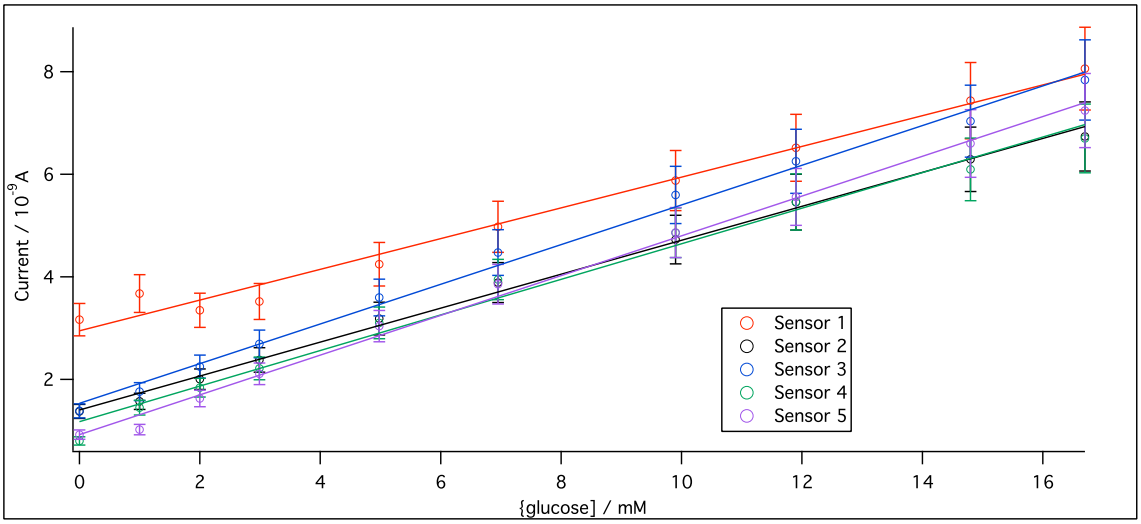


Figure 5.7: Glucose calibration curves for a single batch of devices made using 25mM phenol in the polymerisation cell. These calibration curves demonstrate the intra–batch variability inherent with the process.

5.3.2 pH optimisation

It was found that the presence of acetate in the buffer used for the enzyme stock solution was important for subsequent sensor performance. As the majority of the supporting electrolyte during both the pre-adsorption and polymerisation steps consisted of PBS, the optimisation of the acetate concentration was directly linked to the final pH of the solution. The pK_a of phosphate is 7.2 and that for acetate buffer is 4.5 and therefore the proportion of each was critical to the pH of the final buffer.

Firstly, a 1000 U mL^{-1} stock of the enzyme was made in an acetate buffer, the pH of this stock was 4.52. This stock was split and aliquots diluted to 500 U mL^{-1} and 250 U mL^{-1} using water. The pH of the resultant solutions was 4.56 and 4.66, respectively. Figures 5.8 and 5.9 show the currents recorded when sensors made using the different enzyme stocks were used for a glucose titration. As the two Figures 5.8 and 5.9 show, even an increase in the polymerisation pH of 0.1 units gave improvements in the performance of the sensors.

Even though the enzyme buffer had been made according to the specifications from the manufacturer (with a pH of 4.50), it was decided to check the pH of the polymerisation solution, as described in section 2.7; using the previous, Biozyme formulation. The pH of this polymerisation solution was found to be 6.65, which was more neutral than the pH of the same solution made from the enzyme stock made in house. The pH of the stock, from Biozyme, itself was found to be 4.65. With such a neutral pH there was a small uncertainty about the need for acetate in the supporting electrolyte, as this increased a step in the manufacturing process. The titration currents recorded when using sensors made with only PBS in the supporting electrolyte and in the enzyme stock are shown in Figure 5.10. This test set the required boundaries for the final pH of the solution.

The pH of the solutions made with only PBS were too basic to give good responses from the sensors confirming the need for acetate in stock buffer of the enzyme. The pI of glucose oxidase is 4.2 and therefore it is interesting that in the present set of circumstances the pH plays such an important role as all of the work is done above the pI. A qualitative test was conducted by adjusting the pH of the buffer using HCl, but this did not improve the performance of the sensors, so it was important to optimise both the pH and the acetate concentration of the solutions.

Finally the effect of an acetate 'spike' in the supporting electrolyte was tested. The enzyme stocks were made to a concentration of 1000 U mL^{-1} in PBS and the pH was adjusted by spiking both solutions with a 6.7% (v/v) acetate buffer. This gave a similar pH to the solution made using the liquid formulation from Biozyme (pH $\simeq$ 6.5). Figure 5.11

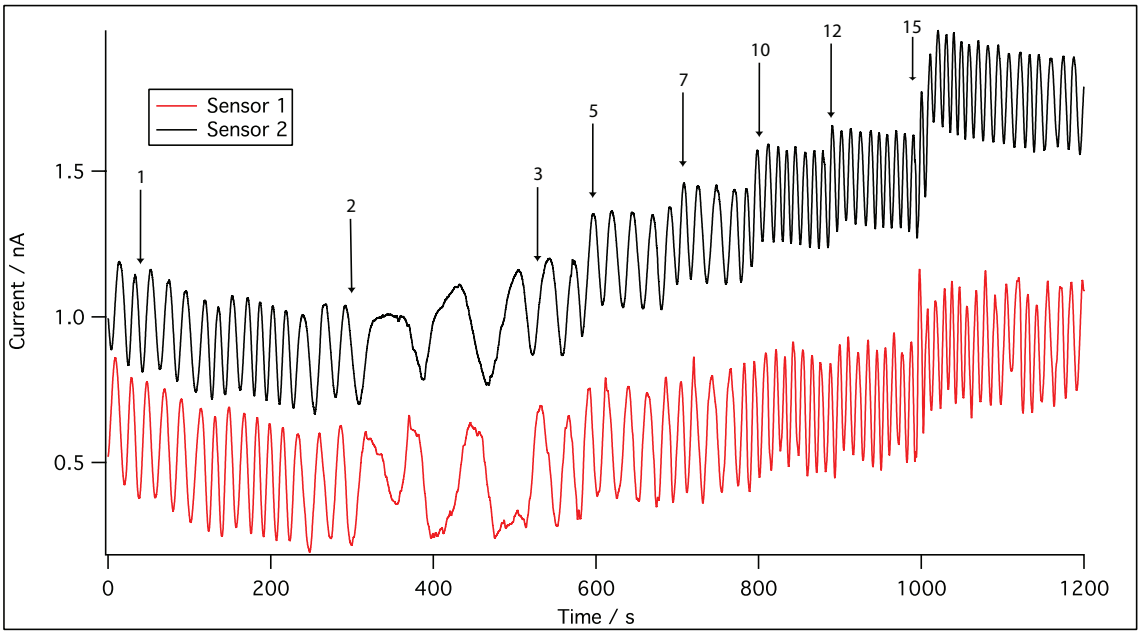


Figure 5.8: Current recorded during a glucose titration for two sensors polymerised in a supporting electrolyte with pH = 4.56. The labelled arrows show the concentration of glucose during the titration.

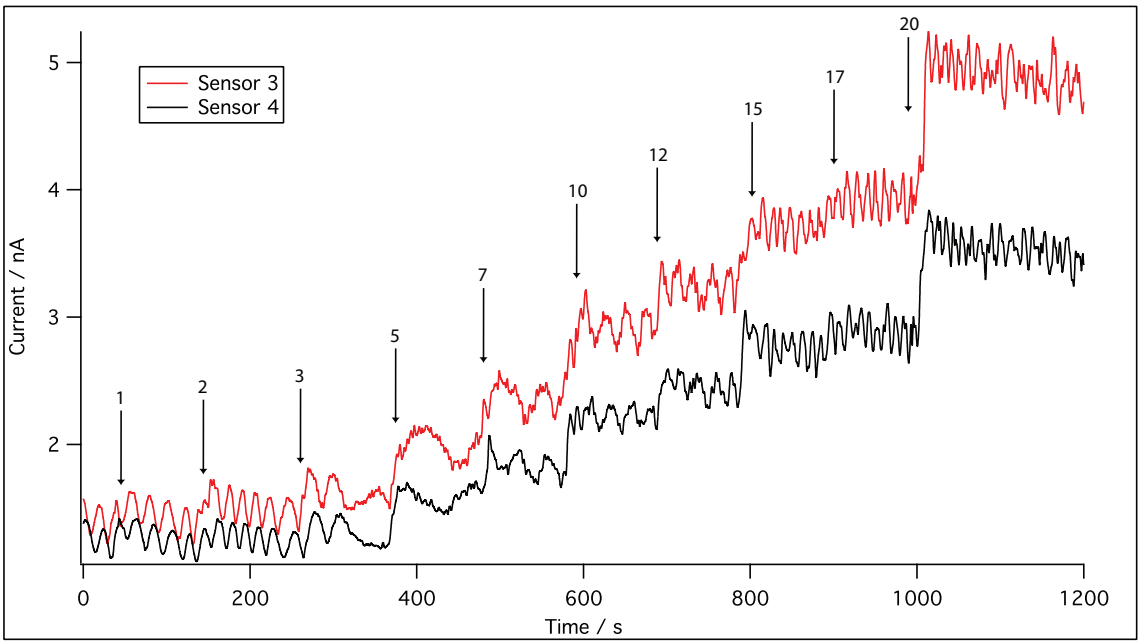


Figure 5.9: Current recorded during a glucose titration for two sensors polymerised in a supporting electrolyte with pH = 4.66. The concentration of glucose in the bulk solution is shown by the labelled arrows within the figure.

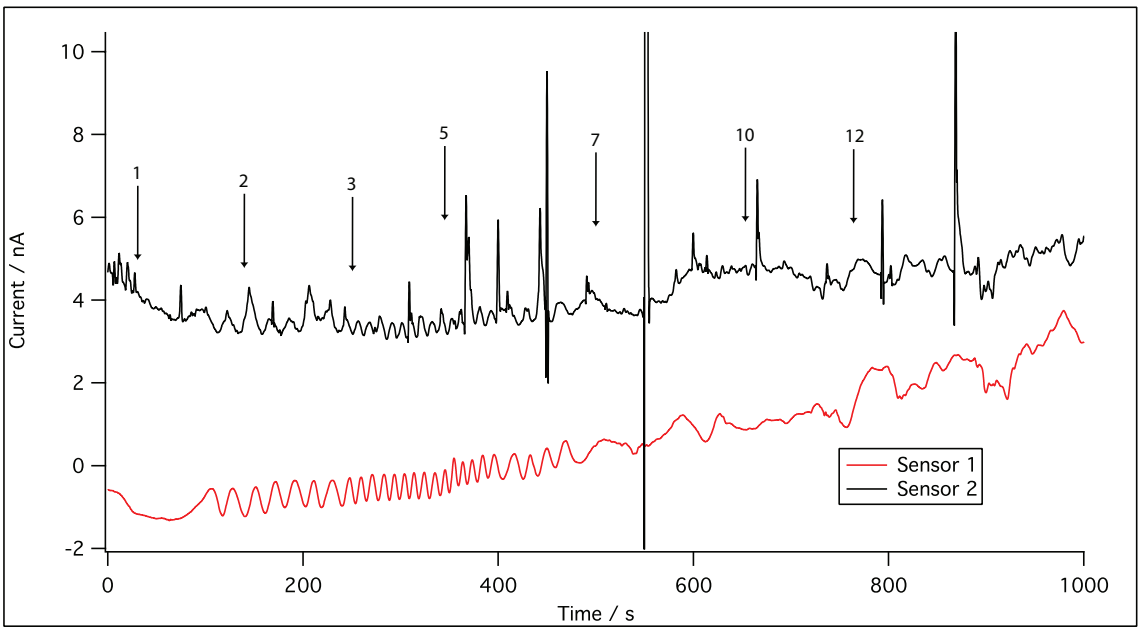


Figure 5.10: Currents recorded during a glucose titration for two sensors that were polymerised in a supporting electrolyte consisting of only 100mM PBS. (pH $\simeq$ 7.2) The arrows indicate the glucose concentration during the titration; in mM.

shows the responses from two sensors.

When sensors made with the two different buffers, from Figures 5.10 and 5.11 were compared, it was found that the calculated acetate spike yielded a better performance than the PBS only polymerisation and the data from the sensors were more reproducible. From these experiments it became evident that both the pH and acetate concentration of the buffer were important in determining the efficiency of the enzyme pre-adsorption. Section 5.4 confirms that this is key to the performance of the described devices. It is also conclusive that the electropolymerisation of phenol is sensitive to the pH of the supporting electrolyte [3].

Therefore the enzyme stock was made in an acetate buffer with a pH of 4.6; this would allow the protein maximum time in favourable media and would make the final solution preparation steps easier. As this method had already been tried with 1000 U ml^{-1} enzyme stock solutions with unfavourable results, it was also necessary to modify the concentration

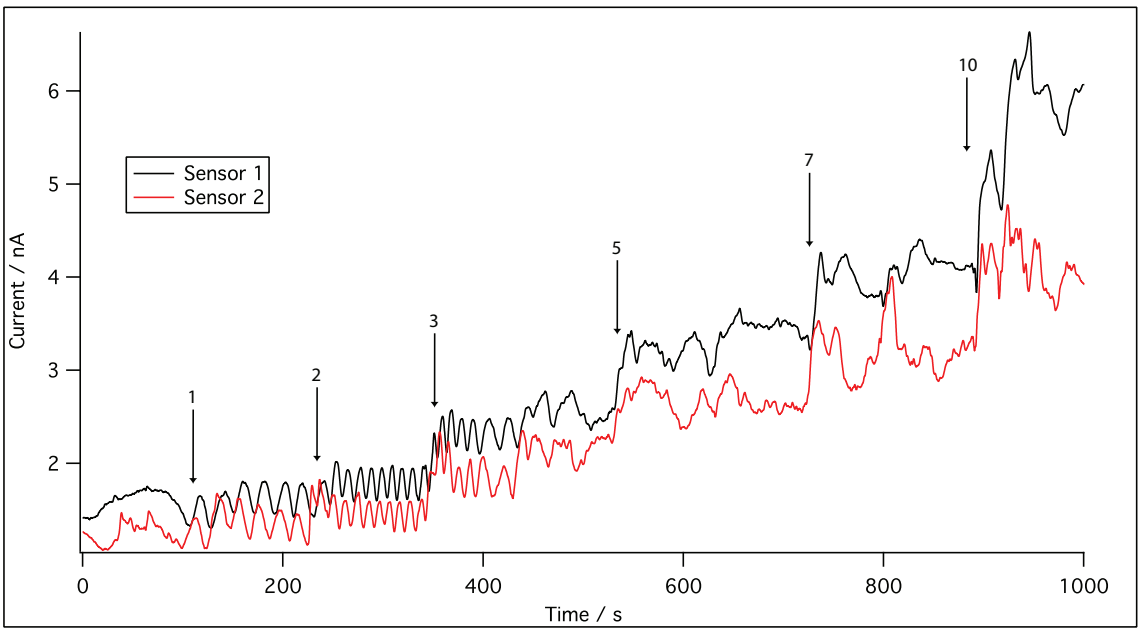


Figure 5.11: Currents recorded using sensors made with PBS as the supporting electrolyte and an acetate 'spike' during electropolymerisation. The labelled arrows show the concentration of glucose, in mM, during the sequential aliquot addition.

of the enzyme stock. The aliquot of enzyme stock to be added to the pre-adsorption and polymerisation solutions had to be 6.7% (v/v) which implied a 15× dilution. This in turn meant that the enzyme stock had to be 7500 U mL^{-1} to give a working concentration of 500 U ml^{-1}. The responses of the sensors made using this protocol can be seen in Figure 5.7. The devices made using this protocol exhibited a good response to changes in glucose concentration and the data were reproducible.

5.4 The importance of pre-adsorption

The protocol for the manufacture of sensors involved the pre-adsorption of enzyme onto the platinum surface. This was a process that was very time consuming and decreased the number of electrodes that could be made in a single day. The utility of this step was investigated in order to ascertain whether the production time could be lessened without harming the operating characteristics of the sensors or their intra-batch variability. The

protocol followed was the same as that described in section 2.7, with the exclusion of the pre-adsorption step.

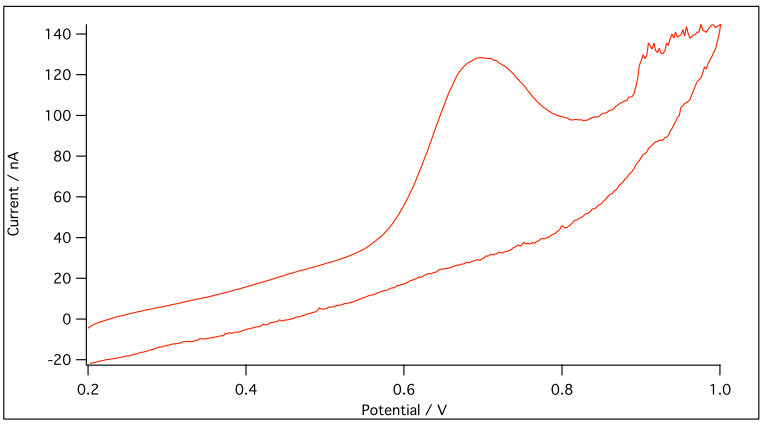


Figure 5.12: CV of 50 mM phenol an a platinum disc electrode that has not been allowed to stand in glucose oxidase solution. Therefore there has been no pre-adsorption of enzyme on the platinum surface.

The CV obtained during the polymerisation of phenol is shown in Figure 5.12. The I_p of this CV is approximately the same as that seen for a bare platinum disc with the same diameter. This meant that the effective area available for the oxidation of phenol was similar to that for the bare electrode. Therefore we should expect a lower enzyme loading and unfavourable operating characteristics, with this sensor.

The currents recorded during the calibration procedure are shown in Figure 5.13. One of the devices shows absolutely no response to changes in glucose concentration in the electrolyte, whereas sensor 2 shows very discrete changes in the oxidation current for each new aliquot of glucose. These responses are translated to calibration curves in Figure 5.14. Here the intra–batch variability is clear; sensor 1 shows a linear response to glucose after only the 5^{th} aliquot has been added. This could mean that there was something preventing the transport of glucose to the enzyme until this glucose concentration was reached. Alternatively, the lower loading of the enzyme may not have provided sufficient oxidation currents that could be detected above the noise. Sensor 1 is the only device that shows a linear response along the entire calibration range, although it shows a lowered

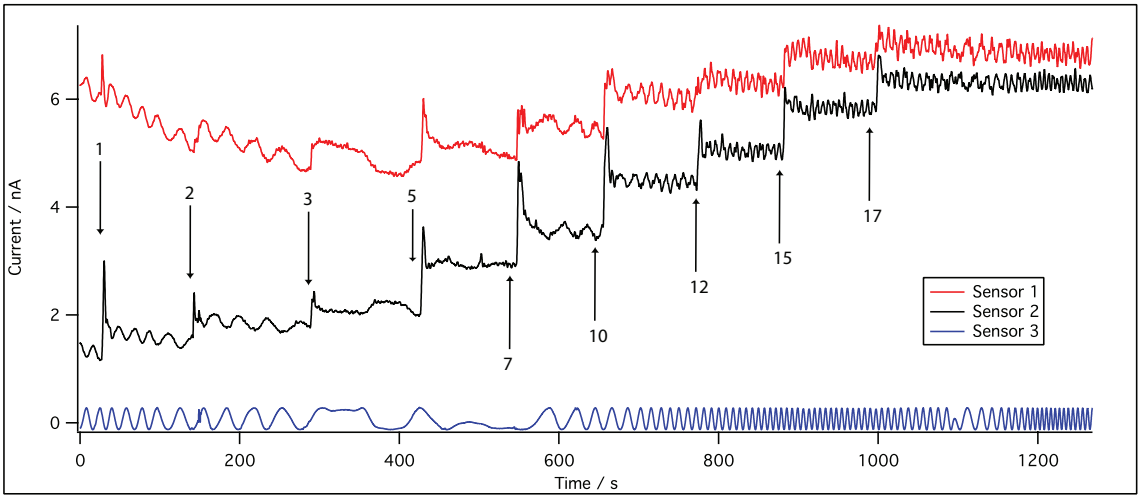


Figure 5.13: Currents recorded during the glucose calibration of three sensors prepared without the pre-adsorption step. The arrows show the glucose concentration, in mM during the titration.

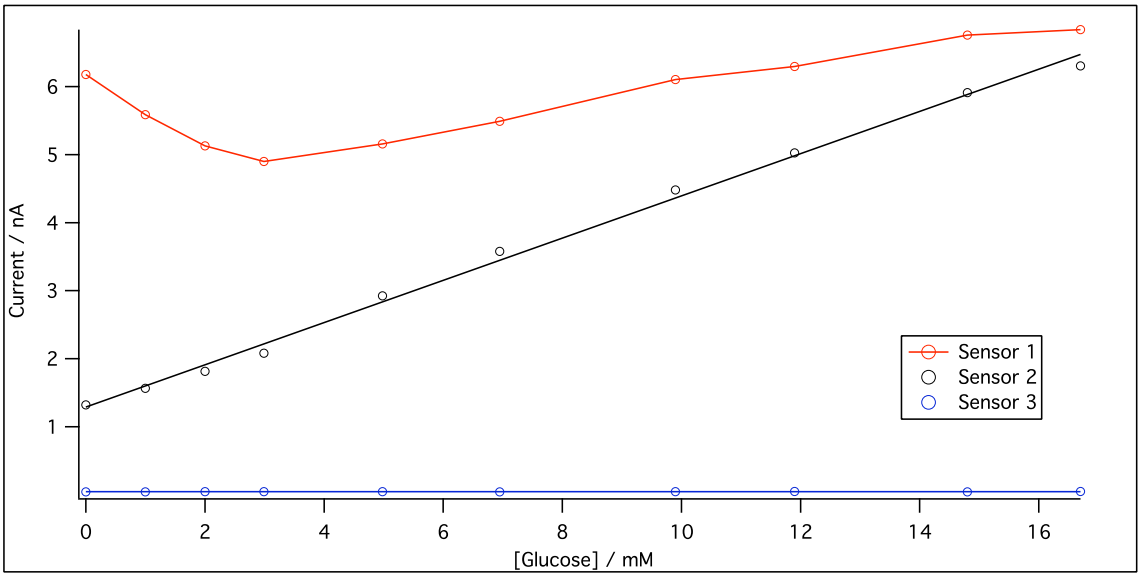


Figure 5.14: Calibration curves obtained from the titration of glucose; for three sensors prepared, as described without any pre-adsorption. The CV in Figure 5.13 corresponds to the trace shown here for sensor 1

sensitivity of only 310pA mM^{-1} of glucose. Even though the sensitivity is lowered, the background current in 100 mM PBS is roughly the same as that expected at 1.29 nA.

The shapes and qualities of the polymerisation CVs and the responses of each of the devices to glucose indicated that pre-adsorption was an important step in the fabrication procedure. The pre-adsorption of glucose oxidase lowers the area available for phenol polymerisation and allows for the formation of a stable protein layer on the surface of the platinum. A two hour period of glucose oxidase adsorption gave sensors that produced reproducible data. This lead us to conclude that although it is time consuming, the pre-adsorption of glucose oxidase is necessary for efficient sensor function.

5.5 Control studies

The responses from the glucose sensors were well characterised, but it was also necessary to study the negative controls. The two negative controls of most value were the addition of PBS aliquots using a fully functional glucose sensor and the addition of glucose using a platinum electrode with only a poly(phenol) film on its surface, there was no enzyme in this film.

One of the standard 200μm disc electrodes was used for the first of these two controls. It was first characterised using a standard glucose titration. The titration was then repeated, but this time the glucose was replaced by 100mM PBS. The two traces in Figure 5.15 show the data collected during each of the two titrations. The addition of glucose shows that the sensor in question is sensitive to glucose. This titration was stopped when the concentration of glucose in the cell had reached 10 mM. It is not known why the background current of this sensor has jumped up from ca. 0 nA to ca. 2.5 nA when the electrolyte was replaced. The background current from the red trace in Figure 5.15 is the expected result. All other experimental conditions were constant between the two set ups. That is there was no difference in the composition of the electrolyte or the stirring in the cell. It seems that the current in the negative control has not even reached a steady state value, as it can be seen

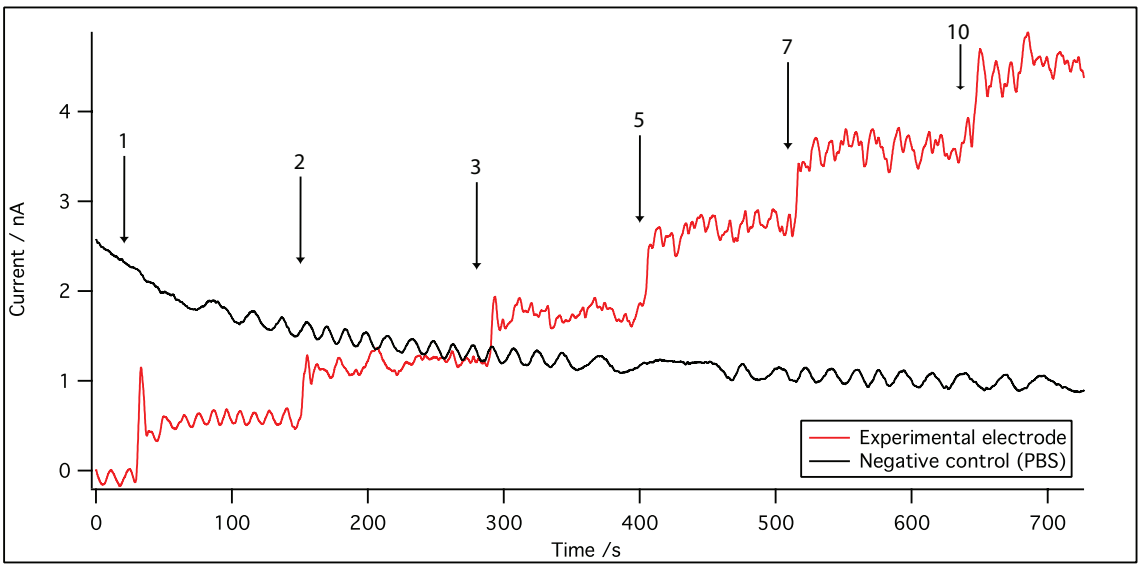


Figure 5.15: Currents recorded on a functional glucose sensor during a standard glucose titration (experiment) and the titration of 100mM PBS (negative control). The concentration of glucose in the cell was increased step wise, this is indicated by the labelled arrows in the figure.

to decay to below 1 nA over the course of 700 seconds.

The important point to note is that the signal from the sensor is not perturbed by the addition of 100 mM PBS; this is the supporting electrolyte in the cell and the medium used to make the glucose standard.

The second control test was the titration of glucose using a platinum electrode with only a poly(phenol) film. This test was conducted on a 1 mm platinum disc with no enzyme present in the cell during the electro-polymerisation and without any preadsorption of the enzyme. The CV recorded during the electro–polymerisation is given in Figure 5.16, scans 2 and 3 are not shown. As a comparison the same CV for an electrode with pre-adsorbed glucose oxidase is also shown. The background currents for each of these devices during the forward scan are similar. At potentials more positive than the oxidation potential, the background current of the poly(phenol) film is lower than that of the glucose oxidase encapsulated film. This is indicative of the latter not being as insulating as the pure polymer film and this is also reflected in the background currents of the reverse scan and the double

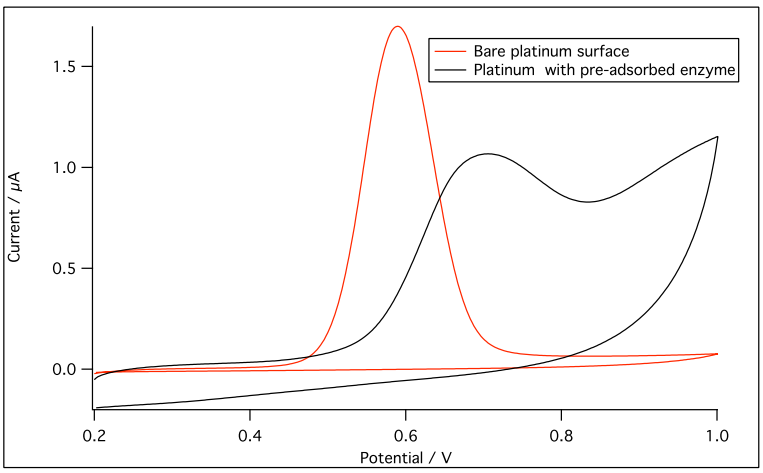


Figure 5.16: CVs for a the oxidation of 50mM phenol on a 1 mm bare platinum disc without any glucose oxidase in the cell and the same electrode with pre-adsorbed glucose oxidase and present in the polymerisation cell.

layer capacitance. Phenol polymerisation is a self sealing process, as any holes in the film will allow current to flow and hence generate polymer. With the enzyme the film does not self seal because the enzyme agglomeration hinders the approach of the reactants to the surface of the platinum.

The two most important features of these CVs are the I_p and E_p for the oxidation of phenol. The height of the oxidation peak at the bare surface is 1.69 μA and that of the glucose sensor is 1.07 μA; this is a 35% decrease. This indicated that the effective area of the electrode once the enzyme had been pre-adsorbed was diminished by a similar factor. The diffusion coefficient in the protein containing media will have an effect on the I_p, but the protein content in the cell is low enough for it not to be significant.

The peak potential of the CV in the presence of glucose oxidase too has shifted to a more positive value. This is because the pH in the cell was more acidic in the presence of the enzyme than in its absence due to the stock buffer. The pH of a pure phenol solution is 7.29 and the enzyme containing solution is at a pH of 6.41. The pH of the enzyme stock buffer (acetate) is 4.6 and therefore the pH of the final polymerisation solution is lower. All other parameters remained constant during each of these polymerisation reactions. This

observation agrees with the reports of the pH sensitivity for the electro–polymerisation of phenol by Arslan et. al. and Gattrell and Kirk [3, 4].

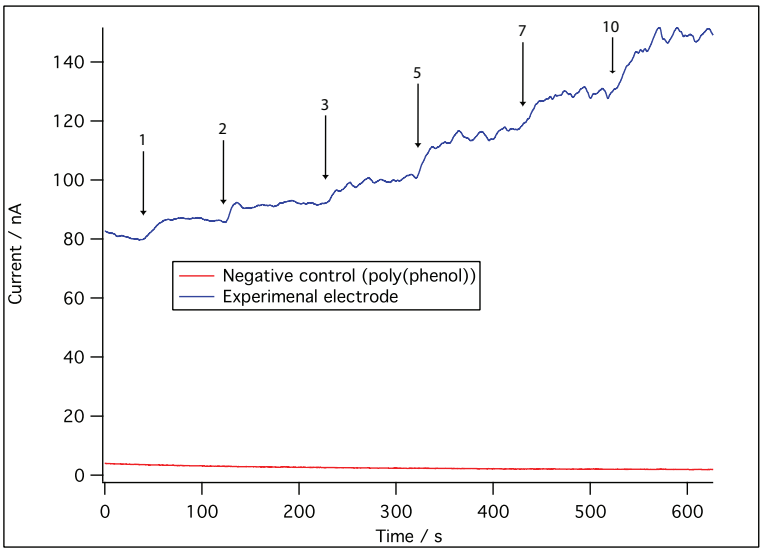


Figure 5.17: Currents recorded during a glucose titration on two 1 mm diameter platinum electrodes. One of the electrodes is a functional glucose sensor and the other is a poly(phenol) film electro-oxidised on the platinum surface. The arrows show the bulk glucose concentration in the cell during the titration.

The responses shown from the poly(phenol) film are shown in Figure 5.17 and here both the devices were calibrated at the same time. The background currents of each of these electrodes are different because the poly(phenol) film is a strong insulator, whereas the presence of glucose oxidase on the surface does not allow for a similar degree of insulation. This titration curve is truncated up to 10 mM. Again it is possible to see from the negative control that the responses form our sensors are due to the presence of glucose oxidase in the film, as poly(phenol) alone does not respond to changes in the concentration of glucose in the electrolytic cell.

5.6 Intra–batch variability

Once an optimised protocol had been developed, it was important to study the the intra–batch variability of the production process. Tests showed that it was possible to make up to 8 sensors in one batch without much change in the operating variability. The calibration curves for one such batch of 5 sensors are shown in Figure 5.7, these were prepared together over a single day. Each sensors' operating slope is shown in Table 5.3. The data shows that

Sensor	Slope / (pA mM^{-1}))
1	300
2	331
3	386
4	347
5	388
mean slope = 351 ± 37.6 pA mM^{-1}	

Table 5.3: Operating slope of a single batch of glucose sensors.

the chosen protocol allowed for the manufacture of a number of glucose sensors that were relatively well matched in sensitivity. The sensor variation was only 10.7% of the mean sensitivity, which is just outside the range of experimental error. The batch shown here is representative of the other batches manufactured in terms of operating characteristics and sensor variability.

The inter–batch variability was significant, the initial calibration of each batch of electrodes compensated for this to a large extent as all further analyses could be conducted using batch and device specific operating conditions. It is not known why there was significant inter–batch variability, but the most likely reason for this would be small variations in the stock buffer concentrations and pH. This would have resulted in variations in the solubility of the enzyme and the final pH of the solutions used for preadsorption and polymerisation. Another possibility could have been the small variations associated with electrode preparation.

5.7 Life–time analysis of the sensors

The life time of the sensors was studied over a period of 7 days. During this time the sensors were stored in 1× PBS at room temperature. Their behaviour over this period of time would allow us to ascertain their viability for long term sensing. A number of devices were used for this test from multiple batches.

The daily calibration curves for three sensors are shown in Figures 5.18 to 5.22. The days on which each of these sensors were tested are described in the legends of each figure. The responses from sensor 'A' are linear for a 6 day period and there is a daily decrease in sensitivity. The largest decrease occurrs between days 1 and 4, which is to be expected due to the extended length of time that had passed between the two calibrations.

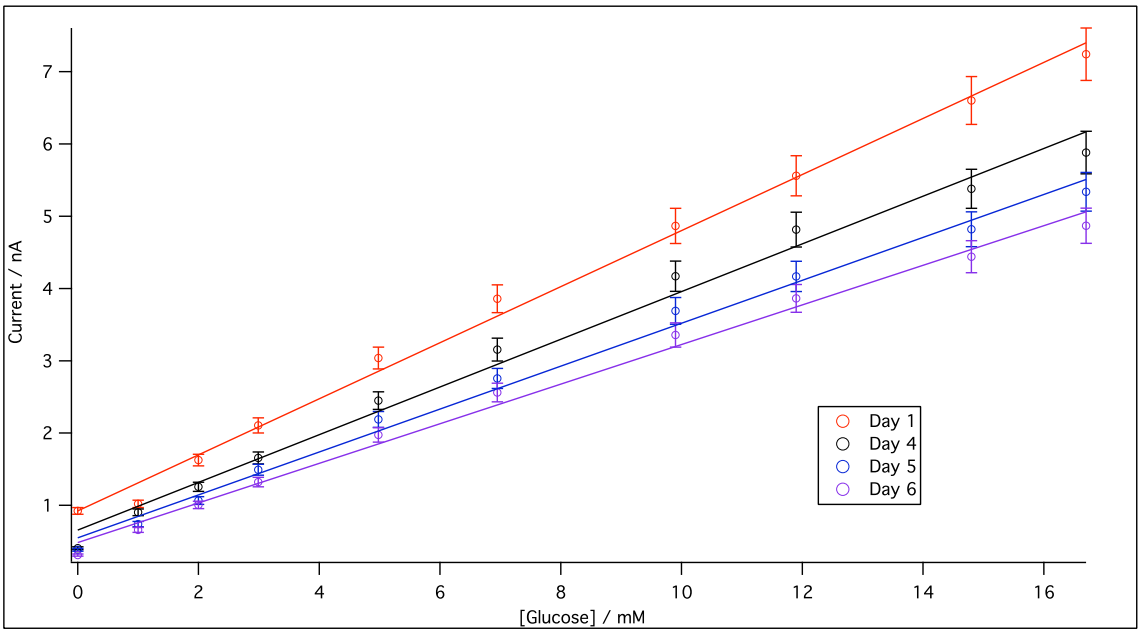


Figure 5.18: Variations in the calibrated responses to glucose on days 1, 4, 5 and 6, for sensor 'A'.

The calibration curves for sensors 'B' and 'C', shown in Figures 5.19 to 5.22, are split in to two different plots to allow greater clarity, although the scales of the plots are the same. This enables a direct comparison of changes in their sensitivity. Both of these devices show a

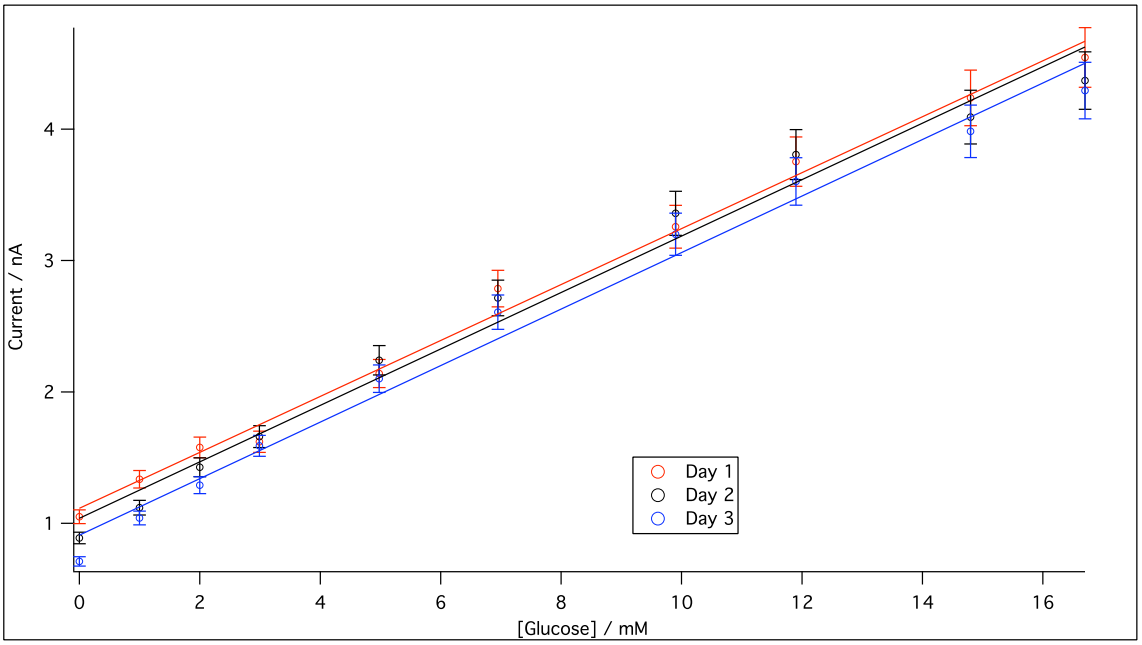


Figure 5.19: Glucose calibration curves, for sensor 'B' on days 1,2 and 3.

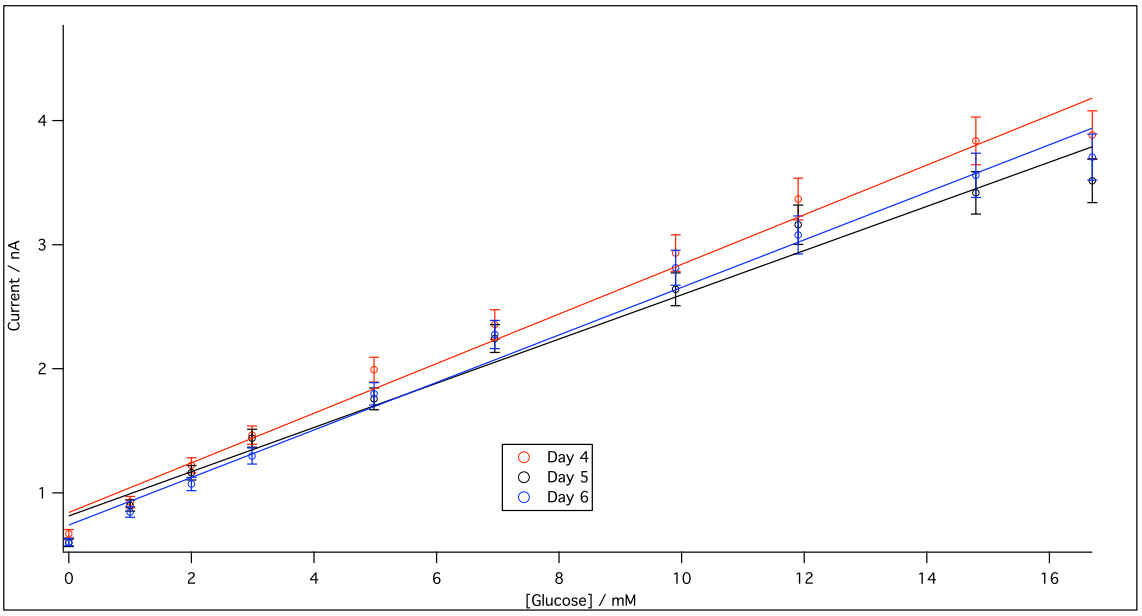


Figure 5.20: Glucose calibration for sensor 'B' on days 4, 5 and 6.

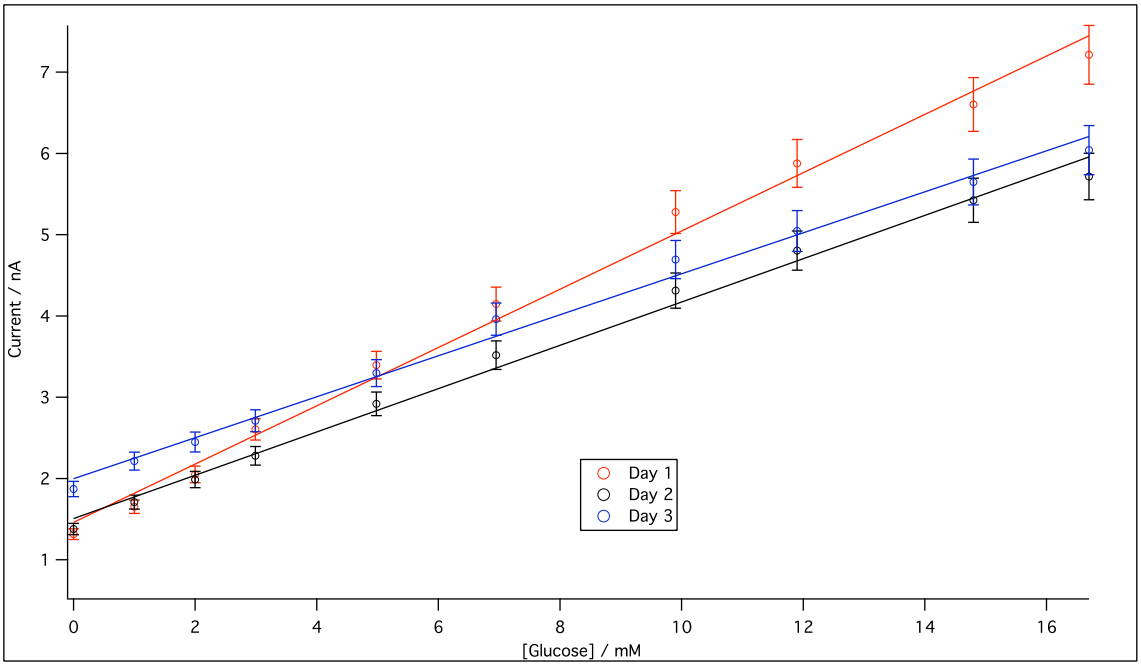


Figure 5.21: Glucose calibration curves for sensor 'C', from days 1 to 3.

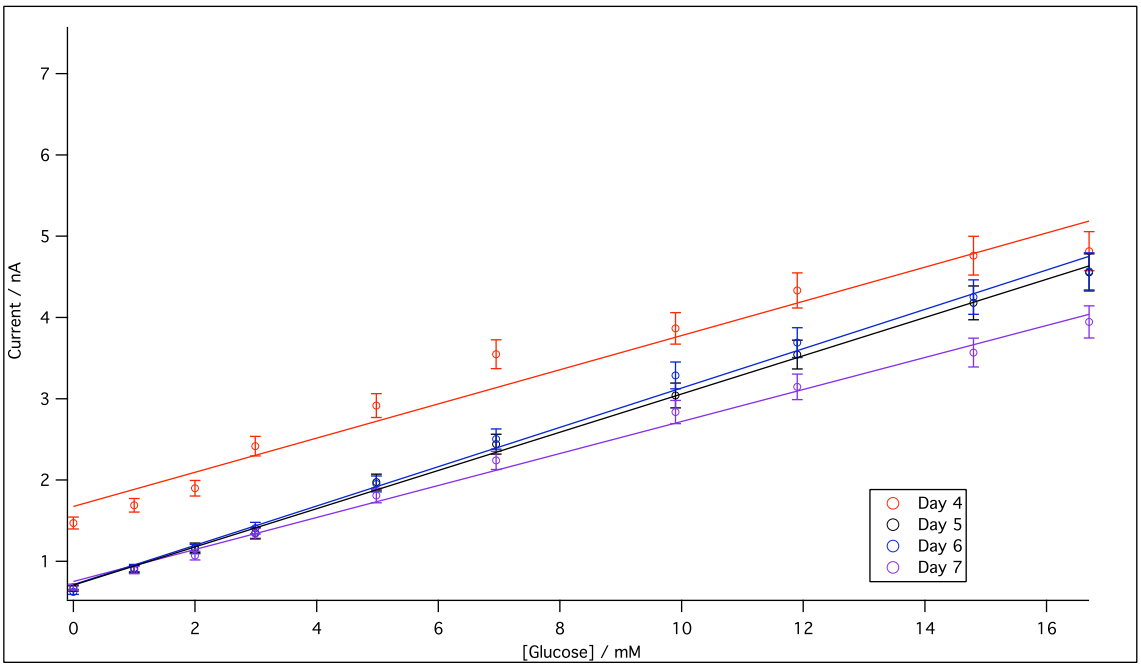


Figure 5.22: Glucose calibration curves for sensor 'C' from days 4 to 7.

large change in sensitivity during the first 48 hours and then their responses tend to stabilise for the remainder of the test period. These three devices represent the characteristics of the other devices tested, whose calibration curves are not shown.

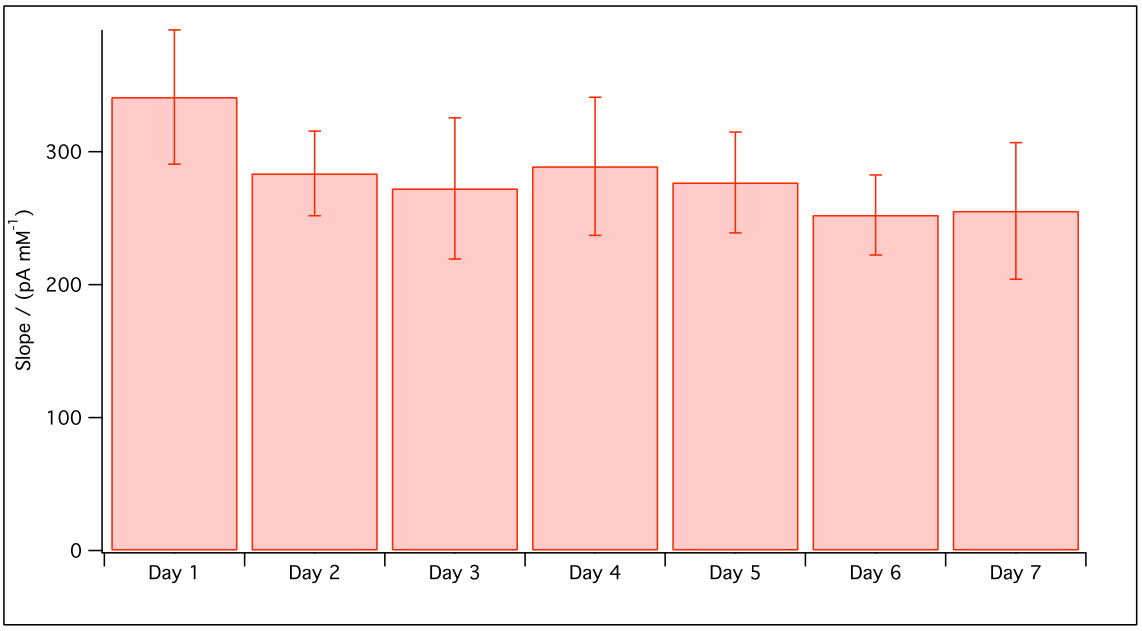


Figure 5.23: Daily variations in the calibration slopes for 7 days.

The operating characteristics show that the sensitivity of the sensors decreases primarily during the first 48 hours. Thereafter there is a slower decay in response. This might be considered to be within experimental error, however, this is not the case. The calibration curves, current responses and less marked steps are clearly indicative of this weak decay during the later days of titration. The error bars in plot 5.23 are very large because the daily variations were studied using data collated from different batches. As it was not possible to use a single batch, the inter-batch variations result in a broad spread of responses. The trend within each individual batch is similar to that shown here, which allowed the use of mixed data for this analyses. This was confirmed by doing an Analysis of Variance (ANOVA) and checking the homogeneity of variance using Levene's test. The results of the test showed that the inter–batch variations could be treated as being part of the same

population; this holds true for both the slopes and intercepts of the calibration curves. The F and P values at 1% significance level are shown in Table 5.4.

	F value	P value
Slope	0.8625	0.4579
Intercept	0.7153	0.5179

∗Values given for a 1% level of significance

Table 5.4: Analysis of inter-batch variance of the operating characteristics of glucose sensors. Obtained by performing and ANOVA on the batches and comparing the homogeneity of variance using Levene's test.

The main reason for this decay in sensitivity is related to the degradation of glucose oxidase, as described in chapter 6. The poisoning of the platinum surface due to the oxidation of H_2O_2 will play a role in the degradation of the sensor, but because these sensors were only used for the purpose of studying a daily variation, their use was limited.

According to Michaelis-Menten characteristics the K_m of the enzyme should remain unchanged. However, it is clearly evident that in the system described above the K_m decreases as the sensors age. This is because what we are seeing is a decrease in the apparent K_m of the system. As the enzyme film ages its responses to glucose change because of small changes to the number of serial processes that produce the signal. An ageing film might result in a reduction of glucose flux to the sensor's surface, or the approach of glucose to the active sites of the enzyme might become hindered. There are numerous reasons why there might be a decrease in the apparent K_m of the system and these would need to be investigated in more detail.

5.8 Summary

The preparation of glucose sensitive films made using the enzyme glucose oxidase attached to platinum discs with electro-polymerised poly(phenol) produces reliable and reproducible

devices. The composition of the electrolyte during the polymerisation and pre-adsorption stages is important in the operating performances of these devices. It was found that the final pH of the supporting electrolyte should be $\simeq 6.5$ and the [acetate] should be 100 mM.

The pre-adsorption of enzyme on to the platinum surface in the absence of the monomer, was also very important in the manufacture of the films. It increased the enzyme loading of the film; this can also be seen in the elevated background currents. These occur as a result of decreased insulation because the coverage of poly(phenol) is less.

Both of the negative controls suggest that the presence of glucose oxidase on the surface produces the oxidation signal following the addition of glucose aliquots during titration. The insulating properties of the pure poly(phenol) film also show that the presence of enzyme elevates the background current of the device, when poised at +700 mV, vs. a Ag|AgCl reference electrode.

The optimised protocol allowed for the manufacture of a number of sensors in a single batch and the variability within batches was only marginally above experimental error. when stored at room temperature the sensors were responsive to glucose for a period of 7 days. Most of the loss in sensitivity occurred during the first 48 hours of testing, with any further decay occurring at a slower rate.

References

[1] P. N. Bartlett and D. J. Caruana, "Electrochemical immobilization of enzymes .5. microelectrodes for the detection of glucose based on glucose-oxidase immobilized in a poly(phenol) film," *Analyst*, vol. 117, no. 8, pp. 1287–1292, 1992.

[2] P. N. Bartlett, P. Tebbutt, and C. H. Tyrrell, "Electrochemical immobilization of enzymes .3. immobilization of glucose-oxidase in thin-films of electrochemically polymerized phenols," *Analytical Chemistry*, vol. 64, no. 2, pp. 138–142, 1992.

[3] G. Arslan, B. Yazici, and M. Erbil, "The effect of ph, temperature and concentration on electrooxidation of phenol," *Journal of Hazardous Materials*, vol. 124, no. 1-3, pp. 37–43, 2005.

[4] M. Gattrell and D. W. Kirk, "A study of electrode passivation during aqueous phenol electrolysis," *Journal of the Electrochemical Society*, vol. 140, no. 4, pp. 903–911, 1993.

Chapter 6

Surface characterisation of glucose sensors

6.1 Introduction

To understand the glucose sensors, their surfaces have been studied using various analytical techniques. This will enable a better understanding of the mechanism of the sensor and in future iterations its performances can be improved.

6.2 Optical analysis

Fourier Transform – Infrared Spectroscopy (FT–IR) and Raman spectroscopy are analytical techniques that utilise the different vibrational properties of molecules for molecular analysis. They give characteristic peaks for functional groups and are therefore powerful tools.

There are two chemical entities on our glucose sensors, glucose oxidase and poly(phenol). With each of these techniques, we wanted to find their distribution within the film. It is possible to study the films using FT–IR and Raman, because the characteristic bands for

the functional groups from both the enzyme and the polymer are well defined and do not overlap each other; as shown in Table 6.1. The aromatic ring breathing mode originates from the poly(phenol) and the three different amide stretch bands can be used to study the distribution of glucose oxidase and also each of these are reported to be strong bands. There might be some contribution to the aromatic band from the tyr, phe and trp residues of glucose oxidase, but the strength of the amine bands will be greater.

Group	Raman band / cm^{-1}	FT–IR band / cm^{-1}
Amide I [1]	1595 - 1720	1595 - 1720
Amide II [1]	–	1540 - 1580
Amide III [1]	1243 - 1269	–
Aromatic ring [2]	1000	1000

Table 6.1: Vibrational bands of functional groups expected to be found in the glucose sensors.

6.2.1 FT–IR spectroscopy

The infra-red spectra from glucose oxidase, in Figure 6.1, shows the bands from Table 6.1. The Amide I and Amide II bonds are what we were looking for on sensors' surfaces. Operating in reflectance mode, spectra were collected at a few points on the surface. The spectra collection points were chosen based on the visual image from the optical microscope.

As we can see in Figures 6.2 and 6.3 the absorbance bands on the spectra collected are weak, these figures are representative of 7 different points that were tested on the same sensor. The signal to noise ratio (S/N) is so low that no inference can be made about the molecules on the surface. These spectra are collected through an aperture that is 100 × 100 μm in dimension. This aperture was the smallest that allowed any indication of IR absorbance. Smaller apertures are required to determine the distribution of glucose oxidase and poly(phenol), but at these smaller apertures the incident IR energy is lower and the

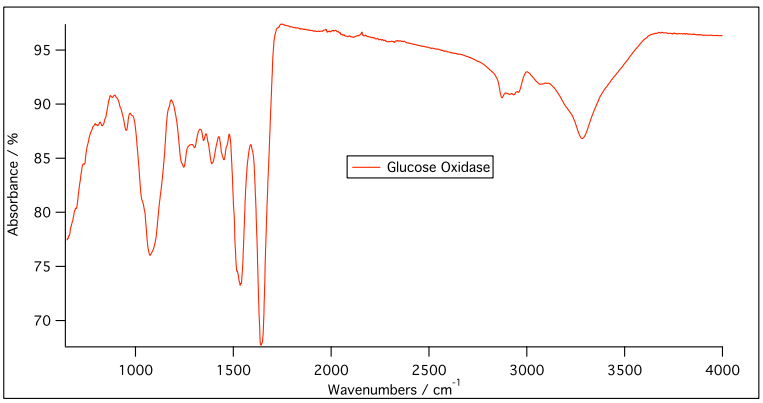


Figure 6.1: IR absorbance spectra for glucose oxidase, obtained using ATR from pressed powder.

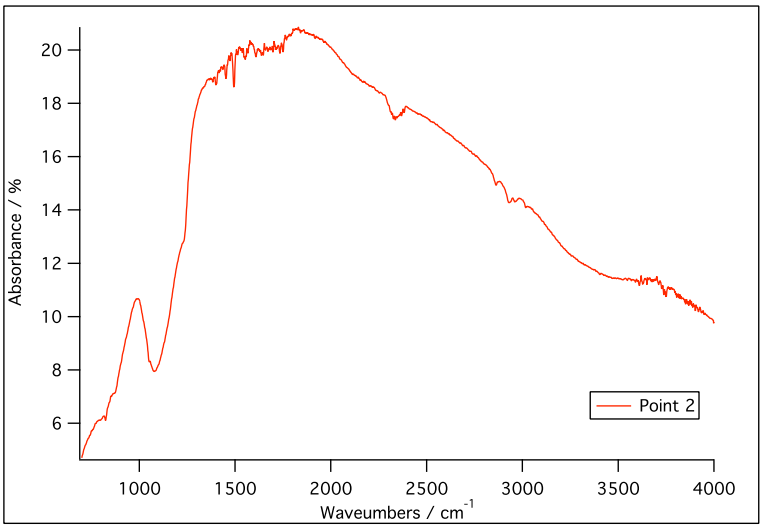


Figure 6.2: IR spectra from the sensor's surface, prepared as a functional glucose sensor. The absorbed signal from the surface is weak and looks similar to a background scan.

signal to noise ratio is even worse. It is clear from Figures 6.2 and 6.3 that the incident beam is not passing through a sufficient amount of material to produce a strong signal.

Films of poly(phenol) and its derivatives have been studied using FT–IR spectroscopy and reports in the literature have shown the ability to distinguish the spectra. Lapuente et. al. use attenuated total internal reflection (ATR) to study films of poly(phenol) and the spectra obtained by them can be used to analyse the composition of the coating [3]. In the

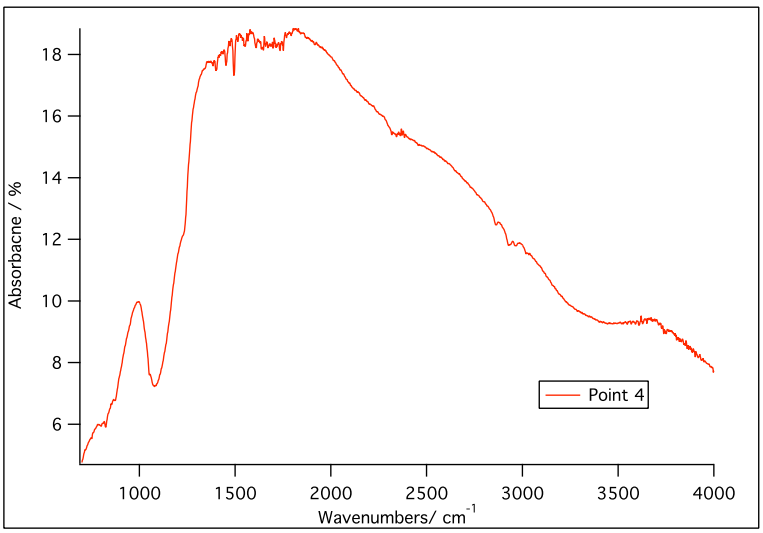


Figure 6.3: IR spectra from from the surface of a glucose sensor. The absorbed signal is weak and none of the characteristic bands can be distinguished.

context of this study there are two limitations with their approach. Firstly, the equipment available did not allow the use of ATR. Secondly, ATR operation does not allow the mapping of the surface, but gives the composition of all the material that is in optical contact with the crystal. Another report by Ferreira and co-workers showed spectra better than those reported in this work, but they are still weak, although the bands can be distinguished [4].

6.2.2 Raman spectroscopy

It was thought that maybe with the use of Raman spectroscopy it might be possible to achieve a better signal and having the ability to tune the power of the incident laser, might improve this. The laser power was defined by the software using a logarithmic scale.

Raman spectra for both the raw materials are shown in Figures 6.5 and 6.4. The crystals of phenol produce a brilliant spectra with a very well resolved and strong peak for the aromatic ring breathing mode at 1000 cm^{-1}. This shows that the signal is strong for a low incident power and that the Raman scattering for phenol can be used as a simple recognition tool. The response from the glucose oxidase sample is relatively weaker, as the

spectra from Figure 6.5 was obtained at a higher laser power. This is because the glucose oxidase was dried on a reflective substrate and then analysed under the laser. This drying process resulted in a much thinner film and consequently weaker spectra.

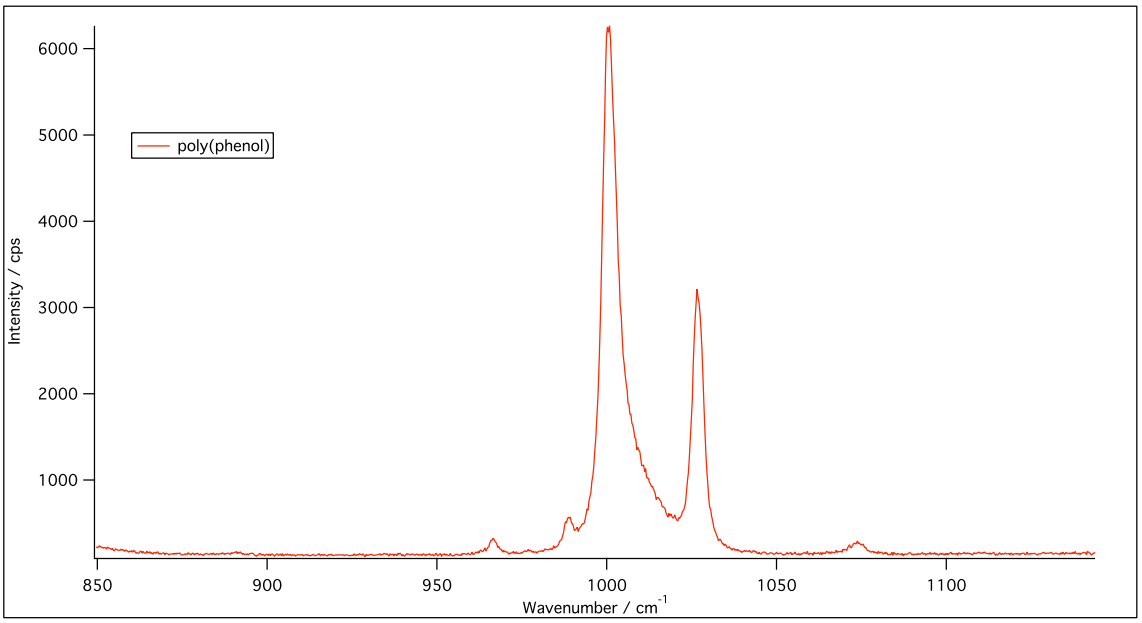


Figure 6.4: Raman spectra for crystals of phenol placed on a glass slide.

Firstly a pure poly(phenol) film was analysed under the Raman laser, the resulting spectra of which, can be seen in Figure 6.6. The lower trace was collected when the power of the laser had been attenuated to 10% of its maximum and the second spectra was collected when the power of the laser had been turned up to 30%. Both these spectra show that the poly(phenol) film is too thin to result in a detectable Raman peaks, at the expected wavelengths.

Then, the surface of a glucose sensor was tested, firstly a short study was conducted to find the optimum power of the incident laser. Figure 6.7, shows that at each setting of the incident laser the aromatic ring breathing mode a 1000 cm^{-1} can not be picked up, so the laser power was optimised based on the amide bands alone. Increasing the laser power increases the background intensity and also harms the film on the surface. From Figure 6.7, it was decided to use a laser power setting of 30%, this is because it shows the maximum

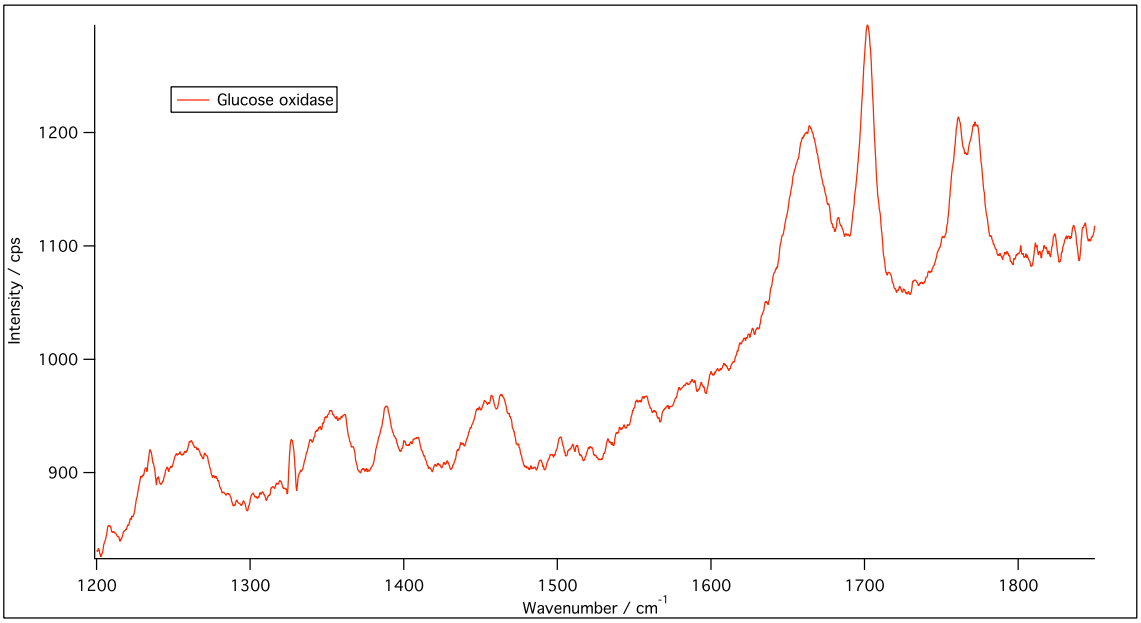


Figure 6.5: Raman spectra for glucose oxidase dried from solution on a reflective substrate.

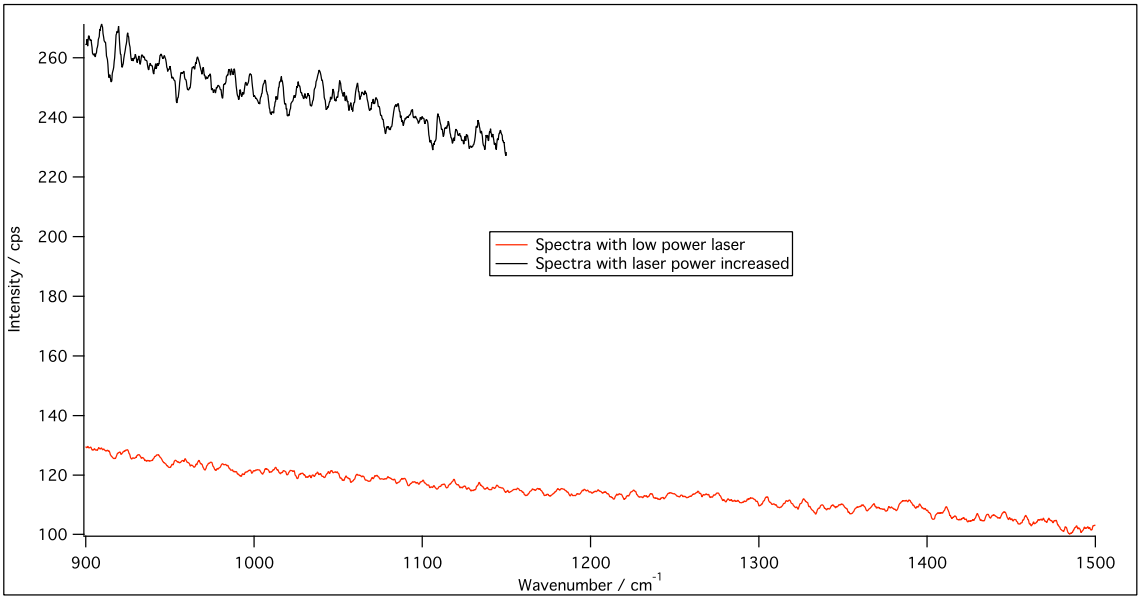


Figure 6.6: Raman scattering for poly(phenol) polymerised on a polished platinum substrate. Two different laser powers were used to assess whether the signal from the thin film could be improved.

S/N ratio. It is possible that the higher laser powers will show an increased signal, but at the same time a large proportion of the thin film was being burnt away by the increased power of the incident laser.

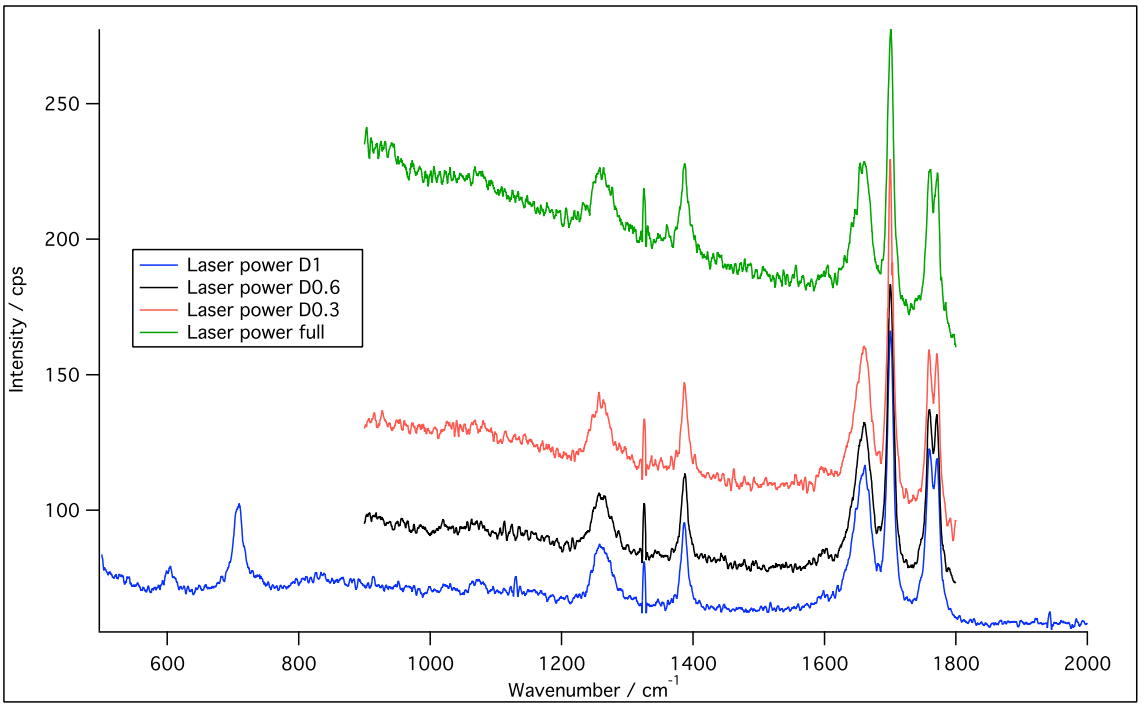


Figure 6.7: Raman scattering for a glucose sensor at different laser power settings.

The Raman was used to develop a map of the scattering bands on an area of the platinum surface. Due to a poor signal, the map is not shown here, but Figures 6.8 and 6.9 show two points each for the collection of spectra which showed some features and those that did not show any. Altering the collection conditions for the spectra did not improve the signal strength, any further.

It should be possible to obtain a better resolution of the chemical characteristics of the glucose sensors using Raman spectroscopy; although this was found not to be the case, as the thickness of the film and therefore the small amount of material that the laser passes through did not allow this. Therefore, in this case, these simple and powerful optical techniques are not suited to draw any conclusions about the morphology of the enzyme

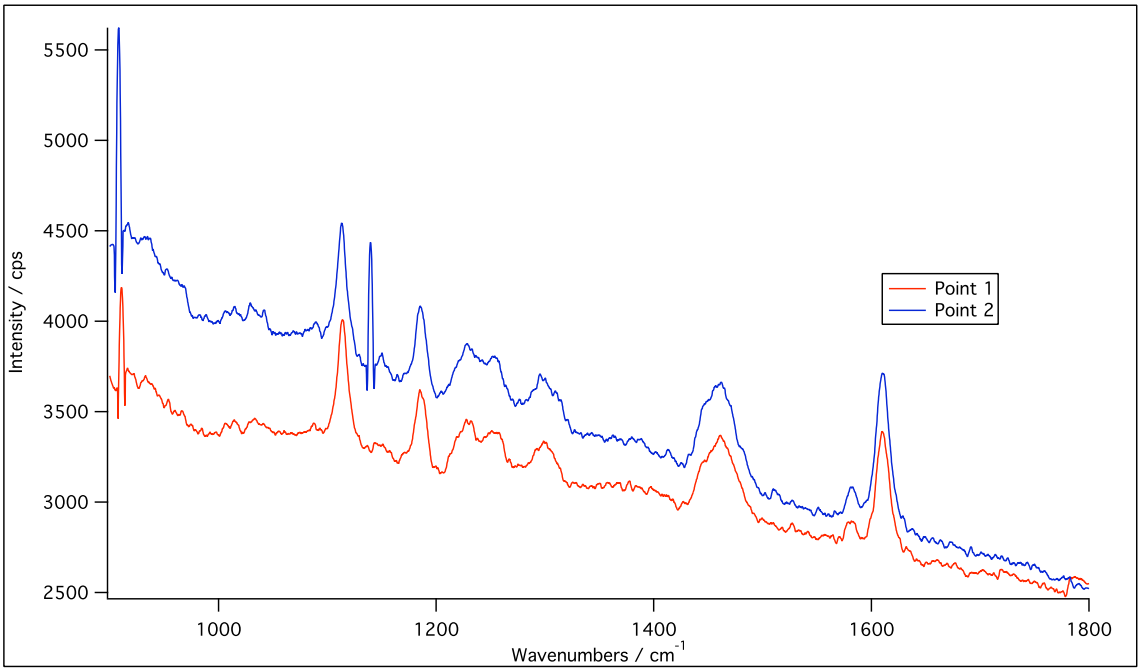


Figure 6.8: Raman spectra from the surface of a glucose sensor showing weak bands.

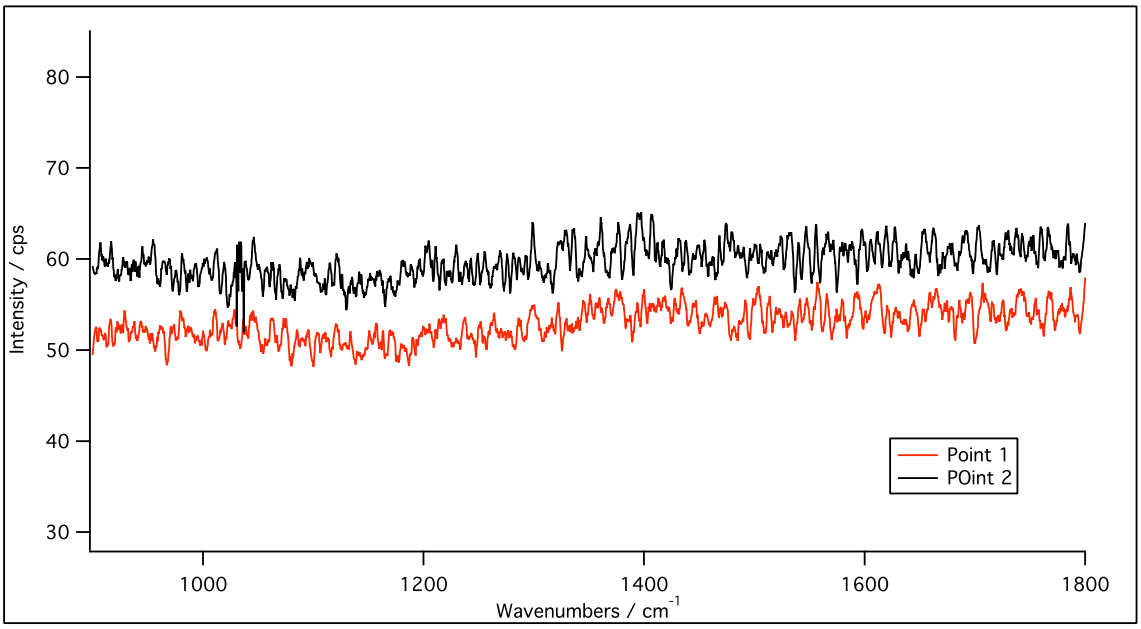


Figure 6.9: Raman scattering from the surface, at points of little or no signal.

film on the platinum substrate. Fleischmann et. al. have reported the Raman analysis of poly(phenol) films on silver electrodes, but in their case the Raman was surface enhanced (SERS). The surface of the silver was electrochemically roughened and then Raman spectra of the polymer collected; this improved the intensity of the Raman spectra [5]. Using SERS might be a method to improve the Raman analysis, but it will affect the electrochemical properties of the devices as well.

6.3 Cyclic Voltammetry

6.3.1 Validation

A poly(phenol) film will passivate the surface of the electrode, but the presence of enzyme in the film alters the degree of insulation. Along with this, the diffusion profile to the surface of the electrode will determine the flux and the quality of response to changes in the bulk concentration of glucose.

The ferrocyanide redox couple was used to observe the accessibility of probe molecules to the surface of the electrode. This test was carried out using a functional enzyme sensor made on a 1 mm platinum disc electrode. During the first test the sensor was tested for its responses to glucose on a daily basis, immediately prior to the ferrocyanide test. The quality of the polished platinum surface and the total area available, on the unmodified electrode, for ferrocyanide redox can be seen in Figure 6.10.

As a comparison to the bare electrode, the initial CVs for the same disc electrode are shown, in Figure 6.11 with a poly(phenol) layer on the surface and as a fully functional glucose sensor. The peak and background currents for each of these surfaces is an order of magnitude lower than that for the bare platinum. This is because the effective area of the surfaces has been changed and the insulating nature of the poly(phenol) film decreases the steady state current.

The forward scan of the poly(phenol) film exhibits the behaviour of a steady state

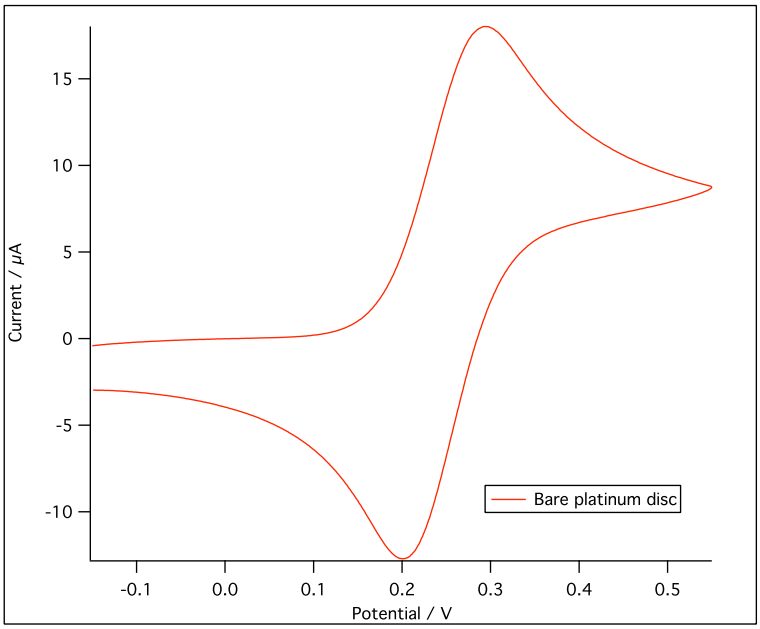


Figure 6.10: CV of 10 mM ferrocyanide in 100mM KCl on a bare 1 mm platinum disc electrode. $\dot{v} = 100$ mV s^{-1} and $C_b = 10$ mM

voltammogram. This points to the fact that the 'pin hole' imperfections in the film are small and spaced far enough apart, so as to give a semi-hemispherical diffusion profile. On the other hand the film containing the enzyme shows behaviour that is more characteristic of regions where the edge effect is not as significant. The charging currents for each of the modified surfaces are of interest as well, and will be discussed later.

As shown in Figure 6.12 there are three types of diffusion profiles for molecules to an electrodes' surface, (a) is a semi-infinite planar diffusion profile, where the characteristic dimension of the electrode is > 20 μm, (b) is a semi-hemispherical diffusion profile with the electrodes' characteristic dimension being < 20 μm and (c) is a hybrid of both of these diffusion profiles. This schematic illustrates the approximate distribution of redox active centres, on a heterogeneous surface, to facilitate any one of these diffusion profiles. For the specific case of (c), the individual diffusion profiles of each active centre overlap and this leads to the formation of a quasi - linear diffusion profile.

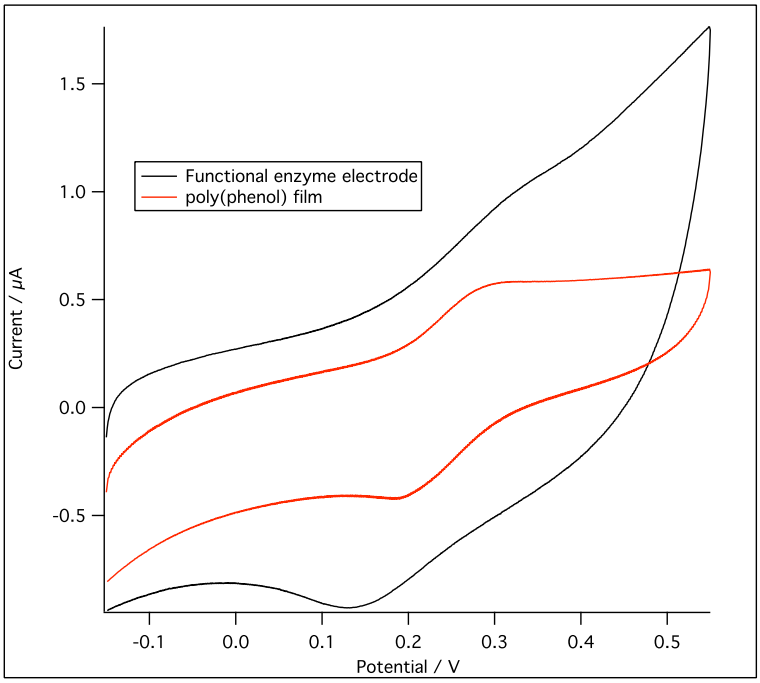


Figure 6.11: CV of 10mM ferrocyanide in 100mM KCl on a poly(phenol) coated and an enzyme encapsulated platinum disc electrode with a 1mm diameter. $\dot{v} = 100$ mV s^{-1} and $C_b = 10$ mM

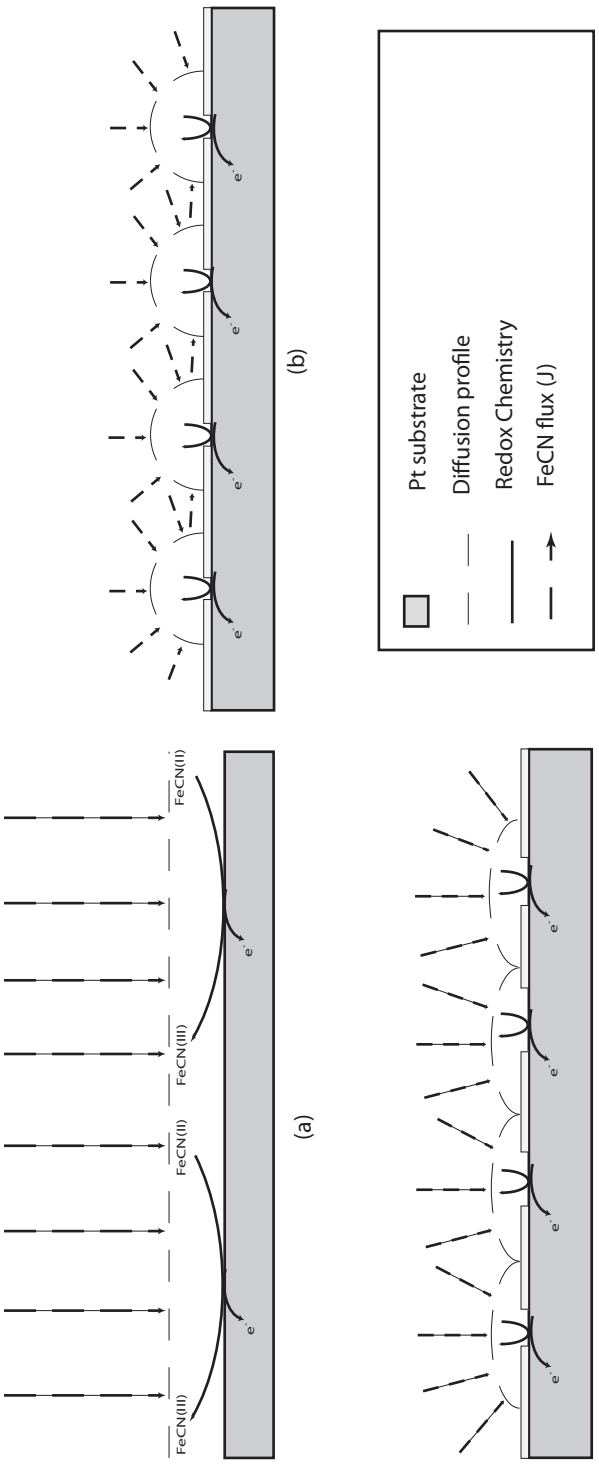


Figure 6.12: Three different types of diffusion profile at an electrodes' surface: (a) planar, macro electrodes; (b) semi-hemispherical, micro electrodes and (c) a hybrid with overlapping diffusion profiles.

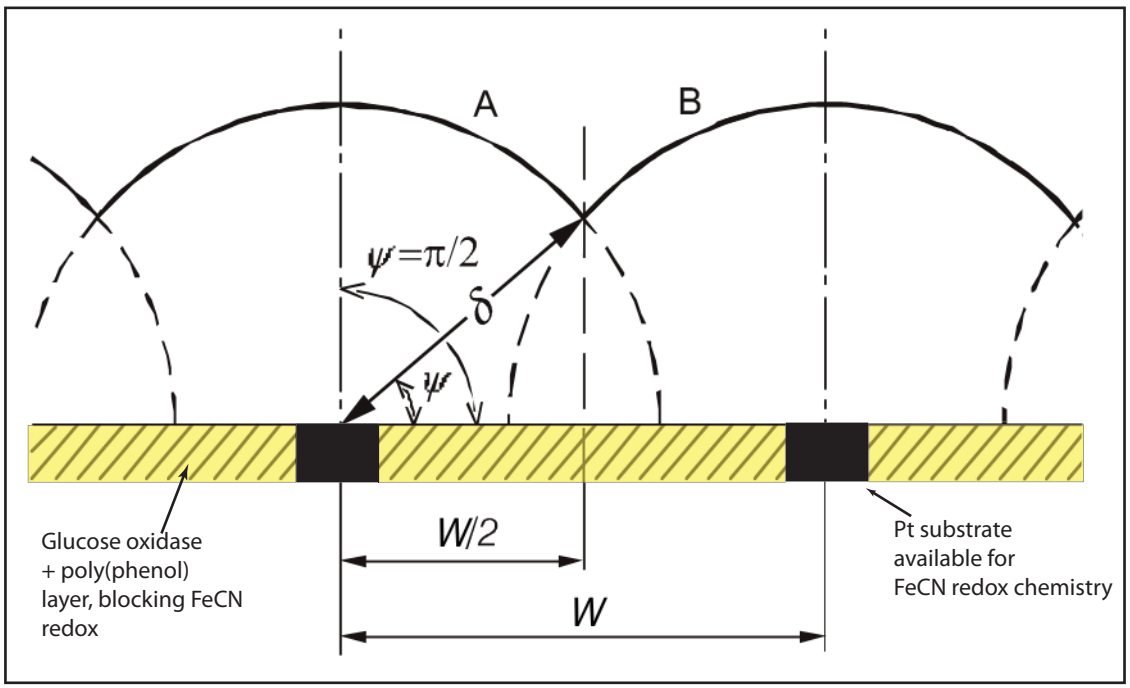


Figure 6.13: The structure of a quasi–linear diffusion profile, adapted from [6].

As can be seen in Figure 6.13 a semi-hemispherical diffusion profile (dashed line) can be attained, around the platinum substrate. The diffusion length (δ) is defined as a function of the diffusion coefficient (D) and time (t). There are two limiting cases that describe the diffusion profiles of (a) and (b) in Figure 6.12, where r is the radius of the electrode or active centre [6].

1. $\delta << r$, in this case the edge effect is not significant and the linear model for diffusion should be used.

2. $\delta >> r$, here the diffusion profile is semi-hemispherical, as the flux at the surface of the electrode is not constant over its area.

$$\delta = \sqrt{\pi D t} \tag{6.1}$$

The other key parameter in obtaining steady state diffusion is the separation between two electrode or active centres (W). This is only possible if the condition in Equation 6.3 is

met, otherwise we end up with overlapping diffusion profiles, as shown with the solid black lines of Figure 6.13. The angle ψ represents the degree of overlap and amongst others, is a function of the electrode separation W. The limiting case where $\psi = \pi/2$ is the case of planar diffusion [6].

$$W = W_e + W_g \tag{6.2}$$

$$W/2 > \delta \tag{6.3}$$

The peak separation for the poly(phenol) film is 100 mV at a scan rate of 100 mV s^{-1}, according to conventional theory based on semi-infinite planar diffusion this would be classed as a quasi-reversible process. This is not entirely unexpected, as the poly(phenol) film is insulating in nature and the electron transfer kinetics may have been affected. If we look at a different model, suggested by Armstrong et. al., which is based on a limited number of active sites for ferrocyanide redox the electron transfer kinetics maybe different [7]. Based on the shape of the voltammogram we can hypothesize that the diffusion profile is not planar, but one based on (b) or (c) from Figure 6.12.

Armstrong et. al. have suggested two tests for reversibility when the number of active sites on the surface is limited, these are shown in Equations 6.4 and 6.5. Where $E_{1/4}$, $E_{1/2}$ and $E_{3/4}$ are the potentials at $\frac{1}{4}$, $\frac{1}{2}$ and $\frac{3}{4}$ of the peak current and E^0_{rev} is the E^0 at a bare electrode with semi-infinite planar diffusion at its surface [7].

$$E_{1/4} - E_{3/4} = \frac{RT}{nF} ln9 \simeq 55mV \text{ [T=298K]} \tag{6.4}$$

$$E_{1/2} = E^0_{rev} \tag{6.5}$$

For the case of the poly(phenol) covered electrode, from Figure 6.11, these tests were conducted to ascertain whether the electron transfer kinetics were indeed quasi-reversible, or if the microscopic model showed that because of the decreased number of sites, the electrochemistry was still reversible. The bare polished electrode shows an E^0_{rev} of 225 mV

and the calculated half peak potential, $E_{1/2}$ from Figure 6.11 is 230 mV. Also the $E_{1/4}$ for this CV is 202 mV and the $E_{3/4}$ is 258 mV, so the difference is 56 mV. This value is also within the 55mV ± 5 mV suggested by Armstrong et. al. [7]. This shows that although the ferrocyanide redox appears to exhibit quasi-reversible electron kinetics when studied under conventional diffusional profiles, its electron transfer kinetics are rapid, if the number of active sites available is taken into account. Armstrong et. al. have reported that the rate of electron transfer in such cases is greater than 1 cm s^{-1} [7].

So, now that we can be certain of the reversibility of this system, using the above model, we can also estimate the radius of the active sites and the degree of sphericity of the diffusion profile. The relationships used to find these are described by Armstrong et. al. and shown in Equations 6.6 and 6.7, where r_0 is the radius of the active centres and β is the sphericity of the diffusion profile. The limit for β, where the diffusion profile tends to linear is zero [7].

$$i_{lim} = \frac{nFADC_o^b\beta}{2}\sqrt{\frac{nF\dot{v}}{DRT}} = 4\pi r_0 nFDC_o^b \tag{6.6}$$

$$\beta = \frac{2}{r_0}\sqrt{\frac{DRT}{nF\dot{v}}} \tag{6.7}$$

An estimate for r_0 for the active centres on the pure poly(phenol) layer, from equation 6.6 is 1.32 μm; where $D = 2.4 \times 10^{-5} cms^{-1}$ and $C_o^b = 10$ mM. From this β can be calculated as 34.5, with a $\dot{v}$ of 100 mV s^{-1}. These two values are in good agreement with those proposed by Armstrong et. al. [7]. This shows that the diffusion profile is approximately 90% spherical, as reported in [7] and that the redox of ferrocyanide through the poly(phenol) film is reversible.

The daily calibration curves for the enzyme sensor are shown in Figure 6.14, where it can be seen that there is no appreciable deterioration in the sensors' performance till day 5.

A fresh batch of 10 mM ferrocyanide was prepared every day and cyclic voltammetry performed at $\dot{v}$ = 100 mV s^{-1}. The redox activity of the surface on days 1 and 2 can be

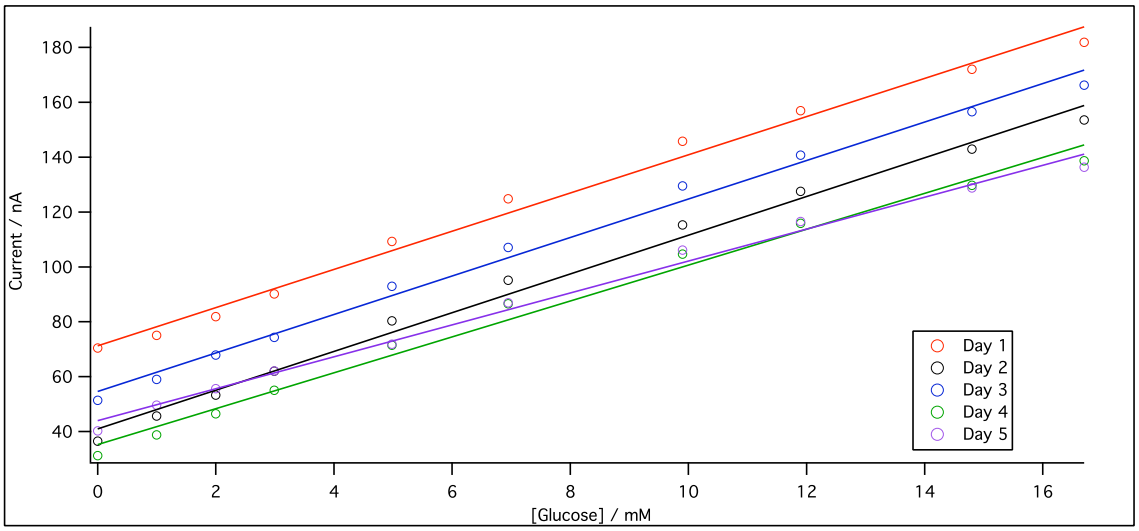


Figure 6.14: Daily glucose calibration curves for the glucose sensors used in this experiment. The sensor is made on a 1 mm platinum disc with pre-adsorbed glucose oxidase encapsulated in a poly(phenol) film.

seen in Figure 6.15 and those for days 3 to 5 can be seen in Figure 6.16. As can be seen in Figure 6.15 there is a weak cathodic shoulder during the forward scan and a stronger anodic peak on day 1. In the same figure it is possible to see that these Faradaic processes on day 2 are greatly diminished.

Figure 6.16 clearly shows that by the 3^{rd} day there is no ferrocyanide redox activity on the surface of the platinum electrode. This observation is very counter intuitive, as it is to be expected that during the life time of the sensor the access of probe molecules to it surface should not diminish. It is thought that the protein adsorbed on the surface of the platinum, is what decreases the effective area of the disc and acts as the primary mass transport barrier to probe molecules. This is supported by studying the responses seen from a plain poly(phenol) film and an enzyme loaded surface, in Figure 6.11. Therefore if the sensor degradation occurs due to a loss in enzyme activity then the access of probe molecules and hence the redox behaviour of ferrocyanide should remain roughly constant. On the other hand if glucose oxidase and poly(phenol) are being lost from the surface then the effective area will increase and so should the electrochemical activity of ferrocyanide.

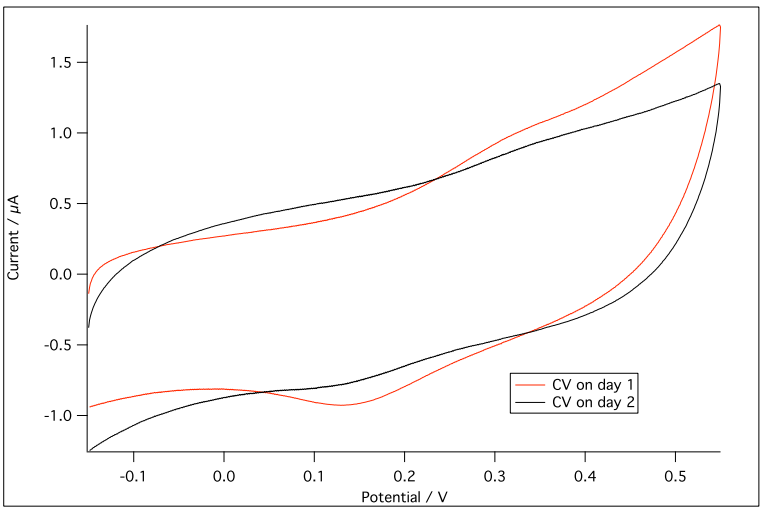


Figure 6.15: CVs of 10mM ferrocyanide in 100mM KCl from the functional glucose sensor on days 1 and 2.

For this experiment these were not the observations.

As seen from the calibration curves, Figure 6.14 the sensitivity of the device remains virtually constant for the time period of this trial. Therefore there does not appear to be a loss of material from the surface of the platinum. There is another very important feature that is being changed during this test. The electrochemical oxidation of hydrogen peroxide, during the calibration of the sensors results in the oxidation of platinum to platinum oxide. The electrochemical redox behaviour of ferrocyanide is sensitive to the oxide content of the platinum surface. In essence during the daily calibrations of the sensors the already limited number of sites available for ferrocyanide electrochemistry were being depleted.

As can be seen from the shape of the CVs from days 1 and 2 the active sites for ferrocyanide are limited, but their distribution is such that the diffusion profile of ferrocyanide remains a hybrid between radial and semi-infinite planar. If the ferrocyanide sites were spread further apart, then a steady state voltammogram might be observed, although the charging currents may be higher than seen for an array of microelectrodes with a similar total area. This is because by altering the surface of the platinum, we have changed the charge storage capacity; again this will be discussed in more detail later.

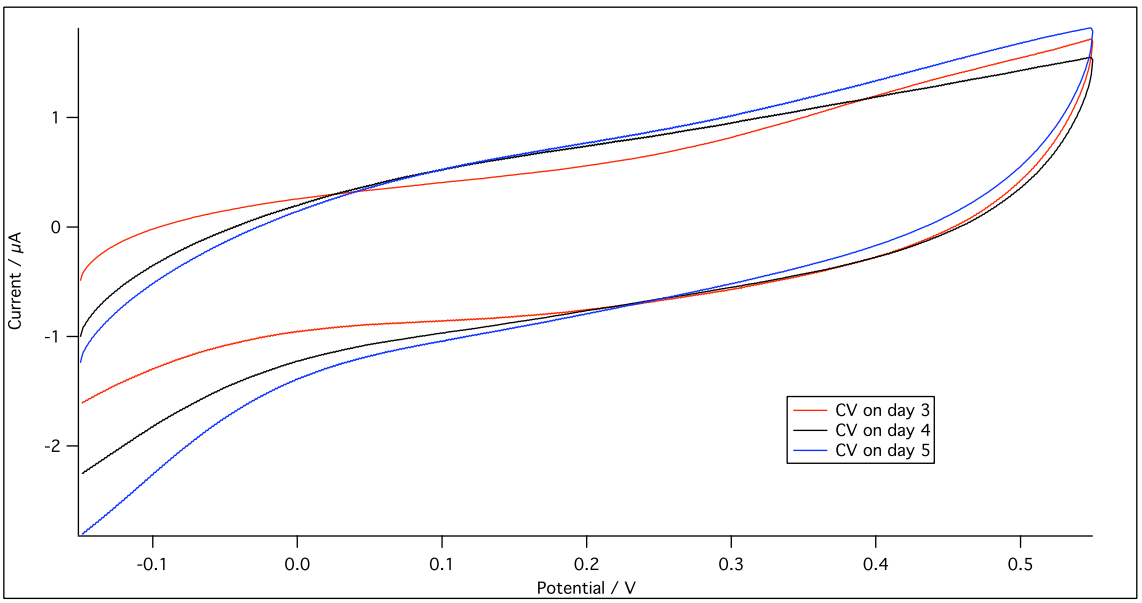


Figure 6.16: CVs of 10mM ferrocyanide in 100mM KCl from the functional glucose sensor on days 3 to 5.

Seeing the results of this trial, it was necessary to alter the experimental procedure slightly. Therefore it was decided not to test the glucose sensor on a daily basis, but to assess its operating characteristics on the first day and then only analyse its behaviour to ferrocyanide electrochemistry. Also it was thought that a scan rate analysis should be performed to understand the system in more depth.

6.3.2 Study of the film's diffusion profile and e^- transfer

Three 1 mm disc electrodes were prepared as earlier. The different films on their surfaces and the nomenclature used to refer to them are shown in Table 6.2. Electrode '2' was used primarily for the purpose of scanning probe microscopy, although it was used in the latter stages of this test as well. During the course of day 3, this sensor was placed in a humidification chamber for two hours, so as to alter the structure of the film. This was performed in order to aid with SECM studies as described in section 6.4.

The initial calibration curves for electrodes '1' and '2' can be seen in Figure 6.17 and the

Electrode name	Surface Modification
'1'	functional glucose sensor
'2'	functional glucose sensor
'3'	poly(phenol) only

Table 6.2: Nomenclature of electrodes used for ferrocyanide CV tests.

operating characteristics in Table 6.3. It can be seen that the calibration response from '1' is slightly better than that for '2' and also that the background current for '2' is substantially suppressed relative to '1'. This indicates that there is a slightly higher enzyme loading on '1' and therefore the coverage of insulating polymer poly(phenol) is slightly lower. The higher enzyme loading facilitates the increased response to changes in glucose concentration on '1', whereas the increased coverage of an insulating film suppresses the background current, on '2'.

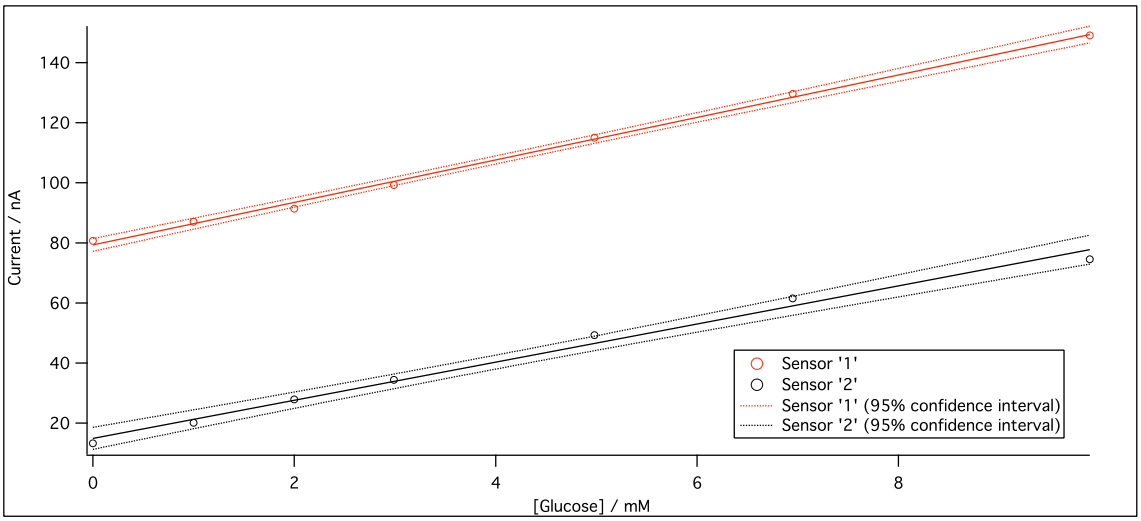


Figure 6.17: Initial calibration curves for '1' and '2' before CV trials.

We know that the electrodes perform to par for the remainder of the 5 days, therefore it will be assumed that their character remains similar to the daily responses seen in Figure 6.14. Whilst this is an assumption, the stability of the electrodes appears to be reproducible,

Electrode name	Slope / (nA mM^{-1})	Intercept / nA
'1'	7.08	79.3
'2'	6.34	14.92

Table 6.3: Initial operating characteristics of '1' and '2'.

and the trade–off with achieving a better response to ferrocyanide without altering the oxide content of the platinum surface is an advantage. Prior to the loading of the films, the polished electrodes were tested in 10 mM ferrocyanide at a scan rate on 100 mV s^{-1}; these scans can be seen in Figure 6.18. The surfaces are of a good quality and are reproducible. The small variations in I_p could be a result of the electrodes having a slightly elliptical shape, or they could be a result of inconsistent surface preparation.

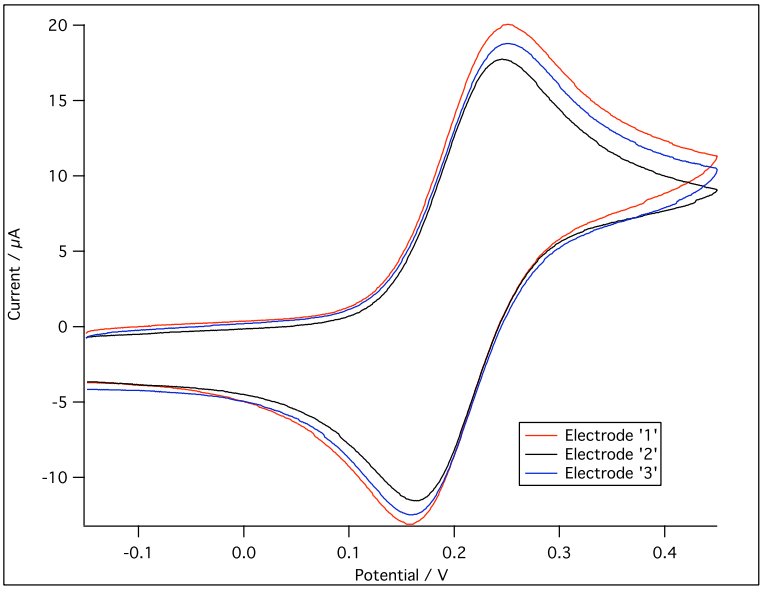


Figure 6.18: CV of 50mM ferrocyanide in 100mM KCl on three 1mm bare platinum disc electrodes, $\dot{v} = 100$ mV s^{-1}.

Firstly, electrode '3' which only has a poly(phenol) film on its surface, is analysed. As we saw in Figure 6.11, we should expect to see a low current response to ferrocyanide in both directions and depending on the distribution of the film's imperfections, maybe a pseudo

steady–state voltammogram. When we look at the CV for '3' on day 1, in Figure 6.19, we don't see any faradaic processes occurring at the platinum surface. This is the case even though the concentration of ferrocyanide in the electrolyte has been increased by a factor of 5 compared to the previous experiment. This was done so that it might be possible to increase the peak currents by a factor of 5 as well, this would mean that they would be more perceptible over and above the capacitance of the films.

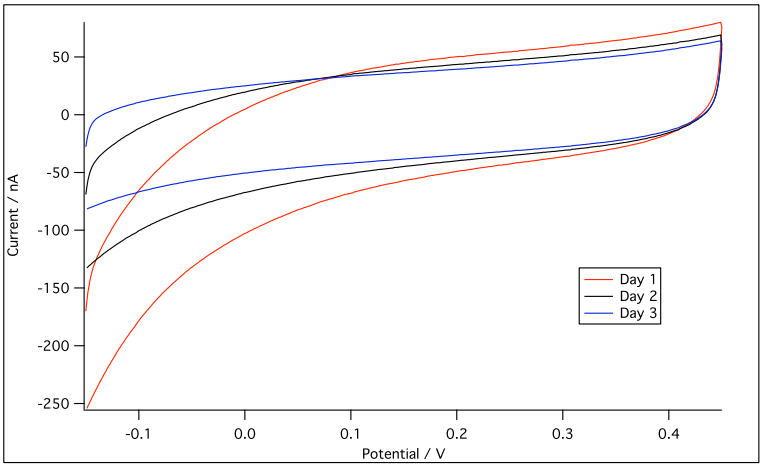


Figure 6.19: Daily CVs of 50 mM ferrocyanide in 100mM KCl for electrode '3' at a $\dot{v}$ of 50 mV s^{-1}.

This implies that the poly(phenol) film on electrode '3' is more insulating than the one in Figure 6.11. As can be seen in Figure 6.20 the CV obtained during the polymerisation of phenol for each of these electrodes shows that a more insulating film might have been predicted for '3'. The peak current for electrode '3', the more insulating film, was higher than that for the film formed for the electrode in Figure 6.11. This shows that more phenol was oxidised on this electrode, resulting in better insulation, the area under the '3' polymerisation peak is approximately 13% higher than the other electrode. Of course, it is difficult to be certain of such small imperfections based on cyclic voltammetry alone. There is also a slight shift in the oxidation peak for phenol, this could be due to a small variation in the pH of the supporting electrolyte, or more likely a reference electrode that had drifted.

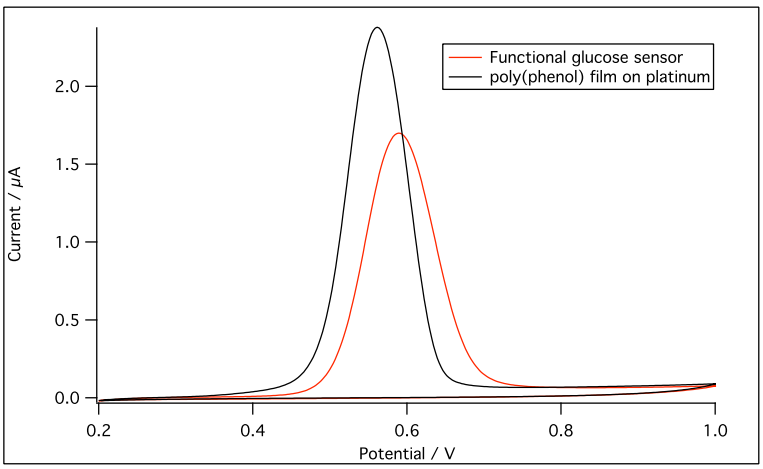


Figure 6.20: Differences in the polymerisation CVs for a poly(phenol) film. Both CVs are for 50mM phenol in 100mM PBS on bare 1mm platinum disc electrodes. Both electrodes have been prepared by abrasive polishing with alumina.

One thing of interest that can be seen in the CVs for '3' in Figure 6.19 is that the transient charging characteristics on days 1 and 2 are distinctive. The electrodes show a high charging current and they require time to achieve steady state, during the course of both the forward and reverse scans. The charging current decreases on day 2 and by day 3 a steady state current is observed from near the start of the first switching potential. The scans for days 4 and 5 are not shown as they are similar to the one for day 3.

When CVs for the functional glucose sensor, '1', are compared for daily variations, as in Figure 6.21, weak faradaic peaks are observed. The scans performed on days 1 and 2 exhibit scans characteristic of a hybrid diffusion profile; although the I_p is substantially lower than that for the bare electrodes, indicating a change in the area and permeability of the film. The scans for the remaining three days exhibit similar redox properties, but their shapes are different due to changes in their charging characteristics.

As mentioned earlier electrode '2' was placed in a humidification chamber for a couple of hours, then after its surface had been scanned, it was tested for another couple of days using cyclic voltammetry, as shown in Figure 6.22. If the hypothesis that the film structure changes while in the dehumidification chamber, then the response of the electrode to the

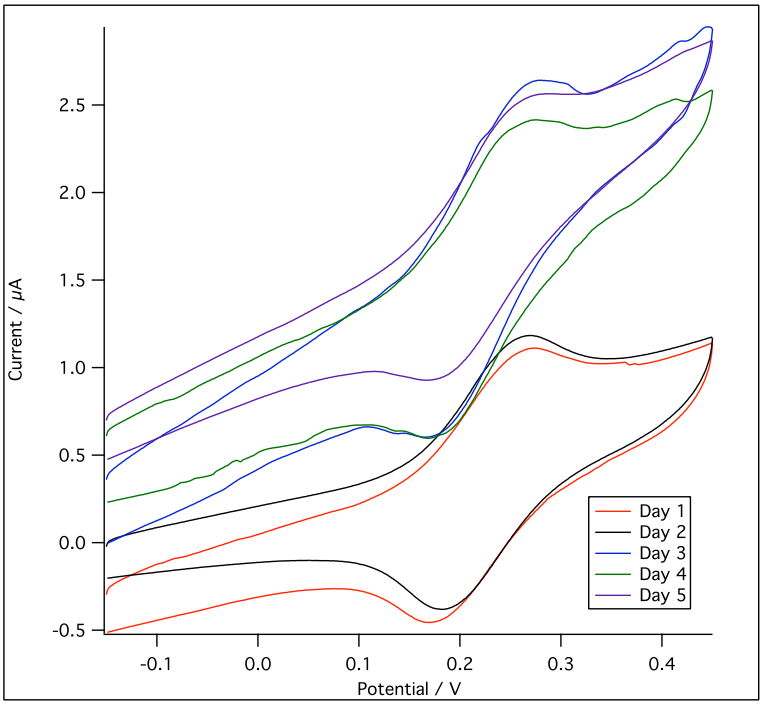


Figure 6.21: Daily CVs of 50mM ferrocyanide at electrode '1', $\dot{v} = 10$ mV s^{-1}.

electrochemistry of ferrocyanide should show differences when compared to the sensor that was not subjected the the same treatment.

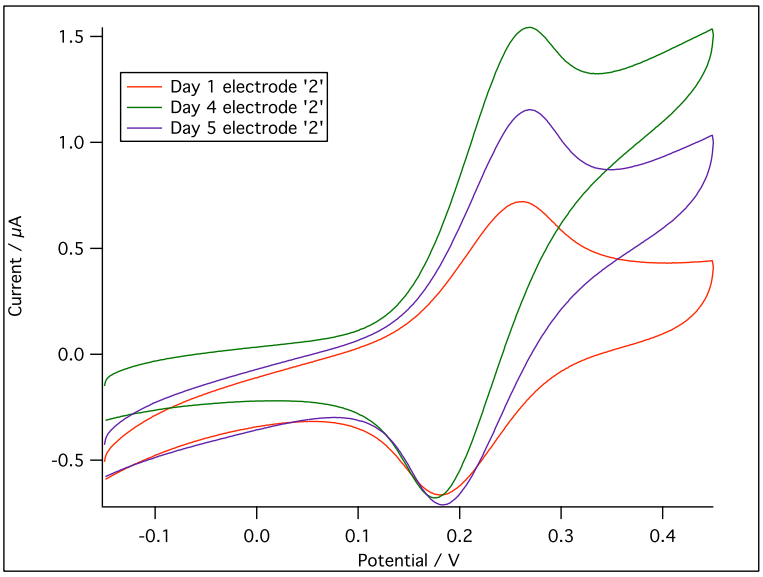


Figure 6.22: Daily CVs of 50mM ferrocyanide at electrode '2', $\dot{v} = 10$ mV s^{-1}.

The CV on day 1 of this electrode is similar to that seen for '1', even the charging characteristics on day 1 are similar. Then, after spending a couple of days in buffer and being in a humidification chamber the responses to ferrocyanide are greatly increased, these can be seen qualitatively in Figure 6.22. The CV on day 4, the day that the electrode was dried, is much stronger than that seen for '1', in Figure 6.21. The background currents during both the forward and backward scans are higher than before, indicating that the insulating nature of the film has decreased. The changes int he film's structure are reversed to a certain degree once the sensor has been rehydrated for 24 hours. The responses for day 5 are slightly suppressed from those on day 4 and the background current returns closer to that seen on day 1. This indicates that the film regains some of its original conformation once rehydrated.

So as to better understand the mechanics of the ferrocyanide redox on the surface of these enzyme sensors studying their behaviour to cyclic voltammetry at different scan rates is necessary, each of the devices was tested daily at different scan rates. CVs at the different scan rates for the two glucose sensors, on day 1, are shown in figures 6.23 6.24 and for '2' on day 4 in Figure 6.25.

As can be seen from the CVs the peak currents increase as the scan rate is increased, also it is possible to see that the peak to peak separation behaves similarly. As seen in Figure 6.26 the peak currents are slightly higher for '1' than for '2', when comparing the operating characteristics of these two electrodes, this could have been predicted. The sensitivity of '1' to glucose is higher and so is the background current. This would imply that the enzyme loading on '1' is higher and as a consequence the poly(phenol) loading is lower. This slight imbalance could have resulted in an increased heterogeneity resulting in more dispersed active sites for ferrocyanide electrochemistry. In turn this would have increased the radial diffusion and therefore flux.

Firstly, we shall discuss the relationship of the peak current with scan rate. The peak current for a reversible process is proportional to the square route of the scan rate, in V

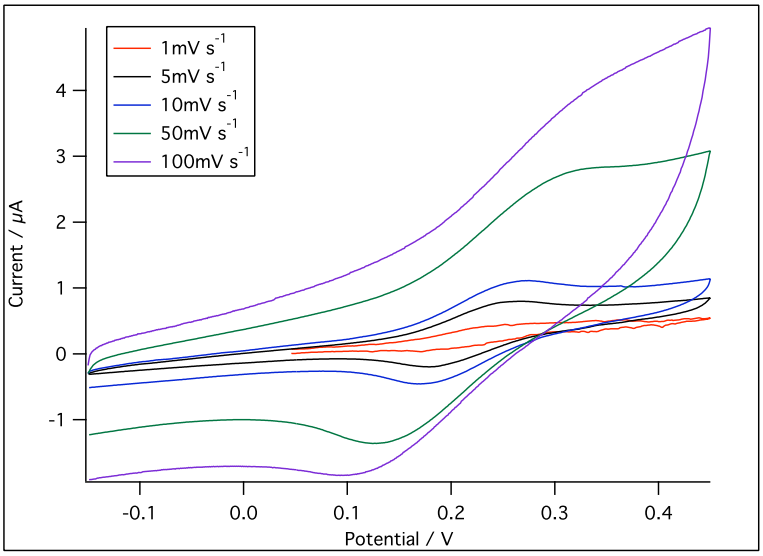


Figure 6.23: Scan rate dependence of 50mM ferrocyanide electrochemistry at electrode '1' on day 1.

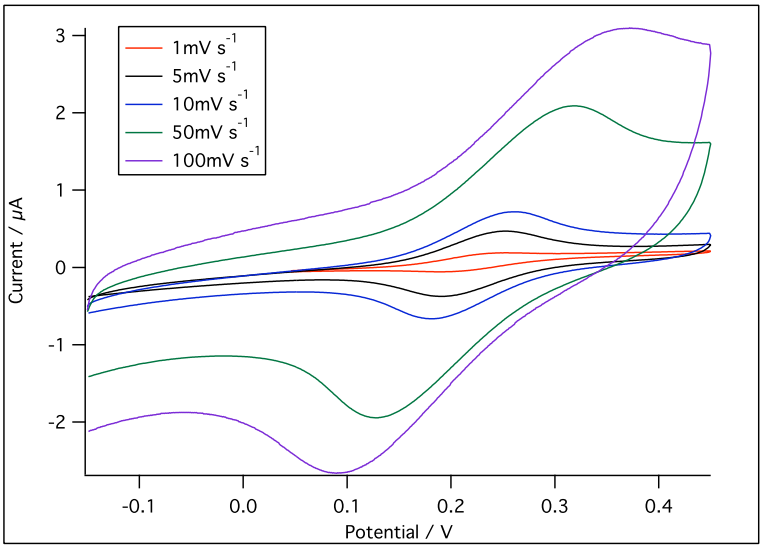


Figure 6.24: Scan rate dependence of 50mM ferrocyanide electrochemistry at electrode '2' on day 1.

s^{-1}. This relationship is shown in Equation 6.8 [8]. Where A is the area of the electrode, D_o is the diffusion coefficient, C_o^* is the bulk concentration and v is the scan rate.

$$i_p = (2.69 \times 10^5) n^{3/2} A D_o^{1/2} C_o^* v^{1/2} \tag{6.8}$$

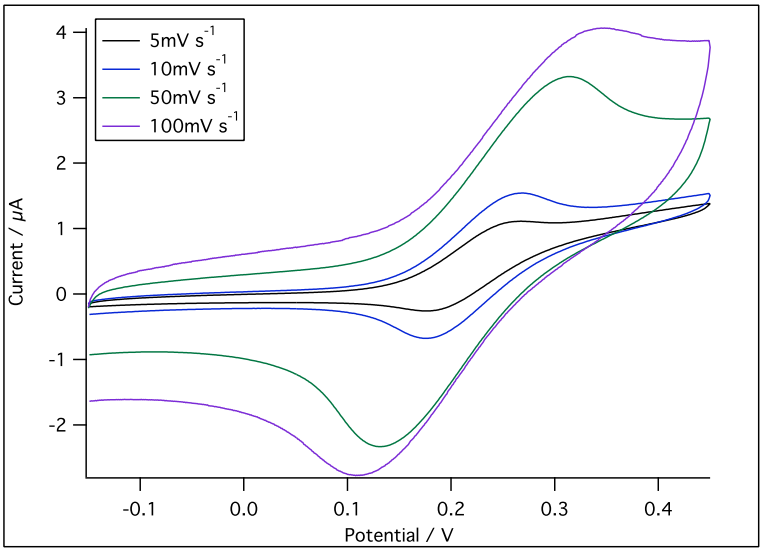


Figure 6.25: Scan rate dependence of 50mM ferrocyanide electrochemistry at electrode '2' on day 4.

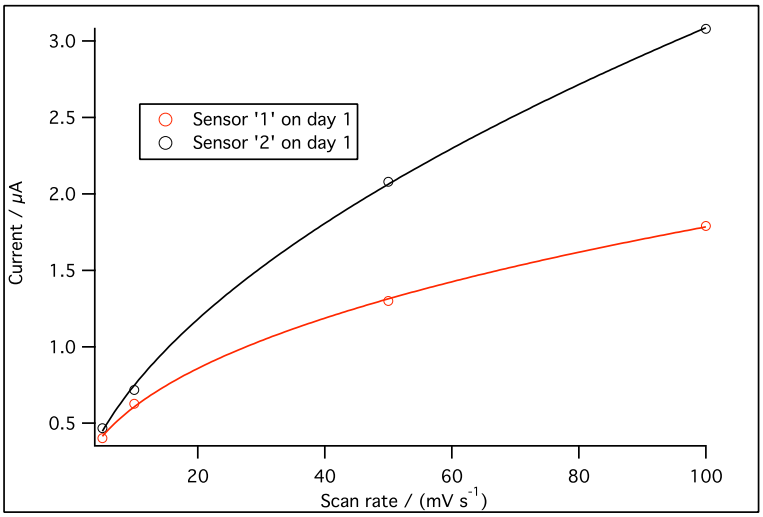


Figure 6.26: Scan rate dependence of I_p for electrodes '1' and '2' on day 1.

For both electrodes, this proportionality was tested daily, figures 6.27 and 6.28 show these for the forward scan. The reverse scan has not been analysed because it is difficult to asses the background current. The capacitive current during the reverse scan is dependent on $E_p, forward - E_\lambda$, where E_λ is the switching potential, and as this is not a constant, it is not possible to accurately assess the base line from which $I_{p,a}$ has to be calculated.

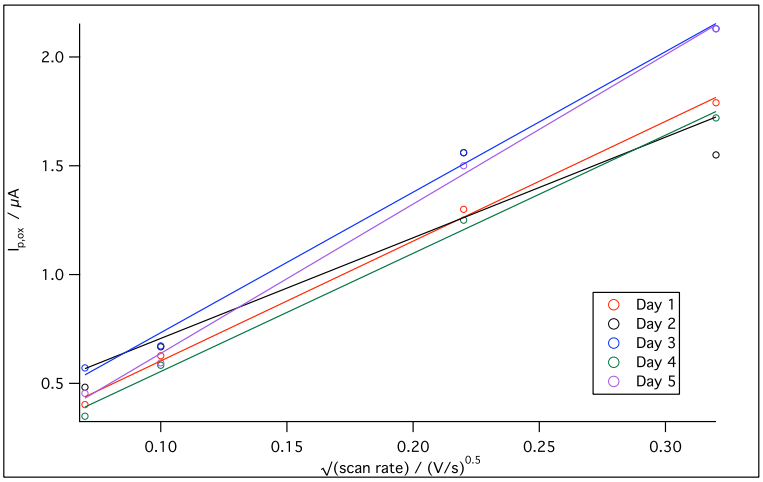


Figure 6.27: I_p vs. $\sqrt{\dot{v}}$ for electrode '1'.

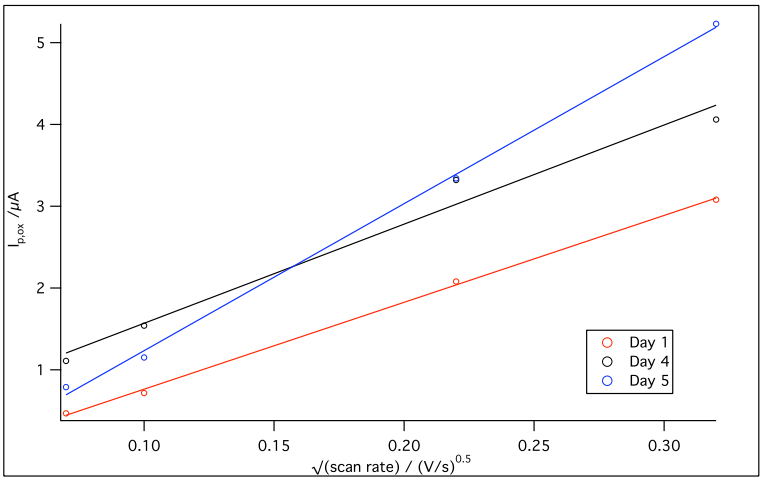


Figure 6.28: I_p vs. $\sqrt{\dot{v}}$ for electrode '2'.

As both figures 6.27 and 6.28 show, the I_p is proportional to the square root of the scan rate for each of the electrodes and on each day of the test. This proportionality would indicate that the redox of ferrocyanide is reversible. From Equation 6.8 it is possible to see that the two parameters that can change during the course of storing the electrode are the electrode area and diffusion through the film; all the other parameters were held constant during the course of the trials. The ionic strength of the electrolyte is not changed, but changes in film permeability are also linked to the morphology of the enzyme film, which

makes it impossible to separate the effect that each of these parameters have on I_p. The slopes of these plots and hence changes in $A.D_o$ are shown in Table 6.4.

Slope / (10^{-7}A (V/s)$^{-1/2}$)	Electrode '1'	Electrode '2'
Day 1	135 ± 2.18	106 ± 2.48
Day 2	136 ± 12.7	–
Day 3	252 ± 3.18	–
Day 4	263 ± 2.61	121 ± 12.7
Day 5	146 ± 2.3	180 ± 5.05

Table 6.4: Slopes of fits from I_p vs. $\dot{v}^{1/2}$ analysis.

As can be seen from the slopes of the lines in Table 6.4, Electrode 1's responses to ferrocyanide electrochemistry increased during the life of the sensor, although on day 5, there is a sudden decrease in the $A.D_o$ term. The same would be expected for the other electrode, but this is not observed to be the case. The change in ferrocyanide activity between days 1 and 4 is not as substantial as that seen for '1' over the same period, although the slope of the line increased between days 4 and 5.

This anomalous relationship can be explained if the diffusion profile of ferrocyanide changes during the lifetime of the sensor. A schematic representation of this can be seen in Figure 6.12. We can see that the shapes of the CVs are indicative of a hybrid, semi-infinite planar and hemispherical diffusion, similar to that reported by Armstrong et. al. [9]. If the morphology of the enzyme film changes, during these 5 days, so that the hybrid diffusion profile of ferrocyanide shifts more in the direction of semi-infinite planar diffusion then the daily variations can not be compared to each other. The converse holds true if the number of sites becomes smaller; as in both cases the flux of ferrocyanide at the surface will change dramatically. It may be possible to become more certain of these changes, if we study the relationship between ΔE_p, scan rate and C_d.

Another piece of information that may help fit the pieces in place is the double layer capacitance of the electrodes. This can be estimated from Equation 3.4, using the steady

state current from the ferrocyanide CVs. The i_{ss} for this trial is estimated using the reverse scan, as the oxidation peak is broad and it is not possible to make an accurate estimation of the steady state current. Most of the currents were measured using the scans at 100 mV s^{-1}, where this is not the case it is shown in Table 6.5 and the C_d are represented graphically in Figure 6.29.

	'1' / μF	'2' / μF	'3' / μF
Bare	36.70	36.7	41.69
Day 1	17.04	18.8	2.051
Day 2	11.08	–	1.336
Day 3	4.77	–	0.897
Day 4	6.70	26.3*	1.097
Day 5	3.28	21.5	0.997

*CV used at scan rate of 5 mV s^{-1}

Table 6.5: Capacitance of disc electrodes.

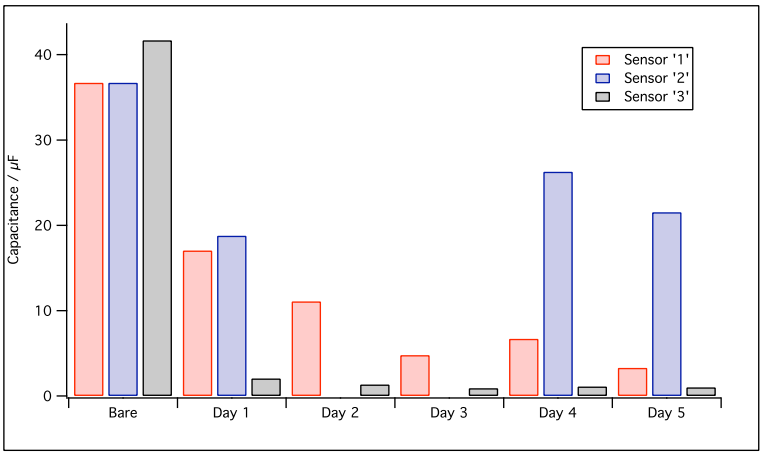


Figure 6.29: Daily variations in C_d for each of the three electrodes.

The capacitance of the bare electrodes is roughly the same indicating a good quality and reproducible platinum surface. If we study the C_d of the electrode with only poly(phenol) on its surface, then we can see the higher charging currents on days 1 and 2, as described earlier, but by day 3 these have reached a steady value of approximately 1 μF. When this is

compared to the changes in C_d for '1', which was loaded with enzyme and placed in PBS for the duration of the experiment, we can see that the charging currents start out much higher, but decay towards the limiting C_d of the electrode '3', although they are still approximately 6 μF. Finally electrode '2' follows a trend similar to '1' during day 1, although its C_d is higher, but once it has been dehydrated the double layer capacitance increases dramatically and approaches 60% of the C_d of the bare electrode. On day 5 this sees a small decrease toward the C_d of day 1.

From these data it is evident that the loading of the poly(phenol) and glucose oxidase decrease the double layer charging current on the surface of the electrode, which is probably a result of a shielding effect between the metal and solution interface. Along with this, their own dielectric constants do not play a significant role in increasing the charging characteristics at the metal–solution interface. One would assume that glucose oxidase being a poly(electrolyte) might have added to the charging currents, but this is not the case; the coverage area may be too small to be of significance.

The increase in the C_d for '2' on day 4, is probably due to more of the surface of the platinum being exposed to the solution. This increases the interfacial area and hence the charging current. As seen with the increase in redox activity and the change in the shape of the CV the area of the metal - solution interface increased on day 4 which was reversed on day 5, resulting in the decreased C_d.

A cursory look at the CVs from figures 6.23, 6.24 and 6.25 shows that the peak to peak separation increased along with the scan rate. These separations are quantified in Tables 6.6 and 6.7.

We know that electron transfer kinetics result in slight increases in the peak separation of CVs when the scan rate increases. A system that exhibits a Nernstian response at one scan rate, may display quasi-reversible behaviour at an increased scan rate. Assuming that the diffusion of ferrocyanide to the surface of the platinum follows semi-infinite planar diffusion, we can use the Method of Nicholson to estimate the rate constant for the quasi-reversible

Scan rate / (V s^{-1})	Day 1*	Day 2*	Day 3*	Day 4*	Day 5*
0.005	63	65	68	67	69
0.01	81	69	76	68	68
0.05	161	136	136	132	133
0.1	197	176	184	168	171

* All values are in mV

Table 6.6: Daily ΔE_p for '1'.

Scan rate / (V s^{-1})	Day 1*	Day 4*	Day 5*
0.005	53	76	60
0.01	67	86	75
0.05	170	166	184
0.1	246	201	258

* All values are in mV

Table 6.7: Daily ΔE_p for '2'.

process [10]. This will allow us to confirm that the kinetics are a result of slow electron transfer and the daily variation might indicate changes in the surface morphology.

Nicholson defined a kinetic parameter ψ which is related to the peak separation, ΔE_p of CVs, this has been tabulated in his paper [10]. Using this it is possible to evaluate ψ for a particular scan rate. It is important to note that the $\dot{v}$ has to be chosen such that the value of ΔE_p falls in the limitation set by the model, although this is generally not a problem. In the determination of these values, he has assumed that $\alpha = 0.5$. He also reports that ΔE_p tends to be independent of α in the range $0.3 < \alpha < 0.7$. Equation 6.9 was used to calculate k_0 and shows the relationship between ψ and k_0. Matsuda and Ayabe have described another parameter Λ to assess the regime of the system. This has been simplified,

by assuming that $D_O = D_R = D$ and is shown in Equation 6.10 [8].

$$\psi = \frac{k_0}{(\pi n f \dot{v} D_o)^{1/2}} \tag{6.9}$$

$$\Lambda = \frac{k^0}{(D f \dot{v})^{1/2}} \tag{6.10}$$

The limits set by Matsuda and Ayabe, for the three regimes of reversible, quasi-reversible and irreversible systems are shown below [8]:

$$\text{Reversible } \Lambda \geq 15;\ k_0 \geq 0.3\dot{v}^{1/2} \text{ cm/s}$$

$$\text{Quasi-reversible } 15 \geq \Lambda \geq 10^{-2(1+\alpha)};\ 0.3\dot{v}^{1/2} \geq k_0 \geq 2 \times 10^{-5}$$

$$\text{Irreversible } \Lambda \leq 10^{-2(1+\alpha)};\ k_0 \leq 2 \times 10^{-5}$$

As tables 6.8 and 6.9 show, the kinetic parameters fall within the limits described for a quasi-reversible system. These were calculated using the peak separations that fell in the range prescribed by Nicholson [10]. This shows that the film on the surface of the platinum results in slower electron transfer, when the diffusion profile for ferrocyanide to the surface is assumed to semi-infinite planar.

Parameter	Day 1	Day 2	Day 3	Day 4	Day 5
ΔE_p [a] / mV	63	65	68	68	68
Scan rate / (V s^{-1})	0.005	0.005	0.005	0.01	0.01
ψ [b]	7	5	3	3	3
k_0 [c]	9.26×10^{-2}	6.62×10^{-2}	3.97×10^{-2}	5.61×10^{-2}	5.61×10^{-2}
Λ [d]	12.4	8.86	5.32	5.32	5.32

[a] Estimated from CVs
[b] Estimated from [10]
[c] Calculated from equation 6.9
[d] Calculated from equation 6.10

Table 6.8: Daily kinetic parameters for '1'.

Parameter	Day 1	Day 4	Day 5
ΔE_p [a] / mV	67	76	75
Scan rate / (V s^{-1})	0.01	0.005	0.01
ψ [b]	3.75	1.72	1.84
k_0 [c]	7.02×10^{-2}	2.27×10^{-2}	3.44×10^{-2}
Λ [d]	6.65	3.04	3.26

[a] Estimated from CVs
[b] Estimated from [10]
[c] Calculated from equation 6.9
[d] Calculated from equation 6.10

Table 6.9: Daily kinetic parameters for '2'.

It was necessary to find out whether the electrochemistry of ferrocyanide on the surface was in fact quasi-reversible or whether, using Armstrong's model the electron transfer kinetics were faster. Testing the enzyme containing film with this model would confirm the electron transfer kinetics and it would also give us a clear indication of the morphology of the film. A reversible ferrocyanide redox at a limited number of active sites would allow us to estimate the radius of the active sites and more importantly the sphericity of the diffusion profile.

Scan rate / V s^{-1}	Day 1*	Day 2*	Day 3*	Day 4*	Day 5*
0.005	181	171	153	131	171
0.01	177	181	162	138	166
0.05	192	196	155	160	182
0.1	210	177	137	172	208

* All figures in mV

Table 6.10: Daily $E_{1/2}$ values for '1'.

The E^0_{rev} for a bare platinum disc is calculated as 206 mV from the CVs in Figure 6.18. When this is compared to the $E_{1/2}$ values from tables 6.10 and 6.12 for both the enzyme films, it is evident that our film fails the first test of reversibility as suggested by Armstrong

Scan rate / V s^{-1}	Day 1*	Day 2*	Day 3*	Day 4*	Day 5*
0.005	38	45	55	48	54
0.01	52	55	45	61	46
0.05	58	64	65	57	68
0.1	67	75	74	55	61

* All figures in mV

Table 6.11: Daily changes in $E_{1/4} - E_{3/4}$ for '1'.

Scan rate / V s^{-1}	Day1*		Day4*		Day5*	
	$E_{1/2}$	$E_{1/4} - E_{3/4}$	$E_{1/2}$	$E_{1/4} - E_{3/4}$	$E_{1/2}$	$E_{1/4} - E_{3/4}$
0.005	184	39	193	51	190	44
0.01	177	45	190	52	192	48
0.05	205	60	215	67	218	71
0.1	222	68	228	74	245	82

* All figures in mV

Table 6.12: Armstrong's tests for '2'.

et. al. [7]. The electron transfer step is considered slow in this model, when $E_{1/2}$ is more negative than the reversible E^0 and when $E_{1/4} - E_{3/4}$ exceeds the ideal value of 55 mV. The results of the second test can be seen in the remainder of the data from Table 6.12 and 6.11. These data do not exceed the ideal values at the lower scan rates, but based on the films failing the first test we can conclude that the electron transfer step is slow, even when we account for the limited number of redox sites of the surface.

It can now be concluded that the electron transfer step for the electrochemistry of ferrocyanide is slow when the electrode is coated with the enzyme film. When we study the kinetic parameters for this in Tables 6.8 and 6.9, we can see indications of the surface morphology. For '1' k_0 and Λ tend to stabilise after a couple of days. The initial e^- transfer kinetics are higher and the electron transfer is faster, than those at which the electrode has stabilised. For '2' the opposite is true, allowing the film to dehydrate increased the speed of electron transfer, which again decreased after the film had been rehydrated.

Along with the shapes of the CVs what these data indicate is that the protein plays a significant role in the mass transport behaviour of probe molecules to the platinum surface and it also affects the electron transfer kinetics. The hypothesis is that during the life time of the sensor, the conformation of the protein changes and this increases the mass transport barrier that the enzyme poses to probe molecules. Changes in the conformation of the enzyme can lead to a loss in its activity. On the other hand dehydrating the film causes conformational changes that reverse the conventional aging of the film and improve the redox of probe molecules at its surface.

6.4 Scanning Electrochemical Microscopy

In this section we will discuss the scanning probe studies that were conducted on the substrate in generation-collection (GC) mode. The sign convention used here is the American one; that is an oxidation current produces a negative signal and vice versa for reduction.

Firstly a bare 1 mm platinum disc was used as the substrate to identify the maximum

response available from the probe. A 100 μm probe was used for this and it was used to measure the reduction of ferrocyanide, while the substrate was generating the oxidised product. An approach curve on the epoxy surrounding was performed, followed by a line scan to ensure that the starting co-ordinates for the map were correct; these are both shown in figures 6.30 and 6.31. The approach curve was halted when the reducing current achieved a value that was approximately 50% of the bulk value, this was to ensure that the probe was not damaged, as a result of a collision with the substrate. In Figure 6.31, there are two line scans, the first one starts at a high current and then approaches the limiting current of the approach curve in Figure 6.30; the reverse happens in the second one. The starting co-ordinates of the were chosen such that the scan began on the conducting substrate and then finished on the packaging, this was reversed for the second x–axis scan.

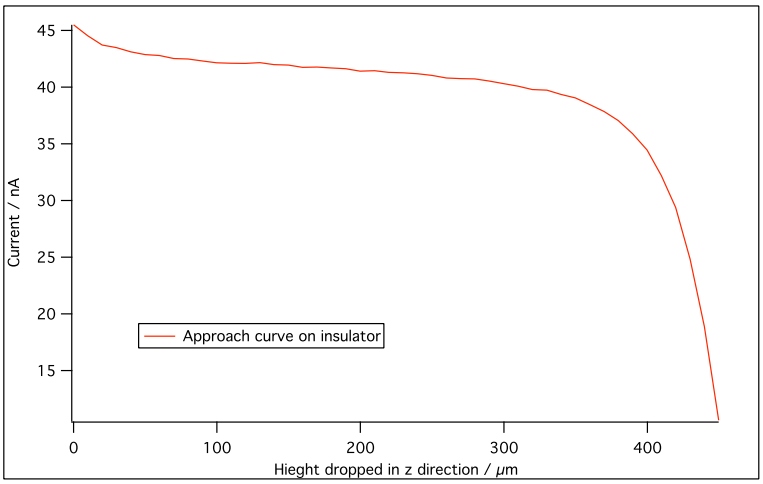


Figure 6.30: Approach curve on the epoxy surround of the substrate. a 100μm tip was used and the bulk electrolyte was 10mM ferrocyanide in 100mM KCl. The tip moved from the its original position in 10μm steps.

It is very easy to see the edge of the disc on the area scan, in Figure 6.32 (a) and (b); also there is a gradual increase in the reduction current until it achieves a steady state value of approximately 30 nA. The reason why the boundary of the disc is not seen as a step is because of the collection area of the probe. The R/G of the probe was approximately 10, this implies that the collection area of the probe is a cylinder with a diameter of 1 mm. This

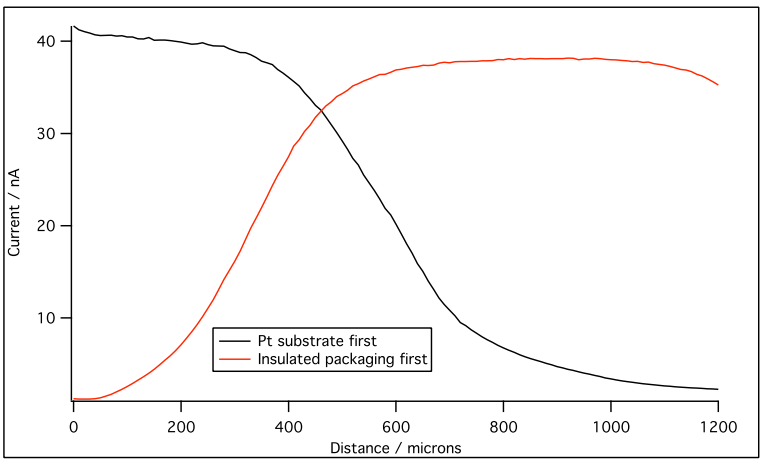


Figure 6.31: Line scans on the bare platinum substrate. The probe distance was set using the approach curve and the bulk electrolyte was 10mM ferrocyanide in 100mM KCl. Each step of the probe was 50μm with a collection time of 2s.

is a limitation of this method of surface scanning, but it does not pose an insurmountable problem.

A preliminary trial following a similar technique was then carried out on the same disc electrode, once it had been prepared with a glucose oxidase and poly(phenol) film; the resultant scan is shown in Figure 6.33. The area scanned for this substrate is not the same as that scanned for the bare one, because the substrate was removed and reoriented so that the enzyme film could be made. The important feature to note with this area scan is the marked decrease in the reduction current, the bare electrode produced a reducing current of about 30 nA and this film structure only produces about 200 pA above the background. Also, the edge of this disc is not as clearly visible as that of the bare platinum substrate.

We know that the initial concentration of oxidised ferrocyanide in the cell is zero; therefore the decrease in reduction current is due a smaller amount of ferrocyanide being oxidised by the substrate once its surface has been modified. Also, the small saddle formation in the bottom left hand corner of the figure indicates that this area has a slightly decreased enzyme loading and is predominantly an enzyme and poly(phenol) interfacial area. Even though it is possible to see a decrease in the oxidation of ferrocyanide at the substrate, the

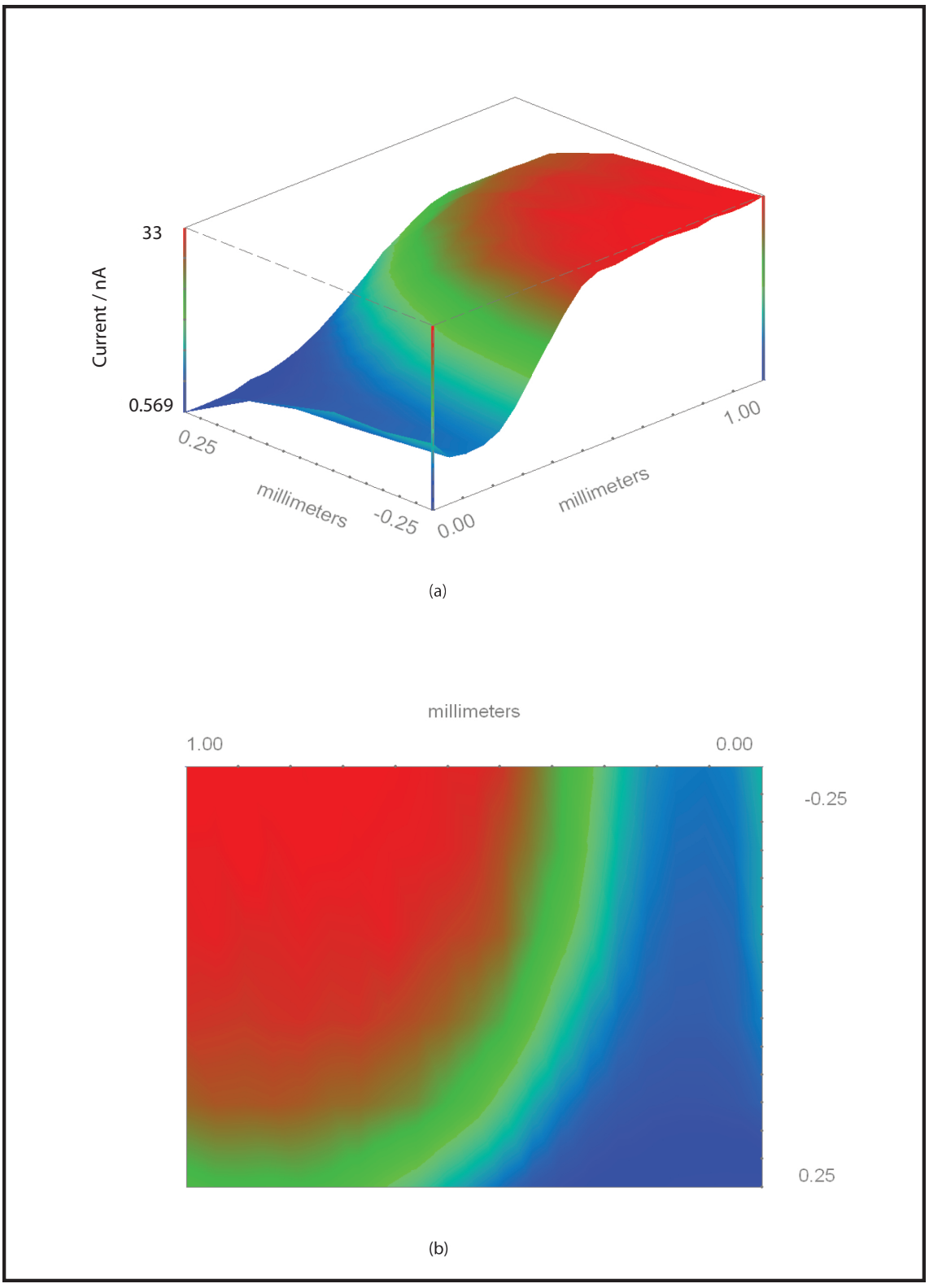


Figure 6.32: Area scan of a bare platinum disc in GC mode with 10mM ferrocyanide in 100mM KCl. This is a 1000 × 500μm scan, 50μm steps are used in both the x and y directions. a) shows the profile of the reduction current and b) shows the plan view mapped substrate.

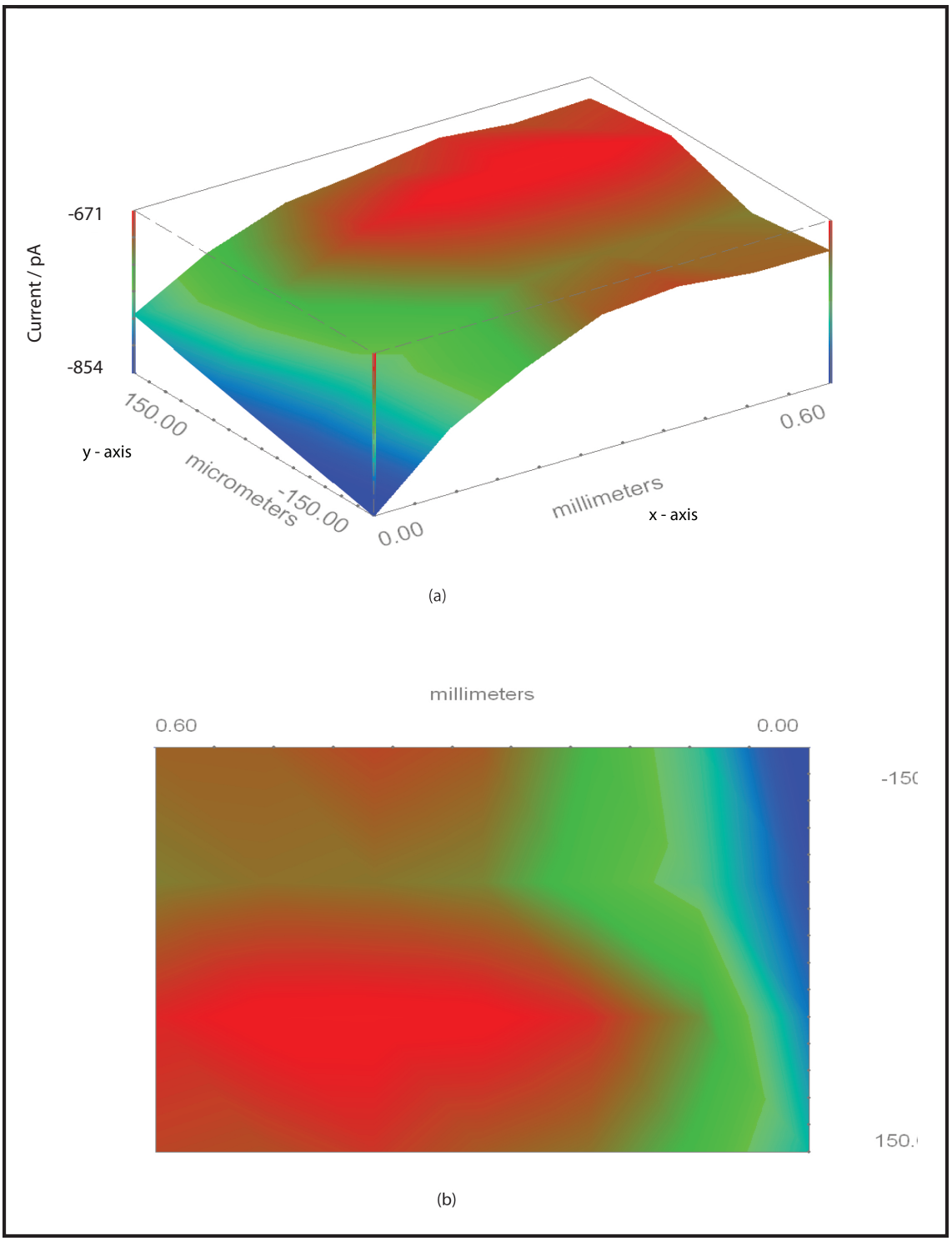


Figure 6.33: Preliminary area scan of a glucose sensors' surface in GC mode with 10mM ferrocyanide in 100mM KCl. The 600 × 300μm area is scanned using 50μm steps along both the axes. The profile of the probe current is shown in (a) whereas (b) shows the plan view of the map.

small currents and the large collection area do not show any more detail of the film. To try and visualise these the experiments were repeated using a smaller probe. The surfaces were also scanned in GC mode for glucose and collection mode for PBS.

A 5 μm diameter probe was used to decrease the collection area, which might allow for more of the surface detail to be observed. One of the resultant scans is shown in Figure 6.34. As the figure illustrates, the currents recorded are very low. The difference between the background current and the ferricyanide reduction current is only 20 pA. It is possible to record these small changes, but the area scans require extensive post processing to remove any points where the collection of the reduction current was noisy. The post processing of the maps is not a problem, although there is a small danger that over compensating for the noise will result in loss of valuable surface characteristics. There are methods of improving the S/N ratio and more work needs to be performed using the smaller probes.

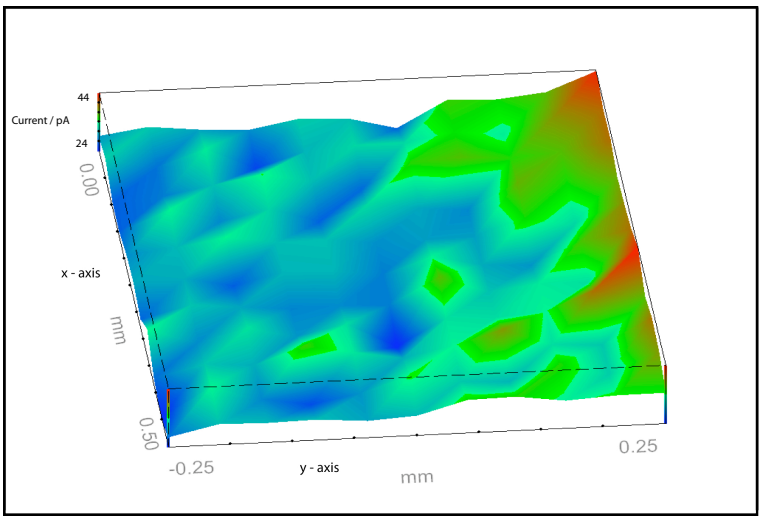


Figure 6.34: Surface scan of a functional glucose sensor as the substrate using a 5 μm probe in GC mode.The bulk electrolyte is 50mM ferrocyanide in 100mM KCl. The area was mapped using 10μm steps in both the x and y directions.

Further scans of the surfaces using the 100 μm probes did not reveal anything of any real interest, so the sensors were 'dried' in a humidification chamber for a couple of hours. Previous work had showed that the sensors lost their responses to glucose, once the film

was dried, so it was apparent that the protein was affected by this. The most likely effect of the drying process would be a loss in the water content of the film, this would result in it shirinking. This diminution in size would manifest itself in an increase in the platinum exposed at the metal–solution interface. Therefore it should be easier to identify features from the surface of the glucose sensor.

Before this process could be attempted, the responses of the sensor had to be tested once it had been dried. Low concentration calibrations were conducted for one of these sensors both before and after the drying process; the results of these are show in Figure 6.35. There is a slight decrease in the sensitivity of the sensor from 4.89 nA mM^{-1} to 4.56 nA mM^{-1}; but this is less than a 10% decrease and within experimental error. The surprising feature from the calibration curves in Figure 6.35 is that there was no change in the background current post drying. This is surprising because we have seen a slight increase in earlier experiments, as in Figure 6.22 and increasing the exposed platinum surface should decrease the insulating nature of the film.

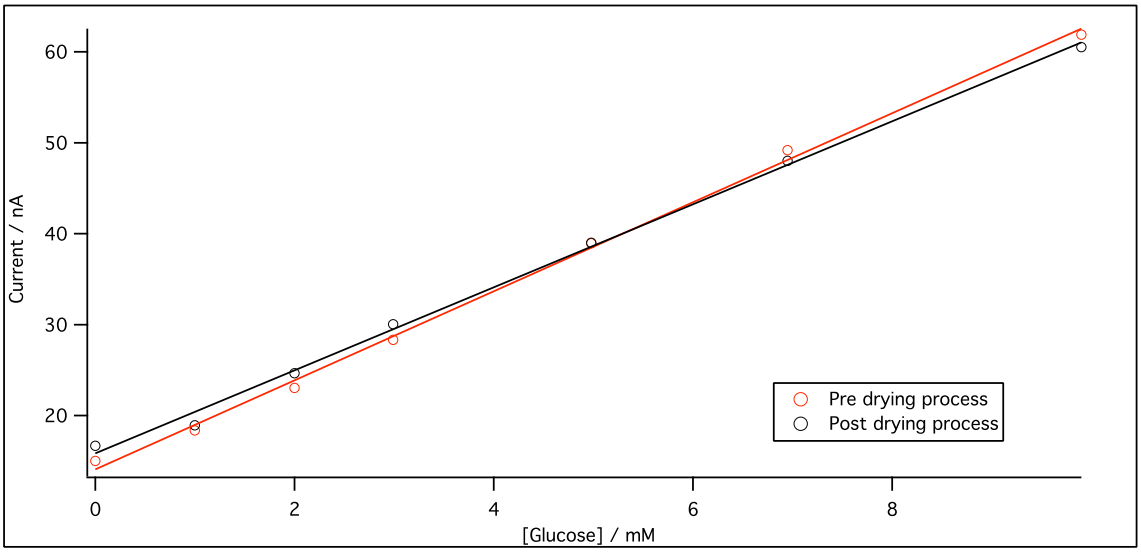


Figure 6.35: Comparison of calibration curves for a glucose sensor before and after it had been placed in a humidification chamber.

A preliminary surface scan using GC mode and a negative control yielded some interest-

ing results, which can be seen in figures 6.36 to 6.38. The colour scales of these figures have been arranged such that red indicates a more positive current and blue a more negative one. What this means for our system is that, when scanning for ferricyanide a red area indicates increased concentration for this species and when scanning for H_2O_2, the same colour indicates a lower concentration of this species; and vice versa for the blue areas. This implies that, when either ferrocyanide or H_2O_2 are collected at the probe, red is indicative of no enzyme and Blue is indicative of the presence of enzyme.

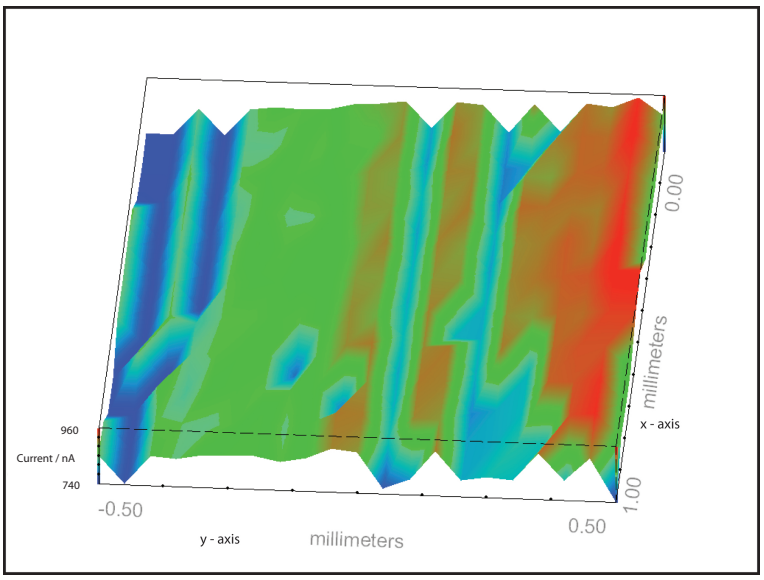


Figure 6.36: Preliminary area scan of the surface of a dried sensor using GC mode with 50mM ferrocyanide in 100mM KCl. A 100μm probe was used and the steps in both directions were 50μm.

The ferrocyanide scan in GC mode shows that at $y \simeq +500\mu m$ there is a long strip where ferrocyanide oxidation is taking place on the surface, this is further confirmed by the lack of H_2O_2 oxidation in the same area of Figure 6.37. There are a couple of important things to note with this preliminary trial, firstly that the area scanned is a square $1000 \times 1000\ \mu m$ in dimension and the diameter of our disc electrode is 1 mm. Even with these dimensions, we were not able to spot the edge of our electrode and the decrease in ferrocyanide activity in the negative y direction, in Figure 6.36, is only apparent in a line parallel to the x – axis.

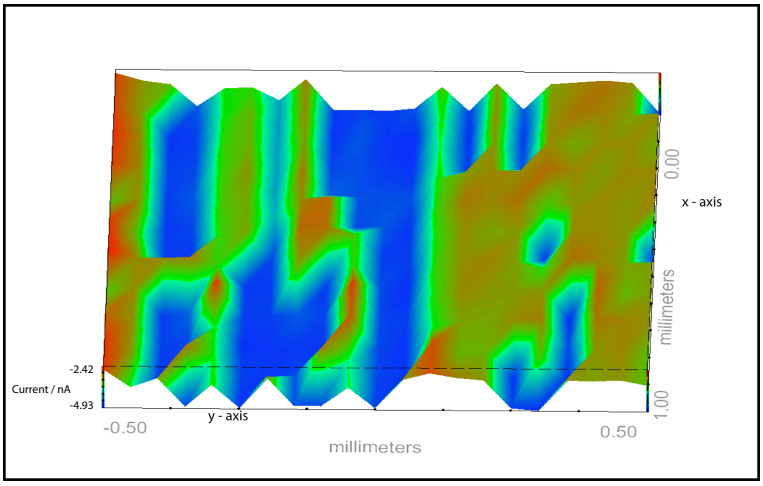


Figure 6.37: Preliminary area scan of the surface of a dried sensor using GC mode; collecting enzymatically generated H_2O_2 at the tip. A 100μm tip was used for this scan and 50μm steps were used to traverse the substrate in both directions.

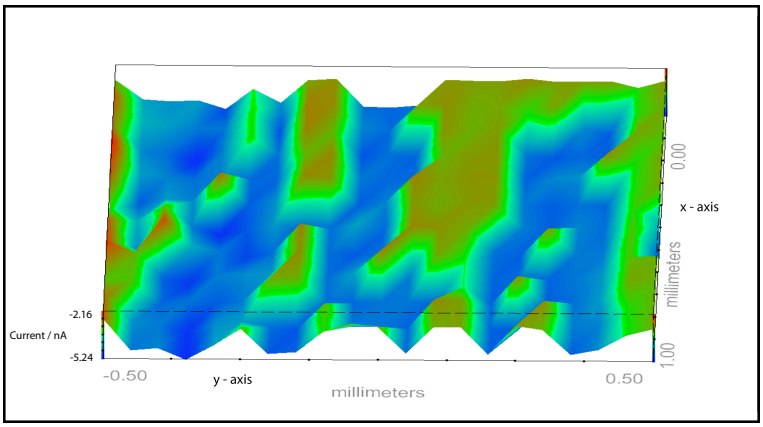


Figure 6.38: A negative control surface scan, with only PBS in the cell.

Secondly the features that we are seeing using both ferrocyanide and glucose are larger than expected. For example the ridge running parallel to the x–axis at y $\simeq$ 200 μm is almost 100 μm in thickness. There is serious doubt about the area that was being scanned here, because of the inability to see the round edge of the substrate. Although the area scan is a square that is the same size as the diameter of the electrode, we would not expect to see a boundary as predominant as in Figure 6.32 or 6.33, but we would expect to see some indication of the substrate's shape from its area scan. This was something that needed to be addressed in future work since finding the edge of the substrate would be the only way to confirm the surface scans.

The process described above of 'drying' the glucose oxidase containing film in a humidification chamber was repeated, to try and find the edge of the disc and gain a deeper insight in to the film's structure. The edge of the disc did not show up when GC mode was used with ferrocyanide, but when the surface was scanned using background electrolyte only, there was an interesting observation. The bottom edge of Figure 6.39 (b) shows a more negative, current than the rest of the map and the boundary is circular in nature.

This shows that the rest of the map is that of the electrode and scanning an insulator gives a more negative current. From this it can be inferred that the green areas of the map are poly(phenol) and the red areas of the map are glucose oxidase. Therefore the enzyme sits in the centre of the electrode and there is an approximately 50–50 split in the coverage of glucose oxidase and poly(phenol) on the surface. Using the same starting co-ordinates and area for mapping, this film was analysed with ferrocyanide and glucose, both of these maps can be seen in Figure 6.40 (a) and (b).

From Figure 6.39 we know that from y $\simeq$ 400 μm we begin to go beyond the edge of the electrode, so this means that we are scanning ca. 700 μm of the length of the disc. The location of the disc is confirmed by the lack of H_2O_2 oxidation when y $>$ 400μm, although from Figure 6.40 (a) we can see the presence of ferrocyanide at the probe in the same area. Also the edge of the electrode, where y $\simeq$ 100μm and x $\simeq$ 0 to 200μm shows increased

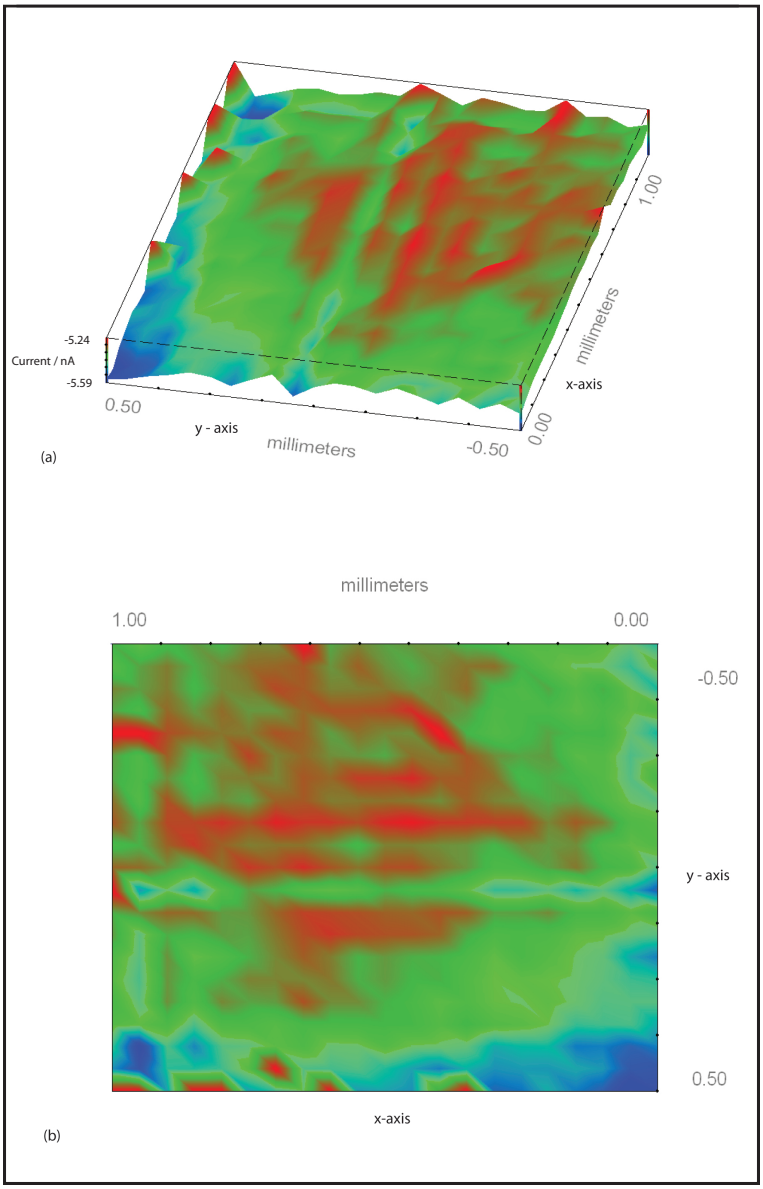


Figure 6.39: Area scan of a functional glucose sensor with only 100mM PBS as the electrolyte. The profile of the probe current is shown in (a) and this is shown as a plan view in (b). The tip was used was 100μm in diameter and 50μm steps were used to travel across the designated area of the substrate.

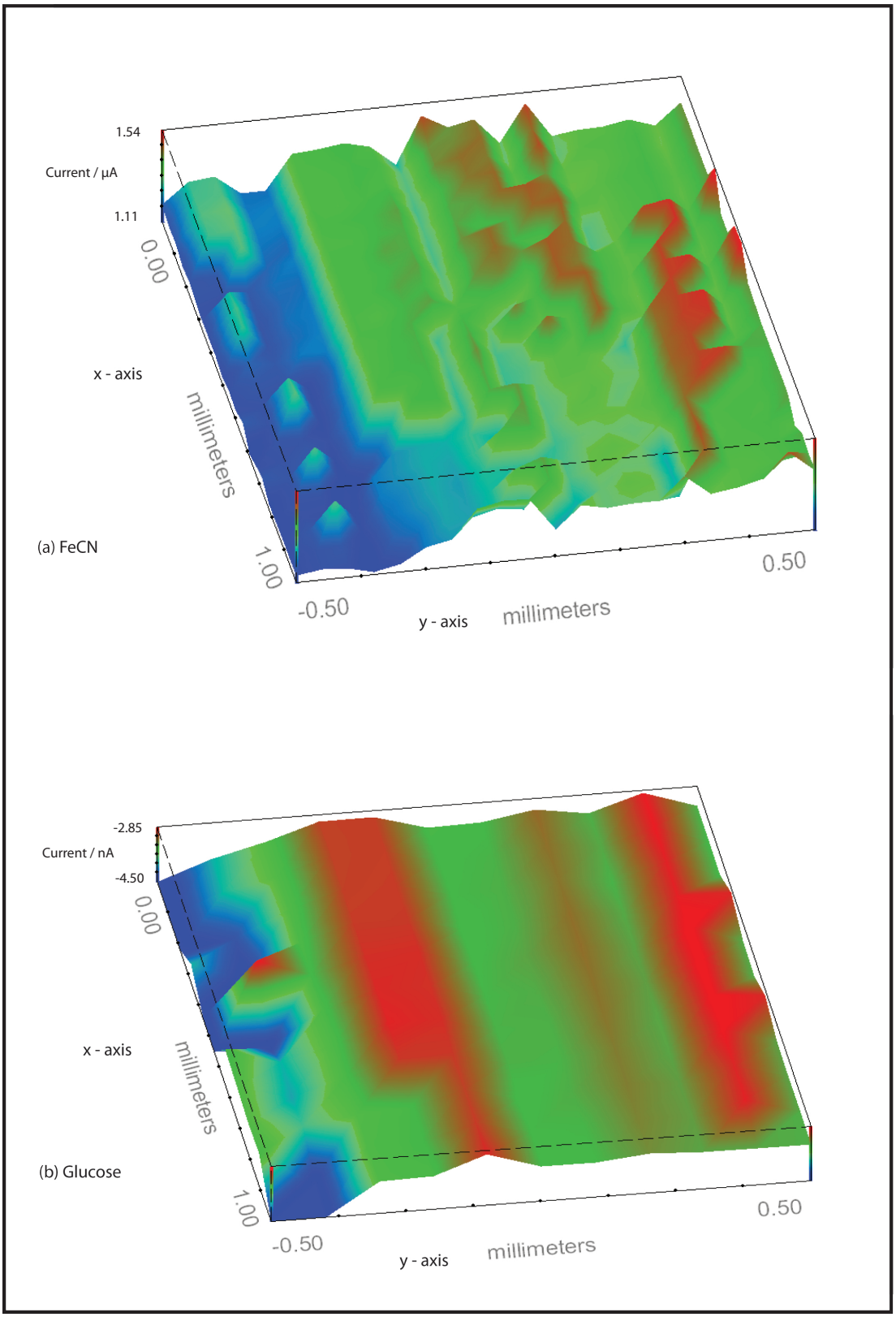


Figure 6.40: Area scans of the same region of the substrate performed consecutively. In (a) the electrolyte is 50mM ferrocyanide in 100mM KCl and in (b) this is changed to glucose in 100mM PBS. All other experimental conditions are the same

ferricyanide reduction, which agrees with the observation that the edge of the electrode has a greater distribution of poly(phenol).

The characteristics of both these maps agree in a broad sense, although there is still a lot of ambiguity and uncertainty within them. The features that we can see from the area scans agree in principle with each other, but in GC mode their sizes are still larger than expected. More work needs to be done in this area to be able to confirm the morphology of the film. However, it can safely be said that both the glucose oxidase and poly(phenol) sit exclusively on the platinum surface and that probe molecules only have access to the surface at the interfacial area.

Another important feature of these scans is the distribution and proximity of each of the two components. From the scans it can be concluded that the active sites for ferrocyanide redox do not possess the characteristic dimensions of microelectrodes and their distribution is heterogeneous but their proximity implies that the diffusion profiles will overlap and tend toward a regime of planar diffusion. A similar diffusion profile will be found for glucose at the enzyme.

6.5 Summary

The optical studies of the glucose sensors did not reveal any information about the film morphology or the heterogeneity of glucose oxidase and poly(phenol) on its surface. The film thickness is reported to be a 7.4 nm for an enzyme sensor and 3 nm for a poly(phenol) layer [11], so the incident light is not passing through sufficient amount of the sample, which in turn gives a low signal to noise ratio. Also, due to the limitations of optics and the structure of the film, which is now known, it is entirely possible that it might not have been possible to observe this heterogeneity and the maps would show a degree of homogeneity in the film.

The cyclic voltammetry studies show that the glucose oxidase and poly(phenol) sit exclusive from each other and that the effective area for ferrocyanide redox is smaller once

the film is loaded on the platinum surface. More importantly the diffusion profile for ferrocyanide is a hybrid between semi-hemispherical and planar diffusion and it shifts in the direction of the latter during the life time of the sensor. This in turn implies that the likely diffusion profile for glucose at the solution film interface is planar, the regime that results in the least flux of glucose at the electrode surface.

Even though the scanning probe experiments have shown some promise, further work needs to be performed with SECM to study the surface of the enzyme electrodes. A detailed study using a probe with a smaller diameter would show a lot more detail, although the smaller currents associated with the smaller diameter needs to be addressed. There are a couple of methods that might be used in achieving this, scanning closer to the surface should improve the S/N ratio. If this is the case then, it is necessary to make sure that the substrate is flatter than was prepared for these experiments. Increasing the collection time, at each collection point should allow for the noise to be diminished. Modifying the surface of the probe could help. Horrocks et. al. have reported the use of horse radish peroxide as a means to scan the generation of H_2O_2 at the substrate [12]. This is useful with the use of a mediator in the cell although in our system where there is no electrochemical interference lowering the oxidation potential at the probe will not improve the S/N ratio. To improve the detail of the surface scan for us, it is necessary to increase the surface area of the probe, without increasing the collection area. The minimum R/G to ensure that the diffusion profiles are hindered is 5, so that is a physical constraint within which to operate. The electrochemical deposition of platinum black on the surface of the probe will increase the area of the electrode, without changing the radius and therefore the collection area. This will vastly improve the information obtained from the surface maps and should be looked at in future work.

References

[1] A. Carden and M. D. Morris, "Application of vibrational spectroscopy to the study of mineralised tissues (review)," *Journal of Biomedical Optics*, vol. 5, no. 3, pp. 259–268, 1997.

[2] H. J. Yvon, *Raman Spectroscopy for Analysis and Monitoring*. http://www.jobinyvon.com/SiteResources/Data/Templates/1imagemap.asp.

[3] R. Lapuente, F. Cases, P. Garces, E. Morallon, and J. L. Vazquez, "A voltammetric and ftir-atr study of the electropolymerisation of phenol on platinum electrodes in carbonate medium, influence of sulfide," *Journal of Electroanalytical Chemistry*, vol. 451, no. 1998, pp. 163–171, 1998.

[4] M. Ferreira, H. Vaerla, R. M. Torresi, and G. Tremiliosi, Filho, "Electrode passivation caused by polymerisation of different phenolic compounds," *Electrochemica Acta*, vol. 52, no. 2006, pp. 434–442, 2006.

[5] M. Fleischmann, I. R. Hill, G. Mengoli, and M. M. Musiani, "A raman spectroscopic investigation of the electropolymerisation of phenol on silver electrodes," *Electrochimica Acta*, vol. 28, no. 11, pp. 1545–1553, 1983.

[6] K. Stulik, C. Amatore, K. Holub, V. Marecek, and W. Kutner, "Microelectrodes. definitions, characterization, and applications (technical report)," *Pure and Applied Chemistry*, vol. 72, no. 8, pp. 1483–1492, 2000.

[7] F. A. Armstrong, A. M. Bond, H. A. O. Hill, I. S. M. Psalti, and C. G. Zoski, "A microscopic model of electron-transfer at electroactive sites of molecular dimensions for reduction of cytochrome-c at basal-plane and edge-plane graphite-electrodes," *Journal of Physical Chemistry*, vol. 93, no. 17, pp. 6485–6493, 1989.

[8] A. J. Bard and L. R. Faulkner, *Electrochemical Methods: Fundamentals and Applications 2nd ed.* J. Wiley, 2001.

[9] F. A. Armstrong, A. M. Bond, H. A. O. Hill, I. S. M. Psalti, and N. Oliver, "Electrochemistry of cytochrome c, plastocyanin and ferrodoxin at edge- and basal-plane graphite electrodes interpreted via a model based on electron transport at electroactive sites of microscopic dimensions," *Journal of the American Chemical Society*, vol. 111, no. 26, pp. 9185–9189, 1989.

[10] R. S. Nicholson, "Theory and application of cyclic voltammetry for measurement of electrode reaction kinetics," *Analytical Chemistry*, vol. 37, no. 11, pp. 1351–1355, 1965.

[11] D. W. M. Arrigan and P. N. Bartlett, "A scanning force microscopy study of poly(phenol) films containing immobilized glucose oxidase," *Biosensors & Bioelectronics*, vol. 13, no. 3-4, pp. 293–304, 1998.

[12] B. R. Horrocks, D. Schmidtke, A. Heller, and A. J. Bard, "Scanning electrochemical microscopy. 24. enzyme ultramicroelectrodes for the measurement of hydrogen peroxide at surfaces," *Anal. Chem.*, vol. 65, no. 24, pp. 3605–3614, 1993.

Chapter 7

Sensors and Cell Cultures.

7.1 Introduction

In this chapter the performance of glucose sensors in cell culture media is analysed. Tests were carried out either, by drawing small aliquots from the extra cellular media or by placing the sensors within the culture vessel. The advantages and disadvantages of each of these techniques is analysed and efforts made to understand the causes of degradation in sensor performance.

7.2 Off - line analysis of Cardiomyocyte cultures

7.2.1 Primary test for validation

This experiment was repeated twice and samples were drawn from the culture every 10 hours. The glucose sensors used to make these measurements were calibrated daily before use and their calibration data are shown in Table 7.1

It was known that the concentration of glucose in the media was higher than the linear range of the sensors, therefore the same sample was measured once it had been diluted by a factor of four. This allowed us to obtain a data point in the dynamic range of the sensor

Day	y-intercept / nA	Slope / (nA/mM)
1	1.34	0.703
2	1.09	0.627
3	1.38	0.494

Table 7.1: Calibration curve data

and then scale up to the actual concentration, as shown in figure 7.1. Using the calibration

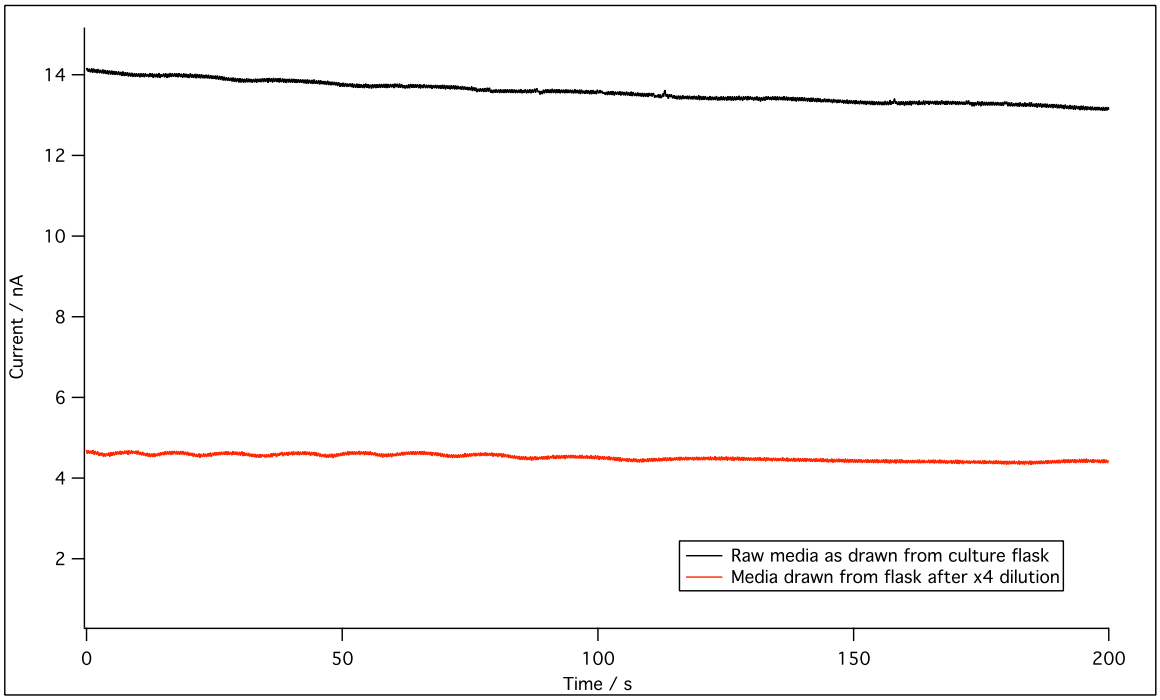


Figure 7.1: Measuring the concentration of glucose in a media aliquot. The raw trace is as taken from the culture (V_{tot}=50 μl) and the dilute trace is the same sample that has been diluted using 100 mM PBS by a factor of 4 (V_{tot}=200 μl).

data from table 7.1, it was straightforward to calculate the glucose concentration for each raw and dilute sample from the current readings.

$$I_{oxidation} = m * [glucose] + c \tag{7.1}$$

$$[glucose] = \frac{I_{oxidation} - c}{m} \tag{7.2}$$

Once the glucose concentration was known, the viability of the media could be assessed. For these particular cells and media composition there was a complication with this approach. The presence of norepinephrine (NE) in the media at a significant concentration of 0.1 mM introduced an electrochemical interference. Although, if it is assumed that the concentration of norepinephrine in the culture stays effectively constant it is possible remove this interference while post processing the data.

We know that the measured current is made up of two components as shown in equation 7.3, where the peroxide is that generated by the enzyme in the presence of glucose.

$$I_{ox,total} = I_{ox,peroxide} + I_{ox,norepinephrine} \tag{7.3}$$

We also know the concentration of glucose in the new media is greater than the linear range of the sensor. So, using the measured current from the first dilution we can calculate the fraction of the total current that is drawn by the oxidation of norepinephrine.

$$\text{Initial concentration of glucose (known)} = 22.55mM$$

$$\text{Initial concentration of glucose after } \times \text{ 4 dilution (calculated)} = 5.64mM$$

$$\text{Expected oxidation current from glucose (calculated)} = 5.31nA$$

$$\text{Oxidation current from total norepinephrine (calculated)} = 720pA$$

As a comparison both the total oxidation current and modified oxidation current have been used to show the changes in the media over the course of the culture. Figure 7.2 shows that the concentration of glucose in the culture does not follow a specific trend. In fact in both experiments the glucose concentration is higher than the initial concentration.

All samples with the prefix 'A' refer to one trial and those with the prefix 'B' refer to the second trial; there were no experimental differences between these two. They are

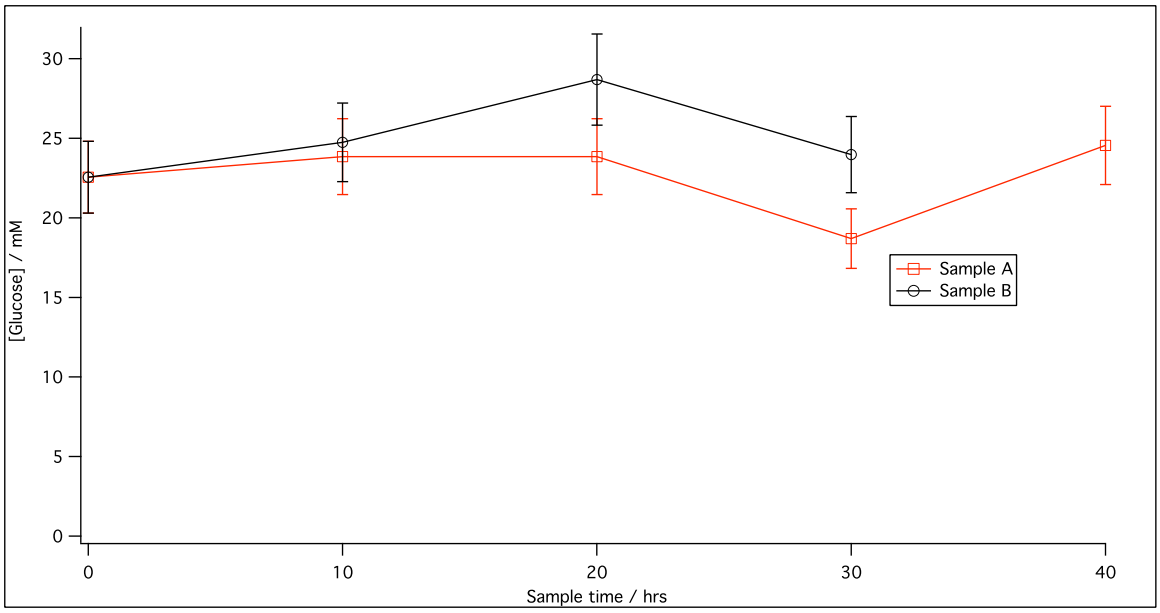


Figure 7.2: Change in glucose concentration not accounting for the norepinephrine, for both trials 'A' and 'B'. Cardiomyocyte cells were cultured in Claycomb media, as described by the manufacturer.

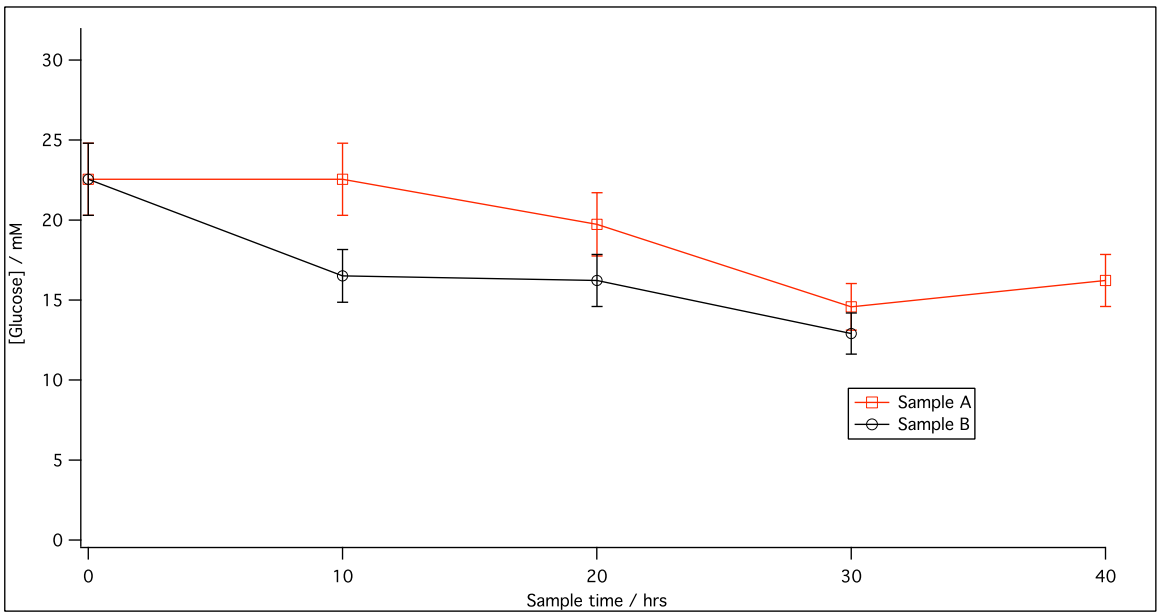


Figure 7.3: Change in glucose concentration when the norepinephrine has been accounted for, for both trials 'A' and 'B'. Cardiomyocyte cells were cultured in Claycomb media, as described by the manufacturer.

experimental repeats, in order to verify the observations.

In the case of sample B the value does not dip below the initial concentration during the entire time that the culture was sampled. This indicated the importance that norepinephrine, as an electro-active species, plays in accurately determining the glucose concentration of the media. Once the oxidation current has been corrected to account for the presence of norepinephrine the glucose concentration for the two cultures can be reconciled as shown in Figure 7.3. Here the glucose concentration decreases from the initial value as the cells grow and consume glucose. The final data point for sample A does not follow this trend, but this error is within experimental bounds and a sensor with a low sensitivity would also explain this.

During the course of these experiments it was found that the cells were not damaged and maintained their growth; even as over 30% of their media was removed for analysis. There is no quantitative information about the cells themselves from these experiments, but the qualitative analysis was positive. Also at no point during the culture period did the glucose concentration fall below 10 mM. All the cultures were carried out by Nir Grossman and the data shown here is obtained from the samples collected by him.

7.2.2 Interference from norepinephrine.

In order to confirm the effect that NE had on our measurements, it was necessary to show that this was proving to be an electrochemical interference. Using the same concentration of norepinephrine as that found in the media the responses from the glucose sensors was studied. The two techniques used for this were cyclic voltammetry and chronoamperometery.

Cyclic voltammetry was conducted in a 50 ml cell, where 500 μl of the norepinephrine stock, was added to PBS. The sensor was cycled from -600 mV to +600 mV at a scan rate of 100 mV s^{-1} [1]. The positive scan was of interest to see if there were any oxidation products that could result in the interference. Figure 7.4 shows that there is a slight shoulder in the

+200 mV region. This oxidation reaction could result in the increased oxidation current observed during the glucose measurements.

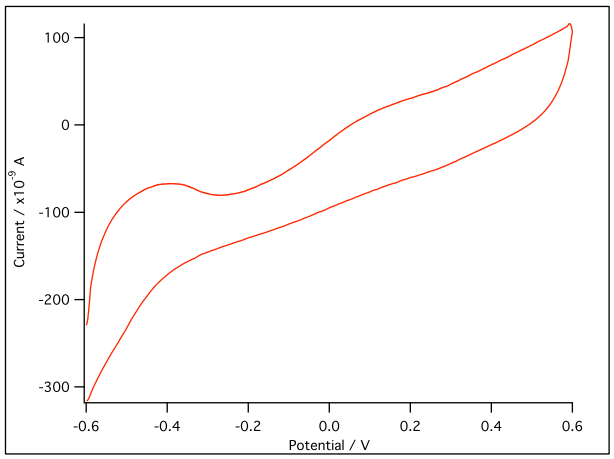


Figure 7.4: Cyclic voltammogram of 100 μM norepinephrine, prepared in 100 mM PBS as per manufacturers specifications. The electrode used is a functional glucose sensor made using glucose oxidase in a poly(phenol) film. $\dot{v} = 100mVs^{-1}$

This interference is further confirmed by using chronoamperometery and adding norepinephrine to the electrochemical cell. The sensors were polarised at +700 mV, the oxidation potential used during all glucose measurements. The response from this addition in figure 7.5 is of the order of 13 nA, for both the sensors. This is clearly much greater than what was seen in any of the other measurements. The probable reason for this elevated response is that all the norepinephrine in the cell was freely available; that is there was no protein in the cell to which the norepinephrine could bind, as was the case in the media.

Lastly, a glucose calibration was conducted in 100 mM PBS and the two calibrated sensors were used to measure the current in fresh and fully supplemented media. The media as used to culture cells is unsuitable as the starting glucose concentration is higher than the upper bound of the sensors' response curve. Therefore, the media was diluted by a factor of 5, and the norepinephrine was added post dilution. The initial glucose concentration would be 4.51 mM and any difference between the background current in the media and the calibration curve at that point could be attributed to norepinephrine interference; this

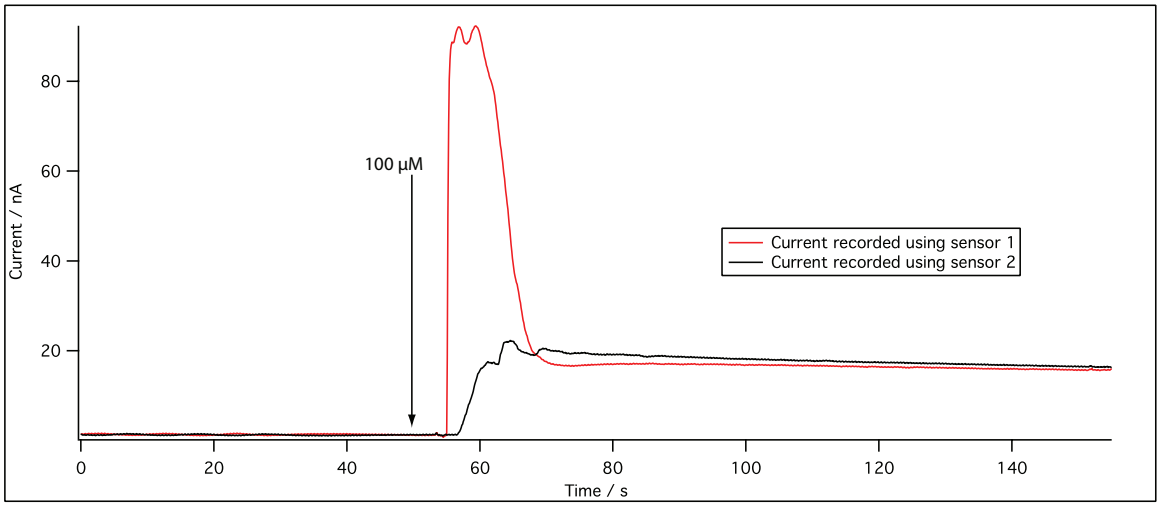


Figure 7.5: Chronoamperometery for a 100 μM titration of norepinephrine in a cell with 100 mM PBS. The electrodes used were functional glucose sensors made using glucose oxidase and poly(phenol).

can be seen in Figure 7.6.

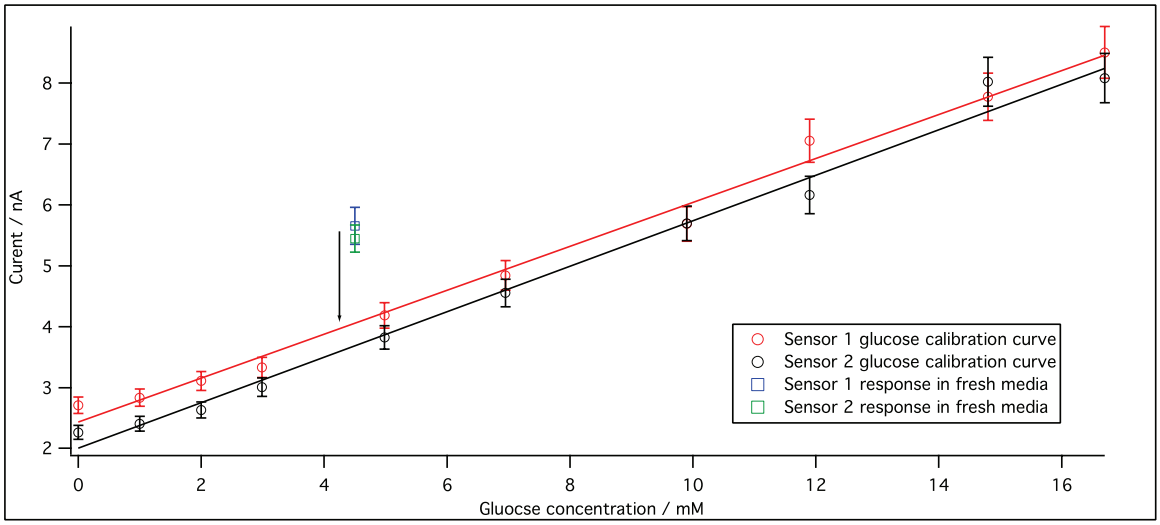


Figure 7.6: The difference between the calibration curve of two sensors in PBS and the responses from the same sensors when placed in fresh media. The error bars of the media points are twice the electrical disturbance during measurement and the arrow indicates the background current of the media, that results in the signal off-set.

For each of the sensors the expected current would be in the 4 nA range, but as seen

in figure 7.6 the media response for the sensors is 5.4 nA. This means that electrochemical interference will result in a 1.3 nA offset in the calculations for concentration of glucose. This value is different from the 700 pA that was calculated for the preliminary experiment. Therefore this estimation of a background current is not the most ideal mode of operation. However, it can now be confirmed that there are electrochemical interference that affect the measurements.

7.2.3 Long term monitoring of cardiomyocytes

A more long term experiment was setup as described earlier. This included a control culture flask and the experimental flask from which regular aliquots were drawn. The samples from the control vessel were drawn from the spent media. The experimental flask was setup in a similar manner, with the exception that in this flask the media was not replenished, but 50μl samples were drawn from it, daily. All samples were treated in the same manner as before, although in certain cases serial dilutions of the sample were performed to try and obtain a more accurate value for the concentration of glucose. The operating characteristics of the sensors used are shown in table 7.2

Sample	y-intercept / nA	Slope / (pA mM^{-1})
0	1.50	330 ± 146
1	1.23	308 ± 84
2	1.95	256 ± 70
3	1.34	207 ± 47
4	0.725	241 ± 57
5	0.757	196 ± 41
6	1.05	237 ± 87
7	0.933	178 ± 54

Table 7.2: Calibration curve data, for the sensors used during the long term monitoring of the media. The sample numbers indicate the calibrations performed before that particular sample was tested.

The data from this long term off-line monitoring is shown in figures 7.7 and 7.8; both

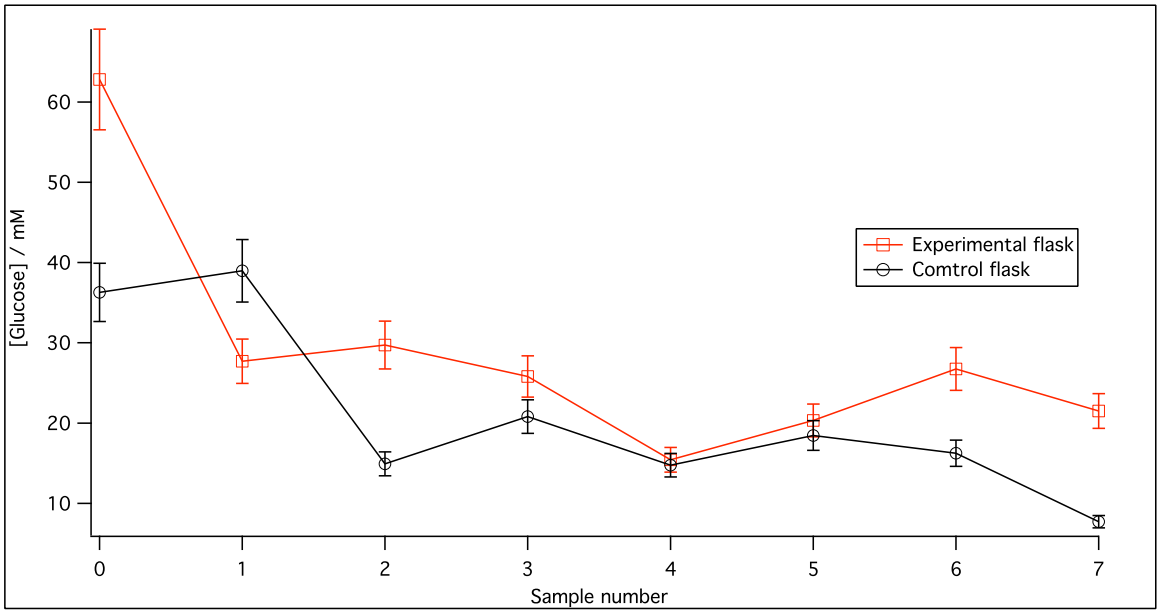


Figure 7.7: Change in the concentration of glucose in Claycomb media during the culture of cardiomyocyte cells, without the removal of the background current.

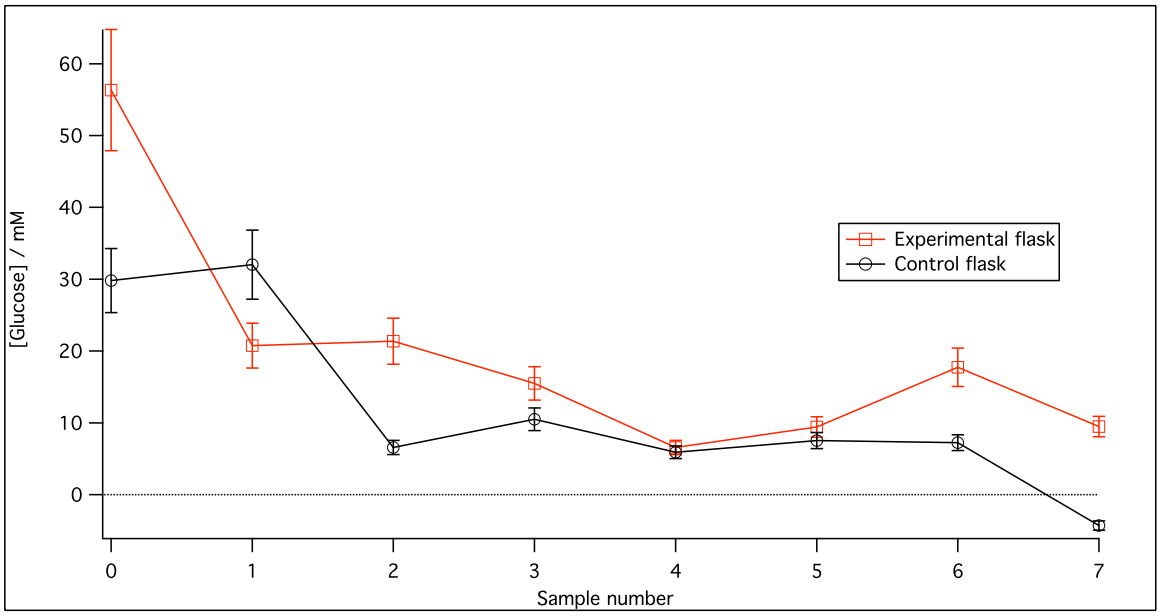


Figure 7.8: Change in the concentration of glucose in Claycomb media during the culture of cardiomyocyte cells, once the estimated background current, has been mathematically removed.

these figures show some unexpected behaviour. The initial glucose concentration is extremely high (the actual concentration should be $\simeq$22 mM) and there was an error in that measurement and it should be discounted. For the other samples, the trend of the glucose concentration can not be reconciled. In this case, even the subtraction of the background current, did not yield any significant improvements. For the purposes of this experiment, the background interference was calculated to be 534 pA.

If the cell density had remained constant then the concentration of glucose in the control flask should have been roughly constant, as the media was replaced at 24 hour intervals. If not, then the glucose consumption in the culture would increase. There is no quantitative data about the cell densities from this experiment, but snap shots of both the culture flasks indicate increasing cell density; as seen in Figure 7.9.

Another possible problem with the collection of the data could have been the pH at which all the glucose measurements were performed. The activity of the enzyme may have been affected, to ascertain whether this was significant, the pH of all the diluted samples was measured and is shown in table 7.3. All the pH values are consistent and are similar to the pH of 100 mM PBS, in which all the calibrations were performed. It is also worth noting that the pH of both media decreases during the course of the culture, as is to be expected. As the cells grow the pH of the media decreases as a result of increased cell growth and metabolism along with being placed in a CO_2 controlled environment.

The reason that this experiment did not yield any consistent results was because of the quality of the sensors. When a background signal is being assumed to be constant so that it maybe subtracted, it is very important that the signal be larger than the background. Any background signal being subtracted has to be stable and its magnitude depends on the tolerance that the analyte shows to error. As the initial sensitivity of the glucose sensors used was about 300 pA mM^{-1}, which then degraded to one third of its original value the sensors were not producing a strong and stable enough signal to subtract the background current in this manner.

Sample number	pH of A	pH of CTR
1	7.47	7.53
2	7.47	7.45
3	7.34	7.37
4	7.31	7.23
5	7.27	7.17
6	7.29	7.09
7	7.40	7.11

Table 7.3: pH of samples diluted with 100mM PBS after being removed from media during the long term monitoring of cardiomyocyte cultures.

It was clearly evident that the cells grown in the control vessel and fed on a daily basis grew at a more consistent rate than those from the experimental flask. The number of cells and their viability can be seen in Figure 7.9. The cells from culture A, show similar growth patterns as the control for the first 72 hours. Then, as the quality of the extra-cellular media begins to degrade and an increasing quantity is removed, the cell growth becomes limited and eventually there are a larger number of cells that die in culture A, as compared to the control.

It is clear that off-line analyses are feasible and can provide information about the state of the media, when it is replenished on a daily basis. There are however disadvantages of off-line measurements that are detailed later. The cell line that was chosen for off-line monitoring and the mode of operation to sense glucose used here are not compatible. Post processing the data to remove background currents is prone to greater error as the independent errors in the measured and background currents propagate. It might be possible to improve the quality f the data collected using differential sensing. If a another sensor was made in the same manner as a glucose sensor, using bovine serum albumin, or other protein, in place of glucose oxidase; then the signal generated by it at the operating potential of +700 mV would be the oxidation of norepinephrine, only. This might be a more accurate method of removing the background current.

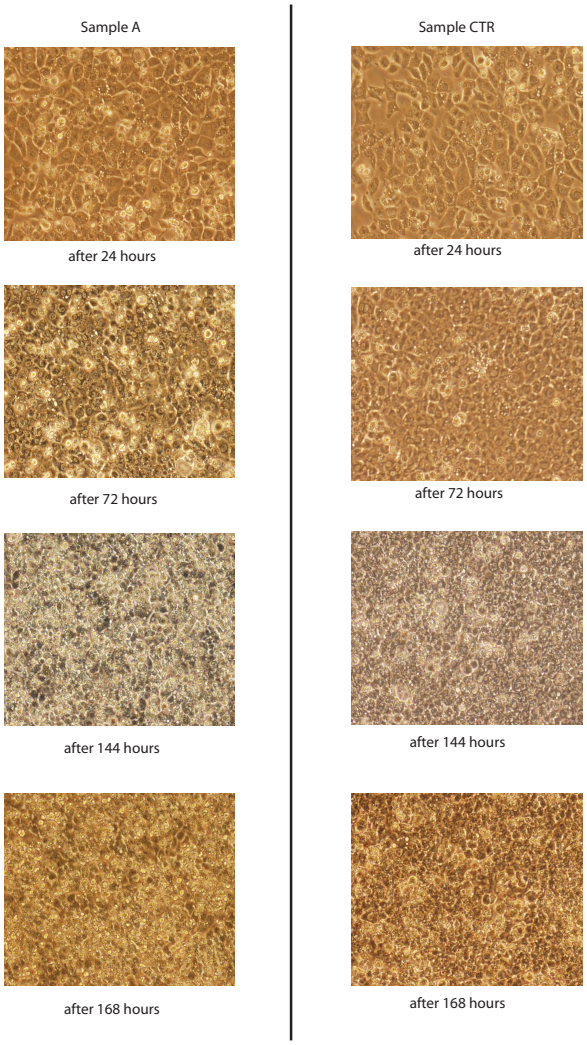


Figure 7.9: Cell growth over 7 days of the second off-line test. (Magnification x20) The two columns show the differences in cell growth in the control and experimental cultures. This illustrates the hindered cell growth and viability in the sample A where the media was not replenished daily.

7.3 *In-vitro* chracterisation and use.

The results from all the *in-vitro* tests and measurements are shown and discussed here. In this section *in-vitro* refers to direct insertion into the culture media. It was important to follow the sequence shown in section 2.11 to ensure that the hypothesis of on-line monitoring was feasible and that the problems, if any, could be ascertained at an early stage.

7.3.1 Toxicity tests

In order to ensure that the glucose oxidase, poly(phenol) and/or the packaging of the device did not prove harmful to the culture, both the bare electrodes and the enzyme sensors were placed in the culture and the cell yield was monitored and compared against the controls.

Research in to the literature on the toxicity of all the materials used did not lead us to believe that any of them would prove toxic. The LD_{50} values available for various forms of exposure did not yield any cause for concern and in some cases these values were orders of magnitude higher than the amounts of material present in the devices. However, from previous experience it was found that the reported toxicity data for humans and other mammals did not necessarily mean that the cultures would not be affected [2]. Table 7.4 shows the results of the toxicity tests. In both the case of the bare electrodes and the enzyme sensors the cell yields between the control vessel and experimental cultures are comparable. This shows us that neither the device packaging nor the analyte specific layer adversely affected the culture of 3T3 Fibroblasts over a period of 7 days.

7.3.2 *In-vitro* life time analysis of the enzyme sensors

As mentioned in section 2.11.2 the life time of the glucose sensors was studied *in-vitro*. Eight sensors were prepared and characterised prior to being placed *in-vitro*. The nomenclature used to identify each of the sensors and the lengths of time that they spent *in-vitro* are shown in Table 7.5. The initial operating characteristics of each of the devices can be seen in Figure 7.10.

Culture details	No. of cells seeded	Cell count at end	Cell viability	Cell yield
3T3 control	20,000	52.500	84%	2.6
	20,000	57,000	86%	2.9
Bare electrodes	20,000	39,600	85%	2.0
Enzyme sensors	20,000	49,500	85%	2.5
	20,000	55,500	84%	2.8

Table 7.4: Results of the toxicity tests

Sensor name	No. of days *in-vitro*
Sensors 1 and 2	1
Sensors 3 and 4	2
Sensors 5 and 6	3
Sensors 7 and 8	7

Table 7.5: Sensor nomenclature for *in-vitro* test.

Each of the sensors was sterilised using ethanol and placed in a 3T3 cell culture. Two sensors were withdrawn from the culture vessel on days 1, 2, 3 and 7. Each pair of sensors was tested for their responses to glucose once removed. While *in-vitro* the sensors were not polarised at their operating potentials, but placed at open circuit. The operating characteristics of the devices both prior to and after removal are shown in table 7.6.

In addition to this each pair of sensors was also tested as follows:

1. Sensors 1 and 2 on days 2, 3 and 7. These were also tested twice on day 2
2. Sensors 3 and 4 on days 3 and 7. These too were tested twice on day 2.
3. Sensors 5 and 6 on day 7 only.

For the main part, we will discuss the pairs of sensors that were withdrawn from the culture on days 1, 2 and 3. As expected the devices that were removed on the seventh day were unresponsive to changes in the concentration of glucose. The calibration curves for all

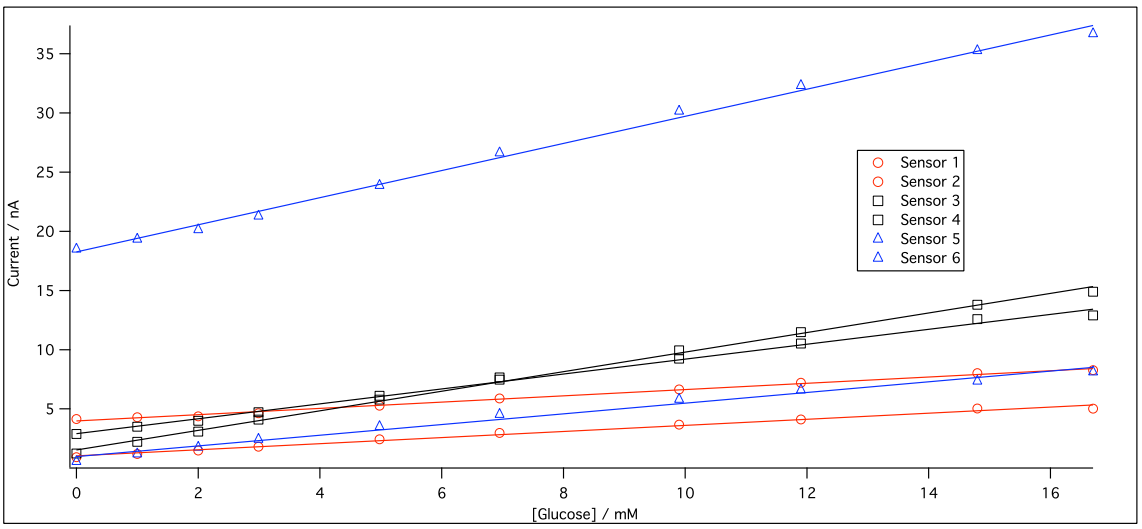


Figure 7.10: Initial calibration curve for sensors before operating *in-vitro*.

three pairs of sensors immediately on removal from the culture vessel are shown in Figures 7.11 to 7.13.

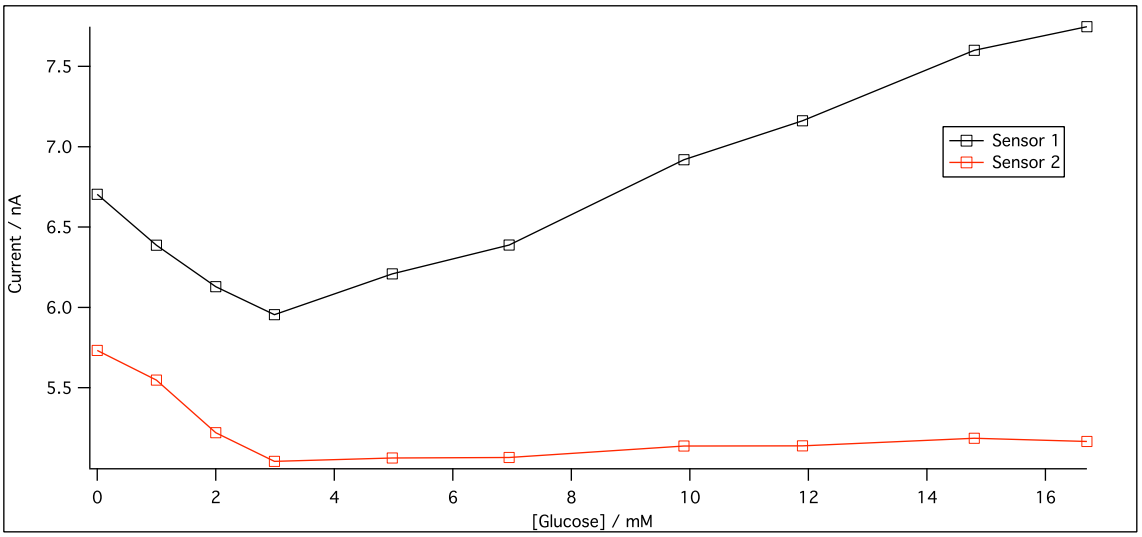


Figure 7.11: Calibration curves for sensors 1 and 2 after one day *in-vitro*.

Each of the daily calibration curves, showed similar responses to changes in glucose concentration. There is an apparent, initial, decrease in the oxidation current for hydrogen peroxide and then the oxidation current increases in a linear fashion. This is the case, for

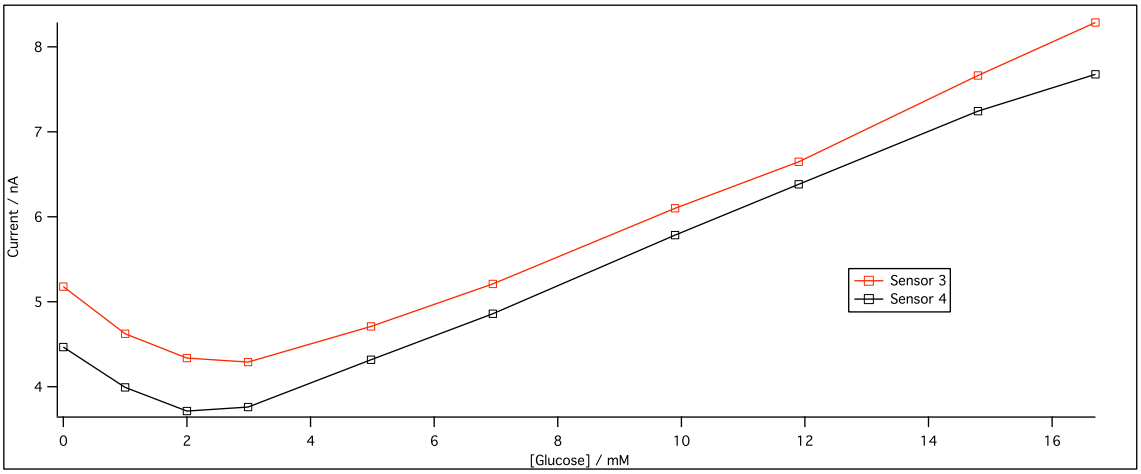


Figure 7.12: Calibration curves for sensors 3 and 4 after 2 days in *in-vitro*.

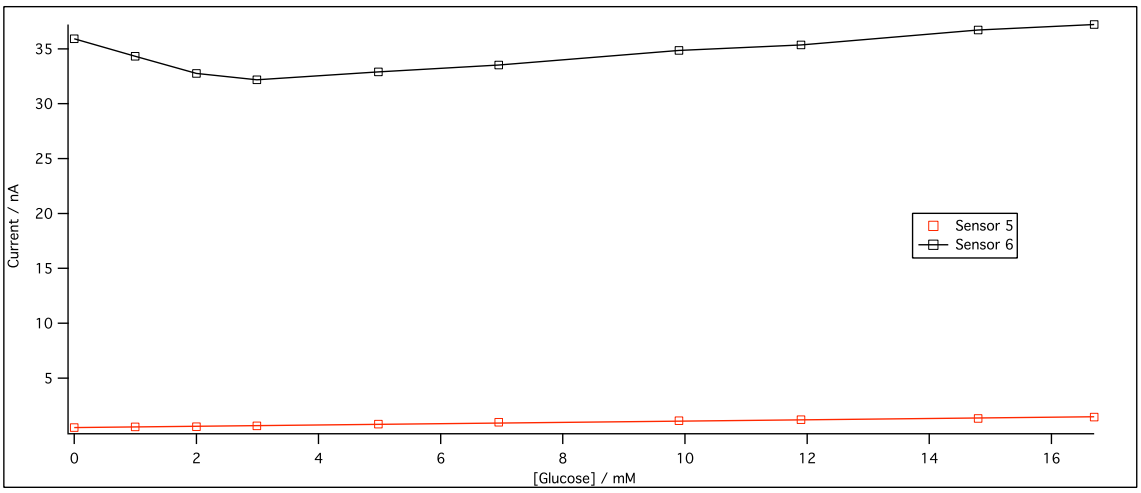


Figure 7.13: Calibration curve for sensor 5 and 6 after 3 days in the 3T3 culture vessel.

all the sensors apart from sensor 5.

To make more sense of the calibration curves it is necessary to split them in to two independent sections and to then analyse each section individually. To allow this, the data is split such that the first portion, includes the current logged till just before the addition of the fourth aliquot of glucose. For each sensor this splits the data in to low and high glucose concentration sections.

Sensors 5 and 6 that were removed from the culture vessel after 3 days, were tested and

as expected the responsiveness of the sensors was very low, sensor 5 exhibits only 10% of its original response and sensor 6 shows a similar shaped response to those of the earlier devices. The sensitivity of sensor 6, in its linear range, is also a mere 58 pA mM^{-1}. The comparative performance of each sensor is shown in Figures 7.14, 7.15; here it can be seen that the top end of the linear range for each sensor is the same as it was before they were placed in the culture, although the sensitivity is decreased from before. Table 7.6 shows the initial operating characteristics and the change in the sensitivity for each of the devices on the day that they were removed from the bio-reactor.

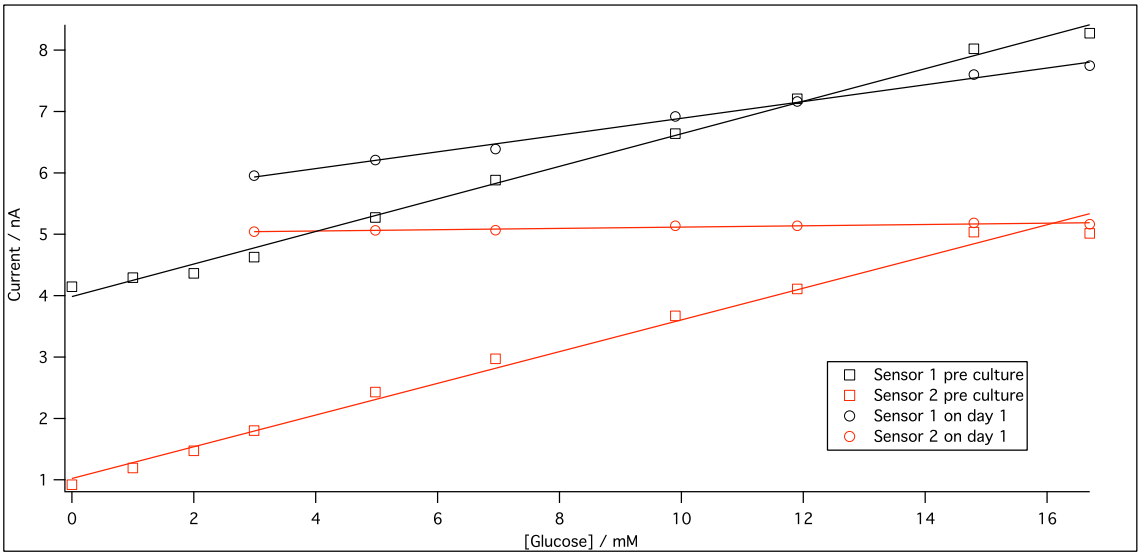


Figure 7.14: Linear section of calibration curves for sensors 1 and 2 on day 1.

The current traces of the sensor responses at the low glucose concentrations, indicate that the current decreased as a function of time. Before beginning the titration the current data was not logged for the first 180 s, so as to allow the Cottrell current to dissipate. The output recorded should have been a steady state current, but in these cases there is a decay in the current from the background.

The fact that the dynamic range of the sensors remains the same; but the sensitivity is lower than before, points to the fact that loss in enzyme activity is not the only reason for a drop in the sensors' response. If this were the only reason for the sensors to degrade then

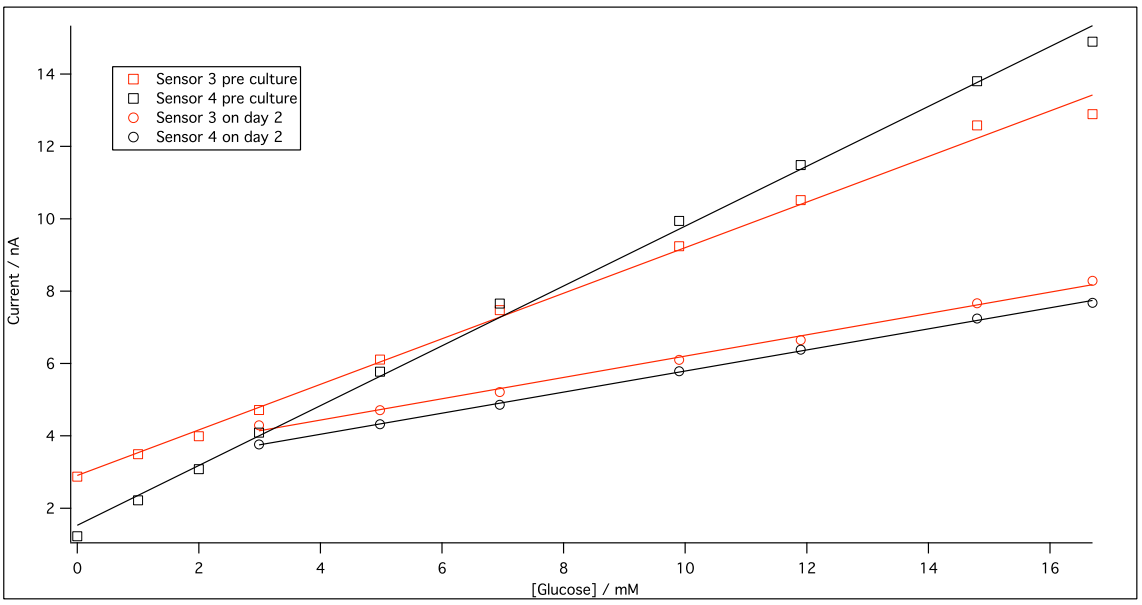


Figure 7.15: Linear section of calibration curves for sensors 3 and 4 on day 2.

the top end of the dynamic range would fall as well, in accordance with the limiting turn over of the enzyme.

For each of the sensors that were removed from the culture, the steady state current persisted till the 4^{th} addition of glucose. This indicated that there was a mass transport barrier between the bulk solution and the active site of the enzyme, which provided a limiting flux of approximately 3 mM glucose. This implied that the flux dampening of glucose through this external barrier affected the performance of the sensors.

A schematic of the possible concentration profiles is shown in figure 7.16, (a) is a fresh sensor and there is no bio-fouling creating an external mass transport barrier. Here even at glucose concentrations < 3 mM the flux of glucose at the enzyme film produces a response, providing a full linear dynamic range. The other two parts show the presence of an external mass transport barrier as a result of being placed in the culture. Only when the bulk concentration of glucose is > 3 mM, is $J_{glucose}$ high enough at the enzyme film to show a response.

We can now say with a degree of certainty that there was a layer on the surface of the

Sensor name	Initial slope / (pA mM^{-1})	Responses after removal / (pA mM^{-1})	Change in sensitivity
1	265.1	136.4	-48.5 %
2	258.3	106.2	-58.9 %
3	629.8	294.8	-53.2 %
4	827	291.2	-64.8 %
5	451.2	58.1	-87.1 %
6	1145.8	37.5	-96.7 %

Table 7.6: Change in linear sensitivity when the sensors are withdrawn from the culture.

sensor that hindered its responses at low concentrations. Also, that most of the degradation in the sensors' responsiveness during the first two days of being placed *in-vitro* was a result of this adsorption on their surfaces. Lastly, based on the fact that the sensors withdrawn from the reactor on day 2 exhibit the same limiting flux as those on day 1, it is safe to assume that the adsorption attains equilibrium during the first 24 hours.

If we know this to be the case, then it is possible to study the characteristics of this film, to try and achieve a deeper understanding of its features and to see if this degradation can be mitigated. Secondly, if this process can be even partially reversed then we can be absolutely certain that a loss in enzymatic activity is not the sole reason for the devices losing their sensitivity.

To see if the degradation could be reversed the devices were calibrated daily and stored at room temperature in a beaker of 100 mM PBS, in between tests. Firstly, we shall look at sensors 1 and 2 that were removed from the reactor after 1 day. The calibration curve for that day can be seen in Figure 7.11, Figure 7.17 shows the calibration after they had been stored in a protein free media for 24 hours. Here too, it can be seen that the pair of devices do not respond to changes in the concentration of glucose at the lower end.

A similar procedure was followed for sensors 3 and 4 that had spent 2 days *in-vitro* and can be seen in Figure 7.15. In order to assess whether repeated titrations would affect the

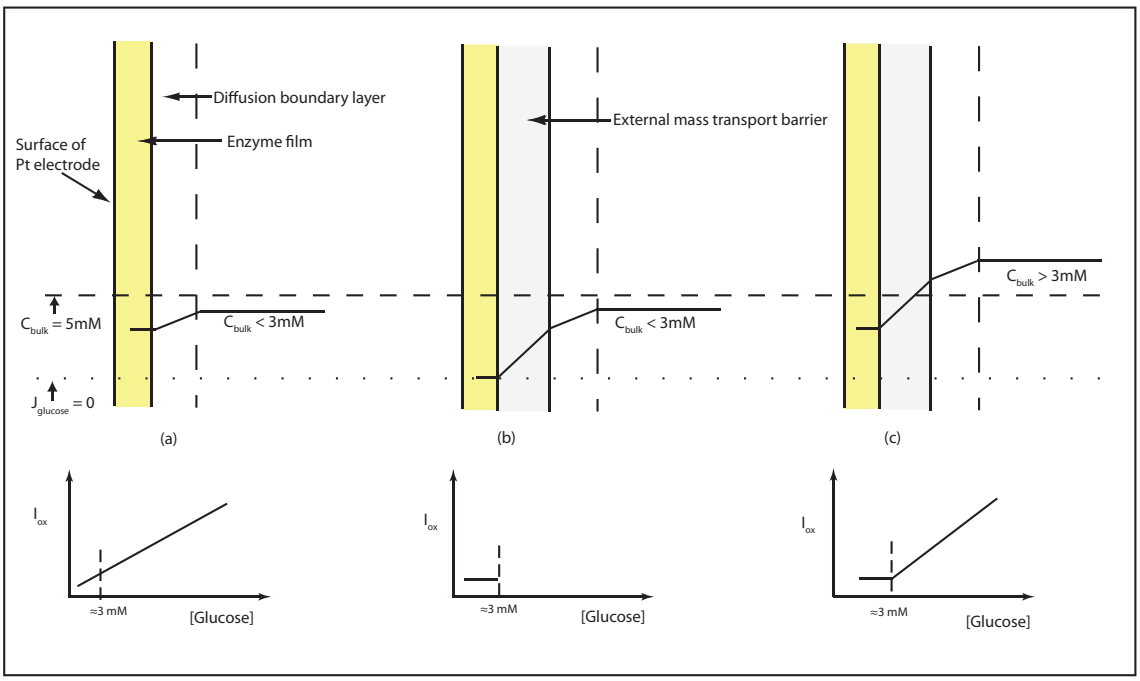


Figure 7.16: A schematic showing the flux of glucose at the enzyme film. Three cases are shown in this figure: (a) A new sensor that displays a full linear range, here the flux of glucose from the bulk to the enzyme is linear relationship. (b) An external mass transport barrier has formed on the outside of the enzyme film. This external barrier means that when the bulk concentration of glucose < 3 mM then the enzyme film does not receive any glucose. (c) This is the same case as (b) with the bulk concentration of glucose now being> 3 mM. As a result the enzyme film is able to receive a portion of the glucose flux, the relationship between the bulk concentration of glucose and its flux at the enzyme film are no longer a simple linear relationship.

mass transport barrier, sensors 1 to 4 were tested twice during the course of day 2. The shear caused by forced convection, during stirring, could result in the fouling layer being removed more effectively. Also, the oxidation of H_2O_2 might affect the manner in which the film adsorbs to the glucose sensitive surface, although this is unlikely as the oxidation occurs in the dissolved phase and there was no visible formation of gas bubbles on the electrode's surface. The shear caused by forced convection is more likely to be the cause of any increased reversibility in the sensor degradation.

As seen in Figure 7.15 the response of both the devices is similar to that seen for sensors 1 and 2. The sensors show a linear response to changes in glucose concentration after a

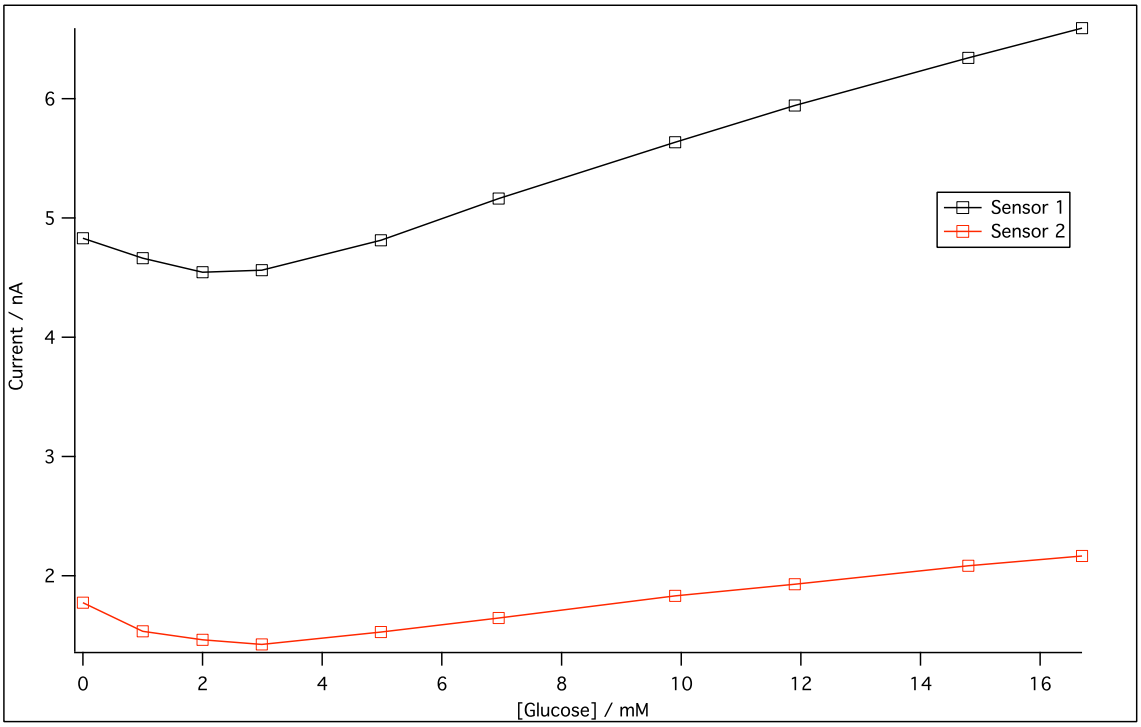


Figure 7.17: Calibration curve for sensors 1 and 2 on day 2.

minimum concentration of 3 mM has been reached in the electrochemical cell. This would indicate that the sensor degradation due to bio-fouling achieves steady state some time in the course of the first day and thereafter the degradation could be attributed to a loss in enzymatic activity. The calibration traces for the repeat titrations for day 2 exhibit an interesting change.

When the traces for the first and second tritrations are compared in Figures 7.18, 7.19, 7.20 it is observed that they begin to show a linear response to glucose after the third addition. This implies that the limiting flux is crossed before the C_{bulk} reaches the previously observed 3 mM. The calibration curve for sensor 4 shows a linear response along the entire range of concentrations, as seen in Figure 7.21. However, the response at lower concentrations is damped compared to that at higher concentrations. The slope for the higher concentration range is 372 pA mM^{-1} and that for the lower concentration range is only 227.6 pA mM^{-1}.

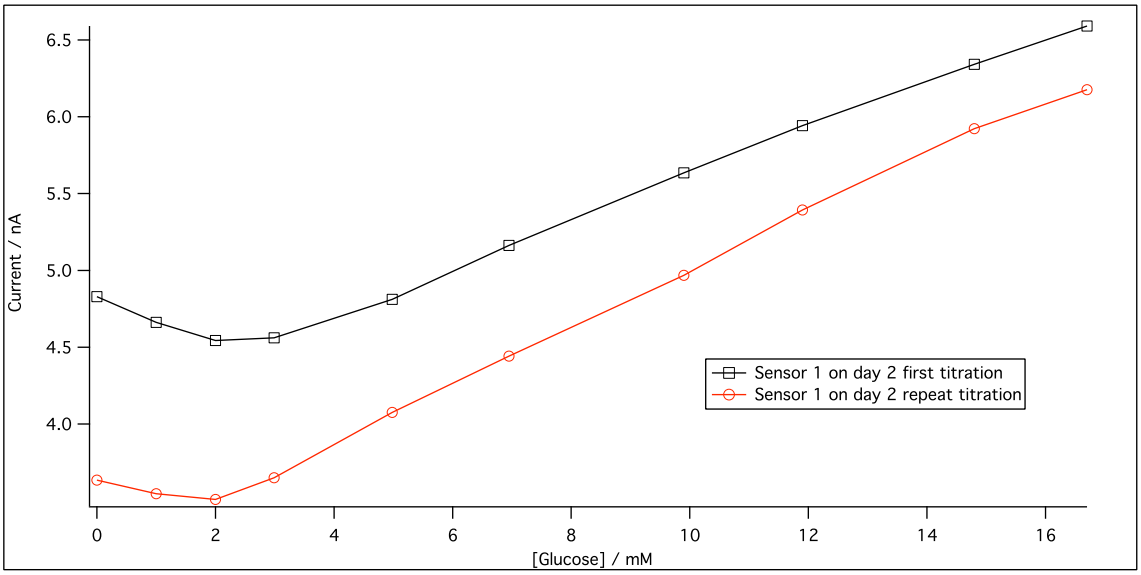


Figure 7.18: Calibration trace for sensor 1 as repeated on day 2.

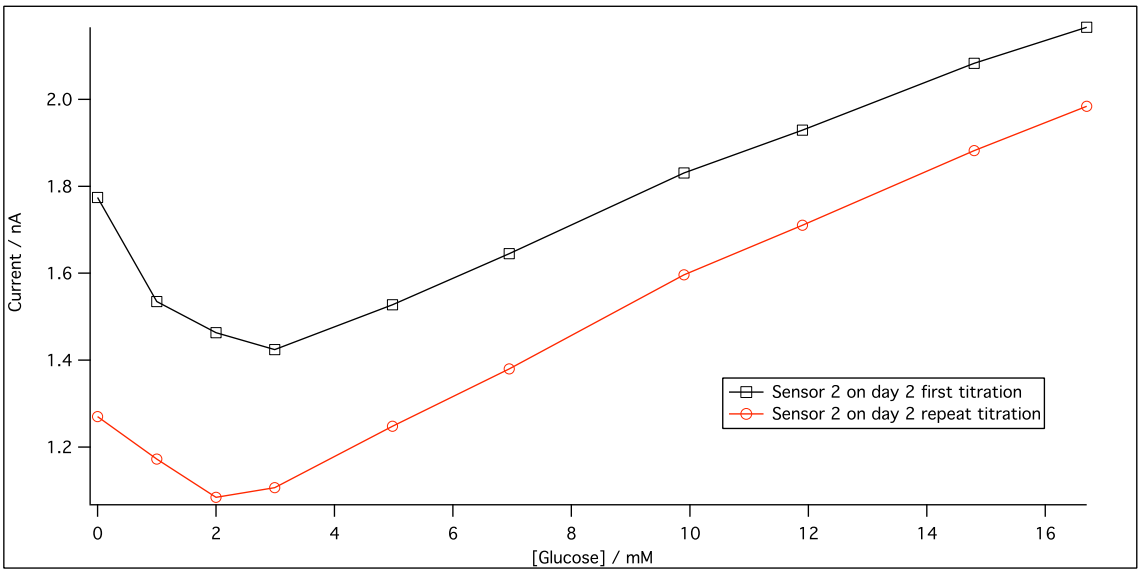


Figure 7.19: Calibration trace for sensor 2 as repeated on day 2.

This evidence indicates a semi-reversible degradation in the sensors' performance, after they have spent two days in the culture vessel. Along with the devices that were removed on day 3, the first four sensors were tested as well. A comparison of these four calibration curves against those for the same devices prior to exposure to the culture are shown in Figures

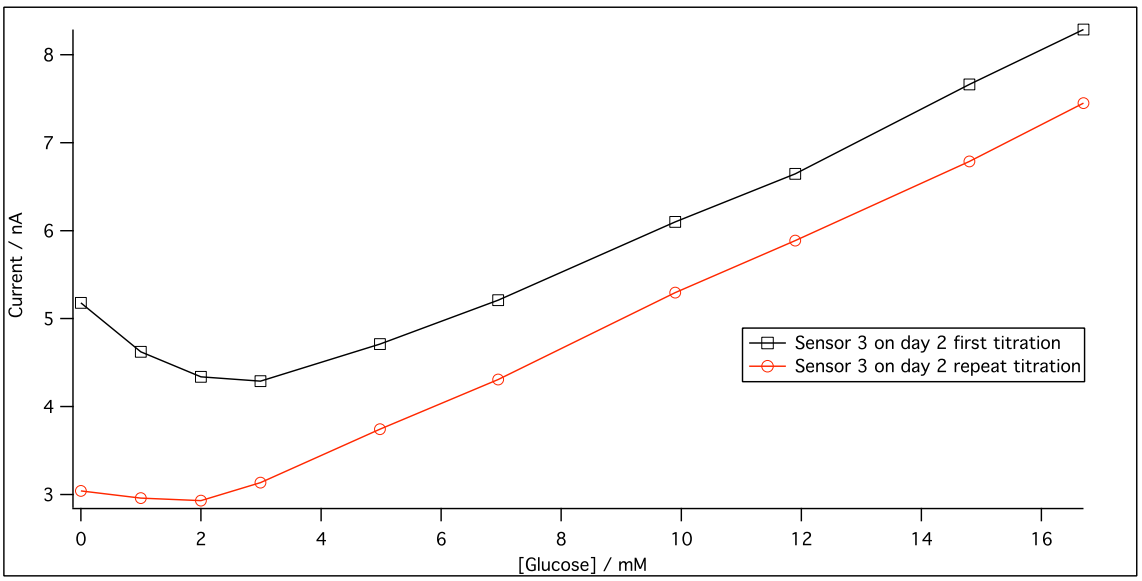


Figure 7.20: Calibration trace for sensor 3 as repeated on day 2.

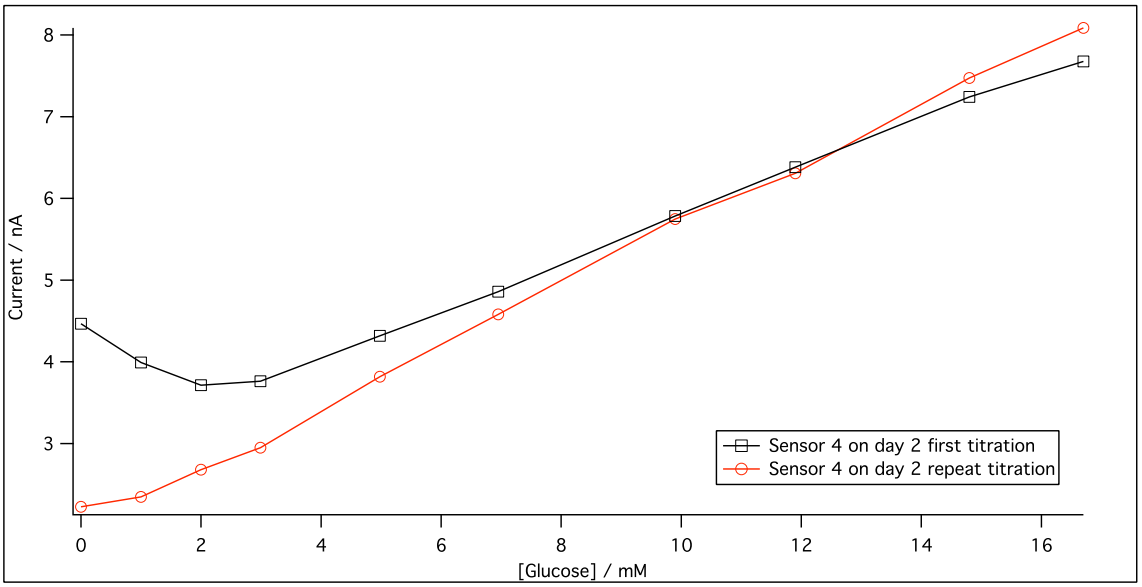


Figure 7.21: Calibration trace for sensor 4 as repeated on day 2.

7.24 and 7.25. The relative performance of sensors 1 to 4, for each of the measurements made using them is shown in Figures 7.22 and 7.23.

As can be seen from these calibration curves, the sensors have regained their full linear range but have lost a substantial degree of their sensitivity, in comparison to their initial

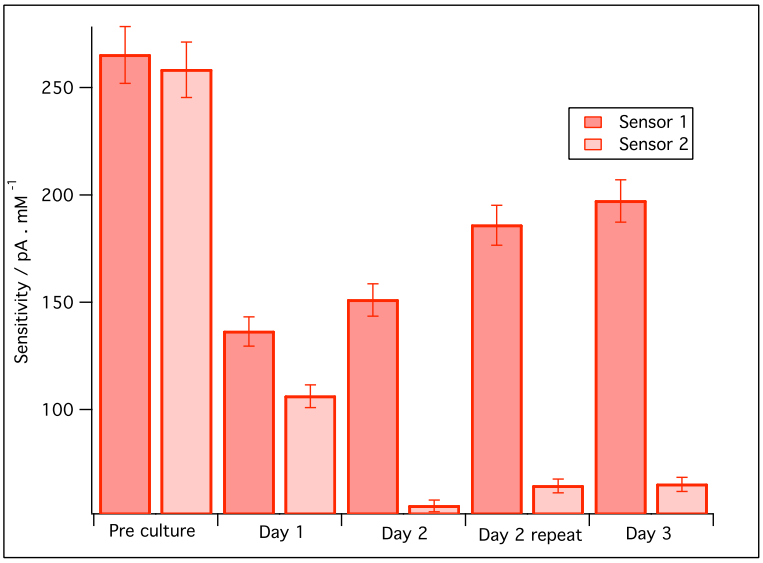


Figure 7.22: The transient nature of the responses of sensors 1 and 2 before they were placed in the culture and during their daily calibrations once they had been removed from the culture after 24 hours.

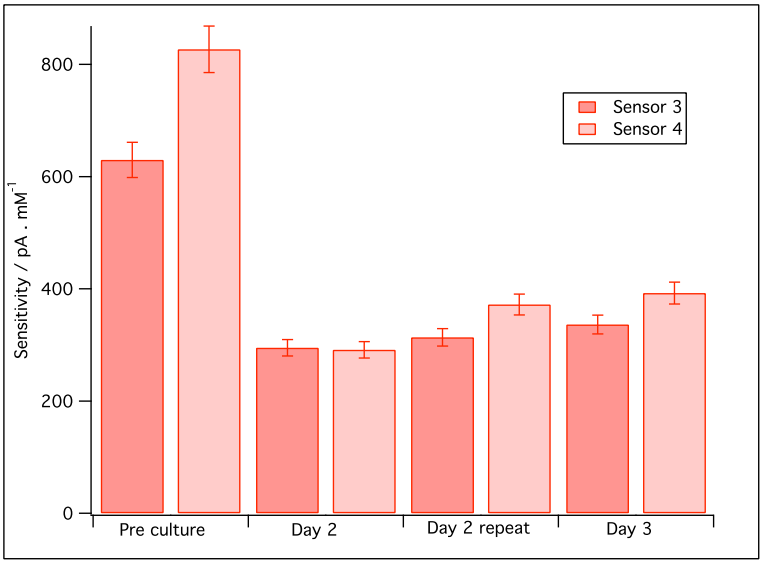


Figure 7.23: The sensitivity of sensors 3 and 4 before being placed in culture compared to their responses on removal from the media.

operating characteristics. Therefore, the removal of the adsorbed external layer allowed the sensing of low concentrations of glucose, but the responses of the sensors may still be damped, due to a diminished $J_{glucose}$ at the enzyme film. It is also possible that being

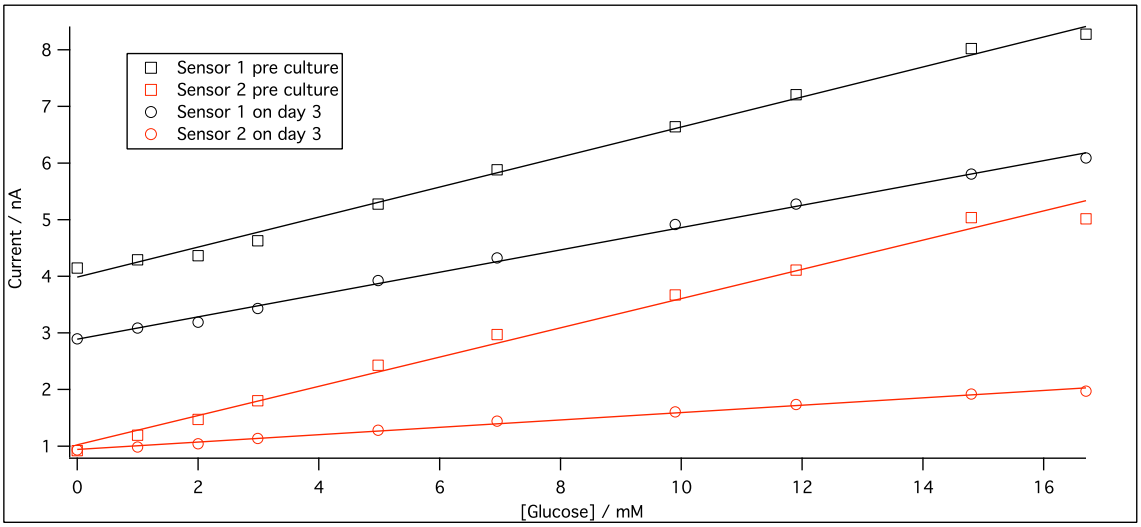


Figure 7.24: A comparison of the calibration curves for sensor 1 and 2 on day 3 compared to the same devices before they were placed in the culture.

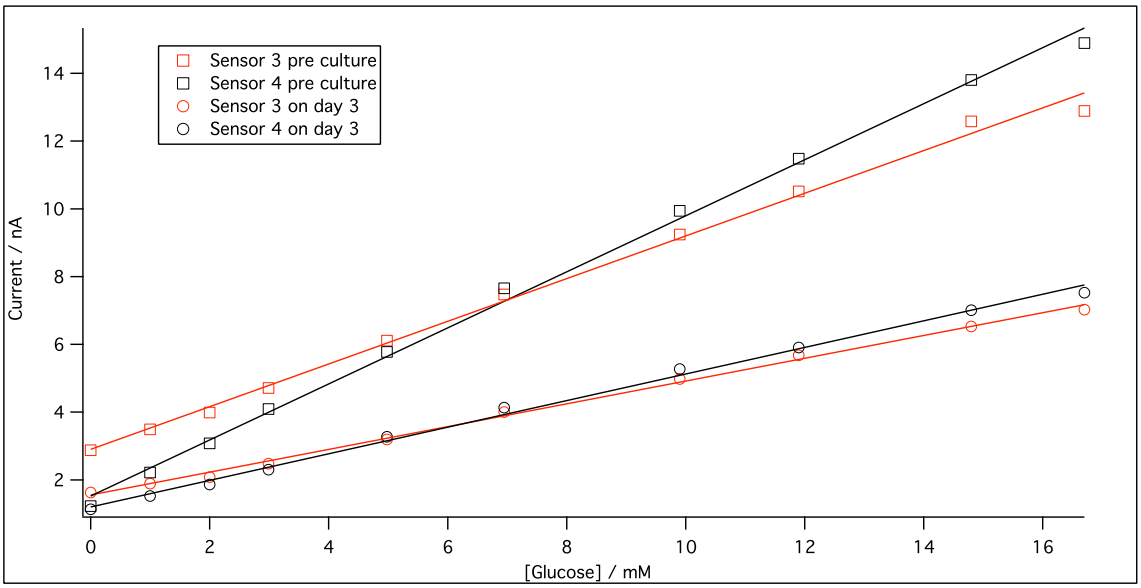


Figure 7.25: A comparative of the calibration curves for sensor 3 and 4 on day 3 and before they were placed in the culture .

present in the cell culture deactivates the enzyme quicker.

7.3.3 The use of H_2O_2 to assess the degradation of the performance of the sensors.

So as to ascertain, whether this particular phenomenon was observed as a result of the external mass transport barrier or inhibited enzyme catalysis, a similar test was conducted to observe the response of the sensors using a different probe molecule after they had been placed *in-vitro* for 1, 2 and 3 days. For this purpose hydrogen peroxide was used as the probe molecule. This was chosen not only because of its size, but also because it was the redox species being used as the signal generator in the glucose sensors and its electrochemistry does not depend on glucose oxidase.

The use of hydrogen peroxide as a probe molecule has some draw backs, primarily its stability. Also, platinum surfaces are prone to degradation, especially with respect to peroxide electrochemistry. However, when the sensor has not been allowed to dry in air and is not polarised for long periods in the presence of hydrogen peroxide, the degradation of the surface should be minimal. To allow for an accurate analysis the concentration of hydrogen peroxide was determined using potassium permanganate ($KMnO_4$) in an acidic environment. The reaction follows the stoichiometry shown in Equation 7.4

$$2MnO_4^- + 5H_2O_2 + 6H^+ \longrightarrow 2Mn^{2+} + 5O_2 + 8H_2O \tag{7.4}$$

Day	Conc. of H_2O_2 / M
0	2.1
1	1.89
2	1.78
3	1.75

Table 7.7: Activity of H_2O_2 verified using a $KMnO_4$ titration.

Using these data, we were able to more accurately assess the responses of the sensors to

hydrogen peroxide, once they were removed from the culture. Three glucose sensors were placed *in-vitro* to be tested daily. Each sensor was characterised prior to being placed in the culture and then again, once it was removed. As before each sensor had been sterilised using ethanol. The sensor responses both before and after being placed in culture are shown in Figures 7.26, 7.27 and 7.28.

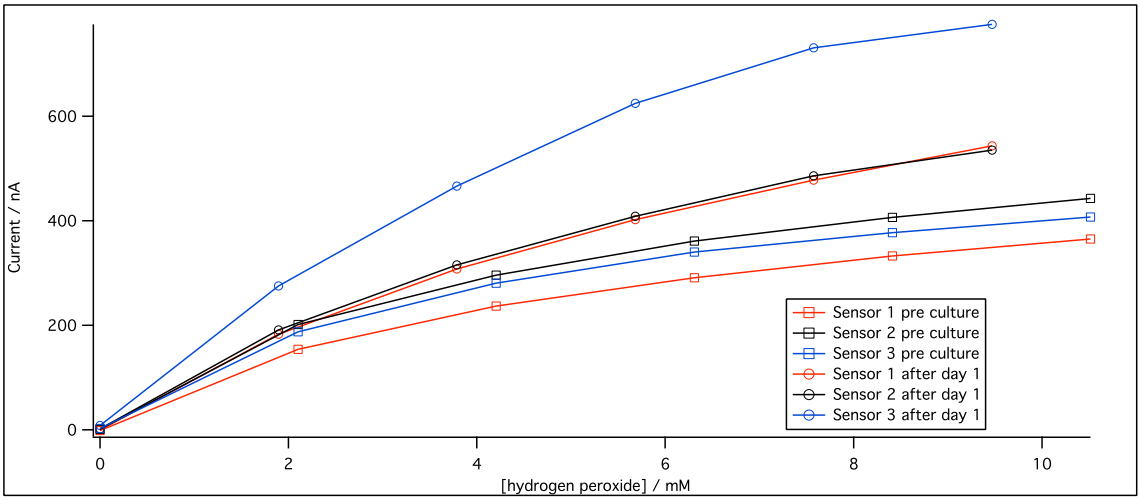


Figure 7.26: Comparative response to H_2O_2 for sensors 1, 2 and 3 before and after being placed *in-vitro*.

The response for all three sensors that spent one day *in-vitro* was higher than that observed before they were placed *in-vitro*. The sensors that spent 2 days in the culture showed a similar response to before being placed in the culture. The final three sensors showed a damped response.

These data do not allow for a rigourous analysis and it can only be surmised that the performance of the sensors was affected by the inherent variations of 'hand made' devices; although, prior to being placed in the culture the operating characteristics of the devices were acceptable. After this initial calibration the sensors were handled on a number of occasions to prepare them for being placed in the culture flask and these steps might have led to sensor damage, as witnessed by their lack of sensitivity toward glucose.

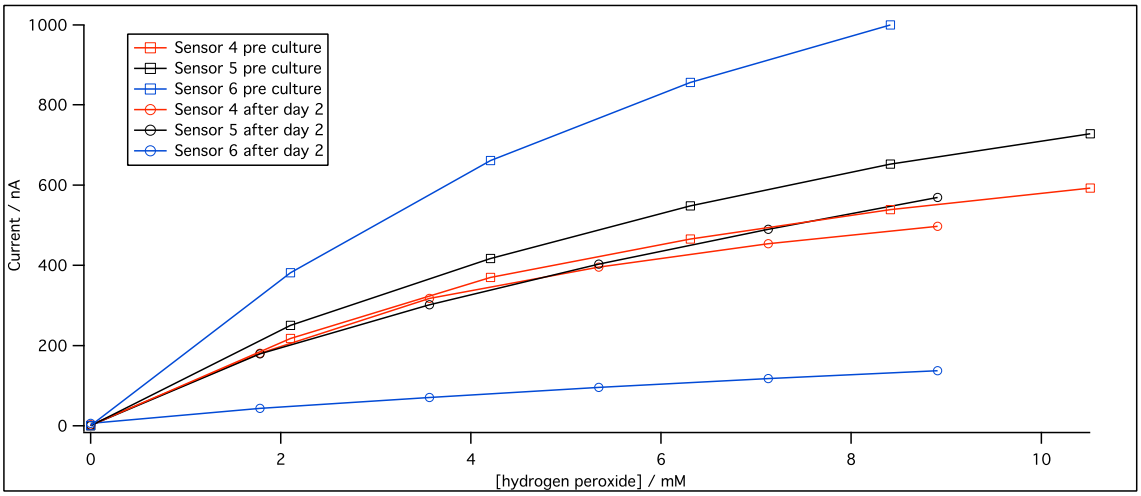


Figure 7.27: Comparative response to H_2O_2 for sensors 4, 5 and 6 before and after being placed *in-vitro*.

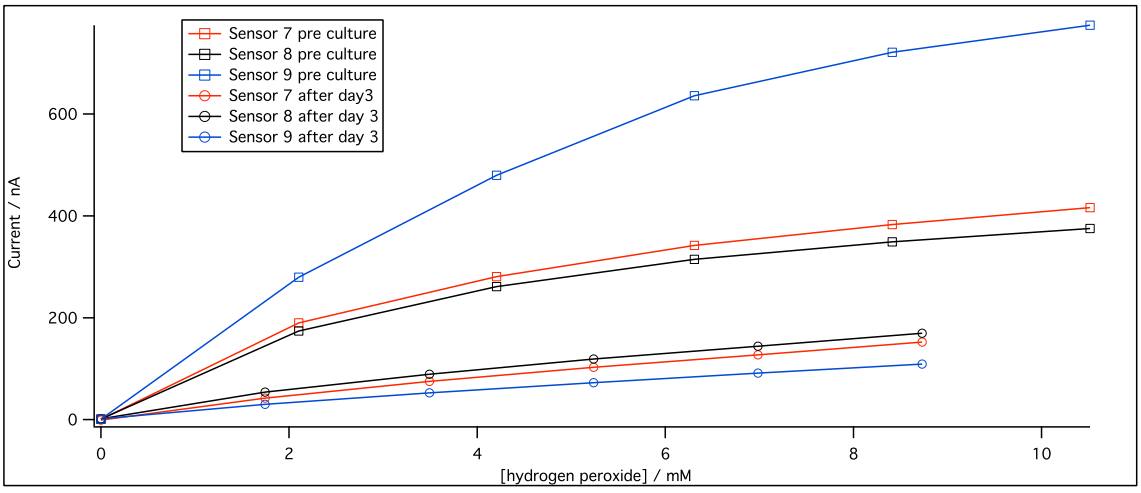


Figure 7.28: Comparative response to H_2O_2 for sensors 7, 8 and 9 before and after being placed *in-vitro*.

7.4 Summary

Off-line monitoring of cell culture media has many advantages, chiefly the ability to use fresh, well calibrated sensors that will result in a high quality and reliable signal. It is also possible to analyse the media using a secondary technique that will allow us to validate the data from home made sensors. These advantages are outweighed by the limited number of time points that are available for analysis. In biological terms a sample every 10 hours or so, maybe sufficient, but it is never able to produce an accurate transient picture that on-line monitoring can give. If reliable and robust sensors are used, then their data can be used and secondary validations performed when required.

The off-line monitoring of the cardiomyocyte cultures showed a great deal of promise and it also makes it patently obvious that in the presence of secondary electrochemical interference it is necessary to tailor the sensors mode of operation to suit the needs of the media. Using a method of differential sensing to subtract the background current from the media sounds promising and more work needs to be done with this.

The sensors did not prove toxic to 3T3 cells over a 7 day culture. This is very promising as it is an important factor to be taken into account when designing sensors for use *in-vitro*. The cell yields for the controls and cultures with sensors present were similar.

When the sensors have spent 24 hours *in-vitro* they develop a mass transfer barrier that lowers their ability to sense low concentrations of glucose, although their linear range is not affected. Their sensitivity is also affected, but this remains similar for the next 24 hours. The degradation in the performance of the sensors is semi-reversible and when it is monitored after removal from the culture it is possible to reacquire 30% of the original sensitivity. It would seem that over the third 24 hour preiod, loss in enzymatic activity becomes significant and coupled with the layer hindering mass transport decreases the sensitivity of the sensor to 10% of its original value. This means that during the culture, we will have to remove the old sensors and insert fresh ones after day three.

Using ‘hand made’ devices or sensors made in small batches in a lab has these inherent

problems. The consistency and reproducibility of the devices can not be maintained due to small variations during each step, that may propagate. This propagation can occur from the preparation of the electrode's surface through to the storage of the sensors. When producing small numbers of devices, it is difficult to iron out some of these errors. The use of micro fabricated devices that have platinum films deposited on them electrolytically can improve the consistency of the surfaces, because they provide a more reproducible crystal structure, even though the deposition procedure has to be carefully monitored. Greater care has to be taken during the preparation of stock solutions, because with the small volumes involved these errors are magnified; if it were possible to make larger volumes of stock then the errors in preparation would be smaller. Due to the need for fresh reagents and to decrease waste, this is not feasible.

References

[1] S.-M. Chen and K.-T. Peng, "The electrochemical properties of dopamine, epinephrine, norepinephrine, and their electrocatalytic reations on cobalt(ii) hexacyanoferrate films," *Journal of the Electroanalytical Society*, vol. 547, pp. 179–189, 2003.

[2] A. Radomska, S. Singhal, H. Ye, M. Lim, A. Mantalaris, X. Yue, E. Drakakis, C. Toumazou, and A. Cass, "Biocompatible ion selective electrode for monitoring activity during the growth and cultivation of human cells," *Biosensors & Bioelectronics*, vol. DOI: 10.1016/j.bios.2008.04.026, 2008.

Chapter 8

Conclusion and recommendations for future work

The work presented here has primarily focussed on the surfaces of glucose sensors, with a small sojourn about iridium oxide, pH sensitive films. This chapter will collate this work and will present the conclusions drawn from it. To conclude there are some proposals for further studies that will build on these findings.

8.1 Conclusions

It was proposed that the variability in responses from iridium oxide pH sensitive films was due to variability in the nucleation sites available during galvanostatic deposition and that increasing the number of nucleation sites would remove these inconsistencies. Acid etching and physi-sorption of gold nano-particles were found to improve the responses from the sensors. These treatments also increased the variability in the operating characteristics of the sensor, specifically the intercept of the linear calibration curve. This was attributed to changes in the interfacial region between the gold and iridium oxide. It was later found that careful preparation of the gold surfaces achieved both better performance and more closely

matched devices.

Increasing the number of nucleation sites on the gold surface can improve the efficiency of iridium oxide precipitation. However, merely providing more sites does not guarantee sensors with closely matched operating parameters. It is more important to have a strict control on the quality of the gold surface, while ensuring that there are sufficient sites available for an effective precipitation process.

The preparation of glucose sensors with poly(phenol) was a process that yielded closely matched devices that could be used *in-vitro* for a period of 3 to 4 days. The performance of the sensors was dependent on the composition of the stock buffer and its pH. Successful pre-adsorption of the enzyme, to the surface of the platinum was also vital. These parameters manifested themselves as variability during the fabrication of different batches of sensors, although for this application these variations were mitigated by initial calibration of each device in each batch.

Surface characterisation of the enzyme sensors using optical techniques provided mixed results. The infra-red mapping did not yield any conclusive results and the data from the Raman maps may have showed some heterogeneity on the surface of the devices. In principle the optical techniques should have shown the heterogeneity on the sensors surface, but the physical limitations of poor resolution did not allow this.

The electrochemical data from the transition metal complexes threw some light on the morphology of the films. A perfectly formed poly(phenol) film passivated the surface of the electrode completely. It was possible to differentiate these from imperfect films because of responsive CVs, the shapes of which indicated that the diffusion profile of the probe molecules was semi-hemispherical in nature. This implied that the imperfections in the film were small and spaced far enough apart to create this diffusion profile.

When the same experiment was repeated on enzyme electrodes, the shapes of the CVs indicated that the active sites for ferrocyanide electrochemistry were neither small nor were they distributed in a manner that showed the features of a steady–state voltammogram.

That is the CVs showed shapes that were characteristic of semi-infinite planar diffusion. Another very important feature of the CVs was the ΔE_p between the forward and reverse peaks. A $\Delta E_p > 59mV/n$ was indicative of a quasi-reversible electrochemical system and this was further analysed using the Method of Nicholson [1]. The analysis clearly showed that the electron transfer kinetics of the probe molecule were quasi-reversible.

With the knowledge that the diffusion profile of the probe might be a hybrid between planar and hemispherical, the data was analysed by another model proposed by Armstrong et. al. [2]. As mentioned previously this model deals specifically with hybrid diffusion and it shows that, although the ΔE_p might indicate this, the electron transfer kinetics of these systems do not necessarily have to be slow. This analysis served two purposes, firstly to ascertain the true electron transfer kinetics and secondly, if this model showed the system to be truly reversible then it would validate the fact that the diffusion profile of the probe was a hybrid and we could then use the model to calculate the sphericity of the diffusion profile.

When the data was analysed using the model it was evident that even by making these changes the electron transfer kinetics were slow. Placing the sensor in a humid environment as opposed to immersed in buffer altered the structure of the film and increased the area available for the electrochemistry of ferrocyanide. This was a slow reversible change and the peak currents returned to values similar to those originally seen when the electrode was re-immersed in buffer, over a period of 48 hours. All of these are indicators of the enzyme and/or polymer being dehydrated and returning to their original state over a period of time.

The data from the CVs were validated using SECM to scan the surface of the sensors, which helped to characterise the film morphology, further. Using two different electrochemical couples in turn, it was possible to study the morphology of the films in generation–collection mode. When ferrocyanide was used as the probe the substrate was electrochemically generating the complimentary couple that was picked up by the probe. In this experiment areas on the substrate that were active toward ferrocyanide electrochemistry could

be seen. In the presence of glucose in the cell, with the tip collecting the enzymatically generated H_2O_2, it was possible to visualise the areas of peroxide generation. When these two maps were compared it was found that these areas tended to be mutually exclusive. More work needs to be done with the SECM as some of the data are inconclusive and this is described in section 8.2.

The mechanism to show the degradation of sensors *in-vitro* is a hybrid of enzyme deactivation and diminution in the flux of glucose at the sensor's surface due to protein adsorption. The data from the experiment in section 7.3.2 showed that the degradation of the sensors during the first three days could be reversed to some extent. This is a clear sign that enzyme degradation is not the sole reason for the loss in the performance of the sensor.

At low concentrations of glucose, ca. 3 mM, there was no response from the sensors. The current logged was similar to the background current in PBS. Thereafter the current increased in a linear fashion on addition of further calculated aliquots of standard glucose solution. This behaviour was observed from all the sensors removed from the culture during the first three days. From this it can be concluded that a mass transport barrier changed the permeability of glucose to the active centres of the enzyme, creating a limiting concentration. This limiting flux was roughly constant for all three days, which in turn indicated that the protein adsorption had equilibrated during the first 24 hours.

Further experiments showed that the process of protein adsorption was reversible to a certain extent. This was observed when the sensors were left to wash in 100 mM PBS under natural convection. The reversibility was a slow process, but the limiting flux regime was removed and the sensitivity of the sensors began to return to their original value. It was also observed that the sensors removed on day 2 regained their operating characteristics quicker than those from day 1; as they were tested twice during the same day. This would indicate that forced convection increased the speed of reversibility and it is hypothesised that the shear caused by stirring is the reason behind this. It is important to note that this can not be concluded from this set of experiments. However, if this hypothesis were

true then it might imply that the performance of the sensors will be improved in a perfused culture, even though the volume turnover in a perfused culture is small.

8.2 Recommendations for future work

The experimental work in this thesis has thrown up some very interesting questions that need further investigation. These studies will give a better understanding of the surfaces and the mechanisms of the degradation of the sensors *in-vitro*.

Firstly, it has been shown that these devices are capable of being used *in-vitro* to monitor the concentration of glucose and the pH of the extra-cellular media. Therefore, it is important to use them as intended and begin to understand the dynamics of the cell culture.

In conjunction with this, the development of a differential sensor to monitor cardiomyocyte cell cultures will give a better understanding of the cell life cycle and its interdependence with the concentration of glucose in the extra-cellular media. The trends seen in this work are indicative of these relationships, but the electrochemistry of norepinephrine needs to be accounted for in a manner that is more accurate than the simple removal of a background current. After the validation of differential sensing, an experiment to assess the dynamics of the cell culture with and without critical growth factors would also provide an excellent foundation on which to design future cell cultures. While performing these experiments it would be critical to perform cell counts and do cell viability studies in order to quantify the effects of the different experimental conditions.

The surfaces of the glucose sensors have been studied using optical techniques and SECM. The optical techniques have shown some limitations, but more work is proposed with the SECM. The work carried out has proposed a model that needs to be verified in greater detail. One of the key limiting factors of the SECM is the trade off between the area of the tip and the R/G ratio of the probe. In order to increase the available surface area without changing the ratio of the tip and the probe, electrochemical deposition of platinum black on the surface of the tip is required. Increasing the available area will amplify

the relatively weak signals that were seen during this work and will not compromise the resolution of the maps. It is very important to note that the tip loaded with platinum black needs to be verified independently using bulk electrochemistry. This is because the crystal structure of platinum black is different from the polished tip and therefore its responses to both the electrochemically generated ferricyanide and enzymatically generated H_2O_2 will be different.

Using an atomic force microscope (AFM) may give a better understanding of the actual morphology of the film, as this may help us to understand the mass transport of the analyte to the active centres of the enzyme. If a finer resolution study can be performed then a clear understanding may emerge of the diffusion profile of glucose to the surface.

For enzyme sensors the flux of glucose at the surface and the enzyme loaded on the surface are the two parameters that underpin the operating characteristics. Therefore, it is necessary to provide an electrode area that is adequate for the enzyme and also to try and achieve a semi-hemispherical diffusion profile. This is not possible using conventional means, but it can be made possible using a randomised array of electrodes and micro-fabrication. A similar set-up has been described by Barton et. al; here the authors have used sonochemically fabricated micro-electrodes to achieve the described results [3].

Once the surface of a functional sensor can be defined, the electrochemical studies performed here can be made in to a more descriptive model. It is then that this model can be used to design the electrode array such that it can maximise the benefits drawn from the enzyme loading and diffusion profile trade–off. Electrochemical studies of the bare and enzyme loaded arrays will be needed to study the actual diffusion profiles. Constructing a model should minimise the number of iterations required to optimise the operating characteristics of the array based device.

Along with the other advantages, multiple analyte sensors can be manufactured using this method. Micro fabrication also provides an excellent opportunity to have devices that are mechanically compatible with the culture vessels. This will make the sensors them-

selves easier to produce in larger batches. It will also decrease the cost so that disposable devices can be made for single use. This will mean a greater consistency in the crystal structure of the noble metal itself and remove the pre-preparatory work required during sensor production; in turn this will allow for a higher throughput of devices.

Finally, it is suggested that a quartz crystal micro-balance (QCM) be used to try and quantify the extent of fouling on the sensors' surface after being removed from culture mdeia. Taking a few snapshots over a 48 or 72 hour period of the bio-fouling on the surface of the crystal may show in more detail the extent of the fouling and the dynamics of the reversal, once it is replaced in a protein free media. Similar results may also be found using an AFM.

Using the techniques described above and by redesigning some of the previous experiments, the results shown here can be used to construct a more detailed and accurate model that can be used to better understand the sensors. This is turn will help in the fabrication of sensors that can be used for a longer time *in-vitro*, while providing useful data from the cell culture.

References

[1] R. S. Nicholson, "Theory and application of cyclic voltammetry for measurement of electrode reaction kinetics," *Analytical Chemistry*, vol. 37, no. 11, pp. 1351–1355, 1965.

[2] F. A. Armstrong, A. M. Bond, H. A. O. Hill, I. S. M. Psalti, and N. Oliver, "Electrochemistry of cytochrome c, plastocyanin and ferrodoxin at edge- and basal-plane graphite electrodes interpreted via a model based on electron transport at electroactive sites of microscopic dimensions," *Journal of the American Chemical Society*, vol. 111, no. 26, pp. 9185–9189, 1989.

[3] A. C. Barton, S. D. Collyer, F. Davis, D. D. Gornall, K. A. Law, E. C. D. Lawrence, D. W. Mills, S. Myler, J. A. Pritchard, M. Thompson, and S. P. J. Higson, "Sonochemically fabricated microelectrode arrays for biosensors offering widespread applicability: Part i," *Biosensors & Bioelectronics*, vol. 20, pp. 328–337, 2004.